The over-expression, purification and crystallisation of the alternative oxidase

Catherine Rebecca Elliott

DPhil

University of Sussex

January 2013

I hereby declare that this thesis has not been and will not be, submitted in whole or in part to another University for the award of any other degree.

Signature:.....

For my Dad.

Acknowledgements

To begin, I would like to express my deep and lasting gratitude to Tony Moore for both the opportunity to undertake this thesis and unwavering guidance throughout, made delightful and gratifying by his tireless, boundless and infectious enthusiasm. Without his support, encouragement and energy this thesis simply would not be. To Mary Albury: your help, knowledge and friendship have quite literally kept me sane, especially after long nights in the lab and failed experiments – thank you. To David Whitehouse: thank you for your encouragement and stimulating conversations about plant biochemistry and teaching undergraduates. I am very grateful to Professors Kita and Iwata for welcoming me into their labs and for all the advice and instruction they provided. To Momi Iwata, Kikukatsu Ito, Yasutoshi Kido, Ewan Main and Darren Thompson, thank you for all your invaluable guidance on the topics of biophysics and structural biology. I would especially like to thank Luke Young and Julia Shearman for all their help and support in the Moore lab – especially for putting up with my inane ramblings. To all the wonderful students I've met along the way (in no particular order – Sarah, Amelia, JJ, Maria, Kirsty, Kyle, Lisa, Sherry, Dong Mei, Elodie and Ben) – thank you all for enriching my time at Sussex both academically and socially.

To Mum, Dad and Lucy – you have been wonderfully supportive during my studies and have offered me confidence and inspiration every step of the way. To my Dad especially, thank you for your proof-reading services (for free, no less!); you made what felt like an insurmountable task manageable. I would also like to thank my *sorores caelestis* (especially Laurie and Silvia) for nurturing my soul and filling my life with such musical beauty.

Finally, to my rock, Matt, I could not have done it without you. Thank you.

CATHERINE REBECCA ELLIOTT

DPhil

OVER-EXPRESSION, PURIFICATION AND CRYSTALLISATION OF THE ALTERNATIVE OXIDASE

SUMMARY

The alternative oxidase (AOX) is an integral monotopic membrane protein which branches from respiratory chain at the point of the Q-pool in the mitochondria of all flowers, some fungi, and some protists such as the human parasite Trypanosoma brucei.

The aim of this project is threefold: to establish an over-expression and purification protocol for recombinant Sauromatum guttatum alternative oxidase (SgrAOX); to use expressed SgrAOX for structural analysis such as crystallography; and finally to use in silico methods to model the alternative oxidase protein. Of these three, only the first and last have been attempted previously, with varying success. The second, namely structural analysis, has never been attempted with SgrAOX.

In order to achieve the aims of this project, primarily laboratory-based protein production were used, in conjunction with downstream analysis using structural biology techniques. The in silico modelling was carried out using a wide range of algorithms freely available on the World Wide Web.

Results of this project are: the determination of an over-expression system and purification protocols in two E.coli strains, producing enough protein to use for the second objective detailed above. While no crystal structure has been obtained, significant steps toward identifying a protocol for rAOX crystallisation have been made. Results from structural analysis support modelling predictions and give novel insights into the thermostability of the protein. New and detailed homology models have been created and critically evaluated, with a very recent crystal structure from our collaborators providing a unique set of data for model evaluation.

The outcome of this project has contributed towards the determination of conditions under which SgrAOX protein may form crystals, and therefore bringing the acquisition of a SgrAOX protein structure closer.

TABLE OF CONTENTS

Abbreviations used

AA – antimycin A

ADP – adenosine diphosphate

AF – ascofuranone

ALA – 5-aminolevulinic acid

AOX – alternative oxidase

APS – ammonium persulphate

ASA – solvent accessible surface area

ATP – adenosine triphosphate

BCA – bicinchroninic acid

BLAST – basic local alignment search tool

BSA – bovine serum albumin

$C_{12}E_8$ – dodecyl octaethylene glycol ether

CD – circular dichroism

CMC – critical micelle concentration

COX – cytochrome oxidases

C-terminal – carboxyl terminus

DDM – dodecyl maltoside

dH_2O – distilled water

DNA – deoxyribonucleic acid

DSSP – Define Secondary Structure of Proteins algorithm

DTT – dithiothreitol

DQ – duroquinone

DQH_2 – duroquinol

DUQ – decylubiquinone

$DUQH_2$ – decylubiquinol

E – redox potential

ε – molar extinction coefficient

e^- – electron

ECL – enhanced chemiluminescence

EDT-20 – *N,N',N'*-polyoxyethylene(10)-*N*-tallow-1,3-diaminopropane

EDTA – Ethylenediaminetetraacetic acid

EPR – electron paramagnetic resonance spectroscopy

ETC – electron transport chain

$FADH_2$ – flavin adenine dinucleotide (reduced form)

FT – flow through

FTIR – Fourier transform infrared spectroscopy

G or ΔG – Gibbs free energy

GFP – green fluorescent protein

H^+ – proton

HAT – Human African Trypanosomiasis

HCl – hydrochloric acid

HRP – horseradish peroxidase

IPTG – isopropyl β-D-1-thiogalactopyranoside

kDa – kilodalton

LA – luria agar

LB – luria broth

LCP – lipidic cubic phase

MMO – methane monooxygenase

MOPS – 3-(*N*-morpholino) propanesulfonic acid

MPL – Membrane Protein Laboratory

NADH – nicotinamide adenine dinucleotide (reduced form)

NMR – nuclear paramagnetic resonance spectroscopy

N-terminus – amine terminus

OD – optical density

OG – octylglucoside

OGS - octyl-gallate

PCT – pre-crystallisation test

PDB – Protein Data Bank

PEG – polyethylene glycol

PMSF – phenylmethanesulfonylflouride

PPT – pellet

PTOX – plastid terminal oxidase

RNR – ribonucleotide reductase

SDS – sodium dodecyl sulphate

SDS PAGE – sodium dodecyl sulphate polyacrylamide gel electrophoresis

SgAOX – *Sauromatum guttatum* alternative oxidase

SN – supernatant

SSE – secondary structure elements

Q/Q_1 – ubiquinone-1

QH_2/Q_1H_2 – ubiquinol-1

TAO – trypanosomal alternative oxidase

TBST – TRIS-buffered saline and TWEEN-20

TCA – trichloroacetic acid

TEMED – tetramethylethylenediamide

TRIS – tris(hydroxymethyl)methyl-2-aminoethanesulfonic acid

Account

The following papers form part of this thesis:

Albury M.S., Elliott C. and Moore A.L. 2009. Towards a structural elucidation of the alternative oxidase in plants. *Physiologia Plantarum* **137**:316-327

Albury M.S., Elliott C. And Moore A.L. 2010. Ubiquinol-binding site in the alternative oxidase: mutagenesis reveals features important for substrate binding and inhibition. *Biochimica et Biophysica Acta* **1797**:1922-1939

Elliott C., Albury M.S., Young L., May B. and Moore A.L. *Manuscript accepted*. Structural elucidation of the alternative oxidase reveals insights into the catalytic cycle and regulation of activity. *Alternative Respiratory Pathways in Higher Plants*. Gupta K.J., Mur L.A.J. and Neelwarne B. (Eds). John Wiley and Sons.

Ito K., Ogata T., Kakizaki Y., Elliott C., Albury M.S. and Moore A.L. 2011. Identification of a gene for pyruvate-insenstive mitochondrial alternative oxidase expressed in the thermogenic appendices in *Arum maculatum*. *Plant Physiology* **157**:1721-1732

Williams B.A.P., Elliott C., Burri L., Kido Y., Kita K., Moore A.L. and Keeling P.J. 2010. Wide distribution of the mitochondrial alternative oxidase in microsporidia parasites. *Plos Pathogens* **6**:2 e1000761

Chapter 1

General Background

1.1 Respiration and the alternative oxidase

1.1.1 Cellular energy and the respiratory chain

Fundamental to the functioning of every cell is the provision of energy in a readily utilisable form. This is provided by the universal energy currency, adenosine triphosphate (ATP), the hydrolysis of which releases 30.5kJmol^{-1} of energy under physiological conditions (Gajewski *et al*., 1986). In eukaryotes, the majority of ATP is supplied during the process of respiration, taking place in the mitochondria and surrounding cytoplasm. During aerobic respiration, the energy harvested from consumed glucose is used to catalyse the phosphorylation of adenosine diphosphate (ADP) by inorganic phosphate (Pi), to make ATP. This catalysis is endergonic, and is the final step in a series of complex and intricate enzymatic interactions.

Ultimately, the process of ATP production begins in the cell cytoplasm with the sequential hydrolysis and decarboxylation of glucose, resulting in: the conversion of glucose to pyruvate; the substrate-level phosphorylation of ADP; and the reduction of nicotinamide adenine dinucleotide (NADH). The pyruvate produced during glycolysis is then decarboxylated and transported into the mitochondria as the substrate of Kreb's cycle, the next stage of respiration. Although the Kreb's cycle is ostensibly a process where the two-carbon substrate is converted to a six-carbon compound and then decarboyxlated in a step-wise manner, important products are released – reduced NAD and reduced flavin adenine dinucleotide ($FADH_2$). It is these products which are necessary for the initiation of the final stage of respiration – oxidative phosphorylation – rather than the carbon compounds metabolised from the glucose molecule during glycolysis and Kreb's.

Oxidative phosphorylation takes place on the inner membrane of the mitochondria, and is carried out by a group of enzymes collectively known as the respiratory or electron transport chain (ETC). In animals, the ETC is formed of a series of membrane-bound complexes, the roles of which are as follows and are illustrated in Figure 1.1 below. Complex I (NADH dehydrogenase), and Complex II (succinate dehydrogenase) strip electrons from NADH and succinate molecules (by way of reduced $FADH_2$) respectively. In addition, Complex I translocates protons across the inner mitochondrial membrane to the intermembrane space. The electrons from these complexes are then passed into a pool of ubiquinone (Q), which is mobile within the inner mitochondrial membrane. The ubiquinone becomes reduced to ubiquinol (QH_2), before becoming re-oxidised by Complex III (bc_1 complex), and the electrons gained from this reduction are transferred to Complex IV (cytochrome c oxidase) via the reduction and subsequent oxidation of cytochrome c, a small molecule which is able to move laterally along the membrane. It is cytochrome c oxidase that facilitates the final step of electron transfer – the four-electron reduction of oxygen to water.

Electron transfer through the ETC is facilitated by reducing iron ions, which are subsequently oxidised back to their original state (i.e. $Fe^{3+} + e^- \rightarrow Fe^{2+} \rightarrow Fe^{3+}$) to allow passage of further electrons in the same manner. The iron ions are not found alone; they exist as metal-metal or metal-nonmetal clusters within domains of the respiratory complexes, as shown in the schematic below, Figure 1.2. Each subsequent complex (with the exception of Complex II, which feeds into the Q-pool directly rather than forming part of the linear chain) has a greater redox potential (i.e. a greater affinity for electrons, E) than the previous complex, thus ensuring the unidirectional flow of electrons through the chain. This is also true of the associated donors and acceptors, which are not found within the enzymes themselves. Reduced NADH – the initial electron donor – has a lower redox potential than oxygen – the final electron acceptor. Since redox potential is inversely proportional to free energy (ΔG; when the value of ΔE is positive, the value of ΔG is negative), when electrons are accepted by a complex with higher electron affinity, free

energy made is available. It is this relationship which accounts for the ability of Complexes I, III and IV to translocate protons across the inner membrane from the matrix to the intermembrane space which would otherwise be energetically unfavourable. This translocation of protons across the membrane establishes a large enough protonmotive force to enable the assembled protons to move back through the membrane, via the trans-membranous enzyme, ATP synthase. It is this movement of protons that results in rotational catalysis of the ATP synthase, causing the phosphorylation of ADP and release of ATP, in an otherwise energetically unfavourable direction (Mitchell, 1961).

1.1.2 The respiratory chain and the alternative oxidase

In addition to the traditional electron transport chain, all plants, some fungi and some protists contain an additional oxidase known as the alternative oxidase. The alternative oxidase is a monotopic membrane protein, found in the inner-mitochondrial membrane and branching from the traditional electron transport chain at the point of the ubiquinone pool (Storey, 1976; Rich and Moore, 1976; Rich 1978). Intriguingly, the alternative oxidase (AOX) is non-protonmotive (Bendall and Bonner, 1971; Moore *et al*., 1978), and instead facilitates the four-electron reduction of oxygen to water and oxidation of ubiquinol to ubiquinone (Rich and Moore, 1976; Moore and Siedow, 1991). The alternative oxidase is insensitive to a number of respiratory inhibitors which are known to affect the other components of the respiratory chain such as cyanide (cytchrome c oxidase inhibitor; Keilin and Hartee, 1938; van Buuren *et al*., 1972) and antimycin A (cytochrome c reductase inhibitor; Chance and Williams, 1956; Rieske *et al*., 1967; for a concise review see Ikuma, 1972 and more recently Moore *et al*., 2013, in press). Instead, the alternative oxidase is sensitive to inhibition by hydroxamic acids such as salicylhydroxamic acid (Schonbaum *et al*., 1971), and propyl gallate (Siedow and Bickett, 1981). More recently, it has been confirmed that the Trypanosomal alternative oxidase, TAO, is sensitive to the antifungal agent ascofuranone (Yabu *et al*., 2003; Minagawa *et al*., 1996), which has proven to be a promising chemotherapeautic agent for the treatment of the Human African

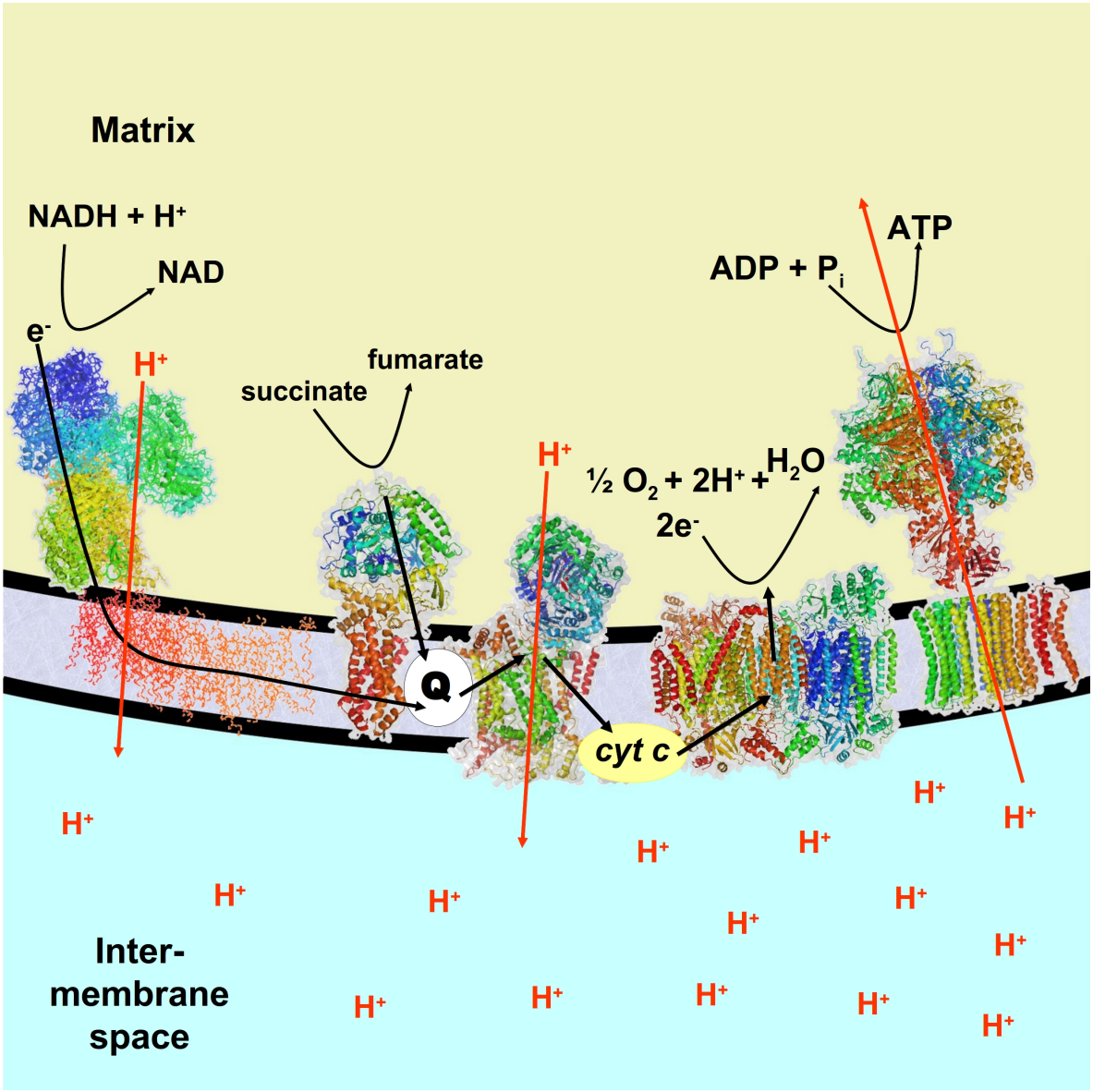

Figure 1.1 – The basic electron transport chain of mitochondria. The complexes in order from left-to-right with PDB accession numbers: Complex I (NADH deyhdrogenase; 3M9S Efremov *et al*., 2010), Complex II (succinate dehydrogenase; 2WDV Ruprecht *et al*., 2009), Q-pool, Complex III (cytochrome c reductase; 1BE3 Iwata *et al*., 1998), cytochrome c, Complex IV (cytochrome c oxidase; 1OCO Yoshikawa *et al*., 1998) and ATP synthase (1C17 and 1E79 – Rastogi and Girvin 1999 and Gibbons *et al*., 2000). Red arrows denote the movement of protons, while black arrows indicate electron flow and reactions occurring in the matrix. The alternative oxidase is located on the leaflet of the matrix-facing membrane between Complexes II and III.

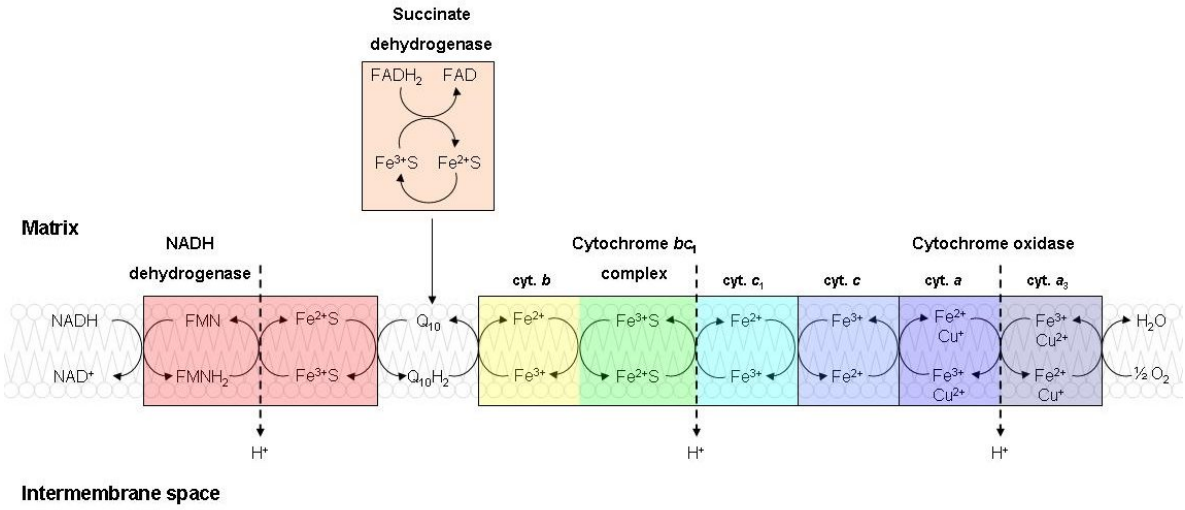

Figure 1.2 – A diagrammatic representation of the reaction centres responsible for electron transfer in the inner mitochondrial membrane. Arrows represent oxidation and reduction as electrons pass from NADH dehydrogenase to cytochrome oxidase. Dashed arrows show proton translocation across the membrane, but do not indicate the exact site of proton shuttling. Succinate dehydrogenase, shown here in orange, is membrane-bound *in vivo* but feeds into the Q-pool independently of NADH deyhdrogenase so is placed separately.

Trypanosomaisis (HAT) also known as African sleeping sickness. The current treatments for HAT are either ineffective or toxic (*cf* Fairlamb, 2003).

1.2 Distribution and function of the alternative oxidase

The alternative oxidase is ubiquitous in all plants (McDonald *et al.*, 2002), and is also found in several other species – including several human parasites (summarised below in Table 1.1). The function of AOX in each case varies depending on the species.

The role of the alternative oxidase in thermogenic plant tissues is well established – the heat released from the non-protonmotive reduction of oxygen to water is used to volatilise aromatic compounds found in the spathes, in order to attract insect pollinators (Meeuse, 1975; Meeuse and Raskin, 1988). The resulting smell is unsavoury to humans and often likened to rotting flesh, but attracts flies and other carrion insects which become

trapped for a short time in the base of the plants before being released, covered in pollen. A thermal image demonstrating the heat generated during this phase in a thermogenic lily found across the UK is shown below in Figure 1.3.

Kingdom	Examples	Reference(s)
Fungi	*Candida albicans* *Pichia anomala* *Chlamydomonas reinhardtii*	Veiga *et al.*, 2003
Protista	*Trypanosoma bruceii* *Cryptosporidium parvum* *Blastocystis hominis*	Chaudhuri *et al*., 1996 Suzuki *et al*., 2004 Stechmann *et al.*, 2008 Williams *et al*., 2010
Archaebacteria	*Novosphingobium aromaticivorans*	Finnegan *et al*., 2003
Animalia	*Crassostrea gigas* *Meloidogyne hapla* *Ciona intestinalis*	McDonald and Vanlerberghe, 2004

Table 1.1 – A summary of the presence of AOX in several kingdoms.

The largest thermogenic lily, *Amorphophallus titanum*, is referred to colloquially as the "corpse" flower; one of its smaller relatives is known as the "dead horse" lily (*Helicodiceros muscivorus*).

However, the role of the alternative oxidase is less apparent in non-thermogenic plants, fungi, and other species, for which there have been several suggested functions of the AOX protein. According to the findings of several groups working with non-thermogenic and fungal models, the alternative oxidase appears not to be constitutively expressed, but rather expressed when the organism experiences stress (such as ageing in potato slices; Hiser and McIntosh, 1990), or disruption of the respiratory chain (such as the

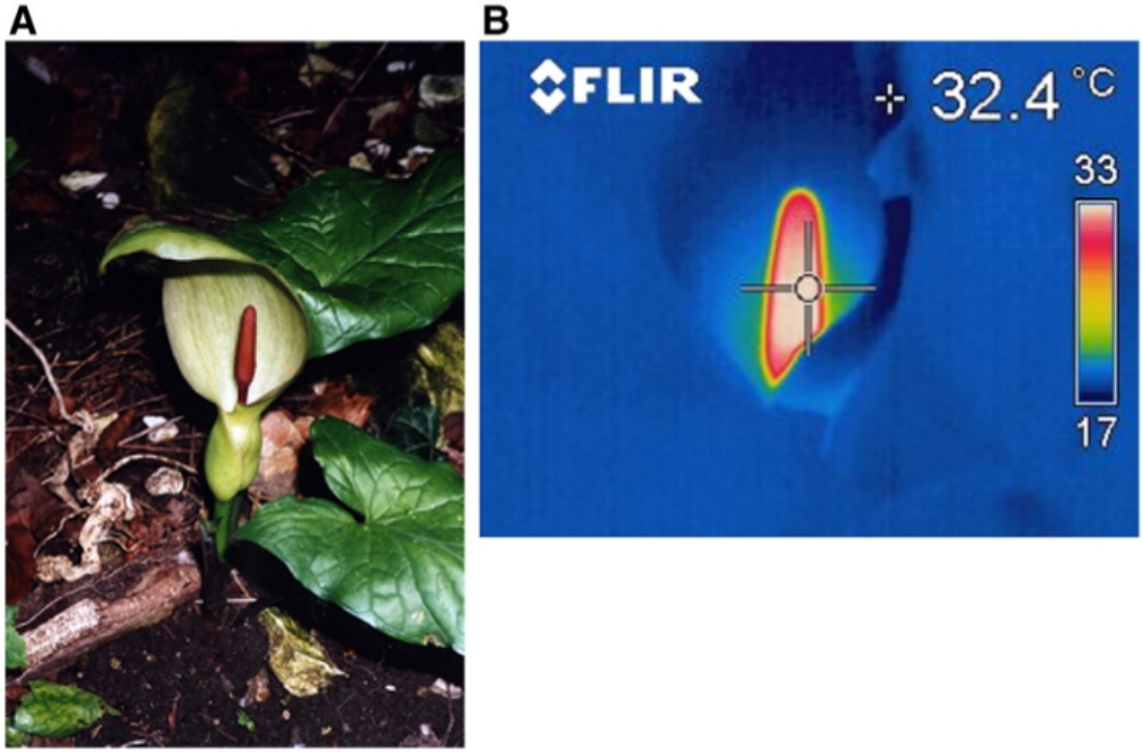

Figure 1.3 – Thermal imaging of an *Arum maculatum* lily during thermogenesis. Image A shows an *A. maculatum* lily found in the grounds of the University of Sussex, UK. The brown-coloured spadix in the centre of the white and green spathe undergoes thermogenesis to volatilise aromatic compounds which attract insect pollinators. The heat generated during this phase is demonstrated in Image B, showing an infrared thermal image of the same plant captured by a FLIR E45 camera. The thermogenesis is driven by the non-protonmotive reduction of oxygen to water by the alternative oxidase enzyme. The images above are taken from Wagner *et al*., (2008) with the author's permission.

effects of chloramphenicol in *Neurospora crassa*; Lambowitz *et al*., 1989). More specifically in relation to non-thermogenic plants, it has been suggested by Bahr and Bonner (1972) and Lambers (1982) that the AOX could be an energy over-flow mechanism, deployed when other respiratory chain components cease to function normally. This has been supported by the findings of Moore *et al*. (1988), Miller *et al*. (1993) and Carré *et al*. (2011), showing that the AOX can be stimulated by both a highly-reduced Q-pool and the α-keto acid, pyruvate. A build up of pyruvate in the cell may indicate a halting

of the Kreb's cycle, meaning that NADH is not being regenerated for use in the ETC. Without electron transfer continuing via the alternative oxidase, normal function of both glycolysis and the Kreb's cycle would cease, suggesting that unused pyruvate may act as the molecular trigger for a feed-forward mechanism, stimulating alternative oxidase activity to ultimately reduce pyruvate levels (reviewed in detail by Finnegan *et al*., 2004). The nature of expression of alternative oxidase in times of stress therefore is temporary, in which respiratory efficiency is sacrificed for survival.

Another theory of the role of the alternative oxidase was suggested by Purvis and Shewfelt (1993), whereby the AOX acts as a mechanism for the removal of reactive oxygen species (ROS) generated within the organism, should the other respiratory chain components be unable to do so (for example, in the presence of inhibitors). This has been supported by findings suggesting that the alternative oxidase can reduce observable ROS numbers in plants cells *in vivo*, as reported by Maxwell *et al*. (1999) and Zheng *et al*. (2008).

In recent years, much research has been conducted to establish the function of the alternative oxidase in human parasites such as such as *Trypanosoma brucei* (causative agent of HAT) and *Cryptosporidium parvum* (causative agent of cryptosporidiosis, a common disease found world-wide, with outbreaks in the UK in recent years). In the case of the former, it was noted that trypanosomes appeared to express an atypical array of mitochondrial components when the organism was in the infectious bloodstream form. Grant and Sargent (1960; 1961) and Clarkson *et al.* (1989) noted that there were no cytochromes expressed, and moreover that the sole terminal oxidase was in fact a plant-like alternative quinol oxidase, branching at the point of the Q-pool. Subsequent studies have shown that inhibiting the function of the AOX in bloodstream form trypanosomes with the inhibitor ascofuranone leads to the death of the parasite (Minagawa *et al*., 1996; Nihei *et al*., 2002). In this case, the ability of the trypanosomal alternative oxidase to reduce oxygen through to water is thought to allow respiration to continue despite the lack of cytochromes

(Chaudhuri *et al*., 2006) thus ensuring the survival of the parasite in the hostile environment of the host's bloodstream.

The alternative oxidase is not expressed in humans, or indeed any higher mammals, so the TAO makes an ideal drug target. Current treatments for African Sleeping Sickness are often ineffective and dangerous to the patient. If effective treatments can be developed for AOX inhibition in those infected with Trypanosomes, then these treatments may well be suitable for therapeutic use against other parasites which rely on AOX for survival such as *C. parvum* and *Blastocystis hominis*, both of which cause disease in humans.

1.3 Structural biology of the alternative oxidase from experimental observations

1.3.1 Identification of the alternative oxidase from thermogenic tissues

Although it is now accepted that both cyanide-resistant respiration and heat producing capabilities in thermogenic plants are a result of the alternative oxidase, these two observable characteristics were not always thought to be linked. When Lamarck commented on the ability of certain plants to raise their own temperature above ambient (1778, as cited in Vanlerberghe and McIntosh, 1997), he did not propose any mechanism by which this heat could be generated. The first mechanism to be proposed was suggested some 160 years later by Van Herk, who postulated that the thermogenic capabilities of lilies could be explained by the presence of a non-cytochrome flavoprotein (1937, as cited in Vanlerberghe and McIntosh, 1997). This remained the best theory of heat generation on a molecular level until attempts were made to isolate what is now known to be the alternative oxidase, 50 years later.

Prior to initial attempts to isolate the molecule responsible for both cyanide-resistance and heat generation from thermogenic tissues, James and Elliott (1955) localized the cyanide-resistant respiration to the mitochondria. Subsequently, attempts to identify the cause of cyanide-resistance were made by Huq and Palmer (1978), who isolated mitochondria from the spadices of the lily *Arum maculatum*, commonly found in the UK in secluded woodland areas. Huq and Palmer's analysis of the mitochondria revealed that

once the cyanide-resistant portion of the protein content had been isolated, no cytochrome could be detected; similarly, no EPR signal corresponding to iron could be identified. They concluded that the activity was likely due to a non-cytochrome flavoprotein, as Van Herk had suggested (1937, as cited in Vanlerberghe and McIntosh, 1997), and furthermore that no iron-sulphur clusters were present in the isolated species. Almost ten years later, mitochondria from *A. maculatum* were isolated by Bonner *et al*., (1986) and their analysis of the *A. maculatum* mitochondria indicated that both the heat generation and cyanide-resistance was in fact provided by a quinol oxidase iron-containing protein, rather than a flavoprotein as previously suggested by Van Herk and Huq and Palmer. At the same time, Elthon and McIntosh (1986) were isolating the mitochondria from another thermogenic lily, *Sauromatum guttatum*, and observed that the activity of the quinol oxidase – the alternative oxidase – was approximately ten times more active in the days leading up to anthesis (flowering), and that at the end of this period the cytochrome pathway activity decreased by 92%. They postulated that the alternative oxidase must therefore be a constituent of the traditional electron transport chain, but that activity was regulated in order to prevent energy wastage through heat production when it was not required. Following on from this work, Rhoads and McIntosh (1991) presented the first alternative oxidase sequence, derived from *S. guttatum* mRNA found in thermogenic tissues, allowing expression of the alternative oxidase in recombinant systems.

1.3.2 Recombinant protein expression

Due to the observed instability and short enzyme life of alternative oxidases isolated from native tissues (as recorded in Moore and Siedow, 1991 amongst others), a key goal has been to express recombinant AOX isozymes with the intention of increasing life-span and improving stability. Therefore, in addition to the groups who have attempted to isolate AOX from thermogenic plant tissues, several have more recently expressed various recombinant alternative oxidases in yeast (*Schizosaccharomyces pombe*; Albury *et al.*, 1996) and bacteria (*Escherichia coli*; Kumar and Söll, 1992 and Fukai *et al.*, 1999). Much

of the work conducted using wild-type/mutant recombinant protein (Albury *et al*., 2001; Nakamura *et al*., 2005) has vastly increased our understanding of the kinetic and structural properties of the alternative oxidase (Moore, *et al*., 1995a; Berthold, *et al*., 2000). Use of the *S. pombe* system has provided a eukaryotic expression system, where the isozymes can be targeted to the mitochondria. However, purification from the yeast system has not been particularly successful due to the lower levels of protein expression observed. However, the use of various strains of *E. coli* have proven useful for purification studies, leading to the production of purified protein stable enough for use in crystallography (Kido *et al*., 2010), EPR (Berthold *et al*., 2002; Moore *et al*., 2008), FTIR (Maréchal *et al*., 2009), as well as circular dichroism (detailed in this thesis). While expression in a prokaryotic system does not allow for the interaction of the alternative oxidase with a eukaryotic electron transport chain, it does provide a mechanism for the production of larger quantities of more stable protein than could be extracted from native samples.

In order to distinguish the activity of the alternative oxidase expressed in bacterial membranes using spectroscopic assays, it has been necessary to inhibit the activity of Complex III using the antibiotic antimycin A as this shares the quinol substrate with the alternative oxidase (*cf* Hoefnagel *et al*., 1997). In order to avoid this, several groups have used haem-deficient strains of *E. coli*, which are unable to synthesise the haem found in Complex III. While this was initially used for the expression of *Arabadopsis thaliana* (Berthold, 1998 and Berthold *et al*., 2002), it was later used by Nihei *et al* (2003) to express TAO. The activity of the alternative oxidase, in all cases, allowed the recombinant cells to survive, despite lacking a major respiratory complex.

Combined observations of both native and recombinant protein have confirmed that the size of the alternative oxidase protein varies depending on the organism in which it is expressed (for example, 38kDa in *S. guttatum* versus 36kDa in trypanosomes), and it is known to associate with the matrix-facing leaflet of the inner mitochondrial membrane (Rich and Moore, 1976; Rasmusson *et al*., 1990). Both native and recombinant protein can be visualized with immunoblotting after SDS-PAGE electrophoresis using anti-AOX

antibodies (Elthon *et al*., 1989), confirming molecular mass from predictions made on the basis of protein sequence information (*cf* Berthold and Siedow, 1993).

1.3.3 Catalytic cycle and active site of the alternative oxidase

Catalytically, the alternative oxidase is known to reduce oxygen through to water, using reduced quinol from the Q-pool as the hydrogen donor (Rich and Moore, 1976; Moore and Siedow, 1991). Whilst the exact catalytic cycle has not been elucidated, it was thought that the pathway of electron transfer within the alternative oxidase is dissimilar to the electron transfers observed in other cytochrome and electron transport complexes. In the latter, the iron clusters at the core of the proteins are reduced and reoxidised by the passage of one electron at a time. However, a recently proposed mechanism suggests that the electron transfer during the oxidation of quinol and reduction of oxygen catalysed by AOX may occur in several steps (Moore *et al*., 2013), rather than one step as previously thought. As previously mentioned, EPR signals of such characteristic reduction and reoxidation are absent in the alternative oxidase; instead, EPR experiments indicate the presence of an iron-only centre (Berthold *et al*., 2002; Moore *et al*., 2008). Whilst initially the AOX was thought to be EPR-silent, EPR analysis of recombinant *A. thaliana* AOX was conducted for the first time in parallel mode (rather than perpendicular) by Berthold *et al*., (2002) which revealed the presence of a non-haem, non-sulphur diiron site in a mixed valent FeII/FeIII state. Experimentation using parallel-mode EPR has been subsequently repeated with recombinant TAO, intact *A. maculatum* mitchondria and native AOX extracted from *A. maculatum* mitochondria. Characteristic signals for diiron centres were confirmed in all three samples. (Moore *et al*., 2008).

The signals observed by both Berthold *et al*., (2002) and Moore *et al*., (2008) share similarities to signals observed in a family of proteins known as the diiron carboxylates. This family is a functionally diverse group containing a non-haem, diiron centre, and members include methane monooxygenase, ribonucleotide reductase and bacterioferretin. All contain four-helix bundles coordinating the diiron centre within the core of the catalytic

units (Berthold and Stenmark, 2003). Most of the members of this family are large, multi-domain proteins unassociated with membranes, though some smaller members do exist, such as ferritin and rubrerythrin (*cf* Berthold and Siedow, 1993; Nordlund and Eklund, 1995). Additionally, both the diiron carboxlyates and the alternative oxidase lack a spectroscopic absorbance above 340nm (Berthold and Siedow, 1993). These experimental observations have lead to the inclusion of the alternative oxidase as a member of the diiron carboxylate family (Moore *et al*., 2008).

In order to identify the potential diiron binding residues of the active site of the alternative oxidase, sequence alignment and comparison of the AOX and the other diiron carboxylates was undertaken. Six key iron-binding residues were identified (Nordlund and Eklund, 1995), corresponding to known diiron binding motifs (E...ExxH repeated twice). The residues are not sequential, but are spread across the four-helix bundle in both the diiron carboxylates and the alternative oxidase. When the proteins are fully folded, the residues are brought close enough together to form a binding scaffold to ligate the diiron centre. The residues are shown below in Table 1.2, and are placed in a model below in Figure 1.4.

By way of confirmation, if any one of the six residues are mutated the activity of the plant alternative oxidase is completely diminished (Albury *et al*., 1998; Albury *et al*., 2002). This has been confirmed in other alternative oxidase isoforms, such as TAO (Ajayi *et al*., 2002; Nakamura *et al*., 2005). Furthermore, it is supported by recent findings from studies highlighting the necessity of iron to the functionality of the protein in plants (Affourtit and Moore, 2004) and other key organisms (such as Minagawa *et al*., 1990, using *Hansenula anomala*, now *Pichia anomala*). When inhibitors of ferric iron are present, activity of the alternative oxidase is inhibited, but when the inhibitor is removed, activity is completely restored.

Residue and number	Helix
Glu178	1
Glu217	2
His220	2
Glu268	3
Glu319	4
His322	4

Table 1.2 – A list of the key residues involved in iron binding. Above are the six residues proposed to ligate the diiron centre of the alternative oxidase, based on the iron ligation motifs found in other diiron carboxylates. Numbering corresponds to *S.guttatum*.

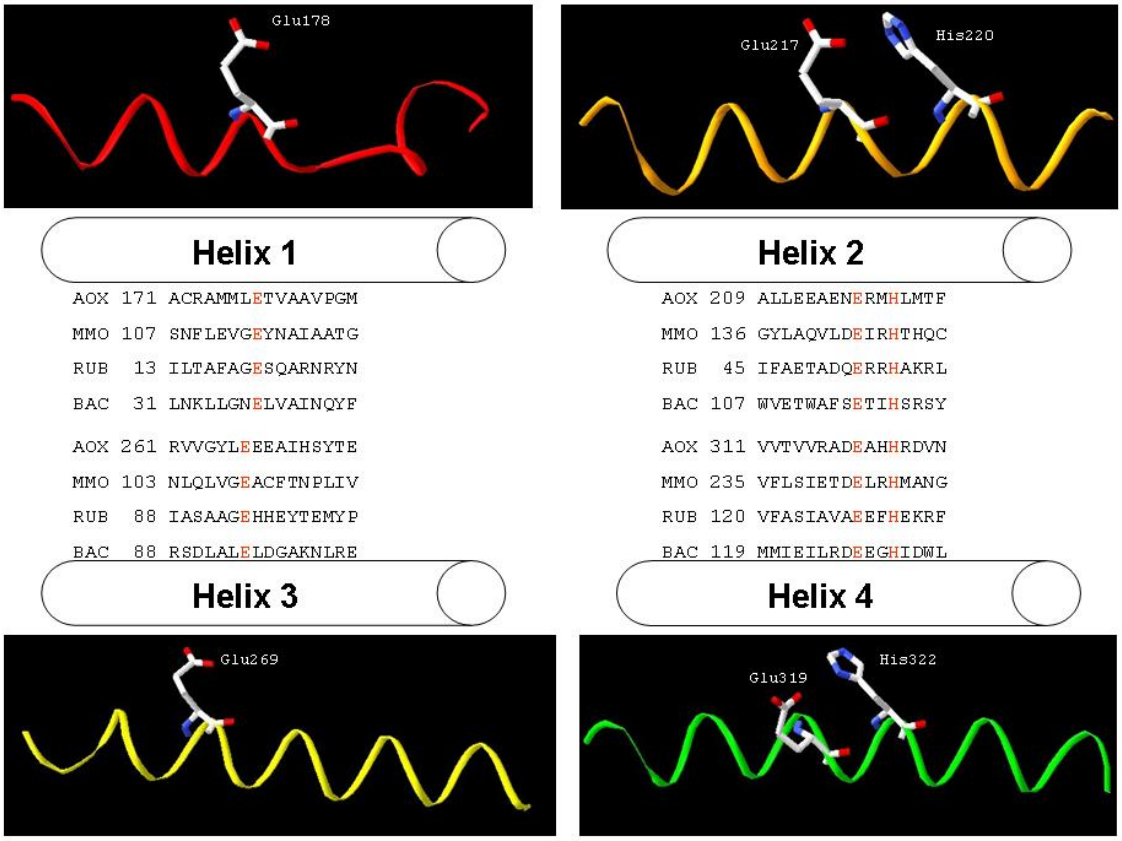

Figure 1.4 – Multiple alignments of each of the four helices involved in iron binding. The multiple alignments above show areas of sequence similarity and the highly conserved iron-binding ligands in several diiron carboxylates and the alternative oxidase. AOX – alternative oxidase; MMO – methane monooxygenase; RUB – rubrerythrin; BAC – bacterioferritin Key residues are highlighted in red.

1.3.4 Regulation of alternative oxidase activity

1.3.4.1 Genetics of the alternative oxidase

Genetically, the alternative oxidase protein in plants is the product of a single family of genes, ranging from a single gene to six genes encoded in the nuclear DNA (*cf* Polidoros *et al*., 2009). Transcription of these genes appears to be determined by the role that the alternative oxidase plays in the organism of interest – in thermogenic tissues expression is significantly increased when required for pollination, whereas in non-thermogenic plant tissues, expression is controlled by various abiotic stressors as demonstrated by Clifton *et al*. (2005) and Clifton *et al*. (2006). By comparison, the expression of the trypanosomal alternative oxidase is controlled developmentally, as it is only expressed during one stage in the organism's life cycle (Chaudhuri *et al*., 1995).

In plants and fungi, there are two main families of AOX genes, which are associated with either inducible stress response (*Aox1; cf* Clifton *et al*., 2006) or constitutive expression (*Aox2*; Considine *et al*., 2002). Thermogenic plants, therefore, tend to contain the latter, while non-thermogenic plants usually contain the former, though this is not always the case. A recent finding indicates that the thermogenic lily *A. maculatum* contains mRNA from the *Aox1* family (Ito *et al*., 2011), and moreover that the different mRNAs are found during different points during the developmental cycle of thermogenesis. Since the different mRNAs isolated from *A. maculatum* are known to give rise to protein isoforms of AOX, this may indicate that the isoforms are performing a variety of roles; though the nature of each isoform has not been established to date. In plant alternative oxidases, it is thought that the nuclear-encoded gene product is transported into the mitochondria in a mature, truncated form (*cf* Tanudji *et al*., 1999) after self-folding (Albury *et al*., 1996).

1.3.4.2 Regulation by changes to the quaternary structure – homodimerisation

Alternative oxidase activity appears to be regulated post-translationally by two different mechanisms which occur simultaneously in some tissues. In plants for example, activity is thought to be regulated in part by reduction and oxidation of the protein. When

the unit is oxidised and less active, two monomers are covalently linked through an intermolecular disulphide bond occurring between the highly conserved cysteine 122 residues (*S. guttatum* numbering; Rhoads *et al*., 1998). When this disulphide bond is reduced, the two monomers become linked non-covalently instead resulting in increased activity (Umbach and Siedow, 1993). In mitochondrial tissue from several plants (*S. guttatum*, *Glycine max* and *Vigna radiata*), Umbach and Siedow (1993) noted the presence of both the reduced and oxidised forms, indicating that the enzymes are able to switch between states – most likely as a result of oxidation and reduction of the quinone pool in the membrane which is known to have an effect on alternative oxidase activity *in vivo* (Moore and Siedow, 1991). In subsequent studies, it was observed that the activity of the alternative oxidase increases up to five times in the reduced state in mitochondrial tissues from soybeans (Umbach *et al*., 1994). Although the exact mechanism by which activity is increased is not known, it is possible that the helices are more stable in the active form. In addition, since the substrate (quinol) is hydrophobic, it may also be possible that the active form allows for greater membrane interaction and therefore increased access to the substrate.

However, this mechanism of regulation does not appear to be the case in organisms such as trypanosomes and fungi, which do not respond in the same way to the reduction and oxidation of the quinone pool. This may be due to the lack of a suitable analogous cysteine residue in the N-terminal region (Chaudhuri and Hill, 1996 and Fukai *et al*., 2002; Sakajo *et al*., 1991 respectively) of their alternative oxidase sequence, though they may be able to form dimers through non-sulphide interactions as indicated by the recent trypanosomal crystal structure which is homodimeric in nature.

1.3.4.3 Regulation by pyruvate and other α-keto acids

As previously discussed in Section 1.2, a build up of pyruvate in the mitochondria may indicate that the Kreb's cycle has ceased to function normally, which would have an impact on electron transport. Therefore, in organisms where the alternative oxidase is

expressed in order to overcome the effects of disruption of the Kreb's cycle or oxidative phosphorylation, it was anticipated that pyruvate could play a part in regulation of the AOX protein. In addition to enzyme reduction increasing activity in plant tissues as discussed above, the activity can also be increased by the addition of pyruvate to non-thermogenic recombinant alternative oxidase (Crichton *et al*., 2005; Carré *et al*., 2011). Pyruvate stimulation is also observed in recombinant alternative oxidases, such as *A. thaliana*, and also thermogenic recombinant alternative oxidases expressed in prokaryotic systems. It is thought that the OH group of the pyruvate interacts directly with the alternative oxidase, forming a thiohemiacetal species (Rhoads *et al*., 1998) with the same cysteine involved in non-covalent dimerisation, C122. While it was initially suggested that pyruvate increased the affinity of the alternative oxidase for its substrate (Umbach *et al*., 1994), it was later suggested that the formation of the thiohemiacetal in non-thermogenic alternative oxidase resulted in a conformational change which lead to increased alternative oxidase activity (Hoefnagel *et al*., 1997), as no increase in substrate affinity could be demonstrated kinetically. Stimulation of alternative oxidase activity by other α-keto acids has also been observed: AOX activity in both tomato (non-thermogenic) and sacred lotus (thermogenic) mitochondria can be stimulated by succinate, for example (Holtzapffel *et al*., 2003 and Grant *et al*., 2009 respectively). Similarly, alternative oxidase activity in soybean seedlings can be stimulated differentially by succinate, malate and pyruvate, with the former two stimulating activity to a lesser extent than the latter (Millar *et al*., 1993).

By contrast, AOX activity in mitochondria isolated directly from thermogenic tissues (*Arum italicum*, Hoefnagel *et al*., 1997; *S. guttatum*, Crichton *et al*., 2005; *A. maculatum*, Ito *et al*., 2011) appears to be insensitive to pyruvate, suggesting that the enzyme expressed in these tissues is possibly fully stimulated by endogenous pyruvate already bound to the protein, resulting in no observed increase in activity with the addition of pyruvate to the medium.

Stimulation of alternative oxidase activity by pyruvate – or indeed other α-keto acids – has not been reported in other species such as fungi and parasites In common with

observations regarding reduced and oxidised enzyme forms as discussed previously, the organisms which are insensitive to pyruvate lack the conserved cysteine residue (C122) which is found in other pyruvate-sensitive alternative oxidases (*cf* Carré *et al*., 2011).

1.4 Predicted structural information from protein sequence data

1.4.1 Modelling the alternative oxidase

To date, there is no crystallographic structural data for the plant alternative oxidase. Based upon sequence analysis, however, there have been two proposed models of the plant alternative oxidase, derived in different ways.

1.4.1.1 The Siedow-Umbach-Moore model

The SUM model was developed after the discovery of highly conserved iron-binding residues ([E]…[ExxH]x2) in the alternative oxidase sequence which were also present in other diirobn carboxylates (Siedow *et al*., 1995) as represented in Figure 1.4 below. Structural data was available at the time for other members of the diiron carboxylate family; namely ribonucleodide reductase R2 (Nordlund and Eklund, 1993) and methane monooxygenase (Rosenzweig *et al*., 1993). The resemblance between the active site for both proteins had been commented on previously (Norlund *et al*., 1992) and this similarity formed the basis for first a model of the alternative oxidase four-helix bundle active site (Siedow *et al*., 1995) and then later the same year, the entire protein (Moore *et al*., 1995a). Emphasis was placed on the highly conserved iron binding residues, and hydrophobicity plots indicated that there were transmembrane helices present in addition to a helical bundle acting as the diiron binding scaffold. In addition, the crucial cysteine residue involved in the formation of the reduced active form (Umbach *et al*., 1994) was included in the model. The model is shown below in Figure 1.5a.

1.4.1.2 The Andersson-Nordlund Model

A second model of the alternative oxidase was proposed in 1999 by Andersson and Nordlund who performed homology modelling using another diiron carboxylate, Δ^9-desaturase, as a template. The structure had been solved after the creation of the SUM model (Lindqvist *et al*., 1996) and Andersson and Nordlund argued that the Δ^9-desaturase shared more sequence homology with the alternative oxidase in helical regions than the other diiron carboxylates. In addition, the AN model postulates that the regions of hydrophobicity observed by Moore *et al*. (1995a) were not indicative of transmembrane helices – rather that the protein was attached to only one leaflet of the membrane through two small helices in a manner similar to the attachment mechanism observed in prostaglandin H_2 synthase-1 (Picot *et al*., 1994). Andersson and Nordlund suggested that this would allow direct access to the active site for the quinol located within the membrane. This model has been recreated for this thesis (as shown below in Figure 1.5b) and is shown as a line drawing in Figure 1.5c also.

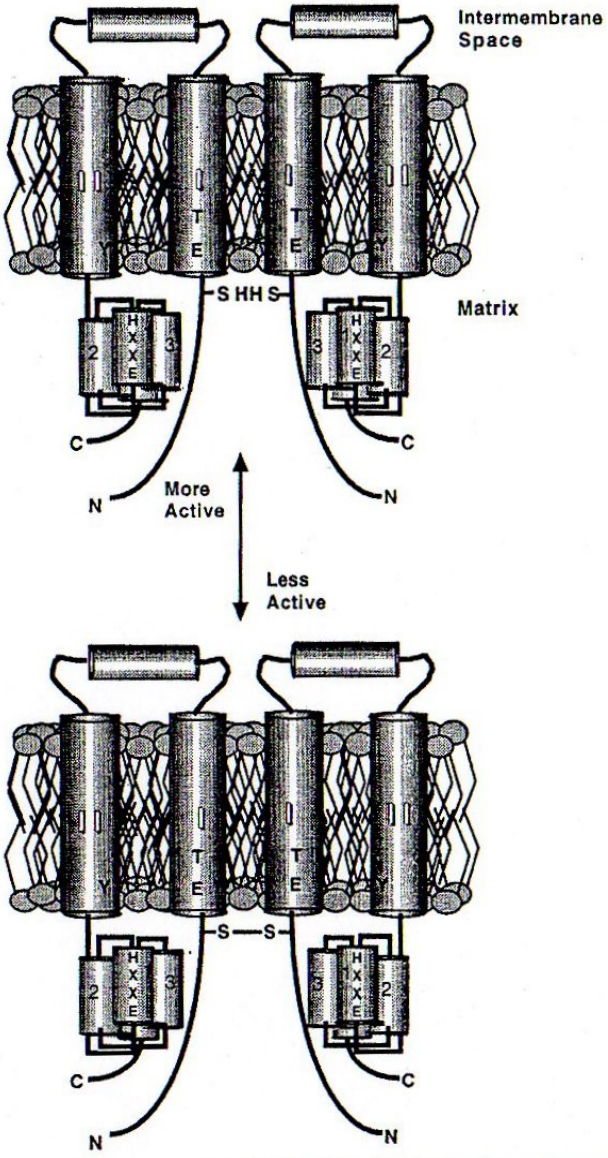

Figure 1.5a – The SUM model of the alternative oxidase. Taken from Moore *et al*., 1995a (reproduced with the author's permission).

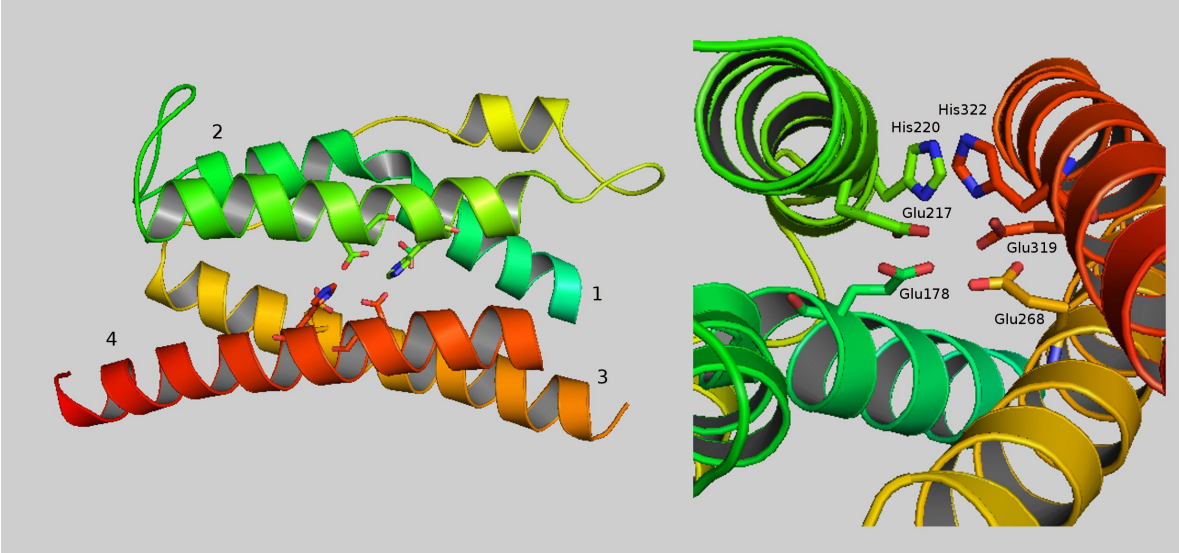

Figure 1.5b – A modified version of the AN model. Iron-binding residues are indicated (right, labelled) within the four helix bundle (left, numbers indicate helices 1-4).

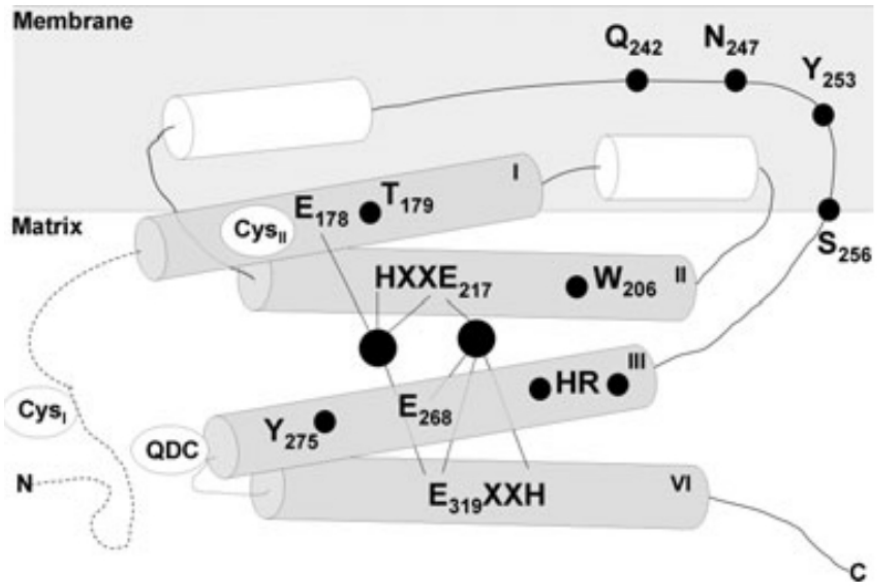

Figure 1.5c – The Andersson Nordlund model of the alternative oxidase. The Figure shows a detailed representation of the Andersson and Nordlund (1999) model, including modifications by Berthold *et al*., (2000). The Figure is taken from Albury *et al*., (2009) and reproduced with the author's permission.

1.4.1.3 Similarities between AOX and other diiron carboxylates

In addition to reported sequence similarity between diiron carboxylates (*cf* Moore *et al*., 1995a and Andersson and Nordlund, 1999), similarities in biochemical characteristics were also noted. For example, methane mono-oxygenase (MMO) lacks a spectroscopic signal above 350nm, which is uncharacteristic for iron-containting proteins; similarly, MMO lacks a characteristic EPR signal found in other iron-containing proteins (Vincent *et al*., 1990; Wilkins 1992; and Lipscomb 1994). It was suggested that while the function of the diiron carboxylates – itself a functionally diverse family of proteins (Nordlund and Eklund, 1995) – differs from the function of the alternative oxidase, they could have similar structures, specifically the construction of the four-helix bundle common to all diiron carboxylates, where the helices act as a scaffold, bringing the iron-ligating residues in close proximity to form the active site (Andersson and Nordlund, 1999; Berthold *et al*., 2002).

1.4.1.4 Recent attempts to model the alternative oxidase

Further alignment and investigation of the alternative oxidase sequences found in the UniProt (www.uniprot.org) database has allowed modelling of both the whole alternative oxidase protein (AN model, as above and Albury *et al*., 2009) and small regions within the protein of particular biological interest, such as the substrate binding site (Albury *et al*., 2010). In the recent attempts to model the alternative oxidase as part of this thesis, a variety of different approaches were taken, such as homology modeling and threading, and comparisons of the generated models was conducted using knowledge-based evaluation. The limitations of such techniques are well understood, and the importance of suitable template choice and accurate alignment of template and target sequences was not overlooked.

1.4.2 Identification of other key residues

In addition to the six essential residues, other highly conserved residues have been identified, and mutated. Areas of particular interest are the substrate and inhibitor binding

regions, the oxygen pathway, and identification of any radicals formed close to the active site that may donate electrons for the purpose of oxygen reduction. A list of such identified residues, their putative roles, and their effect on activity where tested is summarised below in Table 1.3.

1.5 Elucidating the structure of the plant alternative oxidase experimentally

1.5.1 Over-expression of recombinant alternative oxidase protein

Of particular interest in this project has been over-expression of recombinant protein, rather than a focus on extraction of AOX from tissues where it is natively expressed. Extraction of protein from native tissues expressing alternative oxidase has been successful, and the choice to pursue expression using a recombinant system was decided based on the quantity of protein each extraction would provide. Native extraction, as noted by Moore and Siedow (1991) was difficult and samples often lost activity soon after solubilisation; stabilisation of native alternative oxidase (Zhang *et al*., 1996) was a major development in the definition of a purification protocol, and the first highly pure and stable AOX protein isolated from native tissue was prepared from *A. maculatum* tissue (Affourtit and Moore, 2004).

Instability in AOX isolated from native sources is in part due to the protein becoming more labile once released from the mitochondrial membrane; the same difficulties would be expected when solubilising recombinant protein from the vector membrane. However due to the greater quantities expressed using a recombinant system, less overall would be lost to instability, and perhaps having a higher concentration of protein may help to stabilise the protein molecules. Certainly for attempting to crystallise the alternative oxidase, large quantities of relatively stable protein would be required, and therefore recombinant expression offers an advantage over extraction of protein from native tissues. Similarly, tissues expressing alternative oxidase (such as from *A. maculatum*) are only available during certain times of the year, and this would be inhibitory to amassing sufficient quantities of protein.

Residue	Effect	Role	Reference
C172A	Slightly reduced activity; O_2 affinity increased	Regulatory cysteine	Albury *et al*., 2002; Critchton *et al*., 2010
T179A	Slightly reduced activity; O_2 affinity increased	Adjacent to E178; mutant is thought to change the distance of E178 to the diiron centre thus slowing down catalytic cycle	Crichton *et al*., 2010
H261	Not tested; expected activity loss	Putative quinone-binding	Albury *et al*., 2010
R262	Not tested; expected activity loss	Putative quinone-binding	
Y253F	Reduced activity	Possible electron transport or quinol-binding	
G242	Not tested; expected activity loss	Conserved, polar residue in hydrophobic pocket	
N247	Not tested; expected activity loss	Conserved, polar residue in hydrophobic pocket	

Table 1.3 – A list of conserved residues and their putative roles and expected effect on activity if altered. Residues are grouped according to effect on enzyme activity. Numbers correspond to *S. guttatum* sequence.

Generally speaking, there are well-documented difficulties associated with working with recombinant integral membrane proteins (Midgett and Madden, 2007), in particular proteins which do not overexpress to a high level. Therefore, there is a requirement for the development of a reliable and robust expression and purification protocol to allow

sufficient quantities of recombinant protein to be produced. Protein that is produced can be used for many purposes, such as structural elucidation, kinetic analysis, and assessing the impact that mutations have on the overall activity of the protein.

The laboratory of Professor Kita (University of Tokyo) has had much success when expressing recombinant TAO protein, mainly due to their use of a haem-deficient *E.coli* expression strain (FN102), which is discussed in detail in Chapter 4.

1.5.2 Crystallography

To date, no crystallographic data is available for the plant alternative oxidase; however, the crystal structure of the Trypanosomal alternative oxidase has recently been solved to 2.8Å (Shiba *et al*., 2013; initial findings described in Kido *et al*., 2010). The structure was solved after more than a decade of trying to produce suitable crystals. Historically, crystallization of membrane proteins has been a difficult task (*cf* Carpenter *et al*., 2008), and this is reflected in structural databases. For example, in the Protein Data Bank (www.rcsb.org/pdb/home/home.do) there over 74,000 protein structures derived from X-ray crystallography (as of January 2013), but very few of those structures (~600) are membrane proteins. Given that approximately 30% (Bill *et al*., 2011) of the proteomes of living organisms are comprised of membrane proteins, there is clearly a mismatch in the number of membrane proteins known about and those having their structures solved. In part the difficulty in crystallising – and indeed purifying – membrane proteins is their apparent fragility in the absence of a lipophilic environment. Some proteins appear more stable in lower concentrations of the bi-lipid layer (for example Iwata *et al*., 1995 and Svensson-Ek *et al*., 2002), but this is not the case for most membrane proteins.

1.5.3 Circular dichroism

In lieu of crystallographic structural data, there are other techniques available that will supply information about the structure of a protein of interest. One such technique, circular dichroism (CD), utilises circularly polarised light to distinguish features of protein

secondary structure, such as α-helices and β-sheets. Given the predicted predominantly helical nature of the alternative oxidase, this technique is ideal for matching predictions to experimental observations. CD has been used to some success with other diiron carboxylates, such as ribonucleotide reductase (Stubbe, 2003), which is thought to utilise a radical or radicals for electron shuttling in a similar manner to the alternative oxidase; and of a much smaller member of the family, rubrerythrin (Wakagi 2003) which is more like the plant alternative oxidase in size. There exist a number of different algorithms available which allow determination of percentage secondary structure given circular dichroism and protein concentration, which are compared and evaluated in Chapter 5, along with the correlation between predicted secondary structure and secondary structure observed experimentally.

Circular dichroism also offers the advantage of investigating protein stability: for example how increased temperature or presence and absence of cofactors affects the stages of denaturation and disruption of secondary structure.

1.6 Questions remaining in the field of plant alternative oxidase research

In order to consolidate the information presented in this Introduction and shape the aims of this project the following questions have been posed and will be readdressed after considering the results presented in Chapters 3, 4 and 5.

- Is it possible to over-express recombinant *S. guttatum* alternative oxidase protein in a bacterial system?
- Is it possible to the purify the expressed protein, to provide relatively pure protein?
- Its is possible to crystallise recombinant *S. guttatum* alternative oxidase?
- Will recombinant *S. guttatum* alternative oxidase share a similar sensitivity to pyruvate as other AOX isoforms?
- What is the structure of *S. guttatum* AOX and is it similar to that of TAO and predictions made previously?

- Does recombinant *S. guttatum* expressed in a bacterial system form dimers and if so, is it possible to identify the mechanism of dimerisation?
- Is it possible to replicate and expand upon previous attempts to model the alternative oxidase, taking into consideration the large volume of new AOX sequences now available in databases?
- How do previous models of the alternative oxidase compare to the newly elucidated TAO structure?

1.7 The Aims of this project

To date, the structure of the plant alternative oxidase has remained elusive. While significant progress has been made towards a fuller understanding of the TAO, there is still much to be learned about the nature and structure of the plant alternative oxidase. Therefore, the aims of this project were threefold: to overexpress, purify and attempt to crystallise the plant alternative oxidase; to use the expressed protein to gain insight about the structure-function relationship of the alternative oxidase experimentally; and to carry out a comprehensive *in silico* analysis of the alternative oxidase.

Chapter 2

Materials and Methods

2.1 Plasmid vectors and *Escherichia coli* strains

In order to express recombinant alternative oxidase proteins, a library of plasmids was created (Dr Mary Albury, University of Sussex as listed below in Table 2.1), using the pET15b vector system (Novagen).

Plasmid	Organism	Creator
SgAOX-pET15b	*Sauromatum guttatum* (wild-type)	Albury *et al*., 2001
pTAO	*Trypanosoma brucei*	Fukai *et al*., 1999
SgAOX-GFP (pET28(a+)-derived GFP-8His fusion vector; Drew *et al*., 2001)	*Sauromatum guttatum* with green fluorescent protein tag	Dr Momi Iwata (Protein Membrane Laboratory, Diamond Light Source/Imperial College, London)
SgAOX-pET15b mutants: T179A, C172A, Y253F	*S. guttatum*	Dr Mary Albury (University of Sussex)

Table 2.1 – A list of plasmids used and their creators.

The pET15b system offers the advantages of an N-terminal 6-His tag and ampicillin resistance, as well expression being controlled by isopropyl β-D-1-thiogalactopyranoside (IPTG) induction.

2.1.1 Preparation of competent *E. coli* cells

Two strains of *E. coli* were frequently used – a C41 (DE3) cell line tailored for membrane protein expression, kindly provided by Professor John Walker (University of Cambridge; Mirroux and Walker, 1996); and a haem-deficient mutant strain, developed in the laboratory of Professor Kita (University of Tokyo, Fukai *et al*., 2003).

Both major cell strains (C41 and FN102) were made competent using the same protocol, as follows. A streak of frozen, non-competent cell stock was plated out on Luria Agar (LA) plates containing the necessary additives (100μgml^{-1} ampicillin, and then 50μgml^{-1} 5-amino levulinic acid (ALA, Sigma) and 50μgml^{-1} kanamycin for FN102 only) and the plates were incubated overnight at 37ºC. A scrape of cells were used to inoculate 1ml of Luria Broth (LB, containing ALA if necessary). This was then incubated overnight at 37ºC with shaking. Following incubation, the cell suspension was back-diluted 1:100 using fresh LB and incubated at 37ºC until A_{650} = 0.45-0.55. The suspension was then placed on ice for 5 minutes before centrifugation at 6,000 x *g* for 5 minutes at 4ºC. The resultant pellet was the resuspended in ½ volume of ice cold, 0.1m $CaCl_2$. The cell suspension was centrifuged as previously. The resultant pellet was then resuspended in 1:20 volume of ice cold, 75% 0.1m $CaCl_2$, 25% glycerol. The competent cells were then frozen using dry ice, before being stored at -80ºC in 200μl aliquots until needed.

2.1.2 Transformation of competent *E. coli* cells

Both major cells trains were transformed using the same protocol. Frozen cells were thawed out on ice, and then 100μl of cells were aliquoted to separate eppendorfs. Depending on the plasmid used 0.1 and 1μl of plasmid DNA was then added to the cells to be transformed. One tube per plasmid was used as a negative control, and contained only cells and no plasmid. The tubes were then mixed gently and placed on ice for 30 minutes. Following incubation on ice, the cells were then heat-shocked at 42ºC for 90 seconds, before being placed back on ice for 5 minutes. After chilling on ice, 800μl of LB (containing no additives) was added to each tube, and the tubes were incubated at 37ºC for 1 hour in a water bath. After incubation, the cells were centrifuged at 15,000 x *g* for 2 minutes, 4ºC, and after centrifugation, 750μl of LB was removed from each tube and discarded. The remaining ~150μl was used to gently resuspend the cell pellet. The resuspended pellet was spread out on LA plates containing relevant selective antibiotics; typically 100μgml^{-1} ampicillin for C41 cells containing the *Sauromatum guttatum* AOX (SgAOX-pET15b) plasmid and mutants; FN102 containing SgAOX-pET15b and mutants required 100μgml^{-1} ampicillin, 50μgml^{-1} kanamycin, and 100μgml^{-1} ALA; C41 cells

containing the GFP-tagged *S. guttatum* were supplemented also with 50μgml^{-1} kanamycin. Finally, the plates were then incubated overnight at 37^{o}C.

2.1.3 Preparation of transformed glycerol cell stocks

In order to preserve transformed stocks of cells, glycerol stocks were made using cells from a fresh transformation. A loopful of transformed cells was used to inoculate 5ml of LB containing necessary additives and the culture was incubated overnight at 37^{o}C with shaking. After incubation, sterile glycerol was added to a final concentration of 10% (v/v). The glycerol-cell mixture was then aliquoted into appropriate volumes before freezing in dry ice, then stored at -80^{o}C.

2.1.4 Isolation of plasmid DNA

Plasmid DNA was prepared using a Qiagen Midi kit (Qiagen) following the manufacturer's instructions. No changes were made to the protocol. Final purified plasmids were resuspended in distilled water and stored at -20^{o}C until required. Prior to freezing, samples of purified plasmid were electrophoresed on an agarose gel (0.8%, Melford) at 75 volts (Biorad Powerpac 200) for 1-2 hours. The gels were cast containing ethidium bromide dye (Sigma), and fluorescence UV light was captured using a charge-coupled device.

2.2 Protein expression and membrane isolation

The recombinant protein expressed in both *E. coli* strains was associated with the bacterial membrane, so membranes were harvested in order to isolate the recombinant protein.

2.2.1 Expression and membrane isolation from C41

The method of expressing recombinant alternative oxidase using the C41 *E. coli* was based upon a protocol from Berthold *et al*. (2002) with some minor adaptations. Rationale for protocol changes are described more fully in Chapter 4.

A single colony of transformed cells (as described above in Section 2.1.2) was used to inoculate an LB starter culture (20ml broth per 1L of main culture) containing the strain-specific additives (typically 100μgml^{-1} ampicillin, 0.2% glucose, 0.125% $FeSO_4$), which

was the incubated at 37°C overnight with shaking. Following incubation, the whole cell suspension was used to inoculate the main culture (LB, 100μgml^{-1} ampicillin, 0.2% glucose, 0.125% $FeSO_4$). The main culture was then incubated at 30°C for 4 hours. After incubation, the culture flasks were transferred to a pre-cooled 18°C incubator, and left to acclimatise for one hour with shaking. Following the one-hour acclimatisation, the cells were induced using a final concentration of 25-100μM IPTG, and then incubated for 18 hours at 18°C. After 18 hours, the cell culture was centrifuged at 8,000 x *g* for 6 minutes using a JA-10 rotor in a Beckman JX centrifuge in order to separate the cells from the broth. After centrifugation, the cell pellets were resuspended using 50mM TRIS-HCl, pH 7.5, 10mM pyruvate. An approximate ratio of 20ml TRIS:1g of wet pellet was used for the resuspension. The resuspended cell solution was then supplemented with 100mM PMSF in order to reduce protease activity before homogenisation using a glass homogeniser. The cells were then lysed, using either the French Press (two passes at 10k psi; SLM Aminco FA-078 with a FA-032 cell) or sonication (coarse probe at 14 microns, 30 seconds per ml of cell suspension). Following lysis, the cell debris was removed by centrifugation at 20,000 x *g* (Beckman JX centrifuge, JA-20 rotor) for 15 minutes. The centrifugation step was repeated if the pellets were very loose at the end of the first spin. The supernatant was retained and ultracentrifuged at 200,000 x *g* for 2 hours in order to pellet the bacterial membranes (Beckman Avanti XP centrifuge, 70Ti or 70.1Ti rotor). After ultracentrifugation, the supernatant was discarded (though a sample was usually retained for testing the efficiency of lysis), and the pellets resuspended in 50mM TRIS-HCl, pH 7.5, 10mM pyruvate (with additives if required) before homogenisation. Membrane samples were then snap-frozen in liquid nitrogen before storage at -80°C.

2.2.2 Expression and harvest – FN102

The protocol for expression of recombinant alternative oxidase is based on Fukai *et al*., 2003 with several adaptations. The rationale for the adaptations is described in Chapter 4.

A single colony of transformed cells was used to streak LA, 100μgml^{-1} ampicillin, 50μgml^{-1} kanamycin and 100μgml^{-1} ALA. The plate was then incubated for 12 hours at 37°C. After incubation, a single bacterial colony was used to inoculate an LB starter culture

(10ml broth per 1L of main culture) supplemented with 100μgml^{-1} ampicillin, 50μgml^{-1} kanamycin and 100μgml^{-1} ALA. The starter culture was then incubated at 37ºC for 4-6 hours. Following incubation, the starter culture was centrifuged at 5,000 x *g* for 5 minutes in order to remove the ALA from the broth. The resultant cell pellets were resuspended in LB containing no additives, and the centrifugation/resuspension step was repeated twice more. The OD_{650} of the final resuspended pellet was taken (LKB Pharmacia 4050 Ultrospec II), and enough cell suspension was added to each main culture flask to make the OD_{650} = 0.01. The main culture broth (S-broth) contained the following reagents (gL^{-1}): 10g bacteriological peptone (Oxoid), 5g yeast extract (Melford), 5g casamino acid (Oxoid), 10.4g di-potassium hydrogen orthophosphate (Fisher), 3g potassium di-hydrogen orthophosphate (Fisher), 0.74g trisodium citrate (Sigma), 2.5g ammonium sulphate (Sigma), 0.05g magnesium sulphate (Sigma), 0.025g iron sulphate (Sigma), 0.025g iron chloride (Sigma), 0.1g carbenicillin (Sigma/Melford) and 2g glucose (Sigma). The last five reagents were added after autoclaving, and the glucose was autoclaved separately.

After inoculation of the main culture, the flasks were incubated at 30ºC with shaking, and the OD_{650} was monitored. When OD_{650} reached 0.1, the main culture was induced using between 25-100μM IPTG. Following induction, the main cultures were incubated at 30ºC for 8-14 hours (to allow for cultures expressing less active alternative oxidase protein to grow sufficiently). After incubation, the cells were pelleted by centrifugation at 8,000 x *g* for 6 minutes. The resultant cell pellets were then resuspended in 50mM TRIS-HCl, pH 7.5, 10mM pyruvate (with 20% sucrose if performing a sucrose gradient to isolate inner membrane), and supplemented with 100mM PMSF and a Roche Complete Protease inhibitor cocktail tablet (1 tablet per 50ml cell suspension) and then homogenised. After homogenisation, the cells were lysed using either the French Press (two passes at 10k psi; as above in Section 2.2.1) or sonication (coarse probe at 14 microns, 30 seconds per ml of cell suspension; as above in Section 2.2.1). The cell debris was then removed by centrifugation at 20,000 x *g* (Beckman JX centrifuge, JA-20 rotor) for 15 minutes. The centrifugation step was repeated if the pellets were very loose at the end of the first spin.

To prepare the bacterial membrane, the supernatant was ultracentrifuged at 200,000 x *g* for 1 hour at 4ºC (Beckman Avanti XP centrifuge, 70Ti or 70.1Ti rotor). To prepare the

inner membrane fraction, the supernatant was laid over an equal volume of TRIS-HCl, pH 7.5, 10mM pyruvate, 40% sucrose (provided that the cell pellets had been resuspended with TRIS containing 20% sucrose), and ultracentrifuged at 200,000 x *g* for 1 hour at 4°C. Following the first ultracentrifugation step, the middle layer (often slightly yellow in hue) was extracted, and mixed with an excess of 50mM TRIS-HCl, pH 7.5, 40% sucrose, and ultracentrifuged once more at 200,000 x *g* for 1 hour at 4°C. The pellets obtained were then resuspended in 50mM TRIS-HCl, pH 7.5 (with 20% sucrose if isolating the inner membrane) before homogenisation. Following homogenisation, membrane samples were snap-frozen using liquid nitrogen, before storage at -80°C.

2.3 Membrane solubilisation and purification

In order to free the expressed recombinant alternative oxidase from the membrane, a solubilisation step is necessary. Separating the membrane from the protein is required before purification can be carried out.

2.3.1 Membrane solubilisation

Frozen membrane samples (prepared as described above) were thawed out on ice. For small-scale solubilisation (for condition screening), an equal volume of solubilisation buffer (Table 2.2) was added in a dropwise manner to the membrane sample. The buffer and membrane were mixed gently before incubation on ice for 30-60 minutes. For larger-scale solubilisation (for preparatory purposes), approximately 8mg (for inner membrane) or 6mg (for whole membrane) of protein was used per 1ml of solubilisation buffer (Table 2.2). The buffer was added to the membrane in a dropwise fashion. The mixture was then left stirring on ice for 30-60 minutes. After incubation on ice, the membrane-buffer solution was ultracentrifuged at 200,000 x *g* (Beckman TL-100 Ultracentrifuge with a TLA100.3 rotor) for 30-60 minutes at 4°C. The supernatant (soluble fraction) was removed for further purification, and the pellet (insoluble fraction) was resuspended in 50mM TRIS-HCl, pH 7.5 and retained to assess the efficiency of solubilisation.

Optional additive	Rationale
50-300mM NaCl	Recommended additive for downstream affinity purification; limits non-specific interactions with the metal ions of the affinity resin
1-5mM DTT	Can be used to keep the sample under reducing conditions, and limits formation of dimers
10mM pyruvate	In the case of the *S. guttatum* recombinant protein, pyruvate (max. concentration 10mM) appears to stabilise the protein.
20/40% (w/v) sucrose	Required when isolating inner membranes through sucrose-gradient ultracentrifugation.
1% (w/v) DDM	In solubilisation trials this proved to be the best detergent and concentration for the *S. guttatum* alternative oxidases.
1.4% (w/v) OG	Recommended detergent and concentration for recombinant TAO proteins; can be used in conjunction with DDM for *S. guttatum* recombinant proteins. During early detergent screening, it was noted that OG repeatedly reduced recombinant AOX activity and as such OG was not screened to the same extent as DDM.
5-20% (v/v) glycerol	Appears to stabilise the recombinant protein once it has been removed from the membrane; should be incorporated into the solubilisation buffer.

Table 2.2 – A list of optional additives. The optional additives listed above may be used to supplement the standard 50mM TRIS-HCl, pH 7.5 buffer for solubilisation and membrane isolation.

2.3.2 Further purification

The recombinant alternative oxidase proteins were 6-His tagged in order to purify using affinity chromatography. Two main types of affinity resin were used; His-Select nickel affinity resin (Sigma) and His-Select cobalt affinity resin (Sigma). Table 2.3 below lists equilibration, wash and elution buffers used during the purification process.

The soluble fraction (prepared as detailed above in Section 2.2) was retained on ice while the affinity resin was equilibrated. Both types of resin (cobalt and nickel) were equilibrated by first removing the storage slurry, then using 5x resin bed volume of equilibration buffer either at room temperature (batch method) or at 4°C (column method). After equilibration, the solubilised membrane sample was applied to the resin. In batch purification (small scale), this was typically ~600µl of solubilised membrane sample on a

50-100µl resin bed volume. For column (large scale) purification, up to 15ml of solubilised membrane sample was used on a bed volume of 3-6ml. The solubilised membrane sample was allowed to bind by gentle mixing for 1 hour at 4°C (batch method) or simply gravity flow (column method) at 4°C. The resultant flow-through after a low-speed spin (batch method) or gravity flow (column method) was retained and labelled as the flow-through fraction.

Following binding of the sample to the resin, the resin was then washed in stages using 5-10x the resin bed volume of wash buffer (see Table 2.3 below). In each case, the flow-through was retained and labelled as the wash fraction. After washing, the protein was eluted from the resin using elution buffer. In total, 2-3 (batch) or 5-20 (column) applications of 5x the resin bed volume were applied, and the separate flow-throughs were retained as the elution fractions. During elution using the column method, the imidazole concentration was gradually increased.

Buffer	Optional additive	Rationale
Equilibration buffer and wash buffer	Glycerol (5-20%)	Keeps the protein stable once solubilised.
	100mM $MgSO_4$	Appears to keep the protein stable and active during purification
	Detergent (0.5% DDM, 0.5% OG)	Keeps the protein soluble during purification
Elution buffer	20-250mM Imidazole	For elution purposes; disrupts the binding between the 6His-tag and metal ions.

Table 2.3 – optional additives for purification buffers (50mM TRIS-HCl, pH 7.5, 10mM pyruvate).

2.4 Visualisation of recombinant protein

2.4.1 SDS polyacrylamide gel electrophoresis (SDS-PAGE)

In order to visually assess the quality of prepared samples, and to gauge purity of purified recombinant protein, SDS PAGE was used (Laemmli, 1970).

Gels were cast using the BioRad Mini-Protean system (10cm x 8cm x 1mm gels) using the buffers listed below in Table 2.4a. Final acrylamide concentration was achieved using the matrix shown in Table 2.4b. The resolving reagents were mixed gently in a side-arm conical flask, and de-gassed if necessary before pouring. The resolving gel was allowed to polymerise for 30 minutes, whilst overlayed with butan-saturated water to

prevent drying out. After setting, the stacking gel was applied along with a well-comb. The stacking gel was allowed to polymerise for 20 minutes before the apparatus was disassembled.

The protein samples were then mixed with 2x loading dye (Table 2.4a) at a 1:1 ratio, vortexed, and heated at 90^{o}C for 6 minutes. The dye-sample mixture was then loaded into the sample wells along with a rainbow marker (Amersham FullRange Rainbow Markers) and the electrophoretic rig was submerged in 1x SDS-running buffer (Table 2.4a). A current was then applied to the system for approximately 1 hour, 150 volts, or until the dye front reached the bottom of the rig at which point the rig was disassembled and the gels were rinsed briefly in distilled water before either Western blotting or staining using GelCode Blue (Thermo Scientific) following the manufacturer's instructions. Stained gels were destained with distilled water overnight before being dried (BioRad 583 Gel Dryer).

Buffer	Reagents	Comments
TRIS buffer for resolving gel	1.5M TRIS-HCl, pH 8.8	
TRIS buffer for stacking gel	0.5M TRIS-HCl, pH 6.8	
Loading dye (2x)	0.1M TRIS-HCl, pH 6.8, 10mM EDTA, 2% (w/v) SDS, 5% (w/v) glycerol, 0.05% (w/v) bromophenol blue	No β-mercaptoethanol used. Can be supplemented with up to 5mM DTT if reducing conditions are required.
SDS Running (tank) buffer (10x)	0.25M TRIS, 1.92M glycine, 0.03M SDS.	10x stock diluted when required to 1x with distilled water.

Table 2.4a – Buffers required for SDS PAGE.

2.4.2 Western blotting

In order to better visualise the bands containing recombinant alternative oxidase protein on SDS PAGE gels, it was often necessary to perform Western blotting using primary antibodies raised against *S. guttatum* alternative oxidase (Elthon *et al*., 1989).

SDS PAGE gels were run as described above (Section 2.4.1), and rinsed briefly in distilled water. The gels were then transferred to a small amount of chilled 1x transfer buffer (see Table 2.5 below). Meanwhile, an 8x10cm nitrocellulose filter (pore size of

	Final % acrylamide – resolving gel			
Reagent	**7.5%**	**10%**	**12%**	**15%**
30% polyacrylamide	7.5ml	10ml	12ml	15ml
Resolving buffer	7.5ml	7.5ml	7.5ml	7.5ml
10% SDS	300µl	300µl	300µl	300µl
10% APS	300µl	300µl	300µl	300µl
TEMED	20µl	20µl	20µl	20µl
dH_2O	14.38ml	11.88ml	9.88ml	6.88ml
Total	**30ml**	**30ml**	**30ml**	**30ml**
	Stacking gel – 5% acrylamide			
30% polyacrylamide	1.6ml			
Stacking buffer	2.5ml			
10% SDS	100µl			
10% APS	100µl			
TEMED	10µl			
dH_2O	5.7ml			
Total	**10ml**			

Table 2.4b – Final acrylamide concentration matrix.

0.45nm, Protran, Whatman) was also equilibrated in 1x transfer buffer, along with blotting paper and sponges of the same size. A blotting cassette was assembled (see Figure 2.1 below) and placed into the transfer rig along with two ice packs. The blotting tank was then filled with the remainder of the chilled 1x transfer buffer. A current (typically 100V for 1 hour with stirring) was applied to the rig, during which time the temperature of the tank was monitored. If temperature of the buffer in the tank rose above 30°C, fresh chilled 1x transfer buffer was added to the tank, and the ice packs were replaced in order to prevent damage to the nitrocellulose membrane.

Following transfer, the nitrocellulose membrane was washed briefly in 1x TBST (Table 2.5) and then submersed in block solution (Table 2.5) and allowed to equilibrate with gentle shaking for 15 minutes. After equilibration, primary anti-AOX antibody was added to the block solution containing the nitrocellulose to a dilution of 1:5000. The solution and membrane were then incubated at room temperature with gentle shaking for 1 hour. After incubation, the membrane was washed using 1x TBST briefly six times, followed by 6x 5 minute washes with shaking. Following washing, a fresh 20ml aliquot of block solution was added to the membrane along with the secondary antibody (rabbit anti-mouse with a HRP conjugate, Dako BioProducts at a 1:20,000 dilution). The membrane and block were then incubated for a further hour at room temperature with gentle shaking. Following the incubation, the membrane was washed as described previously. After washing, the membrane was placed in 1x blot rinse (Table 2.5) for 15 minutes. The membrane was then gently blotted dry using blotting paper and transferred to a piece of Saranwrap for exposure to the Enhanced Chemiluminescence reagents (Amersham ECL Detection Kit, GE Healthcare) at a ratio of 1:1 for solutions 2 and 1, for 3 minutes and 1 minute respectively.

The membrane was then blotted dry once more before being covered in a single layer of Saranwrap and placed in an extremity cassette (DuPont Ultravision). After securing the membrane in place in the cassette, a single piece of x-ray film (Fujifilm Super RX Medical X-ray film) was placed on top of the wrapped membrane and exposed for between 10 seconds and 1 hour. The exposed films were then developed using a (Konika SRX-101A) auto-rad developer and the positions of the protein markers were noted immediately after developing.

2.4.3 Sample preparation – acetone precipitation

Cold (-20^{o}C) acetone was added to the sample in a ratio of 4:1 and mixed thoroughly, following which the sample was incubated at -20^{o}C for 1 hour. Following incubation, the sample was centrifuged at 13,000 x *g* for 10 minutes (Eppendorf Centrifuge 5415R). After centrifugation, the acetone was carefully aspirated from the pellet, and the pellet was left to air-dry for 30-40 minutes, to avoid over-drying of the pellet. The driedpellet was then resuspended in 2x loading dye and heated for 6 minutes at 90^{o}C before

being loaded onto an SDS PAGE gel, and electrophoresed as described in Section 2.4.1 above.

Buffer	Reagents	Comments
Transfer buffer, 10x	1.92M glycine, 13mM TRIS, pH 7.2	1x working solution made using 8 parts cold distilled water, 1 part methanol, 1 part 10x TB stock
TBST, 10x	140mM NaCl, 20mM TRIS, pH 7.6, 0.1% (v/v) Tween-20	
Block solution	2% (w/v) Marvel milk powder, 3% (w/v) BSA in 1x TBST	
Blot rinse, 10x	10mM TRIS, 5mM ETDA, pH 7.2	

Table 2.5 – Western blotting buffers.

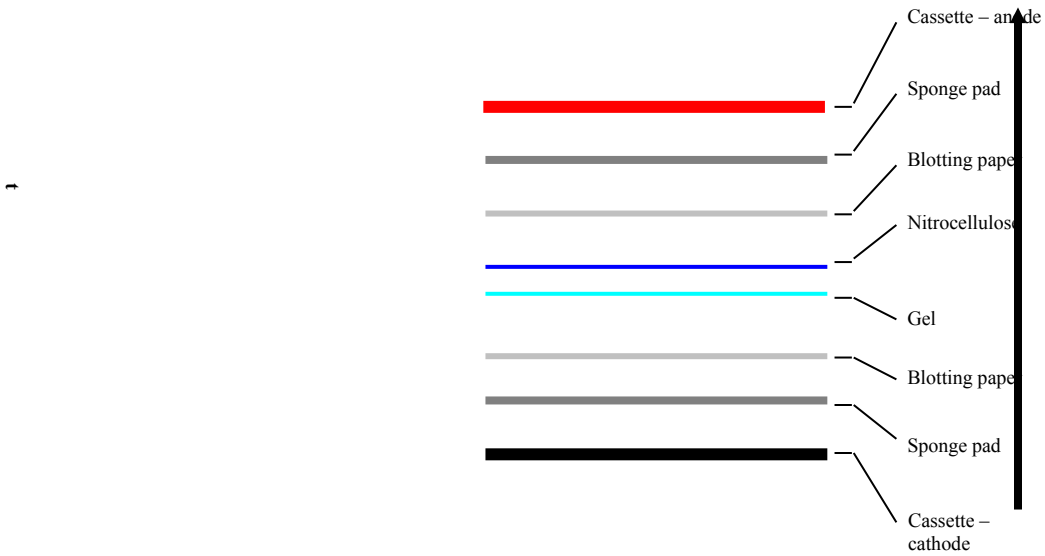

Figure 2.1 – A diagrammatic representation of the transfer cassette. Orientation of the components of the transfer cassette are shown relative to one another. The arrow indicates the direction of the current.

2.5 Protein Assays

A variety of assays were used to assess the protein concentration and activity of prepared samples.

2.5.1 Protein estimation assays

Both of the following methods were used to ascertain protein concentration in any samples prepared; the method used is indicated in the results sections of each Chapter as appropriate.

2.5.1.1 BCA protein concentration estimation method

Protein concentration was estimated using a Pierce BCA protein assay kit (Thermo Scientific, adapted from Smith *et al*., 1985), following the manufacturer's instructions. No changes were made to the protocol, which is summarised as follows. For samples containing substances likely to affect the estimation assay, an acetone precipitation step was required, and was carried out as described above in Section 2.4.3. 100µl of diluted (or resuspended) sample (1:20, 1:50 or 1:100 to dH_2O), standard was added to 100µl of 5% SDS in 0.1M NaOH. Samples were prepared in triplicate and standards (BSA at 0.1, 0.2, 0.4, 0.6, 0.8 and 1$mgml^{-1}$) in duplicate. Blanks (containing water) were also prepared in duplicate. 1ml of BCA working reagent (50:1 of solutions A:B from the kit) was then added to each tube before vortexing. The samples were then incubated for 30 minutes at 37^{o}C. After incubation, the absorbance at 562nm of each standard and sample was then measured spectrophotometrically; the absorbance of the standards was used to plot a standard curve from which the concentration of the unknown samples could be extrapolated.

2.5.1.2 Lowry protein concentration estimation method

This alternative method for estimating protein concentration was used whilst in Professor Kita's laboratory, at the University of Tokyo and is based on Lowry *et al*. (1951).

Several different BSA concentration standards were prepared in distilled water. Samples of protein of unknown concentration were then prepared in two different dilutions (either 1:250, 1:100 or 1:50) with a dilution of 1:50 being used for low concentration

samples. Each of the standards and protein samples had a total volume of 500µl. A 1:1:100 solution was then made of 2% copper (II) sulphate (pentahydrate), 4:% potassium sodium tartrate and 4% sodium carbonate (dissolved in 0.2M sodium hydroxide and 2% sodium dodecyl sulphate) respectively. 500µl of this solution was then added to each of the standards and protein samples, following which 50µl of phenol reagent (Wako) was added. Each tube was vortexed immediately after the phenol reagent was added.

The standards and protein samples were then left at 37°C for 30 minutes before the absorbance of each solution was monitored at 700nm using a spectrophotometer (Shimadzu UV-1201).

2.5.2 Spectrophotometric activity assay

Activity assays were required to assess the functional capability of the expressed recombinant protein, using a variety of substrates. In each case, a 10mm quartz (Hellma, Suprasil) cuvette was used.

Using a Cary 400 UV spectrophotometer[1] (Varian) connected to the Varian spectrophotometer computer suite (CaryWin UV) a scanning wavelength baseline (Scan) was taken to ensure that the sample cuvette and assay buffer (Table 2.6a) did not absorb significantly at the wavelength used to monitor substrate depletion/product formation. Using the Kinetics program, a single wavelength was monitored (Table 2.6b) throughout the duration of the assay. To begin with, only buffer was placed in the cuvette, followed by sample once a flat line was observed. Following addition of sample, substrate was added to initiate the reaction. Additions were made quickly and accurately, allowing the stir-bar to complete the mixing of any substances added to the cuvette. Initial rates were monitored and the reaction was allowed to progress sufficiently before addition of inhibitors or other solutions where appropriate (Table 2.6b). Data collected from each assay was imported into an Excel spreadsheet for further analysis. In order to calculate substrate consumption, the following calculation was used, where ε = molar extinction coefficient of the oxidised substrate.

[1] When at University of Tokyo, Shimadzu UV-3000 was used

$$\left(\frac{slope\,(abs\,\min^{-1})}{\varepsilon\,(M^{-1}cm^{-1}}\right)\Big/\,protein\,(mg)$$

Equation 1

Buffer	Composition
50mM TRIS	50mM TRIS-HCl, pH 7.5, 10mM pyruvate
Yeast Medium A	0.3M mannitol, 1mM $MgCl_2$, 5mM K_2HPO_4, 10mM KCl, 20mM MOPS, pH 7.2 (with KOH)

Table 2.6a – Buffers used for spectrophotometric assays.

Additive	Rationale	Comments
Q_1H_2 (ubiquinol-1)	Substrate	Working concentration 150µM, ε = 15,000 M^{-1} cm^{-1} at 278nm
DQH_2 (duroquinol)	Substrate	Working concentration 250µM, ε = 2,150 M^{-1} cm^{-1} at 283nm
$DUQH_2$ (decylubiquinol)	Substrate	Working concentration 200µM, ε = 4140 $M^{-1}cm^{-1}$ at 289nm
OGS (octyl-gallate)	Inhibitor of the alternative oxidase	Working concentration 1µM
AA (antimycin A)	Inhibitor of the *bc*1 complex	Working concentration 4µM
AF (ascofuronone)	Inhibitor of the alternative oxidase (*cf* Minagawa *et al*., 1996)	Variable working concentration used to determine effect of concentration on inhibition
Pyruvate	Apparent stabilising effect on recombinant *S. guttatum* alternative oxidase; boosts activity	Working concentration up to 10mM. Added to either the assay medium or during membrane harvest

Table 2.6b – Substrates, inhibitors and stabilisers compatible with spectrophotometric assays. In the case of decylubiquinol, the extinction coefficient is taken from Rich (1984).

2.5.3 Substrate reduction protocol

The quinol family of substrates required for alternative oxidase activity must be in the reduced state. They were reduced in-house, using the following protocol (based on Rich, 1981).

Three aliquots of sodium dithionite (Sigma) were prepared by dissolving sodium dithionite in 50ml of distilled water; the quantity of sodium dithionite required is in proportion to the quantity of oxidised substrate used (typically four times as much sodium dithionite as substrate). Oxidised substrate (i.e. 0.25g of duroquinone or 10mg of quinone) was dissolved in 50ml diethyl ether, resulting in a transparent yellow-orange solution. The substrate solution and one aliquot of sodium dithionite were mixed vigorously in a glass separating funnel for 3 minutes in order to allow the dithionite to begin reducing the substrate. After mixing, the solution was allowed to separate into the aqueous phase (containing the water and spent dithionite) and ether phase (containing the partially reduced substrate) and the aqueous phase was carefully discarded to avoid excessive loss of the ether phase. A second sodium dithionite aliquot was added to the ether phase remaining in the separating funnel; this was mixed for 3 minutes, allowed to separate into the aqueous and ether phases, before the aqueous phase was discarded. This was repeated once more using the remaining aliquot of sodium dithionite.

Following the final discarding of the aqueous phase, the funnel and substrate were washed twice using 100ml of saturated sodium chloride (to remove any excess water from the ether phase) and again the aqueous phase was discarded. The ether phase was then removed from the separating funnel, and passed through a second funnel lined with filter paper containing 30g of anhydrous sodium sulphate powder (to remove any traces of water) and collected in a glass beaker. Either a conical funnel or a Büchner funnel and vacuum pump can be used.

A microlance needle was used to make a single hole in the caps of several eppendorf tubes. The filtered ether phase was then transferred to the eppendorf tubes in 1ml aliquots. The tubes were then placed in a heated gyratory evaporator (Savant Speedvac SC110) on low heat (approximately 30^{o}C) until the ether phase had been evaporated, leaving behind a small white residue in each tube (reduced substrate). Each individual tube

was then sealed using Parafilm M (Alcan) and placed in a light-tight dessicator at room temperature until required.

In order to prepare the reduced substrate for spectrophotometric activity assays, the substrate were resuspended gently in 1ml of acidified ethanol (10mM hydrochloric acid), and the concentration was determined spectrophotometrically using the extinction coefficient of the substrate in ethanol at a specific wavelength (see Table 2.6b).

The resuspended reduced substrate was then stored at -80^{o}C after use. The resuspended substrate remained stable for a maximum of 3 months when stored at -80^{o}C. The substrate concentration was verified before each subsequent use by measuring the absorbance of the substrate at the substrate-specific wavelength (as detailed in Table 2.6b) and dividing this value by the extinction coefficient (also detailed in Table 2.6b) and the pathlength of the cuvette (which was always 1cm).

2.6 Crystallography

Purified recombinant protein was used for crystallographic screening. Prior to screening, a pre-crystallisation test (PCT) was carried out to establish whether the protein sample was within the optimal concentration and purity range. The PCT kit used for all tests was supplied by Molecular Dimensions. After carrying out the PCT and adjusting the protein concentration if necessary, screens were set up as follows.

2.6.1 Initial screening – hanging drop method

Initial screening was carried out in the laboratory of Dr. Darren Thompson, University of Sussex. Protein and screen solutions were kept at 4^{o}C throughout the process of setting up the screen. The hanging drop method was used in the initial screening process, with 24-well plates (Molecular Dimensions) and plastic coverslips (Molecular Dimensions). Each well was lightly hand-greased using silicon grease (DuPont). Following greasing, 600-1000µl of screen solution was added to the bottom of each well. See Table 2.6.1 for kits used. 1µl of screen solution was taken from each well, and tip-mixed with 1µl of protein sample on a coverslip. The coverslip was then inverted and placed on top of the relevant well immediately, forming an air-tight seal with the grease. Once filled, the plate(s) were stored at 4^{o}C or room temperature and viewed under a standard light

microscope every 3-4 days for 30-60 days after the screen was set up. Formation of precipitation, microcrystals and larger crystals were recorded and photographed.

2.6.1.1 Seeding and refinement

After conditions producing microcrystals were identified using the initial screening kits, further refinement was carried out along with seeding trials. The conditions (detailed in the product information) were adapted by adjusting pH, precipitant concentration, and salt molarity. Stock solutions of all the components were made, and mixed to create a non-

Kit (manufacturer)	Description
MemStart (Molecular Dimensions), 48 conditions	Sparse-matrix kit developed for membrane proteins
MemSys (Molecular Dimensions) 48 conditions	Developed from the most successful conditions from MemStart
MemGold (Molecular Dimensions) 48 conditions	Non-sparse matrix based on the most successful conditions from MemStart and MemSys
Protein Screen I (Molecular Dimensions) 50 conditions	Sparse-matrix, general protein crystallography screen
Protein Screen II (Molecular Dimensions) 48 conditions	Sparse-matrix, general protein crystallography screen

Table 2.7 – Crystallographic screening kits used.

-sparse matrix. Depending on the complexity of the conditions required, either 24 or 96-well plates were used. Screens were then set up in duplicate as previously described (hanging drop method), or using the sitting drop method (described below in Section 2.6.3). In both cases, the crystals from the relevant successful screen were crushed and mixed using a fine gauge acupuncture needle and then streaked through a drop of protein-solution mix in order to initiate seeding. Plates were then sealed and one plate was incubated at 4 ^{o}C and the other at room temperature. The plates were monitored every 3-4 days for 30-60 days after being set up.

2.6.2 Sitting drop method

In addition to the hanging drop method, the sitting drop method was utilised when working in the laboratories of Professor So Iwata (Membrane Protein Laboratory – Imperial College, London and Diamond Synchrotron facility, Didcot) and Professor Kita (Graduate School of Medicine, University of Tokyo).

The protein sample and screen conditions were kept at 4°C whilst being prepared. In contrast to the hanging drop method, 96-well sitting drop plates (Fisher) were used. Due to the reduced well size, 100µl of screen solution was placed into each well. 0.5µl of screen solution was then placed into the small vapour shelf at the top of the well. To this, 0.5µl of protein sample was added, and mixed gently using the pipette tip. To seal the plate, shireseal was applied. Once sealed, the plates were again incubated at either room temperature or 4°C and monitored every 3-4 days for 30-60 days after being set up.

During screening trials at the Diamond Synchrotron facility, a Cartesian robot was used to aid the setting up of several 96-well sitting drop plates (Innovadyne). In this case the well volume used was 80µl, but the sitting drop volumes were 100nl of protein mixed with 100nl of screen solution. The process was automated.

2.7 Circular Dichroism

Circular dichroism (CD) was used to assess the secondary structure of recombinant alternative oxidase. CD experiments were carried out using a Jasco J715 spectrophotometer, connected to Jasco Spectra Manager software suite and fitted with a Jasco Peltier-type temperature regulation system in the laboratory of Dr. Ewan Main (University of Sussex).

2.7.1 Sample preparation using polyethylene glycol (PEG) precipitation

Protein samples for CD experiments were prepared by first precipitating the sample using PEG. A stock solution of 50% (*w/v*) PEG-6000 (Sigma) was added dropwise to the protein sample, and gently mixed after each addition until the solution became opaque. The sample was then centrifuged at 13,000 x g for 30 minutes at 4°C. The supernatant was removed and retained. The pellet was allowed to air dry for 10-30 minutes at room temperature, before storage at -80°C until required. In order to test the efficacy of the

precipitation, the supernatant was assayed using the techniques described above in Section 2.5.2; if there was significant activity measured, the precipitation was repeated by recombining the supernatant and the pellet, and then the dropwise addition of 50% PEG 6000 (Sigma). The solution was then centrifuged at 13,000 x *g* for 30 minutes at 4ºC. The supernatant was retained and re-assayed. This process was repeated until no activity was observed in the supernatant.

2.7.2 Monitoring secondary structure – multiple wavelength scan

Dried and frozen pellets (as described above) were thawed on ice, and resuspended to an appropriate volume with the relevant buffer. Typically, using a 1mm cuvette, 250µl of dH_2O containing 0.04% DDM was used to resuspend a single pellet. The buffer alone was then added to the cuvette, and a baseline reading (scanning from 300-180nm) was taken to ensure no excessive absorption was observed in this range. The same settings for scanning were applied to the baseline as to the experimental scans, described below.

The resuspended pellet was then transferred to a clean cuvette (Hellma, Suprasil, 1mm), and absorbance across wavelengths of 300-180nm was recorded with a wavelength pitch of 0.1nm. Scans were performed in triplicate and an average taken. Data was then imported into a Gnumeric spreadsheet for further analysis.

2.7.3 Temperature melt CD

Initial multiple wavelength scanning CD indicated that the alternative oxidase was mainly alpha helical in structure. In order to assess how stable the α-helices were, temperature melt experiments were performed. As detailed in Section 2.7.2, PEG precipitated protein was resuspended in the relevant buffer, and placed into a clean cuvette. Absorbance was measured at 222nm and temperature increments of 1ºC from 10-90ºC or decrements of 1ºC between 90-10ºC. Data was exported as a Gnumeric spreadsheet for further analysis.

2.8 *In silico* modelling of the alternative oxidase

A variety of *in silico* analyses were performed and these are described in detail in Chapter 3. Below in Table 2.8 the algorithms used are listed, along with the function of the

algorithm or program. The algorithms were either accessible via a web interface, or downloaded and run from either a Windows or Linux (Ubuntu) machine. Image manipulation throughout the project was performed with the GNU Image Manipulation Program (GIMP; http://www.gimp.org/) and LibreOffice Draw.

Software	Function
AutoDock	Protein/molecule docking software
BioSerf	Automated *ab initio* homology modelling
CFSSP	Chou and Fasman (1974) secondary structure prediction algorithm
ClustalW	Multiple sequence alignment
DeepView	Molecular visualisation software
Dichroweb	Analysis of circular dichroism data
GOR	Garnier-Osguthorpe-Robinson (1978) secondary structure prediction algorithm
Hex	Protein/molecule docking software
HHPred	Protein homology detection and structure prediction
JPred3	Protein secondary structure prediction
NJPlot	Phylogenetic tree drawing software
PHYLIP	Phylogenetic tree drawing software
Phyre2	Protein threading server
PROFphd	Protein tertiary structure prediction
PROSITE	Curated database of protein domains, families and functional sites
PSIPRED 3.0	Protein tertiary structure prediction
PyMOL	Molecular visualisation software
RaptorX	Protein threading server
SeaView	Multiple alignment viewer and editor
SwissModel	Homology modelling server
Treeview	Phylogenetic tree viewing software
VMD	Visual Molecular Dynamics; a Molecular visualisation software

Table 2.8 - Software used during the *in silico* analysis of the *S. guttatum* alternative oxidase. For references, see Chapter 3.

The numbering of residues referred to in this thesis is taken from the *S. guttatum* alternative oxidase protein (UniProt accession number P22185) unless otherwise stated. The other main sequence used in the *in silico* modelling of the alternative oxidase was the Trypanosomal alternative oxidase (TAO; UniProt accession number Q26710, from *Trypanosoma brucei brucei*). Lists of all sequences used can be found in Appendix 1. The accession numbers of any crystal structures used (accessed via the Protein Data Bank,

PDB) are listed in the body of the text. At the time of submission, the crystal structure of the TAO had been recently submitted to the PDB (PDB code 3VV9, Shiba *et al*., 2013). However, the structures themselves were not accessed via the PDB, but came directly from the research laboratory or Professor Kita at the University of Tokyo some time before publication.

Chapter 3

Modelling the alternative oxidase

3.1 The value of bioinformatics

In the absence of structural data, *in silico* analysis of protein sequence may be performed. With careful selection of algorithms and informed interpretation of their output, meaningful and empirically evaluated predictions are possible – from the inference of evolutionary relationships (McDonald and Vanlerberghe, 2006), to predicted secondary structure (Moore and Siedow, 1991) and models generated where homologous protein structure exists (Andersson and Nordlund, 1999). Models of either structure or sequence relationship may then be used to generate hypotheses about the structure-function relationship of a protein, the family to which it belongs, and the evolutionary relationship it may share with other protein families (Gomes *et al*., 2001; Berthold and Stenmark, 2003).

The scope of this Chapter is to revisit previous *in silico* alternative oxidase analysis, and reassess alignments, phylogeny and models in light of new sequence and structure data. For the first time, molecular docking has been attempted, with positive results.

3.1.1 Sequence analysis

The first AOX sequence to be published was that of *S. guttatum* in 1991 (Rhoads and McIntosh, 1991). A filtered[2] Basic Local Alignment Search Tool (BLAST, Altschul *et al*., 1990) search of the UniProt Knowledgebase (http://www.uniprot.org; Uniprot Consortim, 2012) using the *S. guttatum* sequence (UniProt accession number P22185) reveals 607 sequences with similarities ranging from 90% down to 25%. Of the 607 sequences, only 33 have been reviewed and annotated manually. 89% of the 607 sequences are eukaryotic in origin, and the remaining 11% are found in prokaryotic genomes.

[2] An E value cut-off of 1 was applied

Previous sequence analysis of alternative oxidase sequences (Moore *et al*., 1995a) led to the identification of highly conserved residues across both plant and fungal species and earlier (Moore and Siedow, 1991) use of the Garnier-Osguthorpe-Robson (GOR; Garnier et *al.*, 1978) algorithm predicted a primarily helical protein (51%) with 10% β-sheet, 16% β-turn and the remaining 23% attributed to random coil. However, bioinformatic analysis of the alternative oxidase sequences alone did not provide information beyond predicted secondary structure elements, such as metal binding motifs – information which was incredibly important, as the cofactor required for alternative oxidase activity was not known at the time (Moore and Siedow, 1991). Only after the inclusion of sequences from another family of proteins, the diiron carboxylates, did multiple local alignment analysis reveal the presence of several iron binding motifs universally conserved within the alternative oxidase sequences (*cf* Siedow *et al*., 1995; Moore *et al*., 1995a; Andersson and Nordlund, 1999) and ultimately the classification of the alternative oxidase as a non-haem, diiron protein (Siedow *et al*., 1995; Moore *et al*., 1995a; Berthold *et al*., 2002).

3.1.2 Phylogeny

Structure-specific phylogenetic analysis of the alternative oxidase with respect to the diiron carboxylates suggested that the alternative oxidase and the diiron carboxylate family have a common ancestor, most likely a primitive oxygen reductase (Gomes *et al*., 2001). Further phylogenetic analyses were conducted without the inclusion of diiron carboxylate sequences; instead, sequences from plastid terminal oxidases (PTOX) were used in the analysis. PTOX proteins, a family of terminal oxidases expressed in plastid organelles such as chloroplasts, are thought to play an essential role in the desaturation of carotenoids (Carol *et al*., 1999; Josse *et al*., 2000; Carol and Kuntz, 2001). Furthermore, when expressed in *E.coli* membranes, PTOX confers the same cyanide-resistant respiration observed in tissues expressing alternative oxidase which is inhibited by addition of the AOX-inhibitor octyl-gallate (Josse *et al*., 2000). Sequence similarity between the AOX and

PTOX families is very low (25%; Josse *et al*., 2000) despite some similarities in function (as terminal oxidases) and catalytic mechanisms (quinol:oxygen oxidoreductases). However, the iron-binding motifs identified in both the diiron carboxylates and the alternative oxidase are retained in PTOX, suggesting similarity in structure (Carol *et al*., 1999).

Several analyses suggest that AOX and PTOX have a common ancestor of bacterial origin, but that they entered into eukaryotic taxa through different routes shortly after divergence. The alternative oxidase entered into the eukaryotic lineage through the endosymbiotic relationship between proteobacteria, which resulted in the creation of the mitochondria; conversely, the PTOX entered into the plant lineage through the endosymbiotic relationship between cyanobacteria, resulting in the creation of organelles like the chloroplast (Finnegan *et al*., 2003; McDonald and Vanlerberghe, 2006). Phylogenetic analysis of AOX sequences from protozoa, including apicomplexan parasites such as *T. brucei* and *C. parvum* suggests that the parasitic alternative oxidases are descended from the eukaryotic mitochondrial alternative oxidases (Roberts *et al*., 2004; Williams *et al*., 2010).

A particularly popular and adaptable program for generating both multiple alignments and phylogenetic trees is ClustalX (Thompson *et al*., 1994), which allows the user to stipulate which scoring matrices to use for alignments and tree-building. This is particularly useful when analysing distantly related sequences, where certain matrices (such as BLOSUM50 and BLOSUM40) are specifically designed to accurately align more distantly related sequences (Henikoff and Henikoff, 1993).

3.1.3 Previous models of the alternative oxidase

There have been two previous attempts to model the alternative oxidase. In 1995 Moore *et al*. proposed a model in which the active site was located at the centre of four small helices, with two transmembrane helices anchoring the molecule to the membrane (Figure 1.5a). The second model, generated by Andersson and Nordlund (1999) and later

refined by Berthold *et al*. (2002), proposed instead a four helix bundle acting as a scaffold to the active site; by contrast the attachment to the membrane was not via transmembrane helices but by a shorter helix laying parallel to the lipid layer rather than perpendicular to it (Figure 1.5b). The second model is accepted as the most accurate to date. The two models were derived using different methods. In the former, information from hydrophobicity plots, sequence alignment and identification of known iron-binding motifs were combined in a knowledge-based approach to model the AOX without a template. In the latter, homology modelling was used instead, with model evaluation based on existing knowledge of the protein. In between the publication of the first model and the conception of the second, more sequences were made available of both alternative oxidase proteins and diiron carboxylates, on which the second model was based.

3.1.4 *In silico* approaches to modelling proteins with unknown structure

When attempting to predict or model the structure of a protein of novel or unknown structure, there are several approaches that can be taken. Ideally, as many as possible should be pursued and the results compared in order to select the most accurate model based on both statistical analysis and whether the model compares favourably to existing experimental data. Of particular relevance to this project are knowledge-based approaches (such as secondary structure prediction), homology modelling and threading.

3.1.4.1 Prediction of secondary structure

Prediction of secondary structure from sequence data was first explored in the 1960s. For example, Guzzo (1965) noted the recurrence of certain amino acid residues (namely proline, gluatmic acid, aspartic acid and histidine) within structurally-characterised helical regions of myoglobin and alpha- and beta-haemoglobin. It was suggested that the occurrence of these residues in sequence data may be useful in predicting the nature of local secondary structure from a protein sequence (such as where the helices begin and end, for example). A notable early example which both expanded upon and improved Guzzo's

work, whilst taking into account critical analysis from Prothero (1966), was the prediction of alpha-helical regions within proteins (*cf* Kotelchuck and Scheraga, 1969). Additionally, the prediction method incorporated early theoretical work from Zimm and Bragg (1959) regarding the physical transition that polypeptides undergo when shifting from random coil structures to alpha-helical structures and the implication of this theory to the formation of secondary structure. The linking of the Zimm-Bragg coil-helix transition theory to specific amino acids involved in structure determination was a very important step towards the modern structure prediction algorithms in use today.

Early secondary structure algorithms created by Chou and Fasman (1974) and Garnier *et al*. (1978) utilised the quantified propensity for each amino acid to be involved in any given secondary structure element, although the calculation was implemented differently in both algorithms. As the number of structures in databases have increased, along with computing power, prediction algorithms have evolved and improved. Some more recent approaches to the prediction of secondary structure such as PSI-PRED (Jones, 1999; Buchan *et al*., 2010) and PHD (Rost and Sander, 1993) utilise feed-forward artificial neural networks to refine results and improve accuracy. Others, such as the PredictProtein (Rost *et al*., 2004) and Jpred3 (Cuff *et al*., 1998; Cole *et al*., 2008) servers apply multiple algorithms to the sequence of interest, after aggregating information from structural and sequence databases based on sequence similarity. Reported accuracy of modern algorithms varies (see Section 3.1.4.4 below); for novel proteins and those which are underrepresented in the database however, accuracy may be lower than expected compared to proteins where many homologous sequences and structures are known and defined.

3.1.4.2 Homology modelling

Building a three-dimensional model of a protein of unknown structure is beyond the scope of secondary structure prediction algorithms. In order to generate a coordinate map for the atoms in a protein, protein structures with sequences of acceptable similarity can be used as templates in the process of homology modelling. This concept is based on the

recognition that whilst protein sequences from a common ancestor mutate and evolve differently, structure often remains conserved (Chothia and Lesk, 1986; Martí-Renom *et al*., 2000). A comprehensive comparison of how much sequence similarity is required to guarantee identical structures in any two given sequences (Sander and Schneider, 1991) revealed that the similarity threshold was length-dependent, with longer sequences requiring less similarity than shorter sequences. The resulting Sander-Schneider threshold states that at least 25% identically aligned residues must exist across sequences 80+ residues in length in order to confidently state that the fold (tertiary structure) will be the same.

Therefore, the first stage of homology modelling is the selection of a suitable template sequence with greater than 25% similarity to the target sequence of unknown structure. This can be undertaken by the user through manually-evaluated multiple sequence alignments performed with programs such as ClustalX (Jeanmougin *et al*., 1998) using sequences identified after execution of a BLAST search (or similar) and retrieved from databases such as UniProt or GenBank (http://www.ncbi.nlm.nih.gov/genbank/). Ideally, the sequence with the lowest E value and highest similarity should be chosen, although modelling one protein on several similar proteins provides the user with the opportunity to select the most accurate model. Alternatively, a template can be chosen using web-based interfaces such as SwissModel (http://swissmodel.expasy.org/; Schwede *et al*., 2003) and HOMA (http://www-nmr.cabm.rutgers.edu/HOMA/; Srinivasan *et al*., 1993), which perform the multiple alignment and sequence-retrieval automatically with minimal user input.

After suitable template sequences have been chosen, models can be built. During this process, the atoms of the residues in the target sequence are overlaid, segment by segment, onto the atoms of the template structures, to create a set of Cartesian coordinates for the target sequence. Areas with particularly low similarity to the template or few structural templates, such as loop regions, require careful consideration when modelling. Programs such as MODELLER (Sali and Blundell, 1993), for example, use libraries of

known loop sequences and structures to select the most appropriate loop structure, taking account of the spatial constraints of both the surrounding structure and the loops themselves.

Following its generation, the model must be evaluated. In order to evaluate a model, the energy required for the protein to exist in that particular conformation must be calculated and compared to other possible conformations. Model accuracy may be determined statistically; for example the ProSA algorithm (accessible via a web server, ProSA-web: https://prosa.services.came.sbg.ac.at/prosa.php; Wiederstein and Sippl, 2007) provides a measure of structure or model quality given its atomic coordinates, in the form of a standard deviation-derived z-score. In order to generate a z-score, the algorithm calculates an approximation of the potential mean force (PMF) for a protein given the distance between all pairs of C_α atoms (Sippl, 1990). The z-score in this case essentially represents the deviation of the energy distribution for the uploaded protein from the theoretical energy distribution of the same protein were it in a random conformation (Sippl, 1993). The z-score for the uploaded protein can then be compared to z-scores calculated for all current protein structures in the PDB (Wiederstein and Sippl, 2007), thus allowing the user to assess whether the z-score of the uploaded protein is within an acceptable range of z-scores for other proteins of known structure and similar size.

3.1.4.3 Threading

Protein threading is an alternative approach to homology modelling in instances where less than 25% sequence similarity exists between the target and template sequence. Based on fold-recognition, threading algorithms initially construct multiple alignments, comparing the sequence of unknown structure to those in the databases with known structure. The sequence of unknown structure is then threaded onto existing structures, residue by residue, often with iterative refinement. The added advantage of threading over homology modelling is that multiple structures are compared, as opposed to single templates chosen by the user in homology modelling. Examples of popular threading

algorithms include Phyre2 (Kelley and Sternberg, 2009), RaptorX (Peng and Xu, 2011; Källberg *et al*., 2012) and HHPred (Söding, 2005; Söding *et al*., 2005), all of which are available freely via online servers (see Section 3.2.4 below for URLs). The resulting model may be evaluated using the same software as for homology models, such as ProSA-web.

3.1.4.4 Limitations and evaluation of structure prediction and protein modelling

Whilst predicting secondary and tertiary structure is a useful tool when investigating a protein of unknown structure, the techniques used are not without limitations (Wallner and Elofsson, 2005; Ginalski, 2006). The number of sequences available in databases has increased significantly in the last decade due to improvements in DNA and protein sequencing, but some classes of protein remain under-represented. As such, training sets for automated multi-template secondary structure predictions (PHD and PSI-PRED, for example) are likely to biased towards classes of proteins which are well-represented in the databases. Similarly, with homology and threading modelling techniques, novel proteins with no close relatives are unlikely to be modelled accurately. This limitation is particularly relevant to proteins such as the alternative oxidase, where only the structures of distant relatives are available. The only solved structure in the alternative oxidase family is that of TAO (PDB code 3VV9, Shiba *et al*., 2013). In order to encourage improvements in prediction and modelling reliability and accuracy, projects such as the Critical Assessment of Techniques for Protein Structure Prediction (CASP, http://predictioncenter.org/; Moult *et al*., 1995) allow for the overall performance of different approaches to be established. This information is particularly useful for those carrying out structure prediction and modelling, as it highlights the limitations of the techniques and allows for objective appraisal of predicted structures and generated models.

3.1.5 Docking

Molecular docking is the process by which the likelihood of a receptor (R, i.e. protein) and ligand (L, i.e. substrate) forming an energetically stable – and therefore

favourable – interaction is determined. In addition to calculating the probability of a ligand-receptor interaction, cautious interpretation of the results of a docking algorithm may suggest the strength of the interaction. The extent to which the ligand and receptors change conformation in order to achieve the overall best fit is known as the 'induced fit' model. While molecular docking is particularly useful in the field of rational drug discovery, in this project it is a useful tool to assess predicted substrate-binding sites.

There are two main methods by which calculations pertaining to receptor-ligand interactions may be performed; shape complementarity or by simulation of the docking process. In the former, the proposed binding surface of the receptor is given informational descriptors based on the solvent-accessible surface area (ASA). The ASA is given in Angstroms squared ($Å^2$) and derived using information and algorithms first developed in the 1960s and 1970s (*cf* Bondi, 1964; Lee and Richards, 1971; Shrake and Rupley, 1973) which used experimentally obtained crystallographic data to determine the van der Waals radii and therefore surface area of residues and atoms within proteins. Following calculation of ASA, the ligand is given descriptors based on its similarity to the receptor molecule when both molecules are rigid (Shoichet *et al*., 1991; Shoichet and Kuntz, 1991; Helmer-Citterich and Tramontano, 1994). This approach requires assumptions to be made about the molecules; namely that they are in a fixed and rigid state, and that the van der Waals radii/surfaces are accurate from predictions. Therefore, whilst the output from these docking predictions can be obtained with relative speed, they may not accurately reflect the changes in conformation that take place during the process of ligand-receptor interaction, as both molecules adopt minimal-energy conformations to allow an energetically favourable interaction that will not immediately decay.

The second approach is that of simulating the interaction process, starting with the ligand and receptor separated by a physical distance. A finite number of changes are then made to the conformation and physical proximity of the ligand and the receptor; after each such change (or move), the energy in the system (i.e. between the two molecules) is calculated. When the combination with the tightest fit and lowest energy is observed, then

the state of induced fit has been achieved. As a result, this process is far more time consuming, since a very large energy landscape consisting of many possible conformations needs to be calculated and matched. There are many thousands of degrees of freedom generated when both receptor and ligand are flexible, which requires far more computing power to solve than docking simulations where both molecules are rigid. Many docking programs are available as web-based interfaces, such as Hex (http://hexserver.loria.fr/; Macindoe *et al*., 2010) and GRAMM-X (http://vakser.bioinformatics.ku.edu/resources/gramm/grammx; Tovchigrechko and Vakser, 2006) as well as plug-ins for molecular visualisation programs such as AutoDock (Morris *et al*., 2009) which can be used with PyMOL.

3.2 Methodology

3.2.1 Sequence analysis

All protein sequences were taken from the UniProtKB database. Suitable candidates for alignment of the alternative oxidase family were selected using a BLAST search based upon the *S. guttatum* alternative oxidase protein sequence (UniProt accession number P22185). FASTA protein Sequences were then retrieved via the UniProt server interface. Alignments were performed using ClustalX (Thompson *et al*., 1994) and evaluated manually. When aligning the diiron carboxylate sequences to the *S. guttatum* alternative oxidase, the alignment was performed manually. The alignment files (in *.aln format) were viewed and edited using either Clustal X or SeaView (Gouy *et al*., 2010).

3.2.2 Phylogeny

Alignments produced and refined using ClustalX were converted into bootstrapped phylogenetic tree files (in *.phb format), using the neighbour joining method. Trees were viewed in NJ Plot (Perrière and Gouy, 1996) and PHYLIP via the Mobyle server, http://www.mobyle.pasteur.fr/ (Felsenstein, 1989). In order to construct a reliable phylogenetic tree, sequences with sufficiently high sequence homology were indentified

using a BLAST search. In the interest of maintaining a balance between plants, fungi, parasites and prokaryotes a limit of 10 was placed on the number of sequences used from any given phyla.

3.2.3 Homology modelling

Homology modelling was carried out using the Swiss-MODEL modelling server (http://swissmodel.expasy.org/). All features were used, including automated mode and template identification. The *S. guttatum* amino acid sequence (P22185) was modified by the removal of residues 1-63, which are not present in the final expressed protein. Models based directly on Δ^9-desaturase (P22337; 1OQ4; chain A) and TAO (Q26710; 3VV9; Shiba *et al*., 2013) and structures were generated in alignment mode after manual alignment of sequences in SeaView.

3.2.4 Threading

Threading was carried out using the programs and servers listed below in Table 3.1, using a truncated *S. guttatum* sequence lacking residues 1-63 as described above. The user-defined parameters are stated where they differ from default parameters.

3.2.5 Model evaluation

Models were evaluated quantitatively using the ProSA-web server (Wiederstein and Sippl, 2007), from uploaded *.pdb files.

Program/server	User-defined parameters
Phyre2 (Kelley and Stenberg, 2009) www.sbg.bio.ic.ac.uk/phyre2/	Intensive mode
RaptorX (Peng and Xu, 2011; Källberg *et al*., 2012) http://raptorx.uchicago.edu/	Multi-template refinement
BioSerf, including GenThreader (Jones, 1999) and MODELLER (Sali and Blundell, 1993) http://bioinf.cs.ucl.ac.uk/bio_serf/public_job/	None available
HHPred (Söding, 2005; Söding *et al*., 2005) http://toolkit.tuebingen.mpg.de/hhpred	Current and "on hold" PDB libraries

Table 3.1 – Threading software used, with parameters changed from default.

3.2.6 Docking

Docking of a ubiquinone-1 molecule to the alternative oxidase homology model based on TAO was completed using the Hex server (Macindoe *et al*., 2010) and AutoDock as a PyMOL plugin (Morris *et al*., 2009). Few user-defined parameters were available via the Hex server, so all but the correlation type (which was changed to "shape and electrostatic") were left on their default settings. The AutoDock grid was adjusted to contain the whole monomeric protein.

3.2.7 Generating a dimeric AOX model containing a diiron active site

Using the same method as described in Section 3.2.3 above, a second homology model of *S. guttatum* AOX based on TAO was generated using the coordinates of the chain forming the second monomer (chain A) in the dimeric TAO crystal structure. The two homology models were then merged into a single PDB file. In a similar manner, the coordinates for the four iron ions (two per monomer) were taken from the TAO PDB file and merged with the dimer PDB file. To assess the validity of both the dimer PDB and iron-containing models, each model was aligned to the TAO crystal structure.

3.2.8 Building a membrane-AOX model

The dimeric homology model of *S. gutattum* based on the TAO template (as described above in Sections 3.2.3 and 3.2.7) was solvated using the solvate command in Visual Molecular Dynamics (VMD; Humphrey *et al*., 1996). Water molecules were removed above the Z plane where the membrane was to be placed. A membrane patch was built using the membrane modelling script in VMD and the dimer model was placed into the membrane according to the solvation limits generated previously to produce a membrane-AOX model. Finally, using the beta-field command in VMD, lipid molecules within 0.6Å of the protein were marked and removed from the model. The model was solvated once more and any water molecules which appeared between the membrane and the protein were removed.

3.2.9 Visualisation

All molecular visualisation was performed using DeepView (Version 4.1; Guex and Peitsch, 1997) and PyMOL (Version 1.4.1, Schrödinger, LLC).

3.3 Results

3.3.1 Sequence analysis

A multiple alignment was constructed using all 606 sequences identified during an automated BLAST search using the *S. guttatum* AOX sequence (excluding any E values above 1) against the UniProt database. A truncated version is shown overleaf in Figure 3.1.

3.3.2 Phylogeny

Phylogenetic trees were constructed from manually reviewed multiple alignments and assessed for accuracy based on the closeness with which species clades were formed. An example bootstrapped tree is shown below in Figure 3.2.

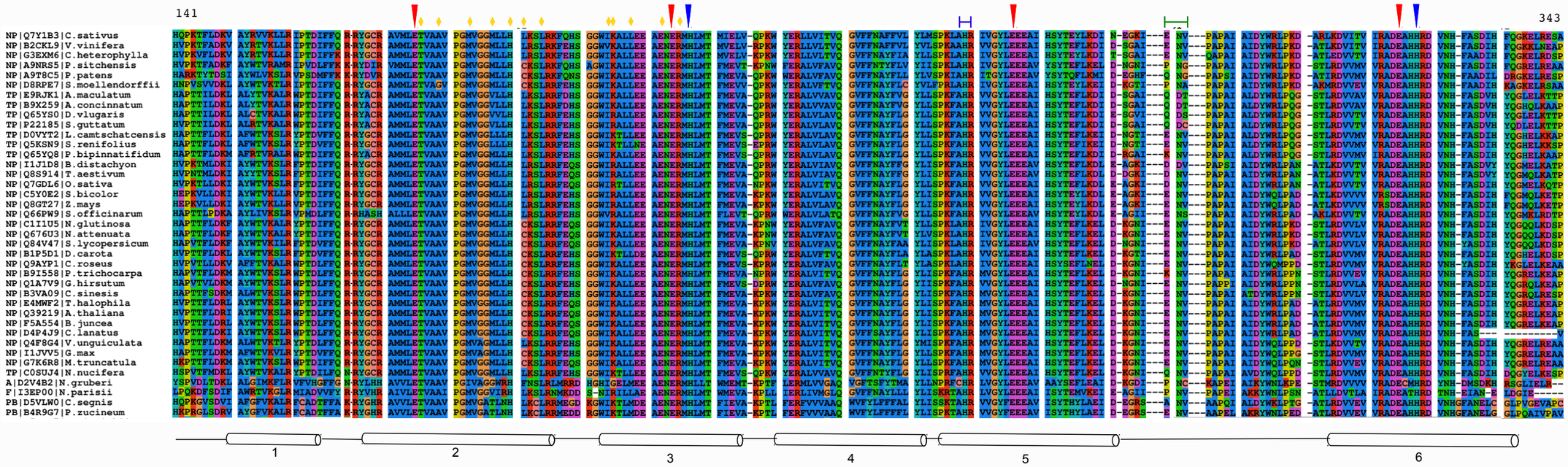

Figure 3.1 – A multiple sequence alignment of alternative oxidase sequences. This Figure shows a truncated multiple alignment of alternative oxidase sequences. UniProt Accession numbers are given along with species names (see Appendix 1 for a list of all sequences used). TP = thermogenic plant, NP = non-thermogenic plant, A = amoebae, F = fungi, PB = proteobacteria, Helices are indicated by numbered cylinders, based on the *S. guttatum* alternative oxidase homology model using TAO as a template. Red arrows indicate the four highly conserved iron-binding Glu residues (178, 217, 268 and 319) and blue arrows indicate the 2 highly conserved His residues (220 and 322) which form the secondary iron ligation sphere. The region highlighted by the blue bracket indicates the previously identified His-Arg pair involved in quinone-binding and the residues highlighted by the green bracket indicates the three-residue region thought to be responsible for determining pyruvate-sensitivitiy *(cf* Crichton *et al*., 2005; Ito *et al*., 2011). The yellow diamonds indicate the potential dimer interface residues as identified in Section 5.3.3 and listed in Table 5.8.

3.3.3 Homology modelling

Two homology models were successfully produced; one based directly on the Δ^9-desaturase structure (1OQ4) and one based on the recently-solved TAO crystal structure (Shiba *et al*., 2013). Both models are illustrated in Figures 3.3a and 3.3b respectively. PDB coordinate files for both models can be found on the compact disc in the back of this thesis in the "Homology Models" directory; the homology model of *S. guttatum* alternative oxidase using TAO as a template is named "HM1.pdb" and the homology model of *S. guttatum* alternative oxidase based on Δ^9-desaturase is named "HM2.pdb". For each model z-scores as determined by ProSA-web are shown below in Table 3.2, along with QMEAN4 scores generated by the Swiss-MODEL server. The z-scores for both models are within range of z-scores for other proteins of similar length and known structure (see Section 3.1.4.2). Two graphical representation of this agreement (as provided by the ProSA-web analysis output) can be found in Appendix 1 for reference.

An overlay of the homology model based on Δ^9-desaturase and the homology model based on TAO is shown below in Figure 3.4a, and both homology models and their respective templates are shown below in Figure 3.4b.

The distance between the 6 iron-binding residues (Glu178, 217, 268, 319 and His220, 322) was measured in both homology models and is shown below in Table 3.3 below.

Model template	z-score	QMEAN4 score
Δ^9-desaturase (chain A)	-1.41	0.14
TAO (chain B)	-3.93	0.25

Table 3.2 – Quantitative analysis of two *S. guttatum* homology models. This Table demonstrates the z-score (ProSA-web) and QMEAN4 score (Swiss-MODEL) for each homology model.

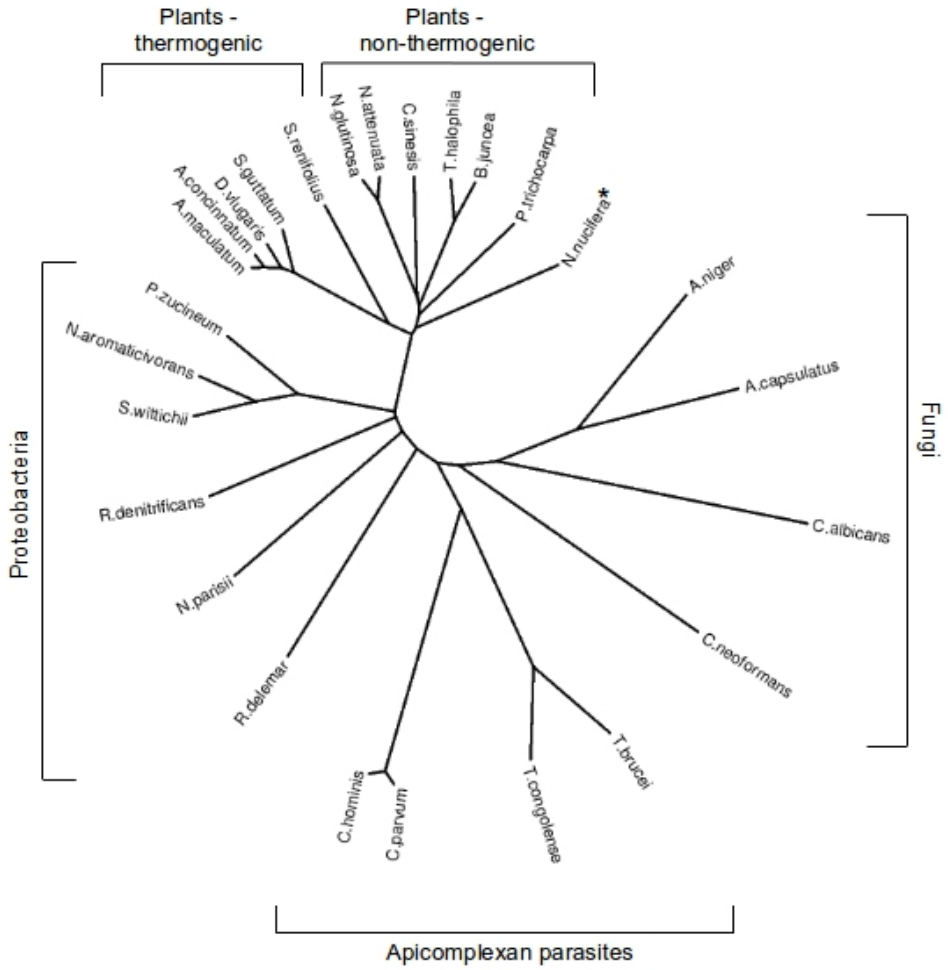

Figure 3.2 – Phylogenetic tree of several AOX sequences. This Figure shows a small bootstrapped, unrooted phylogenetic tree generated by ClastalX (neighbour joining method). Clades are indicated with square brackets, with the exception of *N.nucifera*, which is a thermogenic plant (marked with an asterisk).

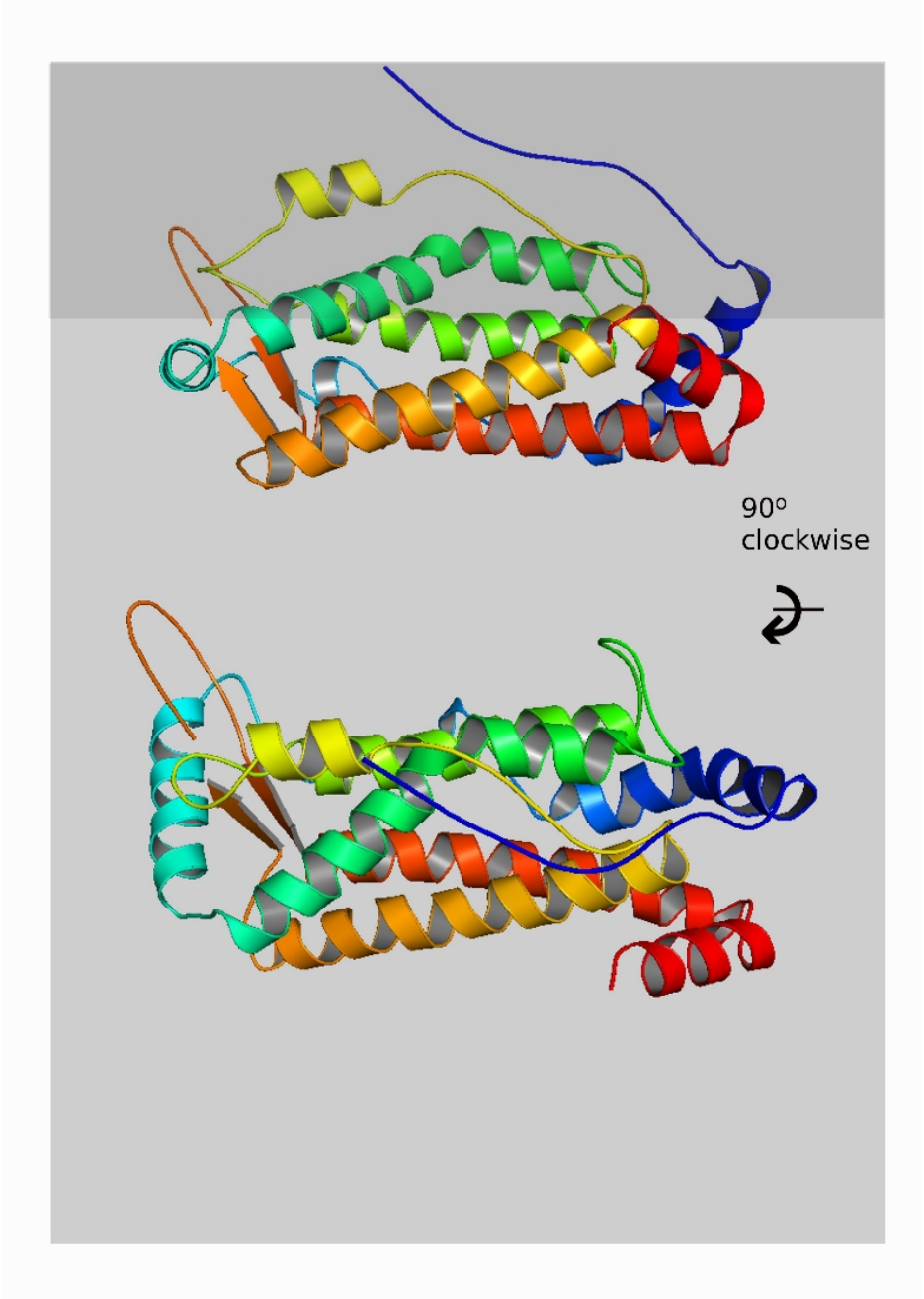

Figure 3.3a – Homology model of *S. guttatum* alternative oxidase using Δ^9-desaturase (1OQ4) as a template. Helices previously predicted to be membrane-associated (*cf* Andersson and Nordlund, 1999) are shown in the grey box in the top image.

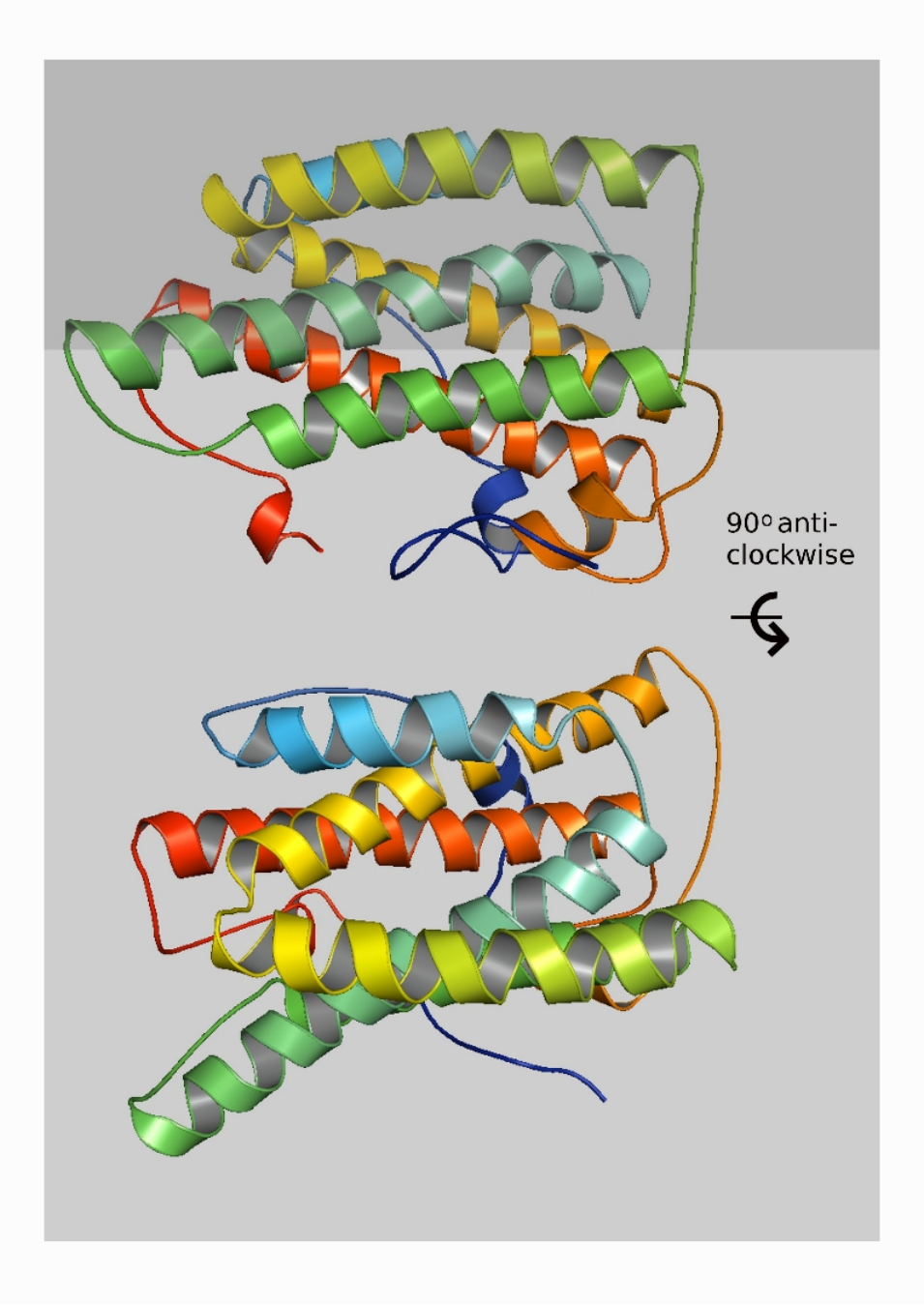

Figure 3.3b – Homology model of *S. guttatum* alternative oxidase using TAO as a template. Helices predicted to be membrane-associated are shown in the grey box in the top image.

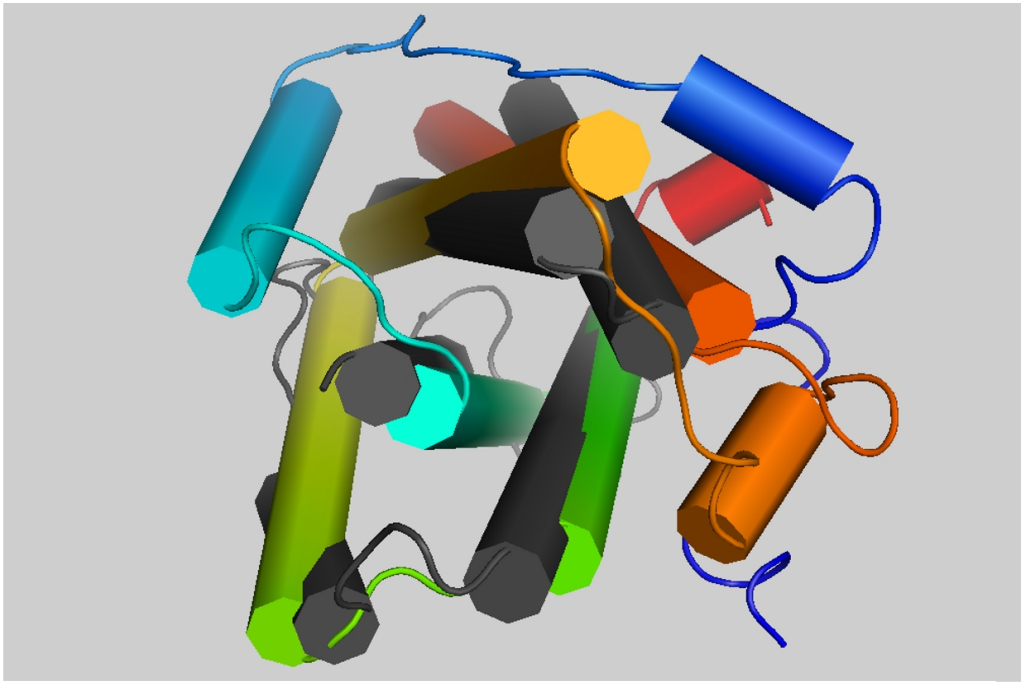

Figure 3.4a – An overlay of the homology models based on Δ^9-desaturase (grey) and TAO (rainbow).

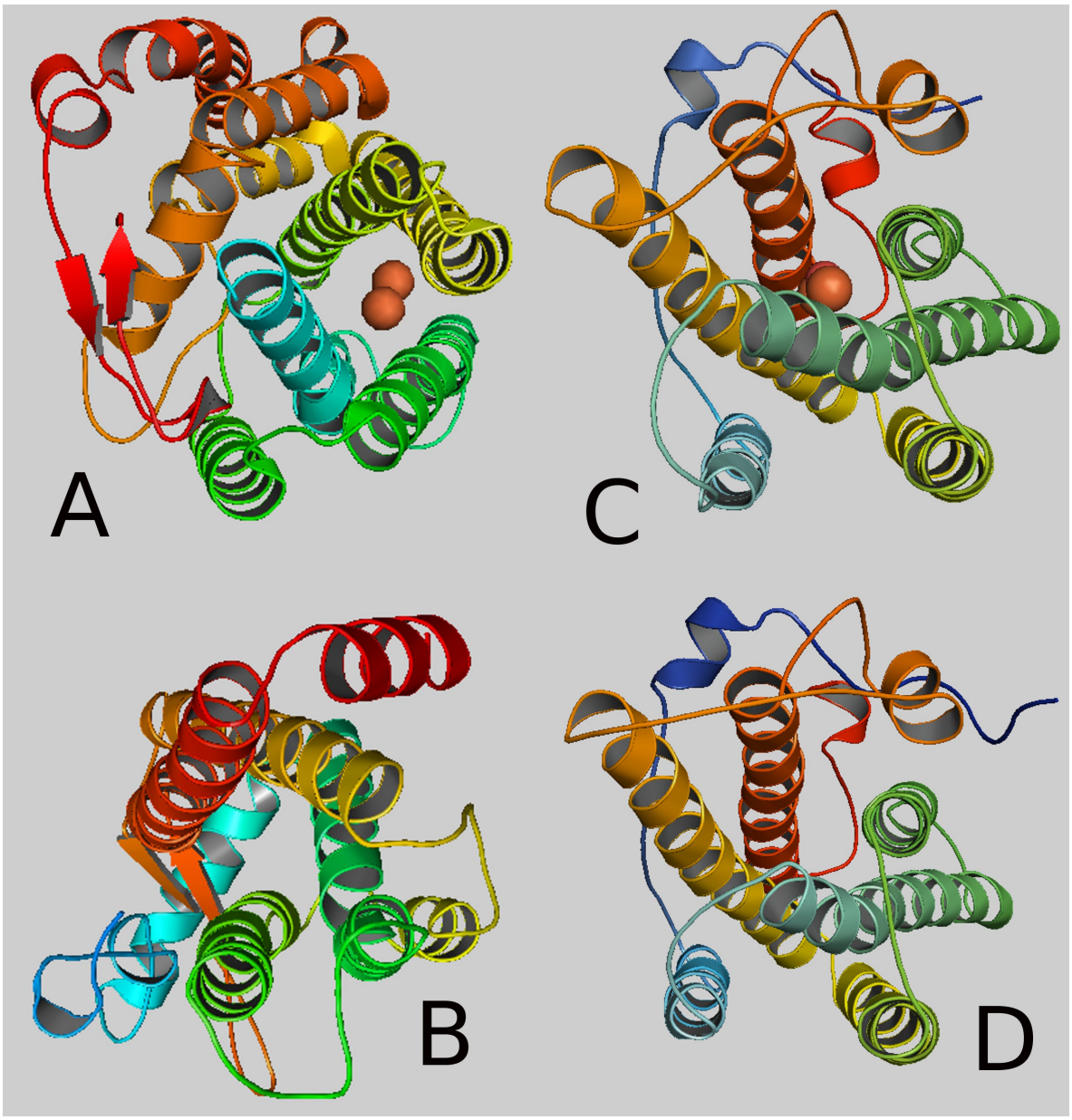

Figure 3.4b – A comparison of each template used to generate homology models of *S. guttatum* AOX and the homology model created. This Figure shows: A – Δ^9-desaturase (1OQ4 chain A); B – the *S. guttatum* homology model based on Δ^9-desaturase; C – TAO (chain B); and D – the *S. guttatum* homology model based on TAO. All orientations show the length-ways view through the four-helix bundle coordinating the diiron active site (red spheres in A and C).

Residue pairs	Distance in Å between residue pairs		
	Δ^9-desaturase-based	TAO-based	TAO structure
E178 → E217	3.4	2.7	3.6
E178 → H220	3.6	3.0	3.0
E178 → E268	8.0	6.7	7.3
E178 → E319	4.5	4.9	3.8
E178 → H322	7.8	7.7	8.1
E217 → H220	3.4	3.3	4.3
E217 → E268	3.8	4.0	3.7
E217 → E319	4.6	3.1	4.1
E217 → H322	5.8	4.8	3.1
H220 → E268	3.4	7.7	6.6
H220 → E319	4.6	4.0	2.6
H220 → H322	7.3	5.4	5.3
E268 → E319	5.6	3.4	3.4
E268 → H322	4.8	6.4	3.2
E319 → H322	4.8	5.7	5.1
Fe → Fe	-	3.1	3.1

Table 3.3 – A comparison of residue-to-residue distances in the two *S. guttatum* homology models and the TAO structure. This Table lists the distances between the 6 iron-binding residues (Glu178, 217, 268, 319 and His220, 322) and iron ions in both the Δ^9-desaturase-based and TAO-based homology models alongside the same distances observed in the TAO structure (PDB code 3VV9, Shiba *et al*., 2013).

3.3.3.1 Generation of a dimeric AOX model containing diiron centres

Alignment and overlay of the generated dimeric AOX model (containing one diiron centre per monomer, see Section 3.2.7) with the dimeric TAO template was absolute, with no deviations between the structures. The dimeric *S. guttatum* AOX model is shown below in Figure 3.5. A PyMOL session file can be found on the CD in the back of this thesis containing this generated structure ("Dimer.pse").

3.3.3.2 Generation of a membrane-AOX model

The dimeric membrane-AOX model is shown below in Table 3.6a. The protein lies approximately 14Å into a single leaflet of the membrane. Figure 3.6b shows the surface of the dimeric homology model with hydrophobic residues highlighted in red (left) and aromatic residues identified as possibly membrane-interacting are shown in green (right); these Figures were generated in an effort to define how deep into the membrane the protein should be placed. The aromatic residues shown in Figure 3.6b are listed in Table 3.4 and may be responsible for membrane-binding in *S. guttatum* alternative oxidase. PyMOL session files can be found on the CD in the back of this thesis containing the dimeric *S. guttatum* alternative oxidase protein in a membrane patch ("Membrane.pse").

Residue number
W160
F165
F166
W232
Y233
F259

Table 3.4 – A list of the aromatic residues predicted to interact with the membrane in *S. guttatum* AOX. The residues correspond to the model shown above in Figure 3.6b.

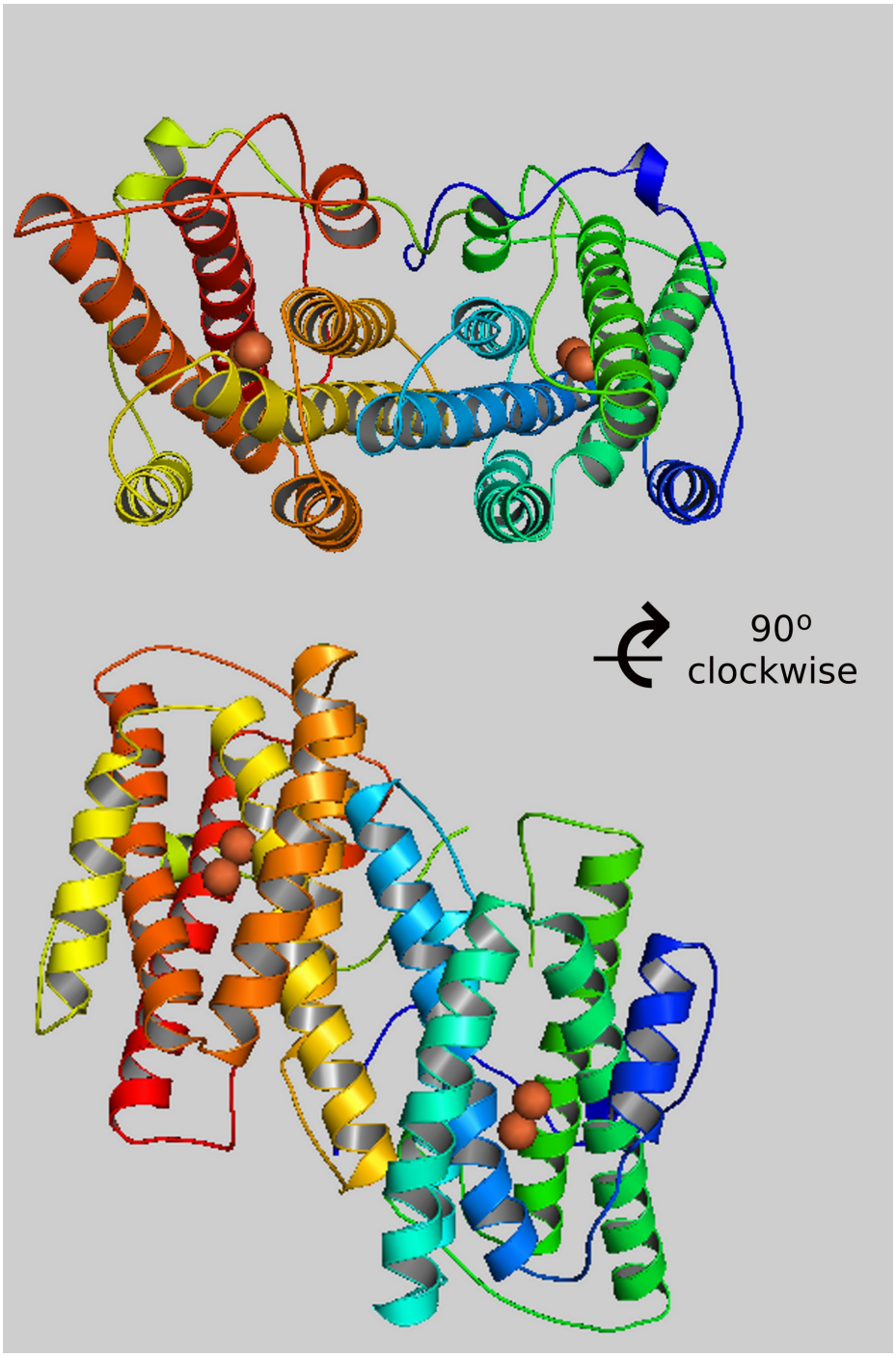

Figure 3.5 – A representation of the dimeric *S. guttatum* homology model. The iron ions of the diiron centres are shown in red.

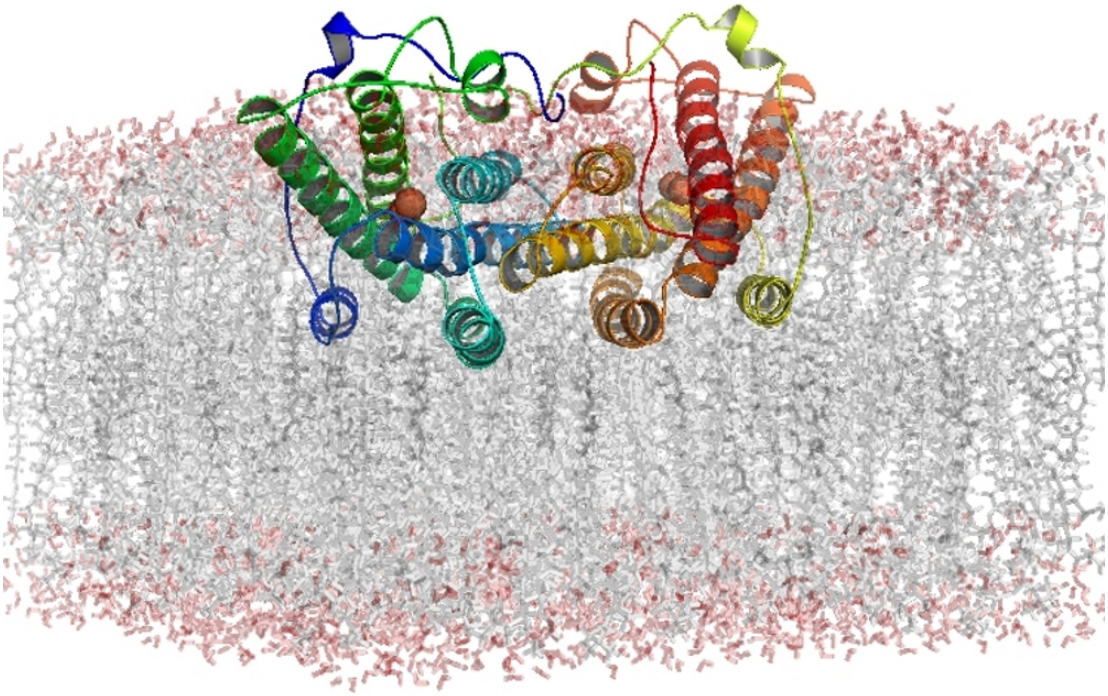

Table 3.6a – The dimeric *S. guttatum* homology model embedded in a membrane patch. Phsopholipids are shown here in grey with water molecules at the membrane surface shown in red. The iron ions of the active site are shown as red spheres.

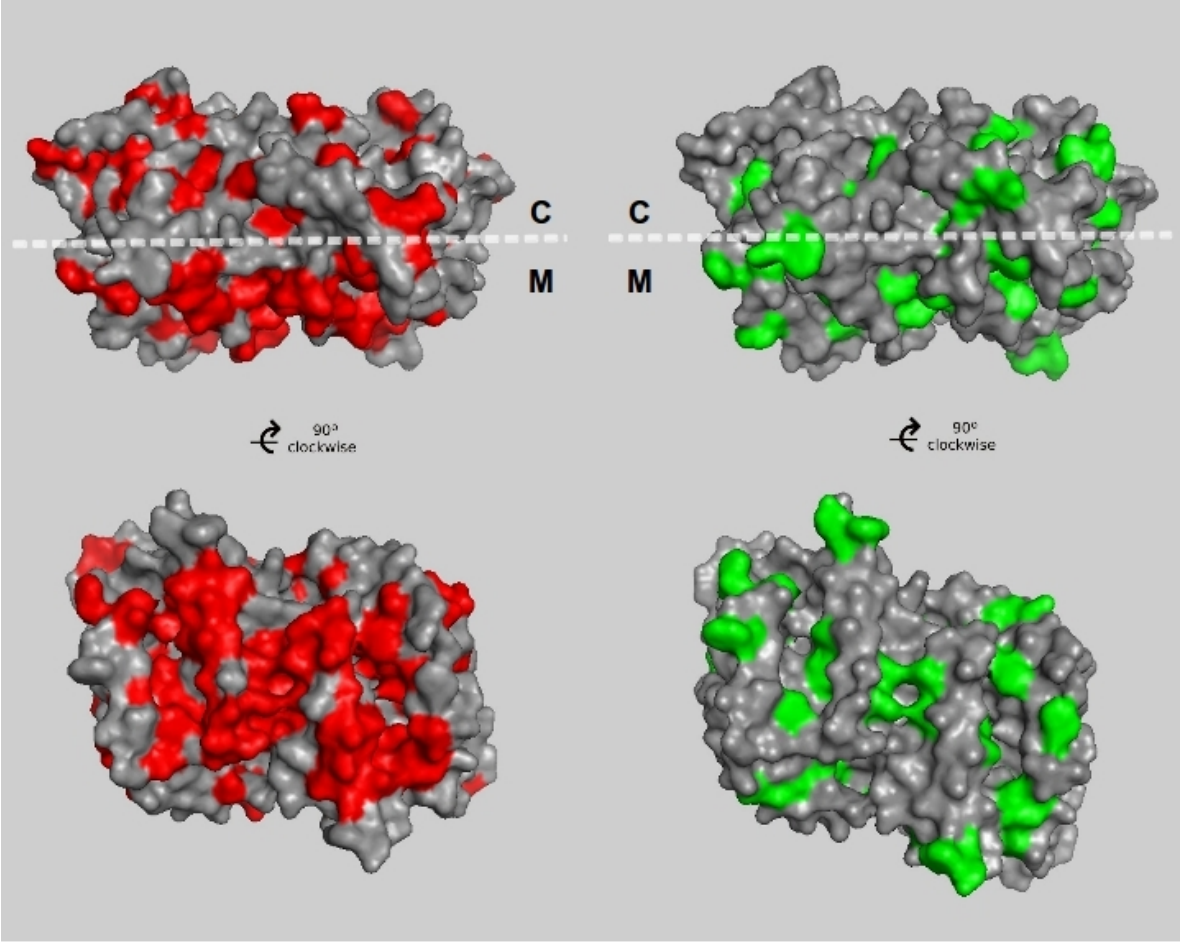

Figure 3.6b – A surface representation of the *S. guttatum* dimeric homology model. Hydrophobic residues are shown in red (left) and aromatic residues are shown in green (right). The dashed white line indicates the proposed placement of the protein in the membrane with C and M indicating the cytosol and membrane sides respectively. The bottom two images represent the portion of the protein embedded in the membrane as viewed from inside the membrane. The orientations of the models shown here are the same as those shown in Figure 3.5.

3.3.4 Threading

Results from each threading algorithm are shown below in Table 3.5.

Program/server	Templates identified
Phyre2	Identified 73 putative templates; two consensus models built
RaptorX	Identified 39 putative templates
BioSerf/GenThreader/MODELLER	Unable to identify suitable template
HHPred	Unable to identify suitable template

Table 3.5 – A list of models generated from each threading algorithm.

3.3.4.1 Threading – RaptorX and Phyre2

RaptorX identified 39 possible templates on which *S. guttatum* was then modelled. None of the models produced replicated the necessary physical proximity of the iron-binding residues (Glu178, 217, 268, 319 and His220, 322; approximate ideal proximity was based on Table 3.3 above). Phyre2 identified 73 templates on which *S. guttatum* AOX could be modelled and subsequently two consensus models were produced. In one model, the aforementioned iron-binding residues were not proximal to one another, but in the second model (shown in Figure 3.7 below) 5 of the 6 residues were proximal (based on Table 3.3) with Glu178 more than 10Å away from all but one of the other 5 residues.

3.3.5 Docking

Use of the AutoDock PyMOL plugin resulted in the generation of 10 possible substrate-protein interaction conformations, with free energy states between -6.33kcal/mol and -4.23kcal/mol. The docking grid encompassed the whole monomeric homology model (Figure 3.3b), but all ten substrate-protein interactions were predicted to occur in the space between helices one and four. The two positions closest to the active site are shown in Figure 3.8 below in green (left, -5.38kcal/mol free energy on binding and 9.2Å from the iron centre) and yellow (right, -4.88kcal/mol free energy on binding and 7.7Å from the iron

centre). The highest-scoring position (-6.33kcal/mol free energy on binding) lies 12.3Å from the iron centre.

A possible substrate-binding site (Figure 3.9, left) has been suggested as a result of docking, found between the membrane-associated helices one and four. A PyMOL session file ("Cavities.pse") can be found on the CD at the back of this thesis.

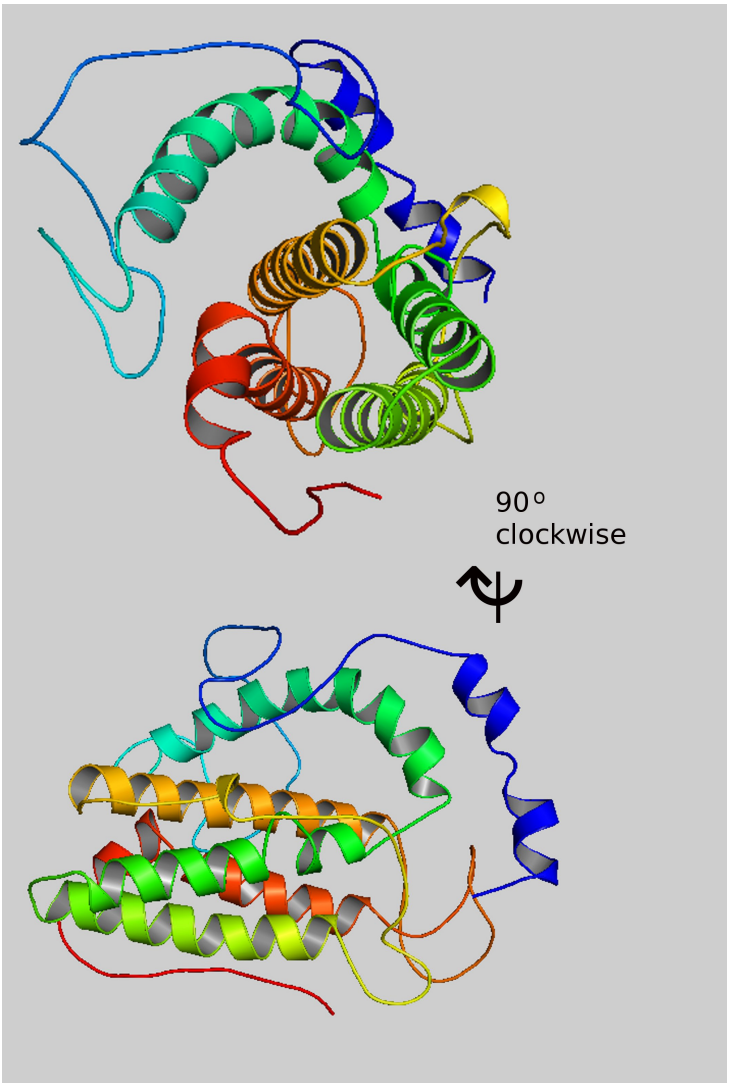

Figure 3.7 – A representation of the consensus model generated by Phyre2.

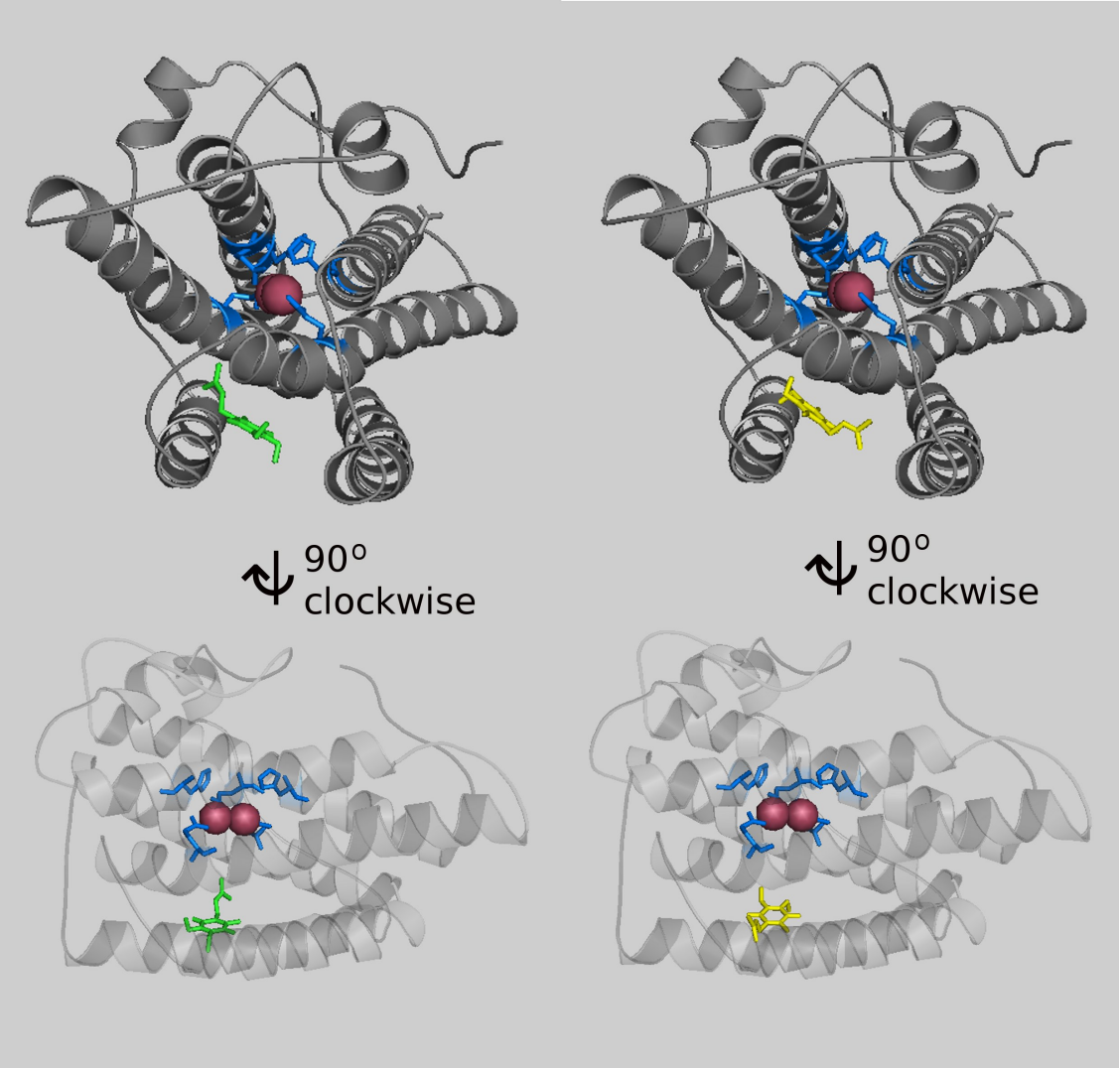

Figure 3.8 – A diagrammatic representation of the potential docking of ubiquinol-1 in *S. guttatum* AOX by AutoDock. The two docked molecules (in green, left and yellow, right) represent the two positions closest to the diiron catalytic centre (9.2Å and 7.7Å respectively). The six iron-binding residues (Table 3.3) are shown in blue with the diirons shown in red.

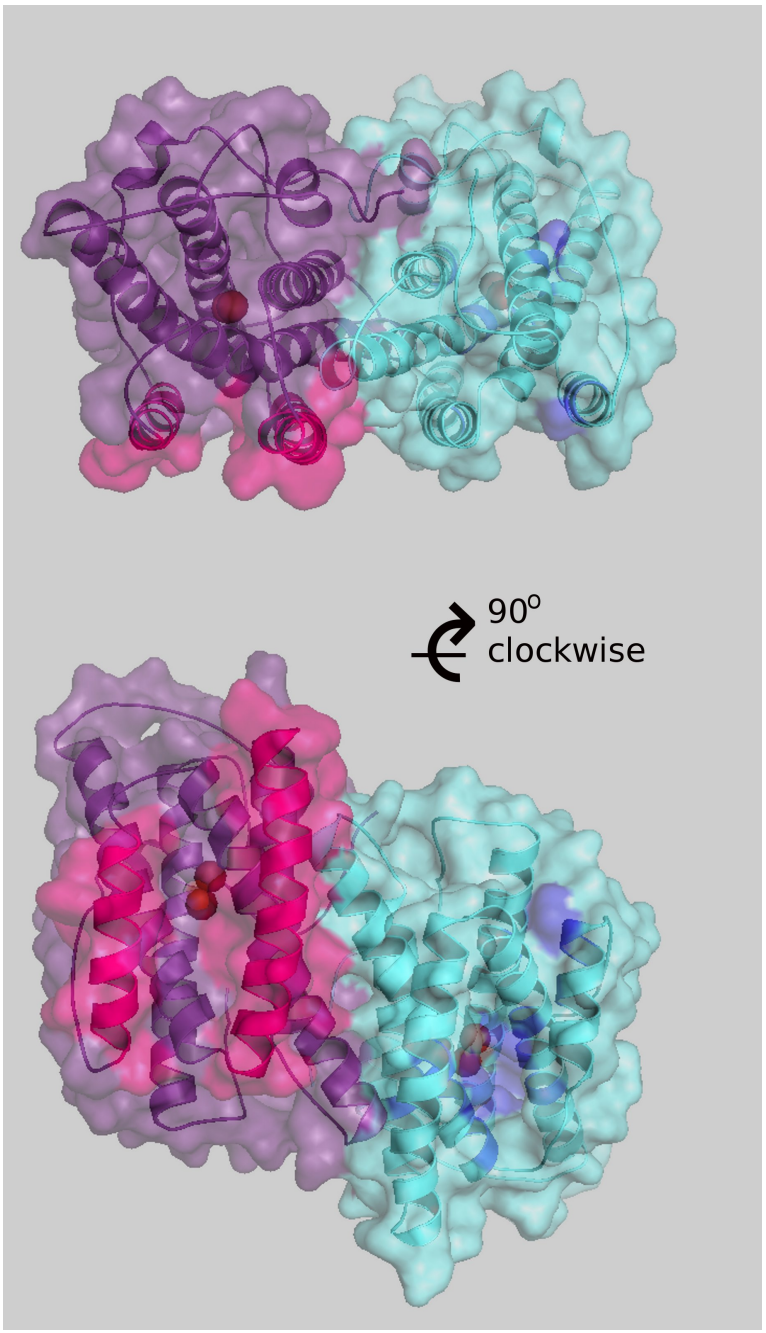

Figure 3.9 – A diagrammatic comparison of two possible substrate binding sites. One possible substrate-binding cavity identified through docking with Autodock (left, in magenta) is compared to the inhibitor-binding site identified by Shiba *et al*. (2013; right, in blue).

3.4 Discussion

3.4.1 Multiple alignment and phylogenetic analysis

In agreement with previous findings *cf* Moore *et al*., 1995 and more recently Williams *et al*., 2010), there is a large amount of conservation observed across proposed helical regions when large numbers of alternative oxidase sequences are aligned (Figure 3.1). The 6 iron-binding residues (Glu178, Glu217, His 220, Glu268, Glu319 and His322) are wholly conserved in all alternative oxidase sequences to date. Sequence variation is observed outside of the helical regions, whilst residues directly up- and down-stream of the 6 iron-binding residues appear to be mostly conserved. Interestingly, there is a high level of variation in the region previously identified as responsible for determining pyruvate sensitivity which is in agreement with previous findings (Crichton *et al*., 2005; Carré *et al*., 2011; Ito *et al*., 2011).

When 100 of the aligned sequences with greater than 60% similarity were used (distributed as evenly as possible between plant, fungi, bacterial and protists) to create a bootstrapped phylogenetic tree, many of the species did not form consistent clades. This suggests that there were errors in the initial iterations of tree construction, perhaps as a result of a relatively low similarity threshold applied across a large number of sequences. By gradually reducing the number of sequences, trees with more appropriate clade patterns could be generated, such as the bootstrapped tree shown above in Figure 3.2. Interpretation of the tree suggests that the modern thermogenic plants found in Australasia (*S. renifoli* and *N. nucifera*) diverged from the common ancestor less recently than the European araceae (*A. conicinna*, *A. maculatum* and *D. vulgaris*), with the *S. guttatum*, native to Asia and Africa diverging after the Australasian species, but before the European species. However, in contradiction with previous phylogenetic analyses of alternative oxidase sequences Roberts *et al*., 2004; Williams *et al*., 2010), it appears that the AOX proteins found in protist parasites (*Trypanosoma* and *Cryptosporidium* species) may be more closely related to prokaryotic AOX proteins than to plant AOX proteins; moreover, the fungal and parasite sequences are more distantly related to the proteobacterial sequences than the plant

sequences are to the proteobacterial sequences. Because the sequences were selected for similarity and familiarity, it is accepted that there is inherent bias and therefore interpretations are made with caution.

3.4.2 Homology modelling *vs*. threading

Several models were produced using both homology modelling and threading. Empirically, the z-scores for the two homology models (Table 3.2, Figures 3.3a and 3.3b) are within an acceptable range (Appendix 1) and the arrangement of the six iron-binding residues in three dimensions is consistent with previously proposed alternative oxidase iron-binding models (Table 3.3). By contrast, the QMEAN4 scores (Table 3.2) are low (0.14 for the homology model based on Δ^9-desaturase and 0.25 for the homology model based on TAO) on a scale where 0 is indicative of a poor model, and 1 is indicative of a very good model. However, low QMEAN4 scores are not unusual for membrane proteins, which are under-represented in the databases used as training sets for algorithms such as SwissMODEL (Benkert *et al*., 2011). Furthermore, accurate calculation of energy distribution in membrane protein models is difficult when the molecules of the membrane are not included in the dataset, so comparison to the energy distribution of other non-membrane-associated protein models of a similar sequence length is not favourable.

A manual assessment of the models shows no disallowed backbone conformations. Empirically and heuristically, the homology model based on the TAO structure must be selected as the most accurate model, as there is the greatest degree of sequence similarity between the target and the template (40%). Models generated using threading techniques were of poorer quality, as none managed to satisfy the proximity required of the iron-binding residue positions relative to one another in the final structure. This is likely to be due to poor template identification. Even using a scoring matrix such as BLOSUM40, which is particularly useful for aligning distantly related sequences, did not lead to any templates on which an accurate model could be based. This is a result of poor sequence similarity between the alternative oxidase and the most closely related family, the diiron

carboxylates (<30%). The accepted iron-binding motifs, $(Ex_nExxH)_2$, are distributed throughout the entire sequence and even with iterative alignment the motifs from several diiron carboxylate sequences are not aligned with those in the alternative oxidase sequence using a BLOSUM40 scoring matrix. At the time of writing, the TAO structure is not available through any of the databases that the threading software discussed herein search, so it is not possible to definitively state whether inclusion of the structure would improve the results of the threading. However, given that the similarity of the two sequences is above the 25% Sander-Schneider threshold, there is a reasonable probability that the threading process would be improved significantly.

3.4.3 Validity, variations and value of the Δ^9-desaturase and TAO homology models

Whilst modelling the alternative oxidase on Δ^9-desaturase is inherently inaccurate due to the low sequence similarity, it was the best model available at the time – especially taking into account the even greater degree of dissimilarity between the alternative oxidase and the other diiron carboxylates (10-20% similarity). This model was used extensively to construct crude representations of both the active site and other important regions such as the quinone binding pocket (*cf* Albury *et al*., 2009). The limitations of the model based on Δ^9-desaturase were accepted; namely the lack of appropriate membrane associated helices and the low accuracy in the loop regions, where the template-target sequence similarity was <1%. Nevertheless, when used with a caveat of empirical limitation, it was a useful tool for physical visualisation of theoretical concepts such as the impact of residue mutation in a three-dimensional space. When the TAO structure was made available before publication, the quality of the working alternative oxidase model improved, especially when modelling virtual mutations and proposing a physical mechanism for the alternative oxidase catalytic cycle (Moore *et al*., 2013) – which may then be presented with an increased level of confidence.

As illustrated in Figure 3.4a above, there is one important difference between the homology model based on the Δ^9-desaturase and TAO templates; the presence of two extra

helices in the TAO-based model. All previous models of the alternative oxidase predicted the presence of four longer helices, with one helix approximately half the length of the others, which was thought to anchor the protein in the membrane in a manner similar to that of prostaglandin H_2-synthase (Andersson and Nordlund, 1999). The extra helices present in the TAO structure, lie below the main four-helix bundle and do not constrain the active site, nor contain any of the iron-binding residues; as such, the previous prediction of a diiron active site coordinated by a four-helix bundle is accurate. The role of the extra helices has not been verified experimentally, although distribution of several aromatic residues (Table 3.4) would indicate that helices 1 and 4 are serving as an anchor to keep the alternative oxidase within the membrane. For reference, an overlay of the model based on Δ9-desaturase and the model based on TAO are illustrated in Figure 3.4a. While the main areas of overlay deviation occur in the unstructured loop regions, the placement of the helices relative to one another is also somewhat dissimilar. Furthermore, the distances between the iron-binding residues for each homology model (Table 3.3) could perhaps indicate that the diiron centre observed in the diiron carboxylate family is not identical to the diiron centre of the alternative oxidase family. This is perhaps some novel evidence that the alternative oxidase, initially placed in the diiron carboxylate family (*cf* Berthold *et al*., 2002) may not belong fully to that family. In fact, the alternative oxidase family has recently recognised officially as a family in its own right (EC 1.10.3.11).

It is worth noting that despite previous predictions that the alternative oxidase may have β-sheet or turn secondary structure elements (*cf* Moore and Siedow, 1991, and Table 5.8, Chapter 5), the TAO crystal structure does not have any β secondary structure elements at all. Since alpha helices are well represented in the databases from which propensity scoring tables are generated (Chou and Fasman, 1974; Garnier *et al*., 1978), this is not the reason why the predictions have been somewhat inaccurate in the past. The degree of variability in secondary structure predictions in Table 5.8 may indicate that the alternative oxidase secondary structures potentially contain residue sequences that are somewhat atypical compared to other residue-structure correlations.

3.4.4 Membrane-AOX model

In the membrane-AOX model (Figure 5.6) generated using VMD and PyMOL, the protein has been placed approximately 14Å into the membrane. This differs from the membrane-TAO model proposed by Shiba *et al*. (2013), in which the protein is placed 8Å into the membrane. Given the relatively even distribution of hydrophobic residues toward the solvent accessible surface of both TAO and the homology model of *S. guttatum* alternative oxidase based on TAO, there is no clear indication from these residues where the protein should sit in the membrane. However, there is a very hydrophobic, surface-accessible cavity in TAO – in which an ascofuranone-derivative molecule has been co-crystallised in each of the four chains presented in the crystal structure – approximately 7Å above the membrane-solvent boundary. This cavity, which is also present in the TAO-based *S. guttatum* homology model (Figure 3.9, right), could potentially allow a quinol-homologue substrate to pass into it, would therefore perhaps be more likely found closer to the membrane-solvent interface, rather than some 7Å above it. In light of this, the membrane-AOX model developed as part of this project has been heuristically modelled to allow the solvent-accessible entrance to the cavity to be placed inside the membrane, rather than outside.

3.4.5 Docking

In addition to the hydrophobic cavity identified in the TAO crystal structure, a second possible substrate binding region has been identified (Figure 3.9) through molecular docking. It was possible to model the interaction between the alternative oxidase and ubiquinol in this proposed binding pocket. The simulated docking outcomes with the lowest energy scores (as illustrated above in Figure 5.6) all place the ubiquinone-1 molecule with the quinone ring in approximately the same orientation (parallel to the membrane), suggesting perhaps that the substrate may be aligned as such *in vivo*. It is accepted that the accuracy of docking algorithms may decrease in the case of the alternative oxidase, as the binding site is likely to be embedded within the membrane *in vivo*, but is partly solvent-

exposed in the homology model. Therefore, calculated physical interactions (particularly electrostatic and hydrophobic interactions) may not be as realistically calculated as required. Bearing this limitation in mind, the outcome of the docking experiments is of interest and would be useful for further refining the exact substrate-residue interactions which take place in the substrate binding pocket.

Interestingly, the newly identified substrate binding pockets do not appear to incorporate any of the proposed quinone-binding motifs as suggested previously, such as the HR pair (H261, R262) and the quinone-binding triad element (LxxxHxxT, corresponding to L137, H141 and T144; Fisher and Rich, 2000). In the TAO-based homology model, the HR pair is greater than 5Å away from both of the proposed substrate binding pockets, and the triad element (L137, H141 and T144) are located in an unstructured region, the position of which varies between chains in the TAO crystal structure. In light of this, the inclusion of the alternative oxidase in group of quinone-binding proteins possessing the HR pair and triad element may need to be reconsidered.

3.4.6 Concluding remarks

It has been possible to model the *S. guttatum* alternative oxidase on both the distantly-related, diiron carboxylate Δ^9-desaturase, and the more closely related member of the alternative oxidase family, TAO. Whilst using TAO as a template for homology modelling undoubtedly produces the most accurate outcome, the homology model based on Δ^9-desaturase provided a useful tool in the absence of a more accurate model. In light of the two newly-identified potential substrate-binding sites, investigation of the key residues within these sites should be carried out using mutagenesis studies to further elucidate the structure-function relationship of these regions. The presence of a four-helix bundle providing a scaffold from which iron-binding can take place had been previously predicted, and therefore remains an essential part of the model, whilst the presence of two membrane-associated – and possibly substrate-associated – helices would suggest that the nature of the

membrane-protein interaction is key to the structure and function of the *S. guttatum* alternative oxidase.

Chapter 4

Expression and purification of the alternative oxidase

4.1 Background

The aim of this part of the project was to define a protocol for the over-expression, solubilisation and purification of recombinant *S. guttatum* alternative oxidase in a prokaryotic expression system.

Alternative oxidase protein has been extracted from native tissues (*cf* Huq and Palmer, 1978; Berthold and Siedow, 1993; Affourtit and Moore, 2004), but the instability and short lifespan of the protein following liberation from the mitochondrial membrane (*cf* Moore and Siedow, 1991) limits the experimental scope of using protein isolated from such tissues. Therefore, in order to conduct experiments where stable, long-lived protein is required, it has been necessary to implement the provision of alternative sources of AOX protein, specifically through recombinant protein expression. Previous attempts to express recombinant alternative oxidase have used both eukaryotic (Albury *et al*., 1996) and prokaryotic (*cf* Kumar and Söll, 1992; Berthold *et al.,* 2002; Kido *et al*., 2010) expression systems, in the form of *Schizosaccharomyces pombe* and *E. coli* respectively. The *S. pombe* expression system has been used successfully as a strain for production of mutated alternative oxidase proteins (Crichton *et al*., 2010) in addition to wild-type *S. guttatum*. This eukaryotic system is ideal for this expression to monitor activity, as the AOX protein product is targeted to the inner mitochondrial membrane and expressed functionally alongside the traditional respiratory chain complexes.

Whilst the *S. guttatum* alternative oxidase has been expressed successfully in a eukaryotic system, extensive expression in a prokaryotic host has not been previously attempted. Other AOX isoforms such as *A. thaliana* and *T. brucei* (*cf* Berthold, 1998; Fukai *et al*., 1999 respectively) have been expressed in prokaryotic hosts however and the

protocols described have formed the basis for expression of *S. guttatum* AOX in specialist *E. coli* strains as described in this Chapter.

In order to ensure a reproducible *S. guttatum* recombinant protein yield can be achieved using a prokaryotic expression system, the previously described expression protocols (Berthold, 1998; Fukai *et* al., 1999; Nihei *et al*., 2003) have been adapted where necessary to account for isoform-specific differences in protein behaviour. Furthermore, it was necessary to define solubilisation and purification protocols for the production of *S. guttatum* recombinant alternative oxidase – which had not been attempted before.

4.1.1 Considerations for designing an expression and purification protocol

4.1.1.1 Expression strains – C41 and FN102

As previously stated, a protocol for expression of recombinant *S. guttatum* alternative oxidase in yeast has been successfully defined (Albury *et al*., 1996). However, the system was not designed to produce protein which can be readily purified. As a result, an additional system may be used to complement this eukaryotic system; namely the use of the gram-negative bacterium *E. coli*. Simple genetics and a short doubling time mean this is an ideal candidate for protein expression (*cf.* Russo, 2003; Terpe, 2006). Furthermore, if the recombinant alternative oxidase is targeted to the bacterial cytoplasmic membrane, it may be separated from the contents of the cell with careful application of cell lysis, solubilisation and finally purification.

Expression of recombinant protein using prokaryotic systems has been a long-established method for the bulk production of proteins of interest for either medical, industrial or research purposes. Much of the early development of this technique was carried out using *E. coli* (*cf*. Cohen *et al*., 1972; Morrow *et al*., 1974) and following the advancement of such protocols and techniques, there exists today a plethora of well-tested and well-documented prokaryotic expression systems for use in protein expression experiments, such as for the over-expression of AOX. Some *E. coli* strains are particularly well-suited to expressing different classes of protein and for this project two strains were

chosen – one strain modified for the general over-expression of membrane proteins (C41), and the other a haem-deficient mutant strain (FN102) with fewer respiratory complexes than other *E. coli* strains.

Historically, over-expression of membrane proteins in standard BL21 (DE3)/T7 RNA polymerase systems has resulted in cell death due to over-expression, causing undesirable effects such as membrane degradation (Dong *et al*., 1995; Grisshammer and Tate, 1995). Similarly, over-expression of globular proteins has been linked to expression-related toxicity (Studier *et al*., 1990; George *et al*., 1994) in the same system. Work carried out by Miroux and Walker (1996) aimed to identify *E. coli* strains which were capable of over-expressing membrane and globular proteins, without succumbing to the toxic effects associated with over-expression. Through numerous rounds of over-expression of the membrane-spanning oxoglutarate-malate carrier protein in BL21 (DE3), Miroux and Walker (1996) were able to isolate surviving cells, which they named C41, that were able to grow to high densities and express significant quantities of protein as inclusion bodies. Further rounds of over-expression of other membrane-bound proteins in the newly-selected C41 strain indicated that the strain was capable of over-expressing membrane proteins (such as the F_1F_0 subunit of ATPase, Arechaga *et al*., 2000) without falling prey to the toxic effects observed in the other BL21 (DE3) cell lines.

A second *E. coli* strain known as FN102 was also chosen for this project, but for different reasons. When expressing recombinant AOX in either yeast (*S. pombe*, as previously described) or bacteria, the protein is targeted to the membrane and is incorporated as a functional (unless mutated; see Chapter 5) protein. As a result, the recombinant protein works in tandem with the respiratory chain present in the organism – and this can be problematic when attempting to ascertain the proportion of activity of the cells that is a direct result of the alternative oxidase. Whilst a suitable solution has been developed in yeast systems (such as the use of complex-specific inhibitors during activity assays, Albury *et al*., 1996), in bacterial systems (where more respiratory complexes are present naturally), the issue is compounded. However, the development of several strains

lacking the ability to synthesise haem A – and therefore to synthesise fully functioning cytochrome *c* oxidase (COX) proteins – have offered a solution to this particular issue (Avissar and Beale, 1989; Kumar and Söll, 1992). Furthermore, when AOX is functionally expressed in haem-deficient strains, it 'rescues' the strain, acting as the final electron acceptor and allowing respiration to continue. Therefore, with no COX activity present, the proportion of alternative oxidase activity should be easier to quantify, which has proved advantageous to parts of this project. Additionally, haem-deficient strains have been used successfully previously to express alternative oxidase proteins (*cf* Berthold, 1998; Chaudhuri *et al*., 1998; Fukai *et al*., 2003) of both plant and parasite origin.

For these reasons, the FN102 strain (as provided by Professor Kita, Tokyo University) was used alongside the C41 strain in order to provide two prokaryotic expression systems, both used in conjunction with a modified pET15b plasmid (Dr Mary Albury, as described in Chapter 2). For the ease of downstream purification of the recombinant AOX a six-histidine tag was encoded at the N-terminal of the recombinant gene sequence inserted into the pET15b vector. The plasmid also encoded for ampicillin resistance, for the purposes of transformant selection and competition reduction. The mitochondrial leader sequence had been removed for expression in *E. coli*, leaving only the mature protein encoded, which was thought to be inserted into the bacterial membranes as though it were mitochondrial in nature. The pET15b plasmid allowed for protein over-expression through the T7 promoter mechanism (Studier and Moffatt, 1986), and also controllable protein expression through the lac operon system (*cf.* Jacob and Monod, 1961 and Hanson *et al*., 1998) using IPTG as a lactose homologue.

4.1.1.2 Growth conditions

It is generally accepted that *E. coli* cultures grow optimally at around 37ºC, which corresponds to efficient enzyme functionality. *E. coli* are relatively hardy however and may also be grown at temperatures below 37ºC if required. For example, growing at 30ºC slows growth during the exponential phase and prevents premature entry into the stationary phase,

whilst growing at 18ºC after induction slows the exponential growth to a greater extent, but also reduces protein aggregation and increases protein solubility (*cf.* Sørensen and Mortensen, 2005).

The media required for growth of transformed C41 and FN102 cells is strain-specific. For C41, standard Miller Luria Broth supplemented with the plasmid-specific selective antibiotic ampicillin (100μg/ml), 0.2% glucose as an additional carbon source and 0.125% iron sulphate was recommended (Berthold, 1998). As shown previously, the availability of iron during protein expression is essential for the formation of functionally active alternative oxidase protein (*cf* Affourtit *et al*., 2004). By contrast, a sodium chloride-free tryptone-peptone buffered growth media was recommended for successful growth of transformed FN102 cells (Nihei *et al*., 2003, see Chapter 2, Section 2.2.2 for exact composition). Other supplements added include two iron sources (iron sulphate and iron chloride) to ensure sufficient iron for inclusion into the recombinant alternative oxidase protein; and magnesium sulphate, which had previously been identified as important for maintaining AOX stability (Nihei *et al*., 2003). In this case, the plasmid-specific selective antibiotic carbenicillin was used in place of ampicillin with no noted negative effects on growth efficiency (Nihei *et al*., 2003). Additionally, all agar plates and starter cultures for the growth of FN102 cells required the addition of ALA to enable the synthesis of haem-complexes prior to the expression of alternative oxidase. A critical step in the growth protocol for the FN102 strain is the removal (by centrifugation) of the ALA from the starter culture prior to inoculation of the main culture medium (Nihei *et al*., 2003).

For both the C41 and FN102 strains, identifying an optimal IPTG concentration is vital (Hansen *et al*., 1998; Kilikian *et al*., 2000), as this directly limits or optimises protein expression. Previous expression protocols (Berthold, 1998; Chaudhuri *et al*., 1998; Fukai *et al*., 2003; Nihei *et al*., 2003) stipulate varying IPTG concentrations for different AOX isoforms, ranging from 25μM-100μM.

4.1.1.3 Membrane harvest and lysis

Whilst for both FN102 and C41 strains the recommended centrifugation speed for pelleting the bacterial cells after the growth was 8,000 x *g* (Berthold 1998; Fukai *et al*., 1999; Fukai *et al*., 2003), the technique for lysis varies. Berthold (1998) and Fukai *et al*. (2003) performed lysis using a French Press, whilst Fukai *et al*. (1999) performed lysis using sonication. When lysing transformed cells with recombinant alternative oxidase targeted to the cytoplasmic membrane, it is particularly important that the cell membranes should be broken into smaller sections, but not eradicated entirely in order to avoid AOX inactivation through premature removal of the lipophilic membrane environment required for protein stability.

4.1.2 Factors affecting solubilisation and purification

The extraction of intrinsic proteins from the membrane requires disruption of the lipid layer and this is most often achieved using detergents. In the case of the alternative oxidase, the association with the membrane is thought to be monotopic (Rich and Moore, 1976), with aromatic residues (see Chapter 5, Section 5.3.3) potentially playing a role in anchoring the protein to the membrane.

Previously, n-octyl-β-D-glucoside (OG; Nihei *et al*., 2003) and deoxybigCHAP (Affourtit and Moore, 2004) have been used to liberate recombinant TAO and native *A. maculatum* from *E. coli* and mitochondrial membranes respectively. However, as *S. guttatum* alternative oxidase had not been previously solubilised from bacterial host membranes, alternative detergents and combinations thereof were tested experimentally. Stronger detergents were considered with caution; sodium dodecyl sulphate (SDS), for example, would potentially lead to protein aggregation and denaturation. By comparison, milder non-ionic detergents such as n-Dodecyl β-D-Maltopyranoside (DDM) and detergents in the polyoxyethylene series are capable of disrupting membranes with limited damage to proteins and have previously been used to solubilise the membrane-bound respiratory enzyme cytochrome *c* oxidase (Rosevear *et al*., 1980). Similarly, the non-ionic

and mild detergent OG has previously been successfully used to solubilise functional membrane-bound respiratory complexes from native tissues (Baron and Thompson, 1975) as well as functionally-active recombinant TAO (Nihei *et al*., 2003). However, other milder detergents shorter chain polyoxylethylene detergents (C_8E_4 or C_8E_5) can often be more inactivating to some recombinant proteins than DDM and other polyoxylethylene detergents with chains of intermediate length (C_{12}-C_{14}) (Maire *et al*., 2000).

For the purposes of solubilisation, it is essential to ensure that the final detergent concentration is equal to or slightly greater than the detergents critical micelle concentration (CMC), as this permits the detergent molecules to form micelles. This process facilitates the disruption of the membrane as well as providing a hydrophobic environment in which the liberated recombinant protein may be sequestered, thus reducing the risk of losing protein conformation (i.e. the exposure of a membrane-bound protein to a hydrophilic environment) and therefore function. The CMCs of most commonly used detergents are well characterised (*cf* Maire *et al*., 2000). Maintaining the concentration of the chosen detergent at or just above its CMC during solubilisation is advised, but following solubilisation the detergent concentration may be decreased to limit micelle size in order to allow for the detergent to be removed downstream.

Following solubilisation of native *A. maculatum* alternative oxidase (*cf* Hoefnagel *et al*. 1997; Affourtit and Moore, 2004) and recombinant TAO (Nihei *et al*., 2003) continued presence of detergent in suspension and purification buffers was required to retain protein activity. The requirement for detergent post-solubilisation is not uncommon for membrane proteins and given the relatively small mass of the alternative oxidase, it is not unreasonable to expect that the solubilised recombinant protein will be localised within the detergent micelles formed during solubilisation. Additionally, the alternative oxidase substrates are hydrophobic in nature (*cf* Hoefnagel *et al*., 1997) and would be sequestered to the core of the protein where the active site is found. As a result, it may be that the AOX not only requires a hydrophobic local environment but also close association with lipophilic structures such as membrane and detergent micelles. An additional lipophilic substance,

glycerol, has previously been added to solubilisation and purification buffers of the TAO (Nihei *et al*., 2003) and is thought to help retain protein activity by limiting conformational flexibility (*cf* Sousa, 1995).

Another additive which had been previously identified as essential for recombinant TAO stability post-solubilisation is magnesium sulphate (Nihei *et al*., 2003). The requirement for Mg^{2+} ions in other membrane-bound proteins (such as ATPase, *cf* Cohen and Thompson, 1975) has been documented, although the exact nature of protein stabilisation by Mg^{2+} ions is not known. One possible interaction that may be particularly relevant to the alternative oxidase is the adsorption of the Mg^{2+} ions onto any negatively charged, solvent-accessible side chains (specifically charged amide groups), thus reducing excessive interaction of these side chains with water (*cf* Collins, 2006).

Crucially, the importance of the addition of pyruvate to buffers used for natively-expressed AOX (Carré *et al*., 2011) and recombinant plant alternative oxidase proteins would indicate that the presence of pyruvate in solubilsation and purification buffers may be essential for recombinant alternative oxidase stability. Whilst the exact mechanism by which pyruvate stabilises the alternative oxidase in unknown, it has been suggested that the pyruvate may interact with the cysteine-122 residue (*cf* Carré *et al*., 2011), which according to recent modelling (see Chapters 3 and 5) would most likely be solvent-facing. In the previously defined purification protocol for TAO (Nihei *et al*., 2003), pyruvate was not added to any of the extraction, solubilisation or purification buffers due to the apparent insensitivity of TAO to pyruvate (Chaudhuri *et al*., 2005). Therefore, the addition of pyruvate to extraction, solubilisation and purification buffers should be considered specific to the extraction of recombinant plant alternative oxidases and potentially other AOX isoforms from species which show pyruvate sensitivity.

4.2 Methodology

Transformation, bacterial growth, cell harvest, membrane solubilisation and recombinant alternative oxidase protein purification was carried out as detailed in Chapter 2, with experimental variations described below.

4.2.1 Expression strains

Modified pET15b plasmids containing the wild-type (*S. guttatum*) gene (as described in Chapter 2) were transformed into C41 and FN102 cells using the previously defined heat shock method (Chapter 2, Section 2.1.2) and grown for a maximum of 12 hours at 37^{o}C on the appropriate LA plates.

4.2.2 Strain-specific growth conditions, membrane harvest and cell lysis

C41

Transformed C41 cells were grown as described in Chapter 2, Section 2.2.1 with no modifications after initial determination of optimal IPTG concentration (minimum 25μM, maximum 100μM). Re-suspension of the cell pellets after growth (harvest) was performed in 50mM TRIS-HCl, pH7.4 in both the presence and absence of sodium chloride (minimum 50mM, maximum 300mM), DTT (minimum 1mM, maximum 5mM) and 10mM pyruvate.

FN102

Transformed FN102 cells were grown as described in Chapter 2, Section 2.2.2 after initial experimentation with starter culture growth times (minimum 2 hours, maximum 8 hours), main culture growth times following induction (minimum 4 hours, maximum 16 hours) and varying IPTG concentration (minimum 25μM, maximum 100μM). Re-suspension of cell pellets after growth (harvest) was performed in 50mM TRIS-HCl, pH7.4 in both the presence and absence of pyruvate (minimum 1mM, maximum 100mM). Isolation of both crude membrane and inner membrane was investigated, based on Kido *et al*. (2010). To determine the effect of ALA on growth, starter cultures were grown in the

presence and absence of ALA, and in one case ALA was not removed prior to main culture inoculation using the starter culture.

4.2.3 Solubilisation

Several detergents were investigated (see Table 4.10 below) using the basic method as described in Chapter 2, Section 2.3.1. Solubilisation time (minimum 30 minutes, maximum 60 minutes) and centrifugation time (minimum 30 minutes, maximum 60 minutes) were varied to determine optimal conditions. Centrifugation speed was kept constant.

4.2.4 Purification

To determine the effect of detergent and glycerol concentration, various concentrations were investigated as follows: DDM – minimum 0.5%, maximum 1%; OG – minimum 0.5%, maximum 1.4%; $C_{12}E_8$ (octaethylene glycol monododecyl ether) – minimum 0.5%, maximum 1%; glycerol – minimum 2.5%, maximum 20%. Similarly, to determine the effect of the presence or absence of 200mM magnesium sulphate, 200mM iron sulphate, 150mM zinc sulphate and 10mM pyruvate these reagents were either included in the purification buffers, or omitted. Small-scale purifications (to test the effect of detergent, glycerol or salt concentration for example) were carried out using the batch method, whilst larger-scale preparative purification was carried out using the column/gravity flow method (Chapter 2, Section 2.3.2).

4.2.5 Protein activity assays

In order to maintain reproducibility, all activity assays were carried out using the spectrophotometric (see Chapter 2, Section 2.5.2) method. A number of substrates were used (duroquinol, ubiquinol-1 and decylubiquinol) depending on availability. The substrate used to obtain the results shown below in Section 4.3 is indicated in each Table information.

4.2.6 Visualisation of recombinant alternative oxidase

SDS PAGE and Western blotting analysis was carried out exactly as described in Chapter 2, Section 2.4.

4.3 Results

Specific and total activity shown in the Tables in this Section are those of wild-type recombinant protein and have been ascertained using ubiquinol-1 as substrate and the BCA method of protein estimation (see Chapter 2, Section 2.5.1.1) from a single preparation unless otherwise stated. The results of over-expression of the various mutants is discussed in Chapter 5; this Chapter is mainly concerned with the over-expression of wild-type (*S. guttatum*) alternative oxidase.

4.3.1 Factors affecting expression

4.3.1.1 Expression strains

It was possible to express active recombinant alternative oxidases from both the C41 and FN102 strains, as shown below in Table 4.1:

Strain	**Average specific activity of membrane (µmols/min/mg)**	**Average protein produced from 5L grow-up (mg)**
C41	0.5 (0.05)	60 (13.8)
FN102	1 (0.1)	20 (2.2)

Table 4.1 – Average specific activity and total wild-type recombinant protein produced per strain. This Table shows activity produced following the Berthold (1998) protocol; 35mM duroquinol substrate. Averages were taken over 5 preparations and standard deviation is shown in brackets.

4.3.1.2 Growth conditions, membrane harvest and cell lysis

4.3.1.2.1 C41

Two methods were used to grow C41 cells expressing recombinant *S. guttatum* based on methods by Berthold (1998) and Fukai *et al*. (1999), the results of which are summarised in Table 4.2 below.

Method	**Average specific activity (µmol/min/mg)**	**Average total protein (mg)**
Berthold, 1998	0.5 (0.05)	60 (13.8)
Fukai *et al*., 1999	0.1 (0.03)	8 (1.5)

Table 4.2 – Average protein activity of membrane-bound recombinant *S. guttatum* AOX. This table shows average protein activity of the membrane-bound recombinant *S. guttatum* AOX and total protein as grown using the two previously described methods using 35mM DQH_2 as substrate. Averages were taken over 5 preparations and standard deviation is shown in brackets.

The Berthold (1998) growth method required little refinement. The growth curves in Figure 4.1 show optical density across a number of preparations, which demonstrates the reproducibility of the growth protocol.

The only change from the Berthold growth protocol was a deviation from the recommended incubation temperature post-induction due to difficulties controlling the temperature of the incubators. When the ambient temperature in the laboratory was high (i.e. in summer), the cooling system on the incubator was unable to chill the flasks to the required temperature of 18°C. The consistently achievable temperature was between 19°C and 20°C, which is under the 21°C temperature threshold recommended for incubation of proteins prone to aggregation or insolubility (*cf.* Baneyx, 1999). Activity and protein concentration from preparations carried out over the winter period (where 18°C was easily achieved) and summer period were compared to ensure that the increase of 2°C did not negatively impact protein expression or protein activity. Two membrane preparations carried out during summer months (exhibiting specific activities of 0.42µmol/min/mg and

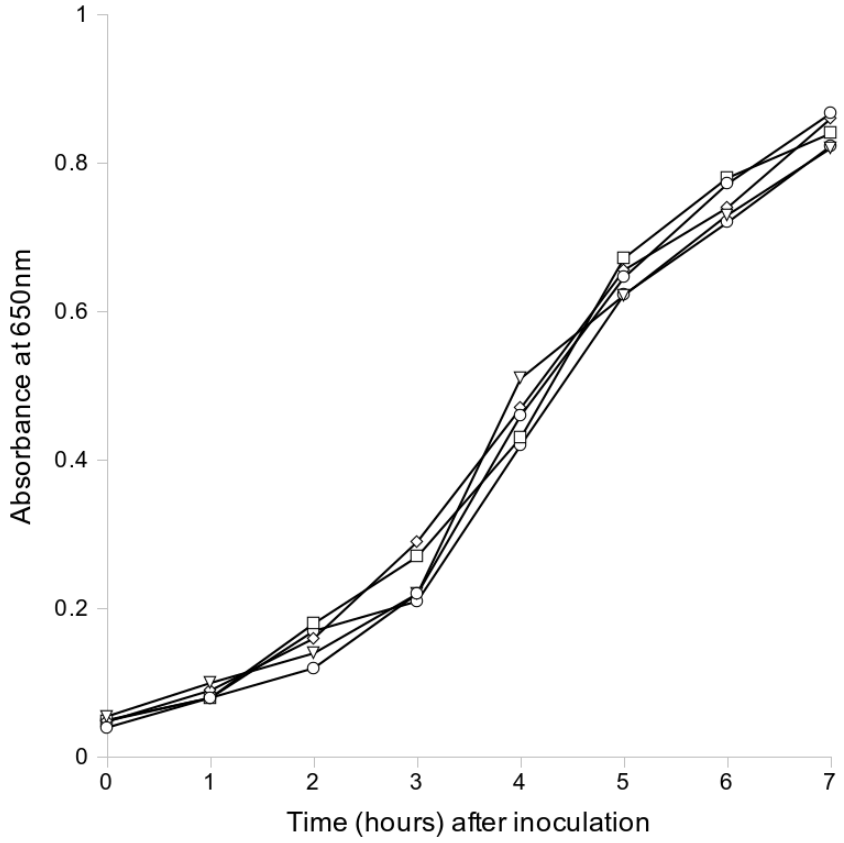

Figure 4.1 Growth curves from five separate cultures using the Berthold (1998) growth method. Cells were induced at 5 hours post-inoculation.

0.48μmol/min/mg and total protein of 52mg and 55mg respectively) were comparable to two membrane preparations carried out during winter months (where specific activities were 0.46 and 0.51 μmol/min/mg and total protein of 55mg and 55mg respectively). Average total activity for the summer preparations was 25μmol/min, and average total activity for the winter preparations was 27μmol/min.

Final IPTG concentrations of 25, 50, 75 and 100μM were investigated and the results are shown below in Table 4.3.

IPTG Concentration (µM)	Total protein in membrane fraction (mg)	Specific activity of membrane fraction(µmols/min/mg)	Total activity of membrane fraction (µmols/min)
25	25	0.12	3.00
50	22	0.08	1.76
75	23	0.07	1.61
100	19	0.03	0.57

Table 4.3 – The effect of IPTG concentration on cell protein concentration and activity of recombinant *S. guttatum* AOX expressed in C41. 35mM duroquinol was used as substrate..

4.3.1.2.2 FN102

As predicted, there was a difference in growth times for FN102 cells expressing recombinant S. guttatum alternative oxidase and published figures for FN102 cells expressing TAO (Fukai *et al*., 2003). Whilst the overnight (12-hour) plate colonies grew satisfactorily (typically 10-50 small colonies per plate), the starter cultures inoculated from the plate colonies consistently took >5 hours to reach optimal optical density for inoculation into the main culture media (optical density of 0.1 at 650nm). Similarly, once the main culture had been inoculated to an optical density of 0.01, the cultures required several hours (minimum of 2, maximum of 8) to reach an optical density of 0.1 and therefore induction density. Growth after induction of FN102 was not as rapid as observed in the C41 strain (see Figure 4.1), although it was not significantly reduced. This is shown below in Figure 4.2.

Figures 4.3a and 4.3b below illustrate the effect that the inclusion and subsequent removal or non-removal of ALA has on the growth curves for FN102 cells. In this experiment ALA was added at the beginning of the starter culture step and then either removed or left in the media prior to inoculation of a larger volume of media. In addition, the cultures were either induced (+ IPTG condition) or not induced (- IPTG condition) to see whether this had a noticeable effect on growth in the presence and absence of ALA.

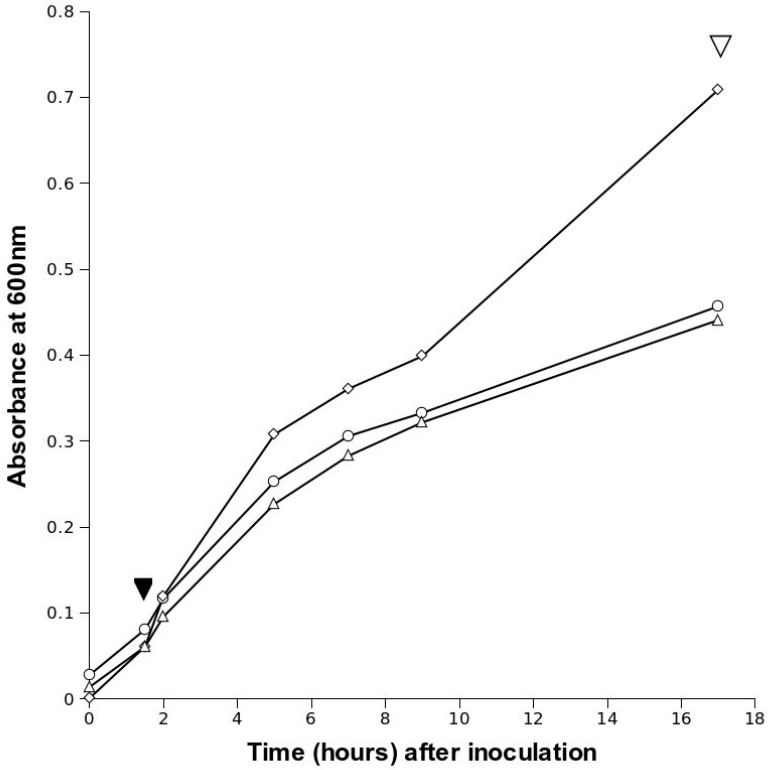

Figure 4.2 – The growth of three cultures of FN102 cells transformed with *S. guttatum* AOX-containing plasmids. Cells were induced at ▼ and harvested at ▽.

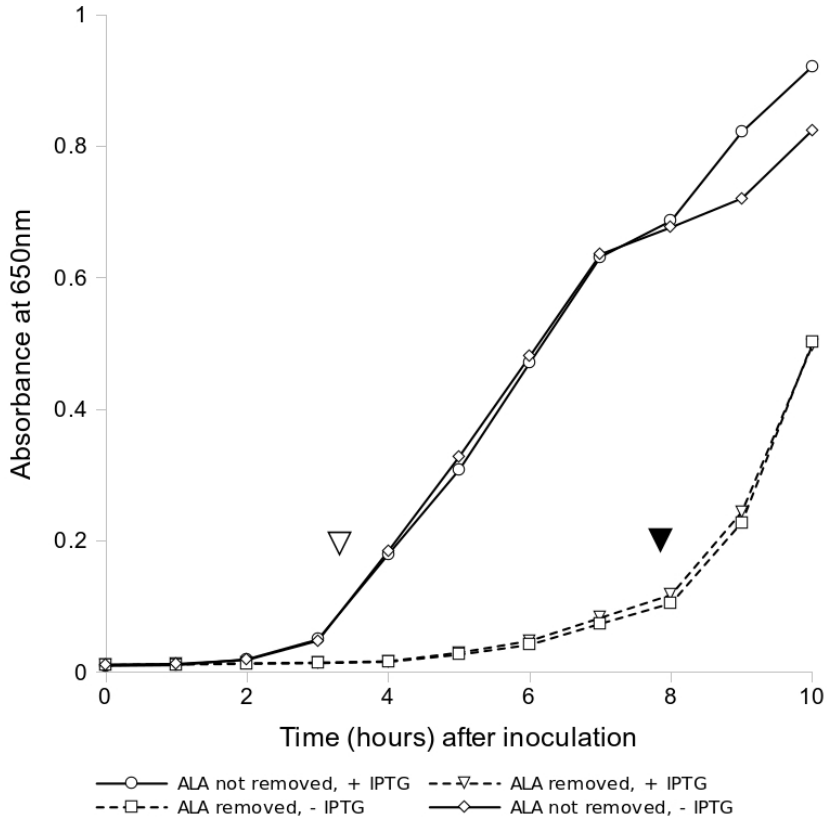

Figure 4.3a – The effect of ALA on growth curves. Comparison of growth curves where ALA was either removed or left in the main culture medium and the effect of subsequent addition or non-addition of IPTG. Induction times of the +IPTG conditions where ALA was not removed and where ALA was removed are indicated by ▽ and ▼ respectively,

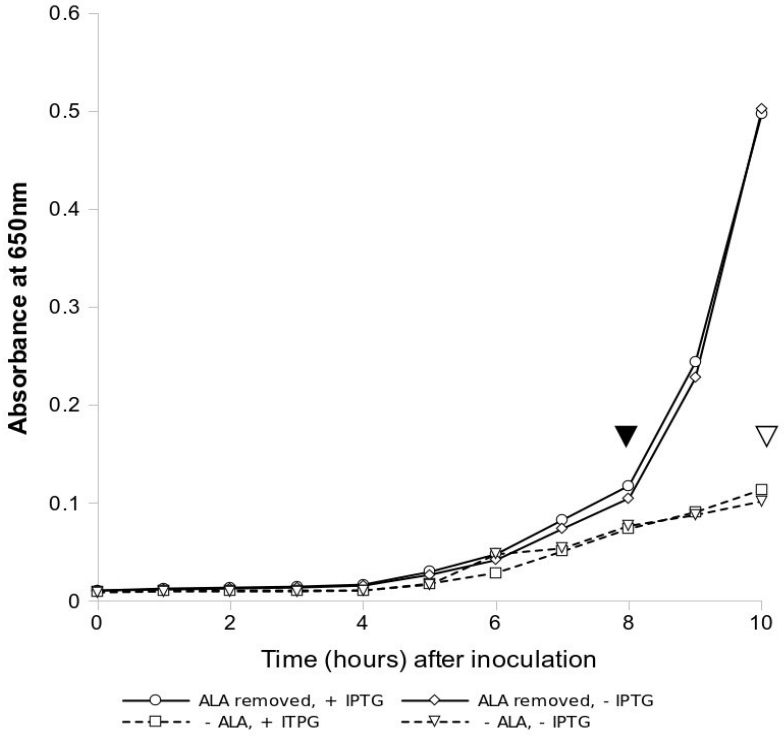

Figure 4.3b - The effect of the presence and absence of ALA in the starter culture on subsequent growth curves. This Figure illustrates the effect of adding no ALA to the starter culture compared to adding ALA to the starter culture and subsequent addition or non-addition of IPTG. Induction times for the +IPTG condition where ALA was removed and ALA was not present are indicated by ▼ and ▽ respectively.

Activity measurements were taken from the samples shown above (membrane-bound recombinant AOX only) after harvest (optical density at harvest not shown in Figures 4.3a and 4.3b) and are shown in Table 4.4 below. Final IPTG concentrations of 25, 50, 75 and 100μM were investigated and the results are shown below in Table 4.5.

Condition	Specific activity (µmols/min/mg)	Total activity (µmols/min)	Total protein (mg)
+ ALA, no removal, + IPTG	0.72	7.92	11
+ ALA, no removal, - IPTG	0.002	0.024	12
+ ALA, removal, + IPTG	1.10	14.3	13
+ ALA, removal, - IPTG	0.001	0.012	12
- ALA, + IPTG	0.11	0.88	8
- ALA, - IPTG	0.00	0.00	7

Table 4.4 – The effect of ALA on activity of membrane-bound recombinant AOX. This Table shows the effect on activity of membranes isolated from FN102 cells +/- ALA, +/- ALA removal, and +/- IPTG (200ml cultures).

IPTG Concentration (µM)	Total protein in membrane fraction (mg)	Specific activity of membrane fraction(µmols/min/mg)	Total activity of membrane fraction (µmols/min)
25	12	0.03	0.36
50	8	0.11	0.89
75	6	0.07	0.47
100	4	0.12	0.49

Table 4.5 – The effect of IPTG on activity of membrane-bound recombinant AOX. This Table shows the effect of IPTG concentration on total and specific activity of subsequent membrane fraction of recombinant *S. guttatum* alternative oxidase in FN102 cells. 35mM duroquinol was used as substrate.

4.3.2 Factors affecting solubilisation and purification

4.3.2.1 Factors affecting solubilisation

In order to solubilise the membrane fraction, and release the recombinant *S. guttatum* AOX from the lipid layer, it was necessary to establish the localisation of the protein within the cell matter. This was achieved using Western blotting in conjunction with activity assays of the relevant fractions. The results are summarised below in Table 4.6

and Figure 4.4. Data shown is taken from single preparations of both C41 and FN102 strains typical of other preparations.

Fraction	Specific activity (µmol/min/mg)	Total activity (µmol/min)
Membrane C41	0.48	26
Supernatant C41	0.001	0.035
Membrane FN102	0.9	18
Supernatant FN102	0.002	0.014

Table 4.6 – Activity distribution in membrane and supernatant fractions from membrane harvest.

The detergents tested and the corresponding activities (all taken from the same preparation of membrane-bound recombinant *S. guttatum* AOX expressed in FN102) are shown below in Table 4.7, comparing activity in the soluble (supernatant) and insoluble (pellet) fractions. The accompanying SDS PAGE gel in Figure 4.5 shows the effect of the detergents in Table 4.7 on sample composition.

DDM was further tested in varying concentrations, with differing incubation and centrifugation run times and speeds. The results are summarised below in Tables 4.8a and 4.8b. A Western blot showing the soluble and insoluble fraction following solubilisation with 1% DDM is shown below in Figure 4.6.

	Specific activity (µmol/min/mg)	
Detergent	**Soluble fraction**	**Insoluble fraction**
1% DDM	0.128	0.041
1% DDM, 200mM NaCl	0.246	0.076
1% DDM, 20mM $MgSO_4$	0.062	0.053
0.1% TRITON X-100	0.040	0.052
1.4% OG	0.020	0.533
0.1% DeoxyBigCHAP	0.087	0.071
3% Digitonin	0.274	0.267
0.1% Tween-20	0	0

Table 4.7- The effect of detergent on activity post membrane solubilisation. All measurements refer to a single preparation of membrane-bound *S. guttatum* AOX expressed in FN102, using the Lowry (1951) estimation method.

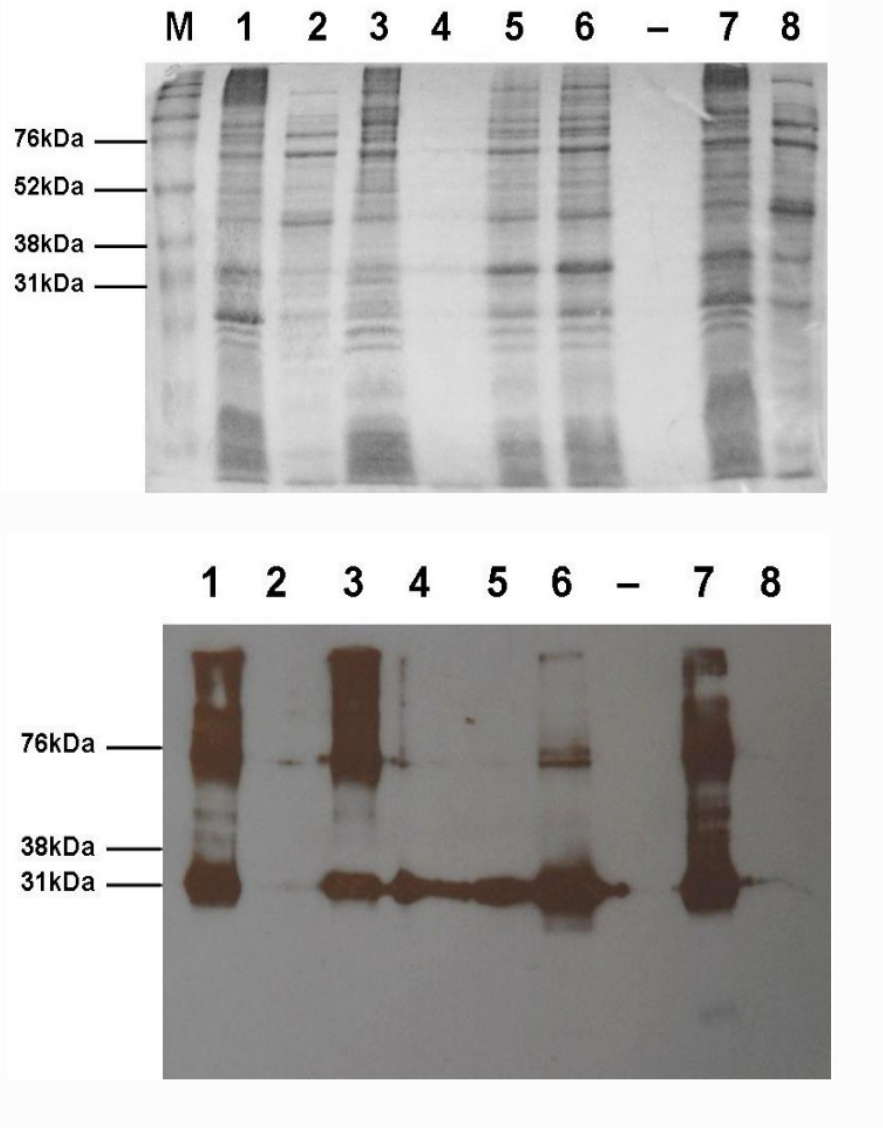

Figure 4.4 – Presence of recombinant AOX during each stage of harvest on SGS-PAGE gel and Western blot. In this Figure, an SDS-PAGE gel (top) and Western blot (bottom) show the presence of the recombinant *S. guttatum* alternative oxidase in the membrane (1) and supernatant (8) fractions during and following membrane harvest: recombinant protein present in the unlysed culture (4); re-suspended cell pellet following initial centrifugation (6); lysed cells (sonication); (5); and top (2) and bottom (3) ultracentrifuge fractions. (-) indicates a gap between lanes 6 and 7. Samples shown are recombinant *S. guttatum* alternative oxidase expressed in C41, using the Berthold (1998) growth and harvest protocol. All lanes contain 15µg of protein. The dark bands present at approximately 76kDa are most likely dimeric recombinant *S. guttatum* alternative oxidase protein.

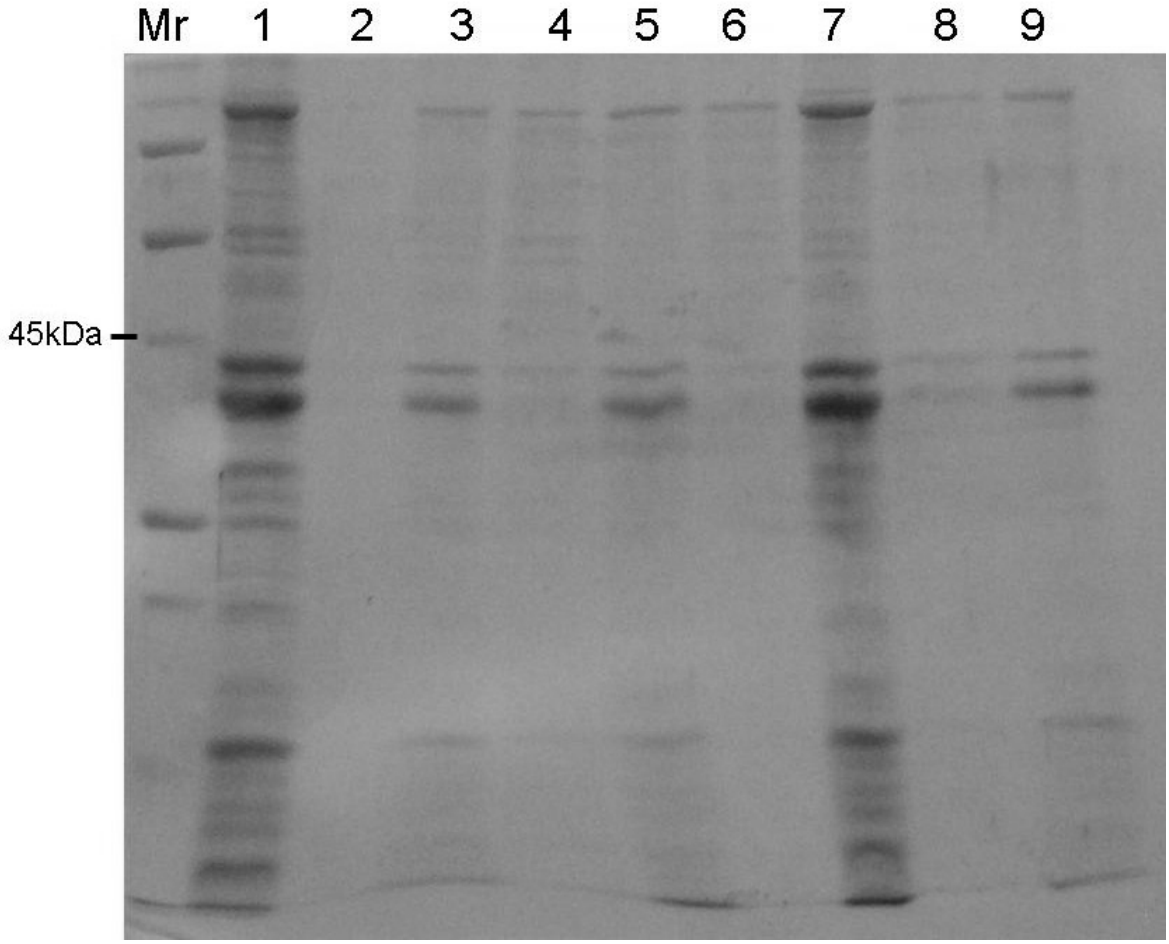

Figure 4.5 – SDS-PAGE gel of solubilisation of recombinant membrane-bound AOX by various detergents. This Figure of an SDS PAGE gel shows the resultant soluble (SN) and insoluble (PPT) fractions following solubilisation with detergents. Lanes: Mr. Marker 1. Membrane; 2. SN Tween-20; 3. PPT Tween-20; 4. SN TritonX-100; 5. PPT TritonX-100; 6. SN DeoxyBigChap; 7. PPT DeoxyBigChap; 8. SN Digitonin;9. PPT Digitonin. All lanes contain protein from the same preparation of membrane-bound recombinant *S. guttatum* AOX expressed in FN102 Concentration of detergents listed reflects those in Table 4.7 above.

Final % of DDM (*w/v*)	Specific activity (µmol/min/mg)
0	0.023
0.75	0.018
1	0.531
1.5	0.130
2	0.274

Table 4.8a – The effect of final DDM concentrations on specific activity. Activities shown correspond to solubilisation with DDM on membrane samples from the same membrane preparation (recombinant *S. guttatum* AOX expressed in C41). 35mM duroquinol was used as substrate.

Conditions		Activity (µmol/min/mg)	
Incubation time (mins)	**Spin time (mins)**	**Soluble fraction**	**Insoluble fraction**
<30	<30	0.001	0.02
30	<30	0.002	0.019
30	60	0.489	0.001
60	30	0.102	0.007
60	60	0.106	0.002

Table 4.8b – The effect of incubation and spin time on activity of solubilised membrane. This Table shows the effect of incubation time and centrifugation spin time on activity of recombinant *S. guttatum* AOX-containing membrane sample expressed in C41 and solubilised with 1% (*w/v*) DDM. 35mM duroquinol was used as substrate**.**

Figure 4.6 – Westen blot showing the soluble (S) and insoluble (IS) fractions after solubilisation with 1% DDM. Sample corresponds to the data shown in Table 4.8a. The dark band present above the 38kDa marker is most likely dimeric recombinant *S. guttatum* alternative oxidase protein.

4.3.2.2 Buffers and additives

Several metal-based buffer additives were tested in order to either stabilise the recombinant protein or otherwise maintain activity during solubilisation and purification. The additives investigated are detailed in Table 4.9 below, illustrating the effect of each additive in the solubilisation buffer.

	Specific activity (µmols/min/mg)	
Additive	+	-
100mM $MgSO_4$	0.498	0.520
200mM $ZnSO_4$	0.001	0.520
150mM $FeSO_4$	0.031	0.520

Table 4.9 – Effect of metal sulphates on specific activity of solubilised recombinant *S. guttatum* AOX. This Table details the effect on specific activity of solubilised protein by the addition of various metal-based additives to the purification and assay buffers. Data corresponds to solubilised recombinant *S. guttatum* AOX expressed in C41 from a single membrane preparation. 35mM duroquinol was used as substrate.

The effect of glycerol concentration on alternative oxidase activity is shown below in Table 4.10.

4.3.2.3 Purification

A number of conditions were tested when purifying recombinant protein and the most effective is summarised below in Figure 4.7. A purification table (Table 4.11) is shown below. SDS PAGE and Western blots showing the membrane, flow-through, wash and eluate fractions using the protocol shown in Figure 4.7 is shown below in Figure 4.8, along with an early attempt at purification for comparison.

% Glycerol	Specific Activity (µmol/min/mg)	Total Activity (µmol/min)	Total Protein (mg)
Membrane	1.43	49.3	34
20	0.32	7.04	22
10	0.31	7.13	23
7.5	0.30	5.7	19
5	0.31	7.13	23
Membrane	1.00	30	30
2.5	0.24	4.32	18
1	0.25	4.75	19
0	0.17	3.74	22

Table 4.10 – The effect of final glycerol concentration on activity of solubilised membrane samples. This Table shows the effetc of glycerol concentration on solubilised recombinant *S. guttatum* AOX expressed in FN102 compared to the membrane fractions from which they were solubilised. Samples were solubilised using 50mM TRIS pH 7.5, 100mM $MgSO_4$, 10mM pyruvate, 1% DDM and 35mM duroquinol was used as substrate.

Fraction	Specific activity (µmols/min/mg)	Total activity (µmols/min)	Total protein (mg)	Purification factor	% recovery
Membrane	0.91	29.7	32.5	-	-
Soluble	0.93	29.5	31.5	1	99
Pooled eluate	20.6	14.6	0.71	22.6	49

Table 4.11 – Purification table for recombinant *S. guttatum* AOX expressed in FN102. This purification table shows activities observed when following the purification protocol as given below in Figure 4.5. Purification factor refers to the factor increase of specific activity compared to the specific activity of the membrane. % recovery refers to the percentage of total activity compared to the total activity of the membrane faction. Activities shown here correspond to samples on SDS-PAGE gel and Western shown below in Figure 4.8.

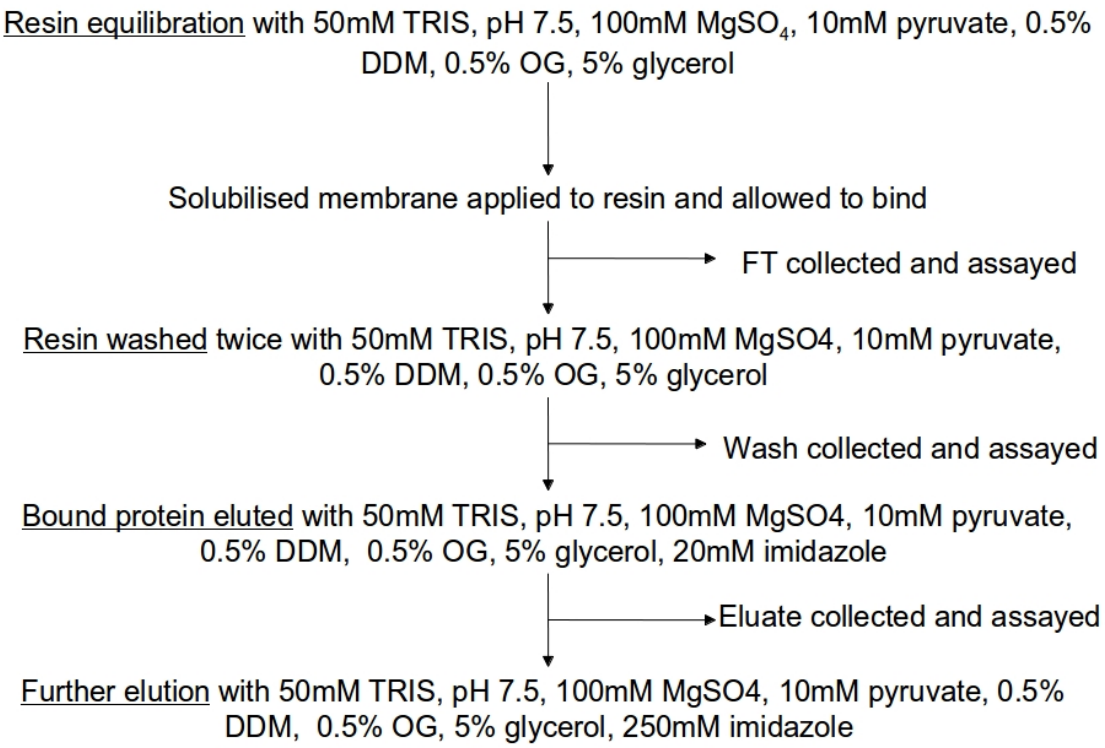

Figure 4.7 – Purifcation workflow. This Figure summarises the final buffer combinations used during the stages of purification for recombinant *S. guttatum* AOX expressed in FN102.

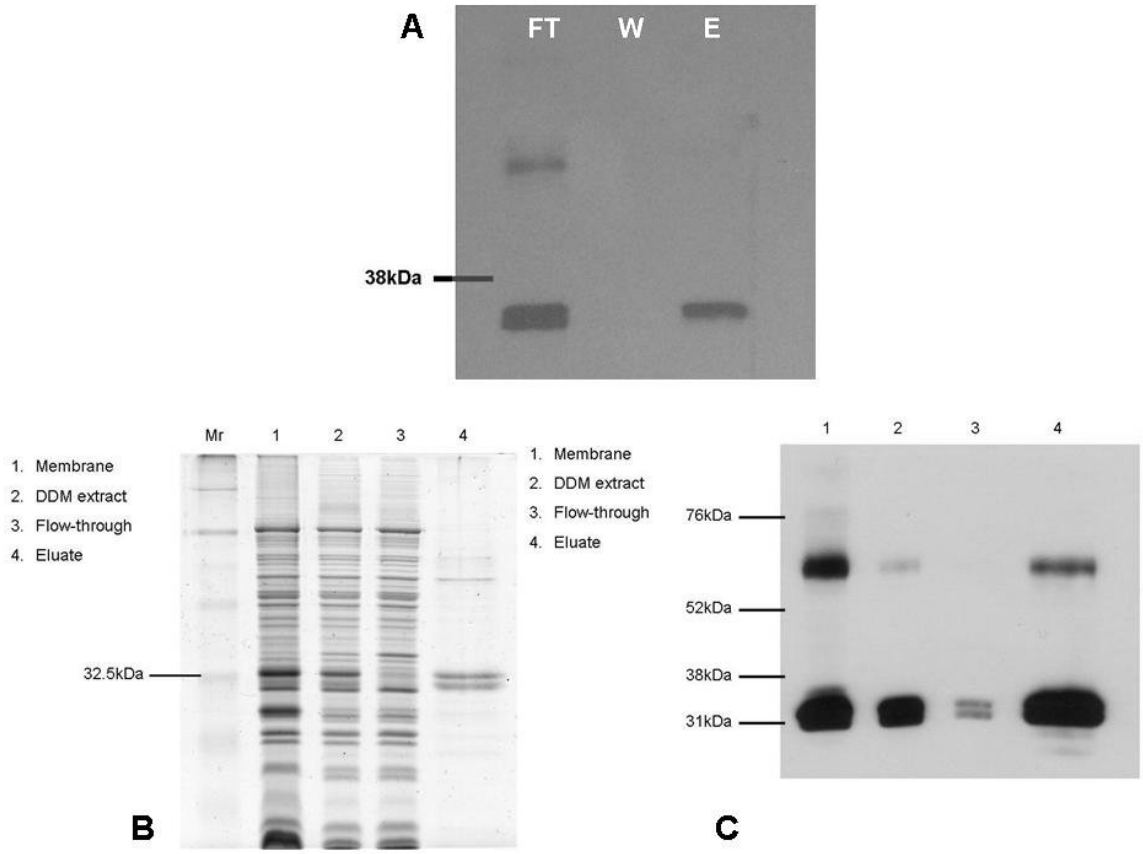

Figure 4.8 – SDS-PAGE gel and Western blots of purified recombinant *S. guttatum* AOX expressed in FN102. A: Western blot showing early attempts at purification (FT flow-through, W wash, E eluate) compared to later attempts (B and C) using the protocol shown above in Figure 4.6. Samples shown in parts B and C correspond to activities listed in Table 4.11 (Mr = marker). The dark bands present between the 76kDa and 52kDa markers are most likely dimeric recombinant *S. guttatum* alternative oxidase protein.

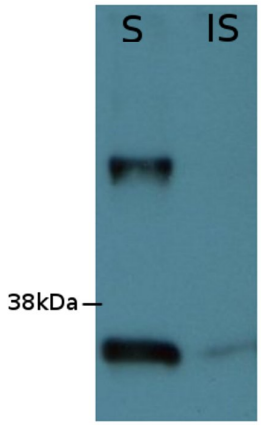

4.3.2.4 The effect of pyruvate on activity

Membrane-bound *S. guttatum* alternative oxidase expressed in FN102 was assayed in the absence and presence of pyruvate. Table 4.12a demonstrates the difference in activity observed in the absence of pryuvate and the presence of 10mM pyruvate in either the assay buffer, the extraction buffer, or both. 150mM Q_1H_2 was used as the substrate, and inhibition of at least 95% by 100nM ascofuranone was demonstrated in each assay.

	Protein (mg/ml)	**Total protein (mg)**	**Specific activity (µmols/min/mg)**	**Total activity (µmols/min)**
Membrane (-)	3.5	5.6	0.5	2.7
Membrane (+A)	3.5	5.6	0.6	3.2
Membrane (+E)	1.9	1.9	2.1	4.0
Membrane (+AE)	1.9	1.9	3.0	5.7

Table 4.12a – The effect of pyruvate on recombinant *S. guttatum* AOX expressed in FN102. This Table demonstrates the effect on activity of the absence of pyruvate (-), 10mM pyruvate added to the assay buffer (+A), 10mM pyruvate added to the extraction buffer (+E) and 10mM pyruvate added to both extraction and assay buffers (+AE).

Table 4.12b below shows the effect of differing the pyruvate concentration in the assay buffer only. The membrane sample assayed had a concentration of 3.5mg ml^{-1} and a total protein of 5.6mg.

The effect of adding 10mM pyruvate to the assay buffer alone when assaying various purification fractions was also monitored and the results are shown below in Table 4.13.

Figure 4.9 below shows the absorbance at 278nm of recombinant membrane-bound *S. guttatum* alternative oxidase in the presence of 150µM Q_1H_2 substrate.

Pyruvate added (mM)	Specific activity (µmols/min/ mg)	Total activity (µmols/min)
0	0.5	2.7
1	0.4	2.1
10	0.6	3.2
15	0.6	3.2
20	0.4	2.4
25	0.5	2.7
50	0.4	2.1

Table 4.12b – The effect of pyruvate concentration on activity of recombinant *S. guttatum* AOX expressed in FN102. The Table demonstrates the effect on specific and total activities when adding pyruvate to the assay buffer. Protein concentration was estimated using the Lowry (1951) method.

		Specific activity (µmols/min/mg)		Total activity (µmols/min)	
Fraction	**Total protein (mg)**	**-**	**+**	**-**	**+**
Membrane	5.6-, 1.9+	0.5	2.1	2.7	4.0
Soluble	0.44-, 0.26+	0.02	3.8	0.01	1.0
Eluate	0.02-, 0.01+	0.12	4.2	0.024	0.042

Table 4.13 – The effect of pyruvate on activity during each stage of purification. This Table shows the effect of adding 10mM pyruvate to the assay buffer alone when assaying various fractions of recombinant *S. guttatum* AOX protein expressed in FN102. Protein concentration was estimated using the Lowry (1951) method.

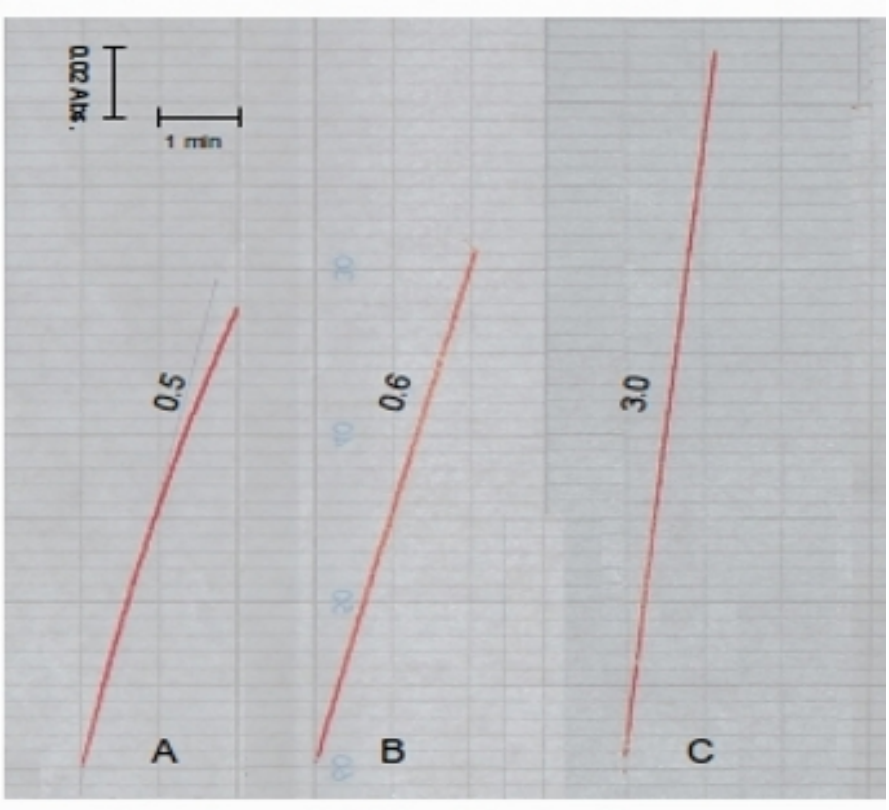

Figure 4.9 – Spectrophotometric trace of the specific activities of recombinant *S. guttatum* AOX protein samples expressed in FN102. This trace shows specific activity (the numbers above each absorbance slope represents specific activity in μmols/min/mg) for several recombinant *S. guttatum* alternative oxidase fractions: A membrane isolated in the absence of pyruvate with no pyruvate added to the assay buffer (Table 4.12a); B membrane isolated in the absence of pyruvate with 10mM pyruvate added to the assay buffer (Table 4.12a); C membrane isolated in the presence of 10mM pyruvate with 10mM pyruvate also present in the assay buffer (Table 4.12a).

4.3.2.5 Downstream processing

In order to concentrate the purified protein several methods were tested as summarised below in Tables 4.14a and 4.14b.

Method	Result
Dialysis	All activity lost, protein precipitated
Ammonium sulphate precipitation	Some of the protein activity retained, although trace $(NH_4)_2SO_4$ was undesirable for downstream protocols and negatively impacted on protein life-span
PEG precipitation	Most of the protein activity retained, and PEG easy to remove via centrifugation. See Table 4.13b below
Ultrafiltration (centrifuge method)	Protein consistently precipitated on filter, and significant protein amount and activity lost
Centrifugation	Results obtained were inconsistent, varying from good activity retention to total activity loss

Table 4.14a – Concentration methods used. This Table lists the various concentration methods used, and general results obtained.

Further to the results shown above in Table 4.14a, it was necessary to ascertain whether PEG had an inhibitory effect on the activity of the recombinant protein and several precipitations were carried out. Typical results are shown in Table 4.14b, and Figure 4.10 below.

Fraction	Total protein (mg)	Specific activity (µmols/min/mg)	Total activity (µmols/min)
Eluate	1.2	0.04	0.058
PEG SN	1.1	0.002	0.003
PEG PPT	0.1	0.122	0.012

Table 4.14b – The effect of PEG precipitation on the activity of purified recombinant *S. gtuttaum* AOX expressed in FN102. SN refers to supernatant and PPT refers to the pellet left following ultracentrifugation.

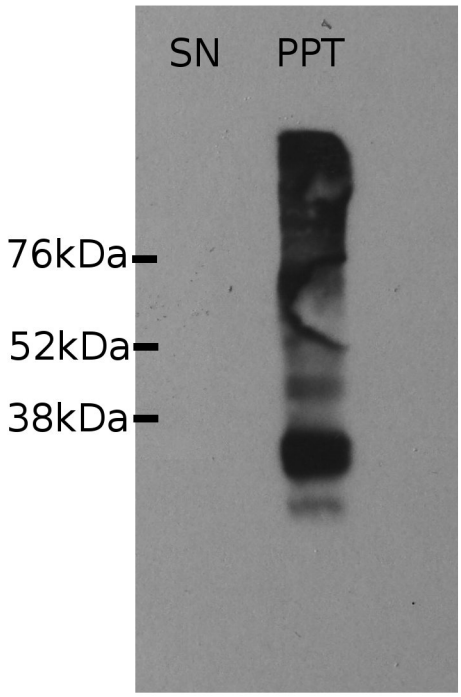

Figure 4.10 – Western blot of PEG precipitated purified recombinant *S. guttatum* AOX expressed in FN102. This Western Blot shows the presence of recombinant alternative oxidase in the PEG precipitation pellet (PPT) and absence in the PEG precipitation supernatant (SN). Sample shown corresponds to the activity shown above in Table 4.14b. The dark bands present above the 76kDa and between the 78kDa and 52kDa markers are most likely dimeric recombinant *S. guttatum* alternative oxidase protein.

4.3.2.6 Quantification, visualisation and activity monitoring of recombinant alternative oxidase

Two methods were used to estimate alternative oxidase concentration, namely the BCA and Lowry methods. In order to identify any differences in sensitivity, the protein content of an active membrane sample (FN102) was estimated on the same day using the two methods. In this case, the Lowry gave an estimation approximately one-fifth (8mg protein total) of that given by the BCA (42mg protein total). In addition when carrying out the BCA estimation method, control protein estimations were performed using buffer containing no protein, but treated in the same manner as experimental samples. These

estimations gave readings of approximately 0.001 at 562nm (0.002 max, 0.000 min). By comparison, the lowest BSA concentration standard, corresponding to 0.1mg/ml protein, had a typical absorbance of 0.202 (±0.021). To further ensure that protein estimation was accurate, any samples where absorbance was below 0.010 were repeated.

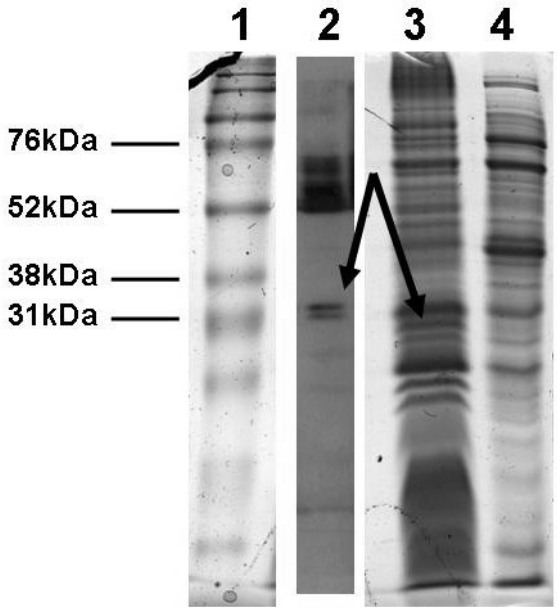

Figure 4.11 – Possible location of recombinant *S. guttatum* AOX expressed in FN102 on an SDS-PAGE gel and Western blot. This Figure shows the probable recombinant *S. guttatum* AOX band on an SDS PAGE gel and corresponding Western blot, as indicated by the arrows. Also observed is the double band often seen when running recombinant *S. guttatum* AOX on SDS PAGE gels. Lanes: 1 – markers; 2 – Western blot corresponding to lane 3; 3 – membrane-bound recombinant *S. guttatum* AOX; 4 – supernatant from membrane isolation. The dark bands present between the 76kDa and 52kDa markers are most likely dimeric recombinant *S. guttatum* alternative oxidase protein.

When conducting activity assays, ubiquinol-1 was the preferred substrate, although not in constant supply as it was donated by Professor Kita (University of Tokyo). Initially,

duroquinol and decylubiquinol were used in activity assays, but lower activity was recorded using these substrates for the same sample, as shown below in Table 4.15.

On each of the Western blots presented in this Chapter a higher-weight AOX species can be seen, typically between the 52kDa and 76kDa markers and above the 76kDa marker. This is thought to be a dimeric recombinant *S. guttatum* AOX which is present unless the protein was placed under reducing conditions.

Substrate	**Average Specific activity (µmols/min/mg)**	**Total activity (µmols/min)**
Ubiquinol-1	0.90 (0.11)	18.0
Duroquinol	0.51 (0.05)	10.2
Decylubiquinol	0.35 (0.13)	7.0

Table 4.15 – The effect on activity of recombinant *S. guttatum* AOX protein of three substrates. This Table shows the specific and total activity observed in one sample using three different substrates. The sample was taken from recombinant *S. guttatum* alternative oxidase expressed in FN102 in the membrane-bound form, containing 20mg total protein. Standard deviation is indicated in the specific activity column.

4.4 Discussion

4.4.1 Strains and growth conditions

It has been possible to successfully express and harvest protein from two *E. coli* expression strains, C41 and FN102 (Table 4.1).

4.4.1.1 C41

Following the Berthold (1998) growth and harvest method for the C41 strain, little refinement of the original protocol was required to produce consistent quantities of recombinant protein (Table 4.1) targeted to the cytoplasmic membrane (Figure 4.6). The optimal concentration of IPTG required for induction of C41 cells expressing recombinant *S. guttatum* was ascertained (25µM, Table 4.3), resulting in consistent protein concentration and specific activity. Furthermore, growth of the main culture post-inoculation and pre-induction (4 hours at 30ºC and 1 hour at 18ºC) appears consistent over a number of

preparations (Figure 4.1). After evaluation of the data shown in Table 4.4, the Berthold (1998) method was selected for all further growth of C41 cultures. The method as defined by Fukai *et al*. (1999) was not used since it consistently produced lower protein concentration and specific activity than the protein produced by C41 cells expressed using the Berthold (1998) method.

4.4.1.2 FN102

The previously defined protocol for over-expression and membrane harvest of FN102 cells expressing recombinant TAO (Nihei *et al*., 2003) has been successfully adapted to express recombinant *S. guttatum* AOX (Table 4.1). Use of 50μM of IPTG to induce FN102 cells expressing recombinant *S. guttatum* alternative oxidase appears to be optimal, giving the highest total activity and sufficient protein content (Table 4.5).

In agreement with previous findings (Chaudhuri *et al*., 1998; Nihei *et al*., 2003) the addition of ALA to agar plates and starter culture is required for FN102 growth. A lack of ALA results in significantly decreased cell growth and subsequent activity as shown in Figure 4.3b and Table 4.4. Retaining ALA in the media leads to increased growth rate, but halves the recombinant AOX activity indicating that whilst the cells are able to express the haem-COX proteins and subsequently the recombinant alternative oxidase after induction, expression of the recombinant AOX while the other COX proteins are present is shown to be decreased. This is demonstrated by reduced AOX specific activity observed in the membrane fraction where ALA was not removed compared to the membrane fraction where the ALA was removed, whilst the total protein concentration remains similar in both conditions (Table 4.4). The reason for this is unclear; it could be assumed that following induction, growth of the FN102 cells without ALA removal should increase more than that of the cells where the ALA had been removed given the additional oxidative role the recombinant protein is performing. However, as this is not directly linked to energy production, there may be additional factors acting on the cells that would explain the observed protein behaviour. For example, when the ATP supply is likely to be steady and

adequate where membrane redox potentials are close to normal for *E. coli* (i.e. when ALA is present and not removed), then the activity of the recombinant protein is reduced, although it is unclear how this may occur. Crucially, in FN102 cells expressing recombinant *S. guttatum* AOX, the time taken to reach the required optical density of 0.1 (at 650nm) after inoculation appears to be longer and more variable than the times given for FN102 cells expressing recombinant TAO (between 2 and 8 hours for *S. guttatum* compared to between 2 and 4 hours for TAO, Nihei *et al*., 2003). Since expression of recombinant AOX in both this project and the previously published work (Nihei *et al*., 2003) is under the tight control of the T7 promoter, with cells grown in lactose-free, glucose-containing media prior to induction, this difference in pre-induction growth cannot be attributed to isoform-specific differences in alternative oxidase protein activity. However, the variation in time taken for FN102 cells expressing recombinant *S. guttatum* alternative oxidase may be explained by naturally fluctuating levels of COX protein production in the presence of ALA; COX activity may decrease after periods of high turnover or remain relatively stable after periods of moderate turnover. The former would produce ATP more rapidly, but levels would also be depleted more rapidly. The variation in time taken to reach inducible optical density results in a less-predictable growth protocol than is observed with C41 cells expressing recombinant *S. guttatum* AOX. Therefore, the growth of FN102 cells post-inoculation requires very careful monitoring of optical density.

4.4.1.3 Cell lysis

Two methods of cell lysis were used during this project – sonication and the French Press. Membrane samples prepared from the same growth, where half the resuspended harvested cells were sonicated and the remaining half lysed using the French Press, no significant difference in specific activity was observed (C41 cells when sonicated: 0.48μmols/min/mg, compared to the French Press: 0.52μmols/min/mg; FN102 cells when sonicated: 0.89μmols/min/mg, compared to the French Press: 0.90μmols/min/mg). Regarding the practicality of each method, there is a preference for the French Press when

the volume of re-suspended harvested cells is >50mls and sonication for volumes of <50mls. The French Press also offers more opportunity to visually assess the lysate for signs of effective lysis (i.e. clarification of the sample leaving the cell) and therefore repeat the lysing process should it appear that lysis has not been effective. However, care must be taken when using both sonication and the French Press as methods of lysis of cells expressing recombinant alternative oxidase, as excessive damage to the membrane during lysis may result in inactivation of the recombinant protein.

4.4.2 Solubilisation

It has been possible to ascertain a solubilisation protocol for the effective liberation of active recombinant *S. guttatum* alternative oxidase resulting in 99% recovery of total acitivity from the membrane fraction (Table 4.11). The protocol consists of the drop-wise addition of solubilisation buffer to the membrane fraction (50mM TRIS-HCl, pH 7.5, 1% (*w/v*) DDM, 10mM pyruvate, 100mM $MgSO_4$, 5% (*v/v*) glycerol), followed by 30 minutes incubation with gentle stirring at 4°C and ultracentrifugation at 200,000 x *g* for 30 minutes at 4°C. After ultracentrifugation, the soluble fraction consistently contains the recombinant alternative oxidase, as verified by activity (Table 4.8b) and Western blotting (Figure 4.6). Previous attempts to solubilise recombinant TAO (Nihei *et al*., 2003) stipulate the requirement for 1.4% (*w/v*) OG, 20% (*v/v*) glycerol and 100mM $MgSO_4$; as such, the DDM and pyruvate are specific requirements for the solubilisation of the *S. guttatum* alternative oxidase. Given the similarity between *S. guttatum* alternative oxidase and TAO, it was unexpected that OG should be so ineffective at liberating recombinant *S. guttatum* AOX protein from the membrane (Table 4.7). Whilst both DDM and OG are mild, non-ionic detergents, DDM has a larger head-group and longer alkyl chain than OG and therefore DDM forms larger micelles than OG (*cf* Baron and Thomson, 1975; Rosevear *et al*., 1980; Maire *et al*., 2000). These differences could suggest that TAO and *S. guttatum* alternative oxidase may have different requirements for lipophilic/hydrophobic association contributing to overall protein stability. However, as OG is known to decrease activity in

some proteins (Maire *et al*., 2000) continued use of DDM for solubilisation is preferable. The 1% (*w/v*) DDM (equivalent to 0.2mM) concentration used for the solubilisation of the *S. guttatum* alternative oxidase is greater than the CMC of DDM (0.17mM; *cf* Maire *et al*., 2000), which would allow for the formation of micelles. It is probable that the recombinant alternative oxidase molecules are at least partially enveloped by the DDM micelles; however, the exact extent of this interaction is not known. If required, the number of protein molecules per micelle could be further elucidated using analytical ultracentrifugation (*cf* Reynolds and Tanford, 1976).

Furthermore, if the recombinant protein molecules are partially embedded within the detergent micelles, this may increase the potential effect of the Mg^{2+} ions present in the buffer; if less protein surface area is solvent-accessible (i.e. buried in the detergent micelles), any Mg^{2+} ions binding to negatively charged groups will reduce the protein solvent-accessible surface area to an even greater extent. Addition of other sulphate salts (zinc and iron sulphate, Table 4.9) does not appear to stabilise recombinant *S. guttatum* alternative oxidase to the same extent as magnesium sulphate, indicating that it may be the magnesium ions rather than the sulphate ions which are stabilising the protein. However, magnesium sulphate alone does not increase activity, so it should be used in combination with DDM, pyruvate and glycerol for optimum effect.

4.4.3 Purification

A protocol has been defined within this project for the purification of recombinant *S. guttatum* alternative oxidase, resulting in 22-fold increase in specific activity from the membrane-bound fraction to the purified fraction and 49% recovery of total activity between the same fractions (Table 4.11). Using 1ml of nickel or cobalt affinity resin per 15mg of recombinant protein, at least three applications of 4x the bed volume of equilibration buffer (50mM TRIS-HCl, pH 7.5, 10mM pyruvate, 0.5% (*w/v*) DDM, 0.5% (*w/v*) OG, 100mM MgSO4, 5% (*v/v*) glycerol) should be used to equilibrate the affinity resin. The soluble fraction should be allowed to bind to the resin for no longer than 15

minutes at 4ºC and following collection of the flow-through, the resin should be washed twice with 5x the bed volume of wash buffer (as per the equilibration buffer, with an additional 25mM imidazole). A final elution buffer (as per the equilibration buffer, with 250mM imidazole) 3x the bed volume may be applied as a single step elution for volumes <4ml, or as a multiple step gradient (25mM-250mM imidazole) elution for volumes >4ml.

This protocol differs from the previously defined protocol for the purification of recombinant TAO (Nihei *et al*., 2003), which does not stipulate the requirement for pyruvate or a DDM-OG combination. As discussed previously, the optimum detergent appears to be isoform-specific; however, any detergent added after solubilisation is unlikely to be forming new micelles, as the concentrations required (0.5% (*w/v*) of both DDM and OG) are below their respective CMCs. The additional detergent may simply be beneficial through the encouragement of the perpetuation of existing detergent-protein micelles by ensuring any detergent molecules lost from the micelles may be readily replaced.

4.4.4 General factors affecting the over-expression, solubilisation and purification of recombinant *S. guttatum* alternative oxidase

4.4.4.1 The effect of pyruvate on recombinant *S. guttatum* alternative oxidase

By adding pyruvate – which would be abundant in the cell cytoplasm if Kreb's had been halted – to membrane-bound recombinant *S. guttatum* alternative oxidase, activity can be increased (Tables 4.12a and 4.13). If the pyruvate is added to the assay buffer alone, the increase is a relatively small 1.2-fold, however when adding pyruvate to the protein membrane extraction buffer, a 4-fold increase in activity is observed. Furthermore, if pyruvate is added to both the membrane extraction buffer and the assay medium, the activity is increased 6-fold. This is generally consistent with previous findings, namely that the addition of pyruvate to native alternative oxidase extracted from thermogenic tissue increases the alternative oxidase activity (Carré *et al*., 2011). This is the first time it has been demonstrated with recombinant *S. guttatum* AOX expressed in *E. coli*. There is a cautious acceptance that the stimulation by pyruvate of thermogenic alternative oxidase

isoforms occurs independently of expression system. However, whether this increase in activity is as a result of a conformational change remains untested, and the data presented in this thesis cannot confirm this suggestion.

Interestingly, before pyruvate was routinely added to the extraction and purification buffers, no inhibition of activity was observed, which is somewhat in contradiction with previously reported findings that an absence of pyruvate leads to the inactivation of the alternative oxidase (Carré *et al*., 2011). It may be that the concentration of endogenous pyruvate present in the *E. coli* cells prior to membrane extraction was sufficient to maintain activity, especially if the pyruvate is bound to the protein (as opposed to being free in the lysate) and did not dissociate during the process of extraction, solubilisation and purification. Similarly, lower than expected rates of activity in early purified recombinant *S. guttatum* AOX samples may have been in part due to depleting pyruvate levels. However, this does imply that at least some of the pyruvate was potentially still bound to the protein as activity was low, rather than absent (Tables 4.12a and 4.13). This supports the suggestion that the pyruvate molecules interact directly – through more than simply transient association – with the alternative oxidase protein.

4.4.4.2 Recombinant protein quantification

Accurate quantification of recombinant alternative oxidase in the membrane and soluble fractions has been a consistent frustration during the course of this project. Since the protein estimation accounts for the total protein concentration rather than recombinant protein concentration only, the estimated protein concentrations used to calculate specific activity were artificially inflated. As a result, the specific activites reported for the membrane and soluble fractions are likely to be lower than the actual activity. This has not been considered in previous attempts to assay recombinant alternative oxidase (*cf* Berthold, 1998; Chaudhuri *et al*., 1998; Fukai *et al*., 1999; Nihei *et al*., 2003).

An alternative method of recombinant protein quantification was considered; expression of GFP-tagged alternative oxidase was attempted, but the attempts were not

successful and were not taken forward. Additionally, quantification through coomassie intensity was attempted, although difficulty in accurately identifying bands on an SDS PAGE gel that corresponded solely to recombinant AOX made this method unreliable (Figure 4.11) and was not taken forward. One possible method for accurately quantifying protein concentration is the use of quantitative Western blotting using flourescence labelling (Bergendahl *et al*., 2003).

4.4.4.3 Downstream processing – protein concentration

As indicated in Table 4.14a, a number of techniques were investigated in order to identify the most effect method to concentrate purified protein samples. Of the methods investigated PEG precipitation proved to be the most effective, resulting in the retention of activity in the pelleted fraction post-centrifugation (Table 4.14b) and demonstrable localisation of the recombinant alternative oxidase to the same fraction (Figure 4.10). The pelleted fraction containing the concentrated recombinant alternative oxidase could also be readily frozen and stored at -80^{o}C until required, with virtually no activity loss observed over 12 months of storage. The other methods investigated (ammonium sulphate precipitation, ultrafiltration, dialysis and high-speed centrifugation) resulted in an unacceptable, irreversible loss of protein activity and so were not used.

4.4.4.4 Substrate preference

As shown in Table 4.15, a higher rate of specific activity is observed when ubiqinol-1 is used as a substrate compared to duroquinol and decylubiquinol in the spectrophotometric activity assays. This is in agreement with previous findings (Hoefnagel *et al*., 1997), but does indicate that when ubiquinol-1 is not available, either duroquinol or decylubiquinol may be used.

4.4.5 Isoform-specific differences in alternative oxidase protein activity

There are significant differences between the specific activity of the three main recombinant *S. guttatum* alternative oxidase fractions (membrane-bound, solubilised and purified, Table 4.11) and the specific activity of other alternative oxidase isoforms, both native and recombinant (summarised in Tables 4.16a and 4.16b below). Particularly noteworthy comparisons are recombinant TAO and native *A. maculatum* (Kido *et al*., 2010 and Affourtit and Moore, 2004 respectively), both of which reported specific activity values for a membrane-bound, solubilised and purified alternative oxidase isoform. For both *A. maculatum* and TAO, the specific activities observed in all fractions are considerably greater than those observed in the equivalent fractions of recombinant *S. guttatum* alternative oxidase. The higher activity exhibited by TAO may be an indication of the high turnover observed *in vivo*; during the blood-stream stage of the trypanosome life cycle when the organism produces ATP through glycolysis only, the TAO acts as the sole terminal oxidase turning over rapidly to reoxidise NADH to ensure glycolysis is sustained (Clarkson *et al*., 1989; Chaudhuri *et al*., 1995; Minagawa *et al*., 1996). The TAO is not subject to regulation, so given sufficient provision of substrate and a suitably lipophilic environment, the enzyme should function at maximum capacity both *in vivo* and *in vitro*. Moreover, TAO has a truncated N-terminal region compared to *S. guttatum* and *A. maculatum* and this region has previously been identified as important in regulation of the activity of many alternative oxidase isoforms (Crichton *et al*., 2005; Ito *et al*., 2011). However, the high turnover rate of the TAO cannot account for the considerably greater protein concentration observed during all stages of expression and purification of TAO compared to that of recombinant *S. guttatum* alternative oxidase. As the expression of recombinant alternative oxidase is controlled by the same promoter for both *S. guttatum* and TAO, the greater quantity of protein produced in FN102 cells expressing TAO may perhaps indicate that either TAO requires less cellular energy to synthesise than *S. guttatum* or that *S. guttatum* recombinant protein is subject to degredation at some point after synthesis. There is some evidence of *S. guttatum* presence in the non-membrane portion of

the cell lysate (Figure 4.4, lane 8) and furthermore there was no AOX activity observed in this fraction when assayed, suggesting degredation may be occuring.

By contrast, the higher activities observed in *A. maculatum* alternative oxidase extracted from native tissues to near homogeneity (Affourtit and Moore, 2004) cannot be explained by a difference in enzyme function – both *A. maculatum* and *S. guttatum* generate the heat required for pollination via the alternative oxidase. Although the two isoforms share 90% sequence similarity, the recent discovery and sequencing of a number of *A. maculatum* alternative oxidase AOX1 gene products expressed at different stages during the process of thermogenesis highlight important amino acid variations (Ito *et al*., 2011) in a region of the AOX previously identified as involved in regulation (Crichton *et al*., 2005). A three amino acid motif, QDC (found at positions 288-290 in the *S. guttatum* sequence) is thought to be responsible for pyruvate sensitivity (Crichton *et al*., 2005); in the recently sequenced *A. maculatum* AOX mRNAs however, the sequence is either ENV, QDT or QNT. Crucially, the *S. guttatum* sequence is the only alternative oxidase sequence to date that contains the QDC motif, which may account for the difference in observed activities presented below in Table 4.16a and above in Table 4.11. Additionally, it is likely that the rates presented by Affourtit and Moore (2004) are the result of the combined activities of two or more of the *A. maculatum* AOX1 gene products. As yet, the exact mechanism for regulation at this site is unknown, although pyruvate and other α-keto acids are thought to play a major role (Crichton *et al*., 2005). Furthermore, the activity assays performed on the *A. maculatum* samples were conducted in the presence of the detergent EDT-20 which is thought to stabilise the AOX protein (Affourtit and Moore, 2004; Carré *et al*., 2011).

Despite the considerable differences in specific and total activity observed in recombinant *S. guttatum* compared to native *A. maculatum* AOX and recombinant TAO, a greater percentage of the total activity (49%) can be retained when purifying *S. guttatum* AOX compared to native *A. maculatum* (31%) and is comparable to the recovery achieved by Kido *et al*. (2010) when purifying recombinant TAO (53%).

Fraction	Total activity (µmols/min)	Specific activity (µmols/min/mg)	Purification factor	% recovery	Total protein (mg)
Mitochondria	116 (58)	1.7 (0.85)	-	-	68
Soluble	84 (42)	5.8 (2.9)	3.4	81	16
Purified	36 (18)	64 (32)	38	31	0.57

Table 4.16a – Purification table for mitochondrial *A. maculatum* AOX. This Table shows total activity, specific activity, purification factor, % recovery and total protein for mitochondrial, solubilised and purified alternative oxidase isolated from *A. maculatum* tissues, adapted from Affourtit and Moore (2004). Total and specific activities refer to µmols of duroquinol consumed and the figures in brackets refer to µmols of O_2 consumed as quoted in the referenced research article. Purification factor indicates the factor by which specific activity is increased compared to the mitochondrial specific activity and % recovery indicates the % of total activity recovered compared to the total mitochondria activity.

Fraction	Total activity (µmols/min)	Specific activity (µmols/min/mg)	Purification factor	% recovery	Total protein (mg)
Inner membrane	3500	23.3	-	-	150
Soluble	2400	63.2	11	69	37.9
Purified	1860	207	35.4	53	8.95

Table 4.16b – Purification table for recombinant TAO expressed in FN102. This Table shows total activity, specific activity, purification factor, % recovery and total protein for inner membrane, solubilised and purified recombinant TAO expressed in FN102, adapted from Kido *et al*. (2010). Total and specific activities refer to µmols of substrate consumed when 150µM ubiquinol-1 was used as a substrate. Purification factor indicates the factor by which specific activity is increased compared to the inner membrane specific activity and % recovery indicates the % of total activity recovered compared to the total inner membrane activity.

4.4.6 Concluding remarks

For the first time, two different prokaryotic expression systems can be reliably used to express recombinant *S. guttatum* alternative oxidase protein. One system (C41) produces

a higher recombinant protein concentration, whilst the other system (FN102) produces recombinant protein which exhibits a higher activity, albeit in smaller quantities. Given the lower specific activity observed in protein expressed in the C41 strain, the FN102 strain is the better choice for expressing protein to use for kinetic profiling as the protein is more likely to reach V_{max}.

Recovery of total activity following solubilisation and purification of the recombinant protein is comparable with other recombinant alternative oxidases (TAO, Kido *et al*., 2010) and greater than the recovery of total activity of alternative oxidase from native tissues (Affourtit and Moore, 2004). The use of the detergent DDM for solubilisation of recombinant *S. guttatum* alternative oxidase is very effective. Furthermore, retaining a lower concentration of DDM and OG post-solubilisation appears to be important for maintaining recombinant protein activity and stability. Therefore, a concentration of 0.5% (*w/v*) of both DDM and OG should be used in conjunction with magnesium sulphate and glycerol in all post-solubilisation buffers. Crucially, pyruvate should be present in all buffers post-harvest, as pyruvate has the most positive effect on stability and activity of recombinant *S. guttatum* alternative oxidase.

Even when using similar growth, solubilisation and purification protocols, the specific activity observed in recombinant TAO is considerably higher than that observed in recombinant *S. guttatum* AOX. This indicates that the activity may be affected by protein structure, as there are differences in sequence, structure and activity *in vivo* between TAO and *S. guttatum* AOX. Although the optimised protocols are not suitable for scaling up much beyond volumes described herein, they can be repeated often with ease allowing quantities of active protein to be produced, pooled and stored. Whilst this approach has the disadvantage that protein quality may vary from preparation to preparation, there is less protein to be lost from one small preparation than there would be for one much larger preparation should an error occur.

With an expression and purification protocol optimised for recombinant *S. guttatum* alternative oxidase, this is a significant advancement towards producing protein for other

experimental procedures to further elucidate the structure and catalytic mechanism of the plant alternative oxidase.

Chapter 5

Structural Biology of the Alternative Oxidase

5.1 Background

The structure of a protein can be described on a number of different levels, from the specific order of amino acids as determined genetically, to the highly complex and stable tertiary and quaternary native states. It is possible to ascertain the global structure of a protein using methods such as X-ray crystallography, but to further probe the relationship between the structure and function of a protein, local structure must also be investigated. Whilst no crystal structure is available for any of the plant alternative oxidases, two TAO structures have been solved in recent months (Shiba *et al*., 2013). In addition, site-directed mutagenesis of key residues identified through sequence alignments has been gathered previously for a number of AOX isoforms, which has lead to the identification and predicted structures of the active site, the substrate binding pocket and the inhibitor binding site.

The results presented in this Chapter show for the first time analysis of the alternative oxidase secondary structure, and describe efforts to define a protocol for the crystallisation of the *S. guttatum* alternative oxidase, which has previously not been attempted.

5.1.1 Primary and secondary structure of the alternative oxidase

The primary structure of a protein is determined by the gene from which it has been transcribed. The amino acids, in specific order, are joined through covalent peptide bonds and unlike the secondary, tertiary and quaternary structures it is not subject to changes in state unless enzymatically cleaved. The primary structure of the alternative oxidase has been known for two decades, with the first amino acid sequence published in 1991 (Rhoads

and McIntosh; *S. guttatum*). To date, there are ~280 reviewed alternative oxidase sequences in the UniProt database (http://www.uniprot.org), from both prokaryotic and eukaryotic organisms. Early sequence alignments were carried out when relatively few sequences were known (*cf* Moore *et al*., 1995a) and areas of high conservation became immediately apparent. Additionally, similarities between alternative oxidase and diiron carboxylate sequences (as reported in Moore *et al*., 1995a and Moore *et al*., 1995b) were observed. Furthermore, the alternative oxidase appeared to share physical properties with diiron carboxylates (like methane mono-oxygenase, MMO) such as the absence of a spectroscopic signal above 340nm (Vincent *et al*., 1990; Wilkins 1992; and Lipscomb 1994), leading to the suggestion that the similar functions of the AOX and diiron carboxylate (the activation of molecular oxygen) might indicate that their structures may also be similar (Moore *et al*, 1995a). This was supported by the similarity observed in the structures (Nordlund *et al*., 1992) of several diiron carboxylate proteins (hemerythrin, Holmes *et al*., 1991; methane mono-oxygenase, Rosenzweig *et al*., 1993; and ribonucleotide reductase R2, Nordlund and Eklund, 1993). Whilst the number of monomers varies for each diiron carboxylate, the monomers have predominantly α-helical structure, with four helices lying anti-parallel to one another to form a scaffold for the diiron active site. Using homology modelling based on another diiron carboxylate, Δ^9-desaturase, Andersson and Nordlund predicted that the alternative oxidase active site was similarly constructed (Andersson and Nordlund, 1999).

Secondary structure, which is the formation of intrinsically coded, locally co-ordinated α-helices and β-sheets, is the result of hydrogen bonding. The resultant structures have regular geometry, as the amide bonds holding the residues together have restricted torsion angles (Ramachandran *et al*., 1963). Helices, for example, are permitted to adopt either 3.6_{13}, 3_{10} or π-helix conformation, with the latter two occurring less frequently in nature than the former. In the 3.6_{13} helix, often referred to simply as an α-helix, there are 3.6 amino acids per turn, which results in hydrogen bond formation between the backbone C=O group of the n^{th} atom of the chain and the backbone N-H group of every n^{th} + 4 residue. The lone pair of electrons found in the C=O group act as an acceptor to allow

hydrogen bonding to take place with the N-H group acting as the donor. One full hydrogen bond – spanning residue *n* to *n*+4 – contains approximately 13 atoms. The resulting helical structure has a square appearance when viewed lengthways through the core of the helix. This is the most commonly occurring helical conformation observed in nature.

By contrast, the 3_{10} formation, which occurs in nature less frequently, contains 3 residues per turn, and a single closed hydrogen bond loop spans 10 atoms. Bonding still occurs between the C=O and N-H groups, but the participating N-H group is found on the n^{th}+3 residue, rather than the n^{th}+4 residue as it is in the α-helix. The 3_{10} helix appears triangular when viewed lengthways along the core, and offers a more tightly packed conformation. In the π-helix, hydrogen bonding occurs between the C=O and N-H moieties found on the n^{th} and n^{th}+5 residues respectively. Recent research suggests that π-helices are more common than previously thought, and may play a role in the formation of kinks in α-helices of some active sites (Cooley *et al*., 2010). All three helices adopt a right-hand conformation in nature.

The physical construction of α-helices was both predicted (Pauling *et al.*, 1951) and verified experimentally (*cf* Kendrew *et al*., 1960). In 1983, Kabsch and Sander devised the Dictionary of Secondary Structure, and developed the algorithm "Define Secondary Structure of Proteins" (DSSP), which allows the user to assign secondary structure elements (SSE) within a 3D structure given the atomic coordinates. The DSSP algorithm identifies SSEs based on hydrogen bonding and atom geometry; for example it can assign α, 3_{10}, and π helices by calculating theoretical hydrogen bond energies between two residues (*n* + 4, 3 or 5 respectively) given their distance and the angle relative to each other. This algorithm cannot be used to predict secondary structure from sequence information, but the description of hydrogen bonding and atom geometry in a mathematical way has been an fundamental tool when taking a knowledge-based approach to structure prediction. Algorithms exist which are able to predict the propensity for any given sequence of amino acids to form particular secondary structure elements. Early calculations were based either on the frequency with which certain residues occur in each structure (Chou and Fasman,

1974) for example, or calculating probability both on residue frequency and the neighbouring amino acid residues (Garnier *et al*., 1978). Both algorithms have since been adapted and improved, and are freely available and widely used.

5.1.1.1 Determining secondary structure experimentally – circular dichroism

Secondary structure may be verified experimentally by a number of different methods, such as X-ray crystallography, nuclear paramagnetic resonance (NMR) spectroscopy and UV circular dichroism (CD). Of particular interest to this project has been X-ray crystallography and CD, and the latter has been used to estimate the extent of α-helical structure within the plant alternative oxidase protein.

CD is a spectroscopic technique in which the differential absorption of left- or right-hand circularly polarised light by chiral molecules, such as proteins, is monitored over several wavelengths. The data obtained, if correctly analysed, can provide information relating to the secondary structure of the protein under investigation (*cf* Chen *et al*., 1974; Chang *et al*., 1978; and more recently Whitmore and Wallace, 2004; Greenfield, 2006b). CD has been used successfully to investigate membrane proteins such as bacteriorhodopsin (*cf* Cogdell and Scheer, 1985). Furthermore, the limitations of using CD in the investigation of membrane protein secondary structure and the implications for data analysis have been described and critically evaluated (*cf* Wallace *et al*., 2003; Whitmore and Wallace, 2008). For example, shifts in the CD peaks associated with α-helices are observed between soluble and membrane proteins, especially when membrane proteins have been solubilised from their native membrane environments (Swords and Wallace, 1993). As such, careful interpretation of CD data obtained from membrane protein samples – whether membrane-bound or solubilised – is advised (Whitmore and Wallace, 2008).

In addition to providing information about the secondary structure of proteins, CD can be used to assess the thermal stability of proteins (Yadav and Ahmed, 2000; Greenfield, 2006a) by monitoring absorbance at a single wavelength (such as 222nm for α-helical proteins) from low to high temperature. If interpreted correctly, data obtained could

indicate not only the temperature at which a protein begins to unfold, but also the extent to which secondary structure is diminished after heating to 90ºC. This is of particular interest in the case of *S. guttatum* alternative oxidase, which is responsible for the dissipation of energy not coupled to ATP synthesis but released as heat during the process of thermogenesis (Meeuse, 1975; Meeuse and Raskin, 1988).

5.1.2 Tertiary and quarternary structure of the alternative oxidase

The tertiary structure of globular proteins is the native state where the elements of secondary structure are both brought closer together and stabilised through the sequestering of hydrophobic residues at the core of the molecule. This state may be further stabilised by the exclusion of water from the core, and formation of intra-molecular disulphide bonds in some cases. In addition, hydrophilic interactions between the solvent-exposed residues and the external environment aid in the maintenance of the compact structure. Relatively little is known about the tertiary structure of the alternative oxidase, and what is known is inferred from experimental evidence and algorithmic prediction.

As previously stated, in light of both homology modelling (Andersson and Nordlund, 1999) and recent TAO crystal structures (Shiba *et al*., 2013), the secondary structure elements of the AOX are highly likely to form an anti-parallel, four-helix bundle, accounting for the vast majority of the tertiary structure. Specific residues involved in stabilising hydrophobic interactions have not been identified. Predicted loop regions between the helices are relatively short and most likely relatively inflexible, aiding in the maintenance of tertiary structure stability. However, relatively little is known about the N- and C-terminal regions, which even in the TAO crystal structures appears to be unstructured. It has previously been suggestion that the N-region in particular – the region with the greatest sequence dissimilarity between species – may act to increase activity of the molecule through interaction with α-keto acids (Crichton *et al*., 2005) in some species. The exact mechanism for this has not been fully elucidated experimentally.

It is thought that the extent of the quaternary structure of most plant alternative oxidases is homodimerisation, which is responsible for regulation of activity (Moore and Seidow, 1991; Umbach and Seidow 1993) in many non-thermogenic species. Homodimerisation is facilitated by the formation of sulphide bonds between the two highly conserved cysteine (C122 in *S. guttatum* numbering) residues present in all plant sequences. In other organisms such as fungi and trypanosomes it is not clear whether homodimerisation occurs, as an equivalent conserved cysteine residue is absent. When both native and recombinant TAO has been purified, no evidence of dimerisation was observed on SDS-PAGE gels (*cf* Chaudhuri *et al*., 1998; Fukai *et al*., 2003). However, the recent structures of TAO show it as a homodimer – despite the absence of a conserved cysteine. This suggests the potential presence a second site for homodimerisation, which may also be applicable to other non-plant alternative oxidase structures.

Further to the regulation of alternative oxidase activity through dimerisation, stimulation by α-keto acids such as pyruvate is also thought to involve the conserved C122 residue (*cf* Rhoads *et al*., 1998 and Carré *et al*., 2011). It is thought that through the formation of a thiohemiacetal bond between the pyruvate and the C122 residue, the tertiary and potentially the quaternary structure of α-keto acid-sensitive alternative oxidase isoforms may be altered. Mutation of the cysteine 122 residue renders the protein insensitive to pyruvate (Rhoads *et al*., 1998), which confirms the importance of the residue, but not the exact mechanism by which the conformational change is facilitated or what the conformational change may be. This implies a certain amount of flexibility within the alternative oxidase structure exposed to the cytosol – which is perhaps aided by the stabilisation of the membrane-associated regions of the protein. It is widely acknowledged that proteins rarely have a fixed or inflexible single structural conformation; there is thought to be considerable movement associated with catalytic activity in ATP-synthase, for example (Boyer, 1975; Abrahams *et al*., 1994). Therefore, the relative flexibility within the cytosolic, non-membrane regions of the alternative oxidase structure is considered an

essential part of its structural biology and an intrinsic part of the structure-function relationship.

5.1.3 Structure-function relationships – mutants

Sequence homology data as analysed by Moore *et al*. (1995a) led to the identification of several conserved residues proposed to be essential to activity; this list was refined by Andersson and Nordlund (1999). When mutated, the six residues involved in the binding of the two iron ions in the active site (E178, E217, H220, E269, E319, H322) cause complete loss of activity in the protein, even though the protein is expressed (*cf* Albury *et al*., 2002). Mutation of the equivalent conserved residues in TAO causes the same loss in activity (Ajayi *et al*., 2002), suggesting that the active sites of the AOX and TAO isoforms function in the same way. Highly conserved residues outside of the active site have also been investigated through mutagenesis, and these are listed below in Tables 5.1a and 5.1b along with proposed function. The location of each mutant in the protein is illustrated in Figure 5.1.

5.1.4 The nature of alternative oxidase membrane association

When first exploring the primary structure of the alternative oxidase, Moore and Siedow (1991) performed an *in silico* hydrophobicity analysis of the AOX sequence which revealed that there were several regions of predominantly hydrophilic residues, and two large regions of hydrophobicity spanning ~25 residues. Initially it was proposed that the hydrophobic regions formed two membrane-spanning helices, with the active site comprised of several smaller helices located on the matrix-facing side of the mitochondrial membrane (Moore *et al*., 1995a), based on previous localisation experiments (Rasmusson *et al*., 1990). However in the subsequent homology model (Andersson and Nordlund, 1999) it was proposed that there were no transmembrane helices in light of similarities between the alternative oxidase and the diiron carboxylates, and that the protein was largely α-helical. The membrane association is now known to be monotopic, and the larger spans of

Residue and mutation	Function	Effect of mutation	Reference
T179A	Proximal to E178 (iron binding), found near active site	Decreases v_{max} and increases oxygen affinity	Crichton *et al*., 2010
W206F/Y	Radical formation	Inactive	Crichton *et al*., 2010
Q242N	Inhibitor/substrate binding in hydrophobic pocket between helices 2 and 3; possible membrane binding.	94% activity lost	Albury *et al*., 2010
N247Q		4% activity lost	
Y253F Y253A		F 39% activity lost; A 72% activity lost	
S256T		93% activity lost	
H261A	HR pair motif found in quinone-binding proteins; also in hydrophobic pocket between helices 2 and 3; possible membrane binding.	95% activity lost	Albury *et al*., 2010
R262K		94% activity lost	
E270N	Proximal to E269 (iron binding), found in active site	Inactive	Albury *et al*., 1998
Y275F	Radical formation	Inactive	Albury *et al*., 2002
Y299F	Radical formation	Retained 100% activity	Crichton *et al*., 2010

Table 5.1a – Previously mutated residues and the effect on activity once mutated. This Table lists previously mutated residues, their proposed function, and the effect of the mutation on activity. Where the expressed isoforms are inactive, expression was confirmed using Western Blotting. Residues highlighted in bold have been expressed as part of this thesis and the results are detailed in Section 5.3.5.

Residue	Function	Effect of mutation	Reference
C122E	Dimerisation site; site of probable α-keto acid interaction; potential interaction with oxygen	Constitutively active; insensitive to pyruvate	Rhoads *et al*., 1998
C122K/R (positive charge added)		Insensitive to pyruvate and succinate; more active than wild type in absence of pyruvate	Umbach *et al*., 2002
C122Q/L (uncharged)		Inactive	
C172A	Possible second dimerisation site; putative α-keto acid binding site	Oxygen affinty decreased	Albury *et al*., 2002; Crichton *et al*., 2010

Table 4.1b – The effect of mutating two key cysteine residues. This Table details previous mutagenesis of the two conserved cysteine residues involved in regulation of AOX activity. Residues highlighted in bold have been expressed as part of this thesis and the results are detailed in Section 5.3.5.

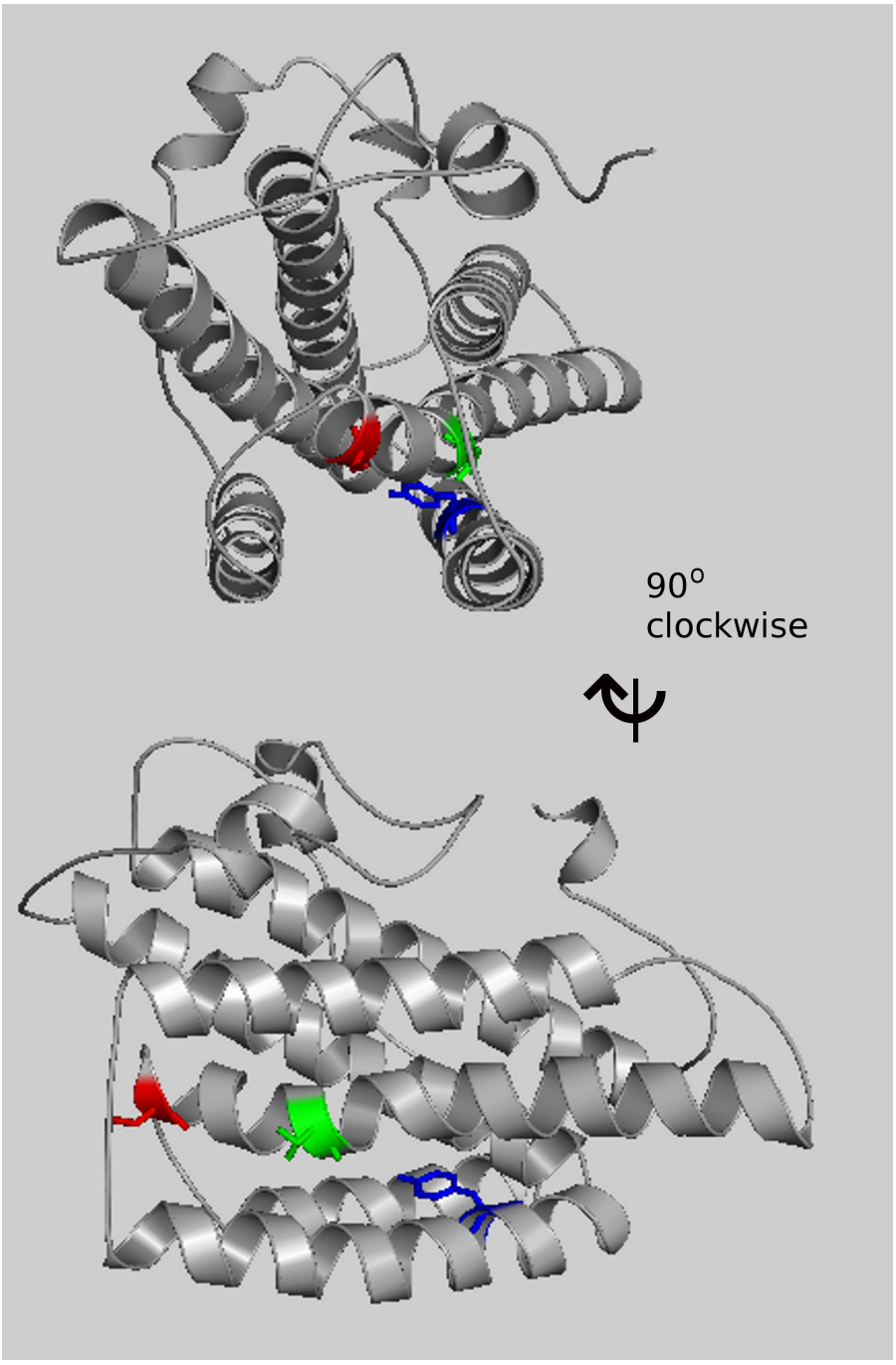

Figure 5.1 – A diagrammatic representation of three residues investigated in this thesis. This Figure shows the location of the mutated residues investigated during this project: C172 is shown in red; T179 in green, and Y253 in blue. The model was generated as described in Chapter 3, Section 3.2.3.

hydrophobicity are more likely to correspond to the substrate binding region (as the substrate is hydrophobic; *cf* Hoefnagel *et al*., 1997) rather than forming transmembrane helices.

In the absence of structural data, bioinformatic approaches may provide useful – albeit limited – information. In order to predict whether a protein contains transmembrane helices, for example, servers such as PredictProtein (*cf* Rost *et al*., 2004) are able to apply several algorithms to user-submitted sequences. Most of the prediction algorithms focus on larger areas of membrane association, such as transmembrane helices (see Nugent and Jones (2012) for a recent review); there are no specific algorithms to predict whether a protein is associated with the membrane in a monotopic manner, as is the case with the alternative oxidase. The lack of monotopic membrane prediction algorithms is partly because monotopic membrane proteins are not as clearly defined as some other protein-membrane association mechanisms (anchors or transmembrane helices for example) – though they are mainly included in training sets for machine learning approaches to membrane-association prediction in order to aid distinction between transmembrane and non-transmembrane proteins (*cf* Jayasinghe *et al*., 2001). Another factor in the lack of monotopic membrane prediction algorithms is the under-representation of monotopic membrane protein crystal structures in the relevant databases. Of the ~74,000 crystal structures available in the Protein Data Bank (PDB), only 65 are identified as monotopic membrane proteins – which represents 0.08% of the database. Included in the 65 structures is the prostaglandin H_2 synthase-1 protein (first solved by Picot *et al*., 1994, PDB reference 1PRH), which has previously been proposed as a template for the membrane-binding region of the alternative oxidase, as the diiron carboxylate structures used as templates for previous models (i.e. Andersson and Nordlund, 1999) are not membrane associated proteins, and therefore lack any membrane-binding regions.

5.1.5 Elucidation of the quaternary structure through crystallography

The first protein structure to be solved using X-ray crystallography was that of myoglobin in 1958 (Kendrew *et al*., 1958). The technique had previously been used to elucidate smaller biologically relevant molecules such as Vitamin B_{12} (Brink *et al*., 1954; Hodgkin *et al*., 1955), but elucidation of a structure several times larger than B_{12} presented a very different challenge.

The first stage in protein crystallography is the production of suitable protein crystals, which can be a time-consuming and non-trivial task. Suitably homogeneous, folded protein is mixed in small volumes with multiple screen solutions (often less than 1µl of protein to an equal volume of solution), covering a wide variety of pH, salt and precipitant concentrations and conditions. The protein-solution mixture can then be aliquoted on to a coverslip and placed above a reservoir containing a larger volume of the screen solution (hanging drop method) and sealed with a lubricant such as silicon grease. Alternatively, the protein-solution mixture can be placed on to a ledge next to a well containing a larger volume of the screen solution in a 96-well plate (sitting drop method). In both cases diffusion of vapour allows movement of molecules between the solution contained in the well and the solution in the sitting or hanging drop, encouraging protein aggregation and ultimately ordered precipitation. In order to achieve ordered precipitation, commercially prepared screen kits contain between 28 and 96 non-redundant solutions ranging from a sparse matrix of conditions previously successful for crystallising proteins (after Jancarik and Kim, 1991), to specialist screens tailored to specific protein classes such as membrane proteins (*cf* Newstead *et al*., 2008). While the protein is initially soluble within the screen solution, the protein solubility must be gradually decreased in order to cause ordered protein precipitation and crystal formation. Since protein solubility is effected by pH, salt concentration and the presence of solvents and precipitants (Chernov, 2003), it is these factors which are varied in crystal growth solutions. The effects of each factor are summarised above in Table 5.2.

Factor	Effect on protein solubility
Salts	Addition of kosmotropic salts (sulphates, phosphates etc.) decreases protein solubility through the removal of water molecules from the surface of the protein. This leads to protein aggregation and precipitation due to hydrophobic protein-protein attraction. Addition of chaotropic salts (iodide, lithium etc.) increases water-protein interactions, leading to increased protein solubility and often denaturation as concentration of the salt increases.
pH	Protein molecules in a solution with a pH above or below their p*I* will be repelled due to exposure of negative and positive charges respectively on the protein surface. Proteins close to their p*I* experience attractive forces, which contributes to the process of aggregation and precipitation.
Solvents	Addition of organic solvents such as alcohols results in protein aggregation and precipitation as water molecules are gradually removed from the surface of the protein, leading to hydrophobic attraction between protein molecules. However, addition of solvents may cause protein denaturation above 0^{o}C.
Other precipitants	Addition of polymers such as polyethylene glycol (PEG) leads to protein aggregation and precipitation through the removal of water molecules from the surface of the protein, causing hydrophobic attractions between protein molecules. Precipitants such as PEG are less likely to denature the protein at temperatures above 0^{o}C.

Table 5.2 – Factors which affect protein solubility.

Initially the individual crystallisation solutions containing the protein of interest are kept at a constant temperature with minimal movement to encourage nucleation. Nucleation is the process by which protein molecules begin to aggregate and align in a regular pattern required to generate crystals. The nucleation event may be as a result of a number of protein molecules aligning in a regular order whilst moving through the solution and forming a surface onto which more molecules may adhere (homogeneous nucleation). Alternatively protein molecules begin to adhere and align on a surface which is not made from other protein molecules (heterogeneous nucleation) such as silicon (Chayen *et al*., 2001). The rate of nucleation is dependent on both the number of clusters formed in the

early stages, which may take a few hours to form for some proteins or considerably longer for others; and the rate at which the protein molecules can diffuse through the solution towards existing clusters. Nucleation and subsequent crystal growth can be described using a phase diagram, which can be derived for a protein by varying the individual parameters for a particular screen condition (*cf* Haas and Drenth, 1999). Following nucleation, the protein molecules should continue to aggregate and align in a regular order in part initiated by the reduction in protein concentration as molecules forming the nuclei are removed from the solution. However, the conditions required for nucleation are often not the same as the conditions required for further crystal growth and it is at this point that the small sites of nucleation can be removed from the original drop solution and placed in a highly concentrated protein solution. The nuclei are transferred to the concentrated protein solution using a fine gauge needle and act as seeds for further crystal growth. Predictive models of the process of nucleation and subsequent crystal growth have been attempted (Rupp and Wang, 2004), although the models require large quantities of data from previously successful crystallisation conditions. As such the models cannot confidently be applied to proteins with no previous crystals, or those classes of protein which are under-represented in the database – especially membrane proteins (see Section 5.1.3.4 below; Rupp and Wang, 2004). Once conditions have been identified which consistently lead to nucleation and initial crystal growth, further optimisation is required. A range of new reservoir solutions can be created by gradually altering the original conditions one factor at a time, as illustrated in Table 5.3 below, to give a new matrix of conditions. Following optimisation and successful crystal growth, the process of collecting and analysing diffraction data can begin, the final result of which is the production of a three-dimensional description of the protein structure.

	pH	Salt concentration	Precipitant
Original	5.6	0.1M NaCl	30% PEG 400
Variation	4.6-6.6	0.1M NaCl	20-40% PEG 400

Table 5.3 – An example demonstrating the variants created from an original solution. In this example, 48 new, unique solutions were created.

5.1.6 The challenges of membrane protein crystallography

To date, there are in excess of 74,000 X-ray crystal structures available in the PDB. However, there is a distinct under-representation of certain classes of protein, such as membrane proteins. Of the ~600 structures identified as membrane-associated proteins in the PDB, just under half (281) are described as integral membrane proteins, suggesting that of the 74,000 crystal structures[3], only 0.8% are membrane-associated proteins, while just 0.38% are integral membrane proteins. Compared to the prevalence of membrane proteins within eukaryotic organisms – approximately 30% of the proteome corresponds to membrane proteins (Bill *et al*., 2011) – there is a clear discrepancy between natively expressed protein and solved structures within the database.

This does raise the question as to why there are so few membrane-associated protein structures in structural databases – is it due to lack of research interest, or are there other inhibitory factors involved? As far as the former is concerned, it is not down to a lack of interest or impetus; with membrane proteins playing vital roles in processes such as cell signalling and respiration, they are not a class of proteins of limited merit – indeed, they are often identified as important drug targets. So on to the latter, and the relatively well-documented difficulties associated with the crystallisation of membrane proteins.

The first membrane protein crystal structure was presented in 1985 – some 33 years after the first protein structure (Deisenhofer *et al*., 1985). While there are specific problems associated with expression of membrane proteins in hosts such as *E. coli* (as described previously in Chapter 4), there are further limitations experienced when expressing and

[3] As of September 2012; http://www.rcsb.org/

purifying membrane proteins for the purpose of crystallography (Carpenter *et al*., 2008). A major obstacle in the crystallisation of membrane proteins is the requirement of detergent for protein stability: membrane proteins often rely on areas of hydrophobicity for conformational stability, which is provided by the membrane. When extracting expressed recombinant protein from the membrane, detergent is required to disrupt the membrane itself. Whilst this is not necessarily problematic from the perspective of protein purification (as detergent can easily be incorporated into purification buffers), it is often inhibitory to the production of crystals as the resultant detergent-protein complexes can disrupt formation of well-ordered crystals (Privé, 2007). Therefore, the smaller the detergent micelle, the more likely successful crystallisation is; octyl-glucoside is preferred over dodecyl-maltoside for this reason. Additionally, the presence of detergent decreases the likelihood of sufficient protein aggregation and precipitation; the protein molecules sequestered in the detergent micelles may not be affected by the factors leading to precipitation described above in Table 5.2.

In order to avoid excessive use of detergent, lipidic materials may be incorporated into the crystallisation solutions, providing both sites of nucleation and a lipidic environment required for membrane protein stability (Landau and Rosenbusch, 1996; and more recently reviewed in Caffrey, 2009 and Cherezov, 2011). Such systems have proven successful in the field of membrane crystallography, with several structures solved in recent years using Lipidic Cubic Phase (LCP) techniques (notable examples are Katona *et al*., 2003 and Cherezov *et al*., 2007).

5.2 Methodology

5.2.1 Circular dichroism

Purified recombinant *S. guttatum* protein expressed in FN102 and TAO protein (provided by Dr Yasutoshi Kido, University of Tokyo, Japan) was concentrated using the PEG precipitation method as previously described in Chapter 2. When required the PEG precipitated pellets were gently thawed on ice and resuspended in chilled (4ºC) buffer,

before being loaded into a 1mm glass CD cuvette (Hellma). Absorption measurements were taken with a Jasco J715 spectrophotometer, and the block temperature was controlled using a Jasco Peltier-type system. Data was recorded using the Jasco Spectra Manager software suite and exported to Microsoft Excel or Gnumeric for analysis. Two experiments were conducted – multiple wavelength scans and single-wavelength variable temperature assays to asses secondary structure and thermal stability respectively.

In order to predict the percentrage of each secondary structure element from the raw CD data, three algorithms were used via the Dichroweb server (Whitmore and Wallace, 2008; http://www.dichroweb.cryst.bbk.ac.uk/html/home.shtml): K2D (Andrade *et al*., 1993), CDSSTR and SELCON3 (*cf* Sreerama *et al*., 1999; Sreerama and Woody, 2000). The K2D algorithm was selected as it did not require selection of a Reference set in order to perform the analysis. This was considered important because the Reference proteins used to generate the Reference sets provided by Dichroweb are all soluble proteins (with the exception of SMP180, described below) and therefore may be biased against membrane proteins (*cf* Wallace *et al*., 2003 and Whitmore and Wallace, 2008). The Reference set SMP180 (Abdul-Gader *et al*., 2011) does contain membrane proteins (albeit large and transmembranous proteins) and is suitable for use with the SELCON3 algorithm. It was not possible to analyse the TAO data using SMP180 Reference set, as it requires data from 180nm, whilst the TAO dataset contained data from 190nm and above only. The CDSSTR algorithm was chosen along with Reference set 4 (optimised for 190-240nm) as CDSSTR is considered relatively accurate (*cf* Whitmore and Wallace, 2004) as the algorithm selects reference proteins from the Reference set with similarities to the protein of interest (*cf* Sreerama and Woody, 2000) and the Reference set most closely matched the wavelength range of the *S. guttatum* AOX data where the HT was less than 600 volts.

5.2.2 Prediction of secondary structure

The *S. guttatum* protein sequence (UniProt accession number P22185; full sequence can be found in Appendix 1) was input into the programs listed below in Table 5.4 to predict secondary structure.

5.2.3 *In silico* investigation of dimerisation site

In lieu of experimental evidence confirming the nature of the dimerisation mechanism, an homology model of the *S. guttatum* alternative oxidase (based on TAO, see Chapter 3 Section 3.2.7) was studied in PyMOL (http://www.pymol.org) to assess the likelihood of dimerisation through salt bridge formation, hydrogen bonding networks and interfacial water hydrogen bonding. Other structures with non-sulphide dimer linkage were studied for comparison; especially those with a known monotopic membrane association such as external NADH dehydrogenase (PDB accession numbers 4G9K, 4GAP and 4GAV – all Iwata *et al*., 2012).

Program	Server/URL	Reference
PSIPRED 3.0	PSIPRED http://bioinf.cs.ucl.ac.uk/psipred/	Jones, 1999; Buchan *et al*., 2010
CFSSP	http://www.biogem.org/tool/chou-fasman	Chou and Fasman, 1974
GOR	NPS@ http://pbil.ibcp.fr/htm/index.php	Garnier *et al*., 1978; Combet *et al*., 2000
JPred3	http://www.compbio.dundee.ac.uk/www-jpred/	Cuff *et al*., 1998; Cole *et al*., 2008
PROFphd	PredictProtein http://www.predictprotein.org	Rost and Sander, 1993; Rost, 1996; Rost *et al*., 2004
PROSITE		Bairoch *et al*., 1997

Table 5.4 – Algorithms used to predict secondary structure for the *S. guttatum* alternative oxidase.

5.2.4 Crystallography

Protein for crystallisation screening was prepared using concentrated eluate (see Chapters 2 and 4) containing expressed recombinant alternative oxidase protein. Concentration was carried out using PEG precipitation (as described in Chapter 2) and final protein concentration was typically <10mg/ml. Initially, to ensure that the concentration was optimal, a pre-crystallisation test (PCT; Hampton Research) was carried out as per the manufacturer's guidelines.

Concentrated protein was then used to set up crystal screen trays using both hanging and sitting drop methods. 1µl of protein was used for both methods. A variety of screens were used in the laboratory of Dr Darren Thompson (University of Sussex, UK), the laboratory of Professor Kiyoshi Kita (University of Tokyo, Japan) and the laboratory of Professor So Iwata (Imperial College London and Diamond Light Source, UK). The screens used are listed below in Table 5.5. It should be noted that initial screens (at Sussex and Diamond) were chosen because they had been specially designed for membrane proteins, while the screens used in the Tokyo lab were recommended by Dr Shiba based on previous success when crystallising the TAO.

Sussex	Tokyo	Diamond
Mem Start (MD1-21)	CS I (HR2-110)	Mem Start (MD1-21)
Mem Sys (MD1-25)	CS II (HR2-112)	Mem Sys (MD1-25)
	MembFac (HR2-114)	Mem Gold (MD1-39)

Table 5.5 – Crystal screens. This Table shows the crystal screens used in the three labs where screening took place. The manufacturer (MD Molecular Dimensions; HR Hampton Research) and product reference number are shown in brackets.

In the laboratory at the University of Sussex, the hanging drop method was used (see Section 2.6.1), whilst at the University of Tokyo, the sitting drop method (see Section 2.6.2) was used exclusively. At the Membrane Protein Laboratory at the Diamond Light Source, both hanging and sitting drop methods were used. In all cases, the plates were

checked regularly and care was taken to avoid crystal degradation by excessive plate handling.

5.2.5 Expression of mutant isoforms

A variety of *S.gutattum* mutants were created by Dr Mary Albury (as detailed above in Tables 5.1a and 5.1b in bold and Figure 5.1) and expressed using FN102 *E. coli*. The purification of these recombinant mutant proteins was carried out as described in detail in Chapter 4, and assays were performed using 50mM TRIS, pH7.4 buffer. A substrate (ubiquinol-1) concentration of 150mM was used in each assay, and 100nM ascofuranone was used as the inhibitor. Assays were carried out on a Shimadzu UV-3000 spectrophotometer. SDS PAGE and Western blots were performed as previously described in Chapter 2.

5.2.6 Variable temperature activity assays

Membrane-bound and purified recombinant *S. guttatum* protein was assayed to determine the effect of temperature on AOX activity. The protocol as defined in Section 2.5.2 was modified to control buffer and protein temperature using a Fisher (DriBlock DB1, Techne) heating block prior to assay, Cary Temperature Controller connected to a Cary 400 spectrophotometer (Varian) to control the sample temperature for the duration of the assay. The inhibitor (octyl-gallate) was not heated due to the small quantity added to the cuvette; the substrate (ubiquinol-1) was not heated to avoid evaporating the acidified ethanol in which it was suspended. The assay buffer used in all experiments was 50mM TRIS, pH 7.5, 10mM pyruvate; 150mM of ubiquinol-1 was used as the substrate, with 1μM octyl-gallate used as an inhibitor.

5.3 Results

5.3.1 Circular dichroism

5.3.1.1 Wavelength scan

Figure 5.2a below shows mean residue ellipticity, [θ] (mdeg cm^2 $dmol^{-1}$) against wavelenght for purified recombinant *S. guttatum* alternative oxidase at a concentration of 5μM, whilst Figure 5.2b shows the same trace overlaid with purified recombinant TAO at a concentration of 4.25μM. Figure 5.4 shows the effect of varying TAO concentration on mean residue ellipticity.

Table 5.6 below shows the outcome of raw CD analysis by the K2D, CDSSTR and SELCON3 algorithms (as accessed via Dichroweb) along with the Reference protein set used. For K2D, wavelengths 200-260nm were selected (as the HT values shown in Figure 5.2a) exceed 600 volts for absorbance readings below 200nm; for CDSSTR wavelengths 190-240nm were used and for SELCON3, wavelengths of 180-240nm were used, as required by the algorithms.

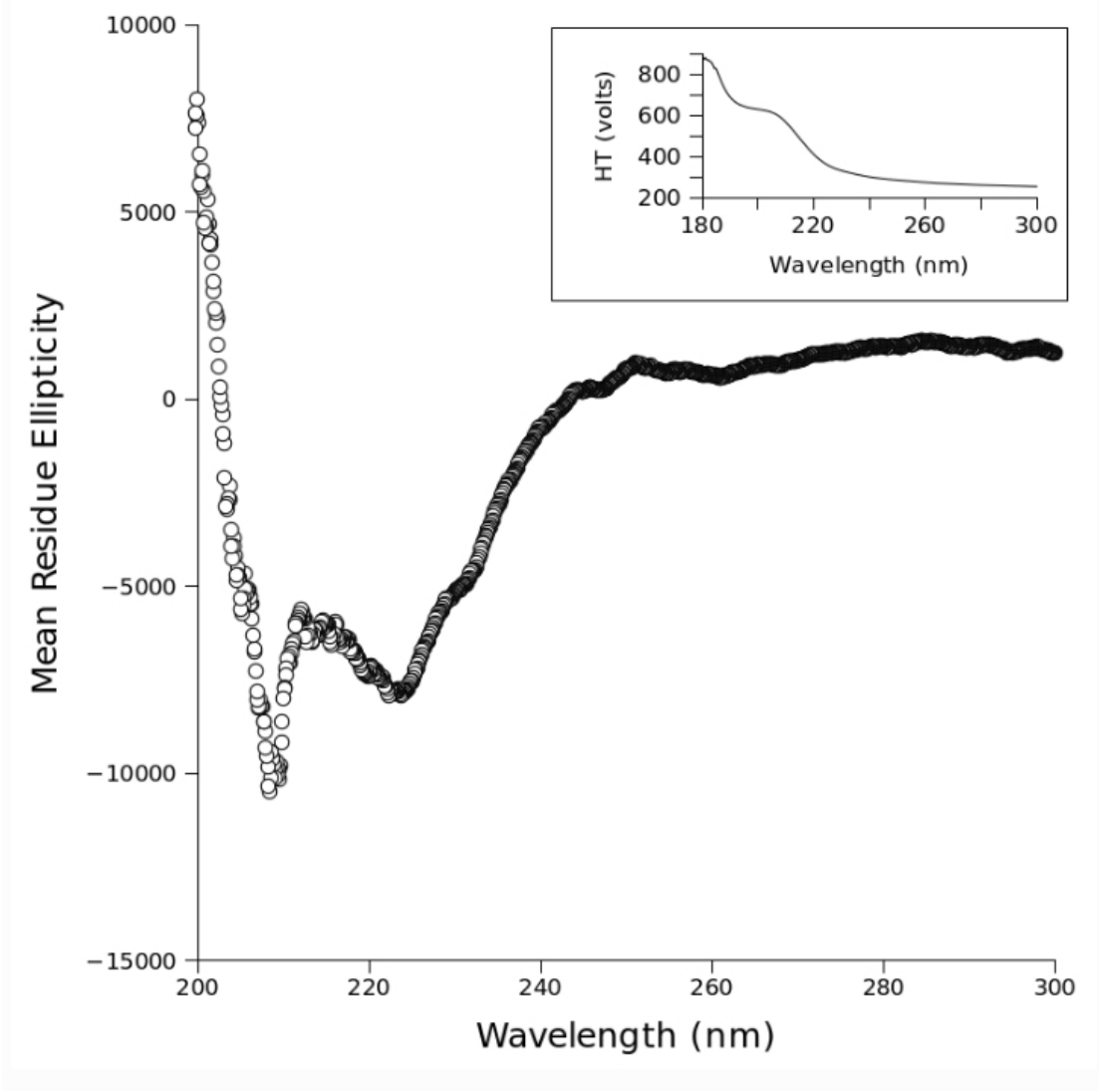

Figure 5.2a – Circular dichroism of purified recombinant *S. guttatum* AOX expressed in FN102. This CD trace shows the mean residue ellipticity ([θ] (mdeg cm^2 $dmol^{-1}$)) of purified *S. guttatum* recombinant alternative oxidase at 5μM. The second plot (top, right) shows the high tension (HT, in volts) values for the data shown to demonstrate why the data has been truncated at 200nm.

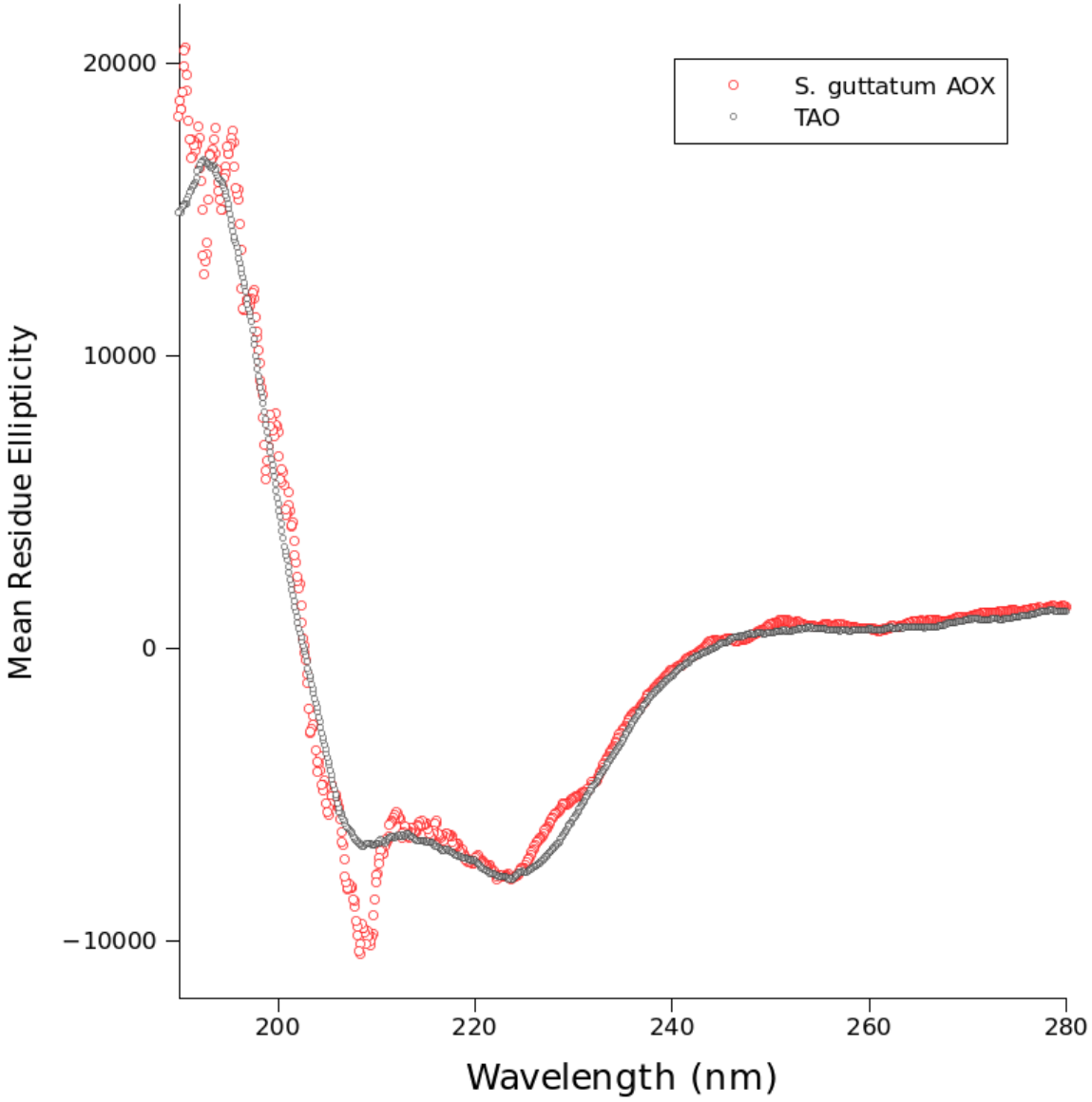

Figure 5.2b – Comparison of circular dichroism of purified recombinant *S. guttatum* AOX and TAO expressed in FN102. This CD trace demonstrates the trace from Figure 5.2a overlaid with the mean residue ellipticity ([θ] (mdeg cm^2 $dmol^{-1}$)) of purified TAO at a concentration of 4.25µM.

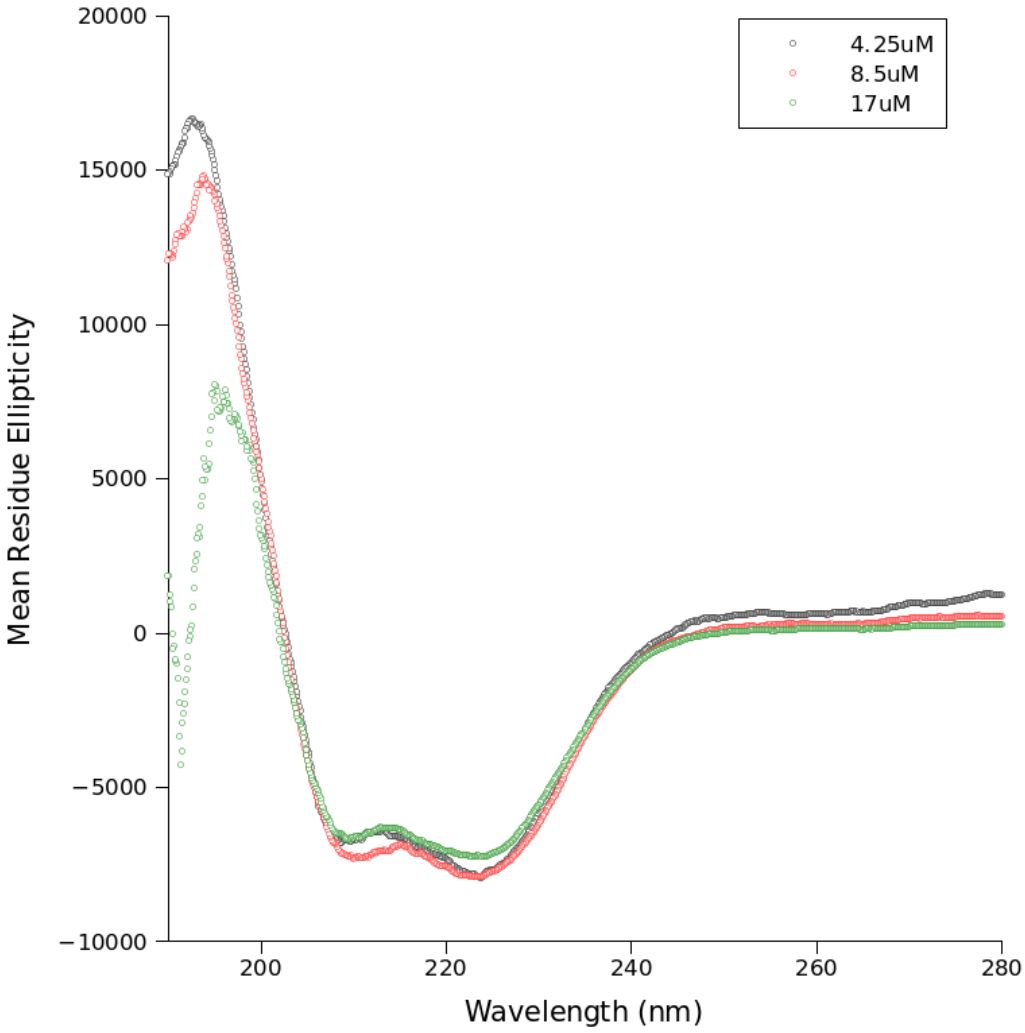

Figure 5.3 – Circular dichroism of recombinant TAO expressed in FN102. This trace shows mean residue ellipticity ([θ] (mdeg cm^2 $dmol^{-1}$)) of purified TAO at 4.25µM, 8.5µM and 17µM.

5.3.1.2 Variable temperature

Figure 5.4 below shows the degree of conformational change observed as a function of mean residue ellipticity versus temperature for purified *S. guttatum* AOX and TAO respectively at a wavelength of 222nm.

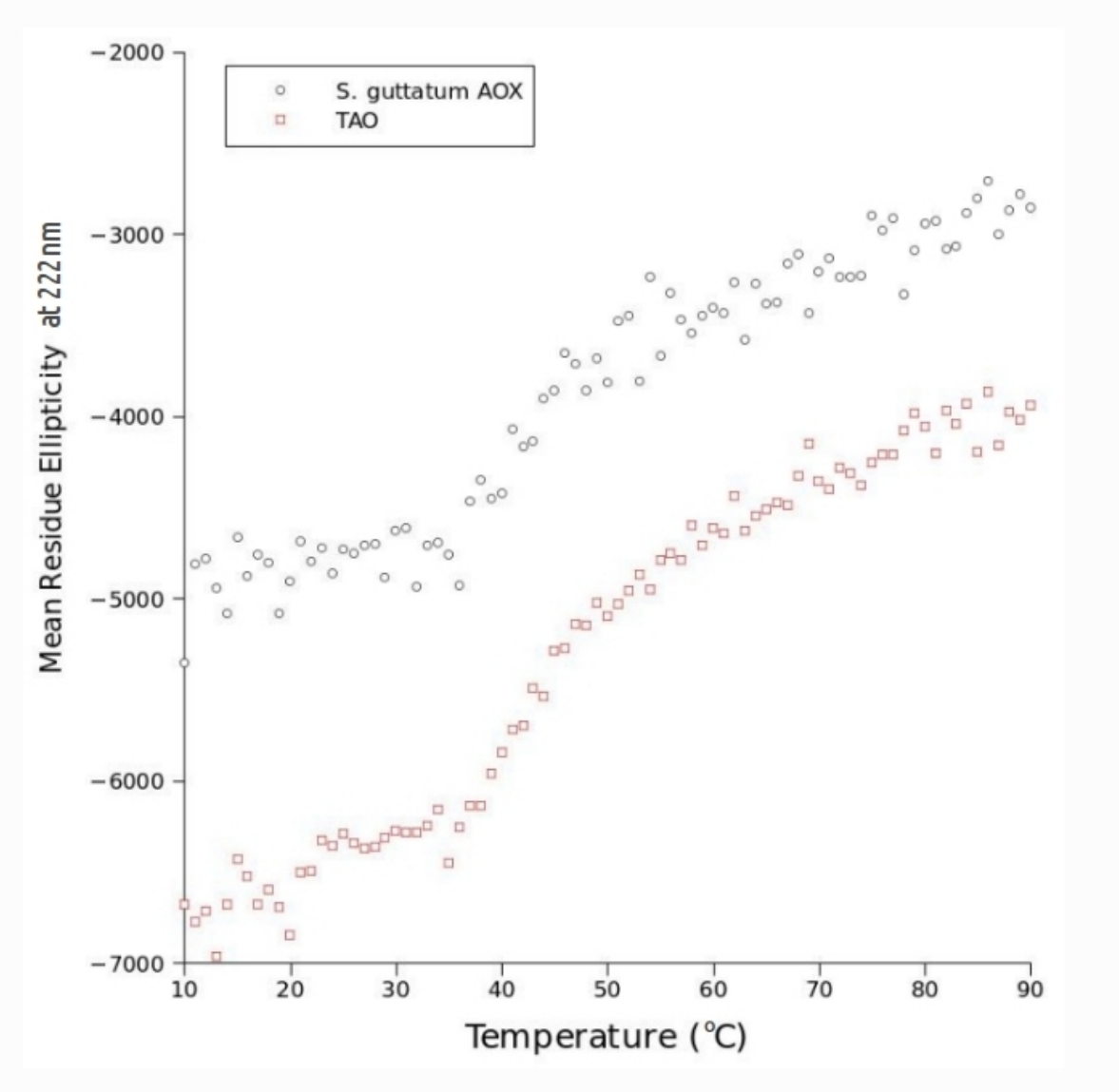

Figure 5.4 – The effect of temperature on mean residual ellipticity at 222nm. This Figure demonstrates the effect of temperature on mean residual ellipticity at 222nm ([θ] (mdeg cm^2 $dmol^{-1}$)) of purified *S. guttatum* alternative oxidase (○) and purified TAO (□) from 10°C to 90°C.

Sequence	Algorithm and Reference set	Predicted secondary structure elements (%)					
		α_1	α_2	β_1	β_2	Turn	Coil
S. guttatum AOX	K2D, no set	49	-	0	-	-	51
TAO	K2D, no set	36.5	-	26	-	-	37.5
S. guttatum AOX	CDSSTR, Set 4	45	10	12	9	3	21
TAO	CDSSTR, Set 4	36	6	18	12	7	21
S. guttatum AOX	SELCON3, SMP180	54	22	8	2	4	10

Table 5.6 – Calculated % secondary structure from raw CD data submitted to Dichroweb. Data from wavelengths 190-240nm was analysed by CDSSTR, 180-240nm by SELCON3 and 200-260nm for K2D. The Reference set chosen for each analysis is indicated, except for K2D which required no Reference set. α_1 refers to regular α-helices, α_2 refers to disordered α-helices, β_1 refers to regular β-strand. β_2 refers to disordered β-strand, Turn refers to turns and Coil refers to random coil (after Sreerama *et al*., 1999). K2D Andrade *et al*., 1993; Set 4, CDSSTR and SELCON3 *cf*; SMP180 Abdul-Gader *et al*., 2011.

5.3.2 Predicted secondary structure

Results of the prediction programs detailed above in Table 5.4 are shown below in Table 5.7.

Number of residues per secondary structure element [%]						Program
Helix		Strand		Coil		
163	[46.7]	0	[0]	186	[53.3]	PSIPRED
251	[71.9]	151	[43.3]	30	[8.6]	CFSSP
126	[36.1]	30	[8.6]	193	[55.3]	GOR
164	[47.0]	15	[4.3]	170	[48.7]	JPred3
173	[49.6]	4	[1.1]	172	[49.3]	PROFphd

Table 5.7 – Predicted secondary structure elements by different programs. The data is displayed as number of residues and [percentage] of the total sequence length (286)

Additionally, the PROFphd algorithm predicted the presence of two transmembrane helices between residues 175-193 and 237-255; and that residues 194-236 would be found within the membrane – but not as transmembrane helices.

5.3.3 Identification of potential dimerisation sites

Using the dimeric homology model generated from the TAO crystal structure (see Chapter 3 Section 3.2.7), 12 residues on helices 2 and 3 were identified which may form a dimer interface (Table 5.8). The criteria for selection was that the residues must be within 10Å and oriented towards the counterpart helix and furthermore must be relatively well conserved across most species. The residues identified are shown in Table 5.5 below and the conservation of these residues is indicated on Figure 3.1. Dimerisation through interfacial water molecules was discounted as a mechanism, as the limited space between helices 2 and 3 would not permit water molecules to form hydrogen bonds with the residues.

Residues on Helix 2	**Residues on Helix 3**
T179	I207
A182	R208
M186	L211
V190	E215
H193	R218
L194	
L197	

Table 5.8 – Potential dimer interface residues. This list shows the residues identified on helices 2 and 3 as potentially involved in formation of a dimer interface. The conservation of these residues are indicated on Figure 3.1.

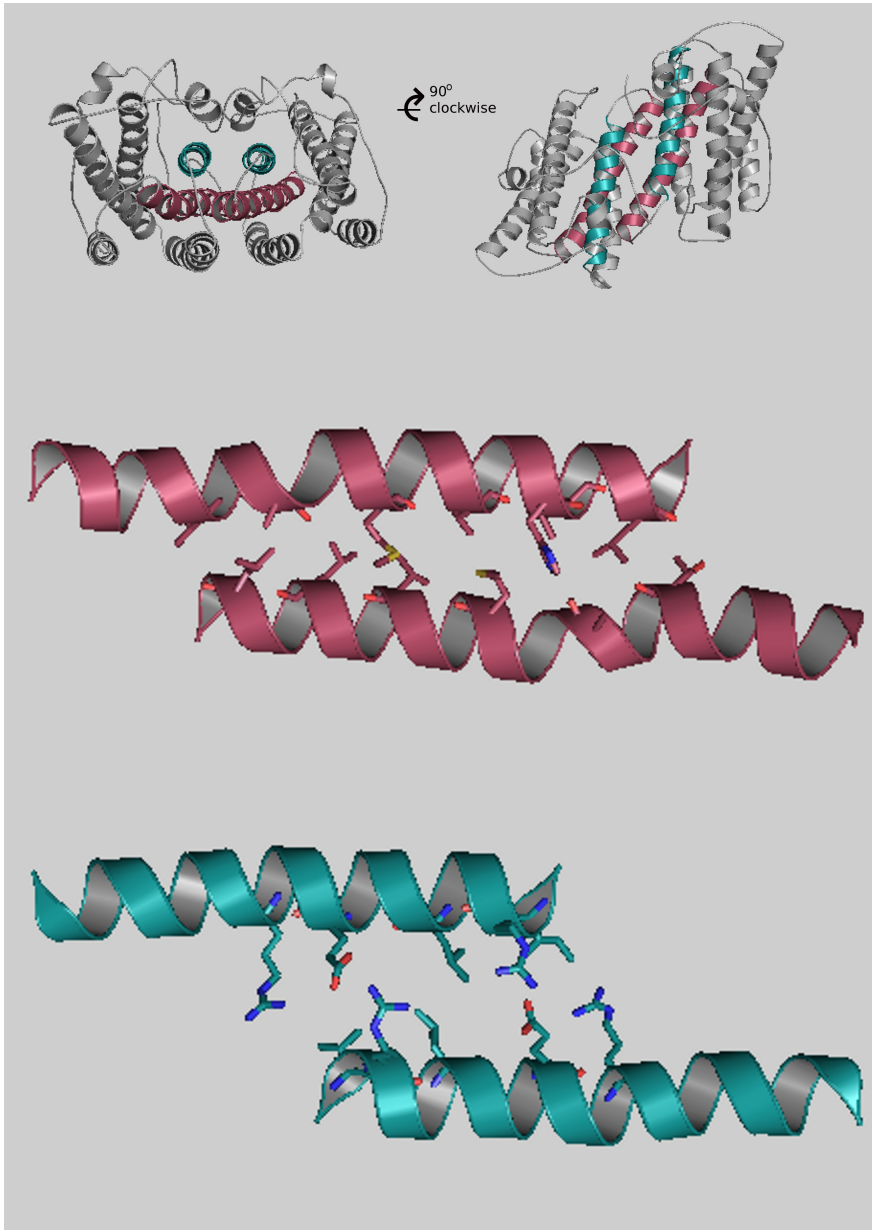

Table 5.5 – A diagrammatic representation of the potential dimer interface. This Figure shows the residues on helices 2 (red) and 3 (teal) that may form a dimer interface. The four helices are shown in their relative positions in the dimer images (top).Residues on helix 2 (red, bottom helix of the pair) from left to right: T179, A182, M186, V190, H193, L194, L197. Residues on helix 3 (teal, bottom helix of the pair) from left to right: I207, R208, L211, E215, R218.

5.3.4 Crystallography

No crystals of diffraction quality were produced from purified recombinant *S. guttatum* alternative oxidase. Any microcrystals produced (a sample of which can be seen below in Figure 5.6) either disintegrated during viewing (i.e. moving the screen tray from the bench or refrigerated unit to the light microscope) or during seeding. The few microcrystals which continued to grow following seeding disintegrated spontaneously within 1-2 days of transfer. However, several conditions consistently produced microcrystals and they are listed in full in Appendix 1. Figure 5.7 below shows the salt type, precipitant type, and pH found in these conditions.

5.3.5 Mutants

Activity assays were conducted on *S. guttatum* mutants (C172A, T179A, Y253F) expressed in FN102, using both membrane-bound, soluble and purified fractions. For all assays ubiquinol-1 was used as a substrate, and at least 95% inhibition was demonstrated using 100nM ascofuranone. SDS PAGE gels and Western blots are shown for each mutant. Activities are shown below for each mutant in Tables 5.9, 5.10 and 5.11. Figure 5.8 shows expressed *S,guttatum* mutants as membrane, soluble and purified fractions on SDS PAGE gels and Western blots.

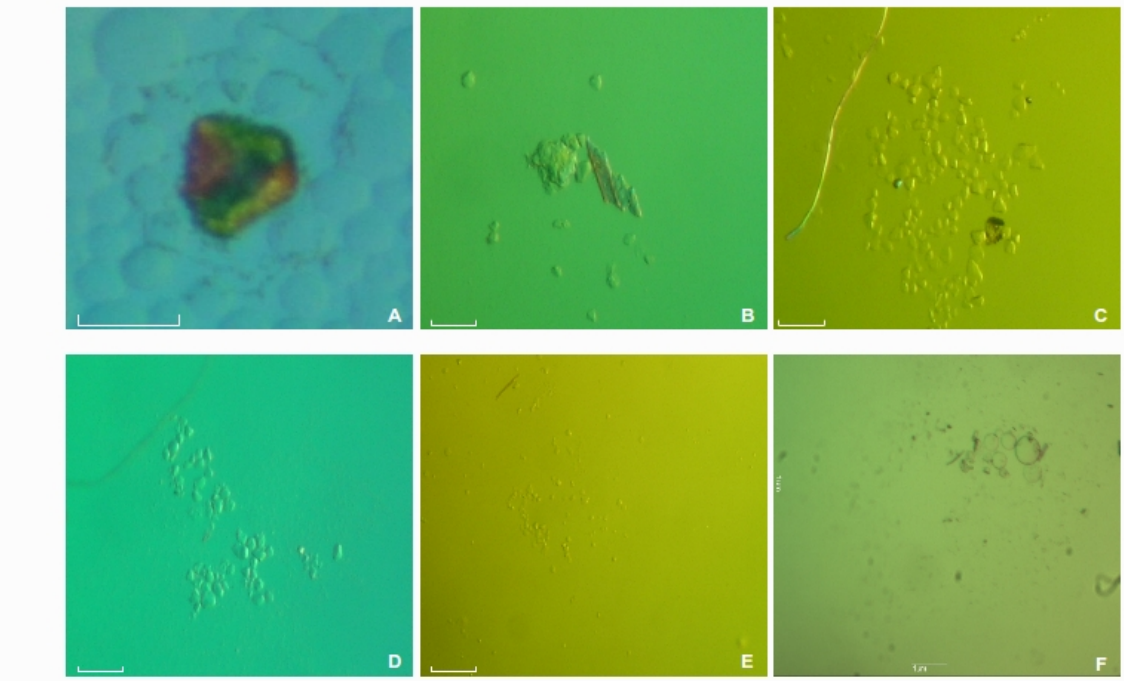

Figure 5.6 – A selection of images taken during crystallographic screening. White scale bars indicate a length of1μM. A an early crystal, when detergent concentrations were too high; B a small crystal, which disintegrated when an attempt was made to seed from it; C microcrystals from Memstart, condition #21 (see Appendix 1 for a full list of screen conditions); D microcrystals from Memstart #23; E microcrystals formed after seeding from Memstart #23 (same conditions); F amorphous precipitate, the result of seeding from Memstart #31.

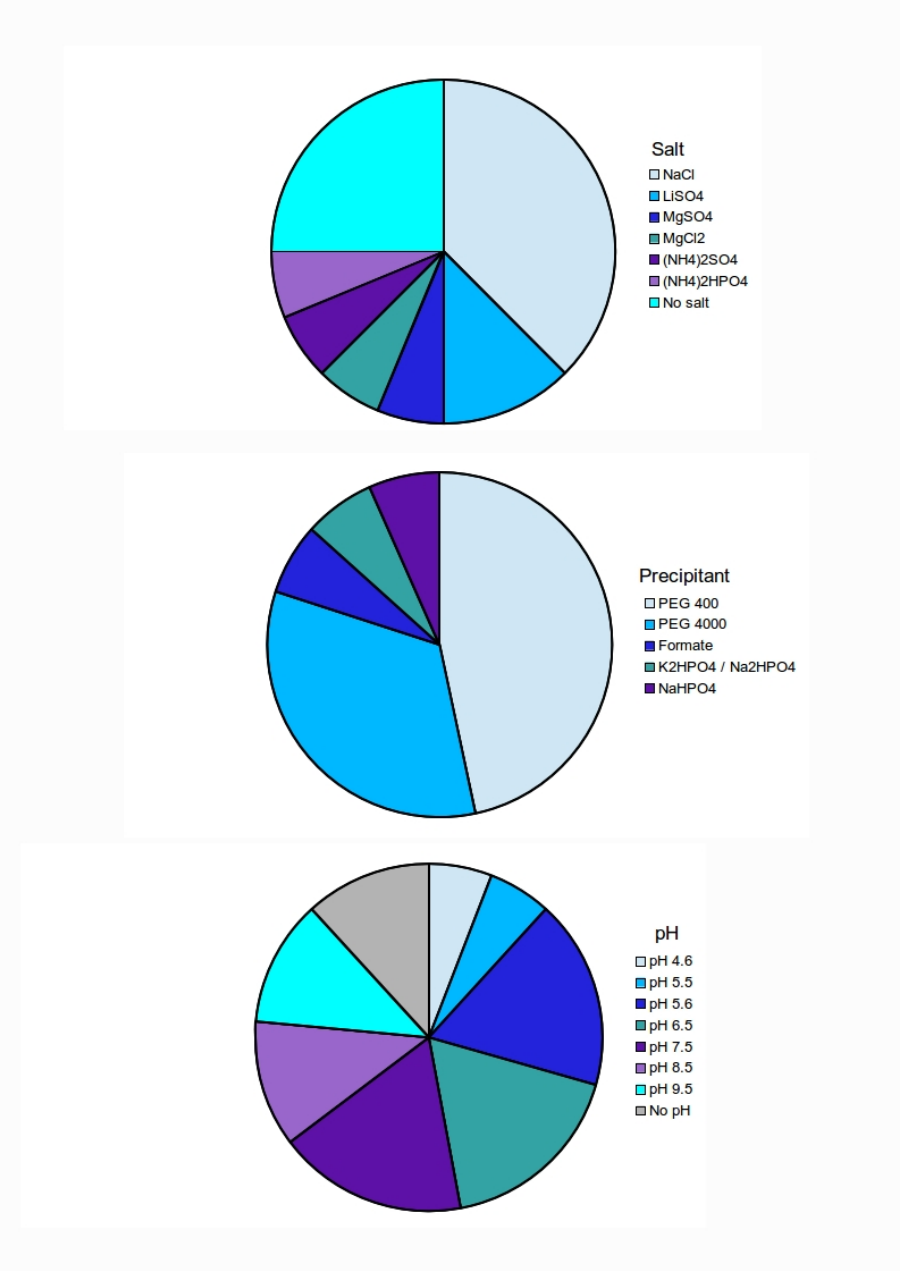

Figure 5.7 – A graphic representation of the number of screens with particular conditions. This Figure shows the number of screens in which particular salt (top), precipitant (middle) and pH (bottom) conditions occurred (out of the 16 screens detailed in Appendix 1)

4.3.5.1 C172A

Fraction	Protein (mg ml^{-1})	Total protein (mg)	Specific activity (µmols min^{-1} mg^{-1})	Total activity (µmols min^{-1})
Membrane	1.0	0.6	3.05	1.83
Solubilised	0.2	0.12	0.54	0.065
Purified	0.27	0.11	0.01	0.001

Table 5.9 – Specific and total activities for the *S. guttatum* C172A mutant expressed in FN102.

4.3.5.2 T179A

Fraction	Protein (mg ml^{-1})	Total protein (mg)	Specific activity (µmols min^{-1} mg^{-1})	Total activity (µmols min^{-1})
Membrane	1.8	1.1	0.19	0.21
Solubilised	0.2	0.11	0.11	0.012
Purified	0.28	0.1	0.01	0.001

Table 5.10 – Specific and total activities for the *S. guttatum* T179A mutant expressed in FN102.

4.3.5.3 Y253F

Fraction	Protein (mg ml^{-1})	Total protein (mg)	Specific activity (µmols min^{-1} mg^{-1})	Total activity (µmols min^{-1})
Membrane	1.9	1.1	0.15	0.165
Solubilised	0.3	0.2	0.04	0.008
Purified	0.22	0.09	0.02	0.002

Table 5.11 – Specific and total activities for the *S. guttatum* Y253F mutant expressed in FN102.

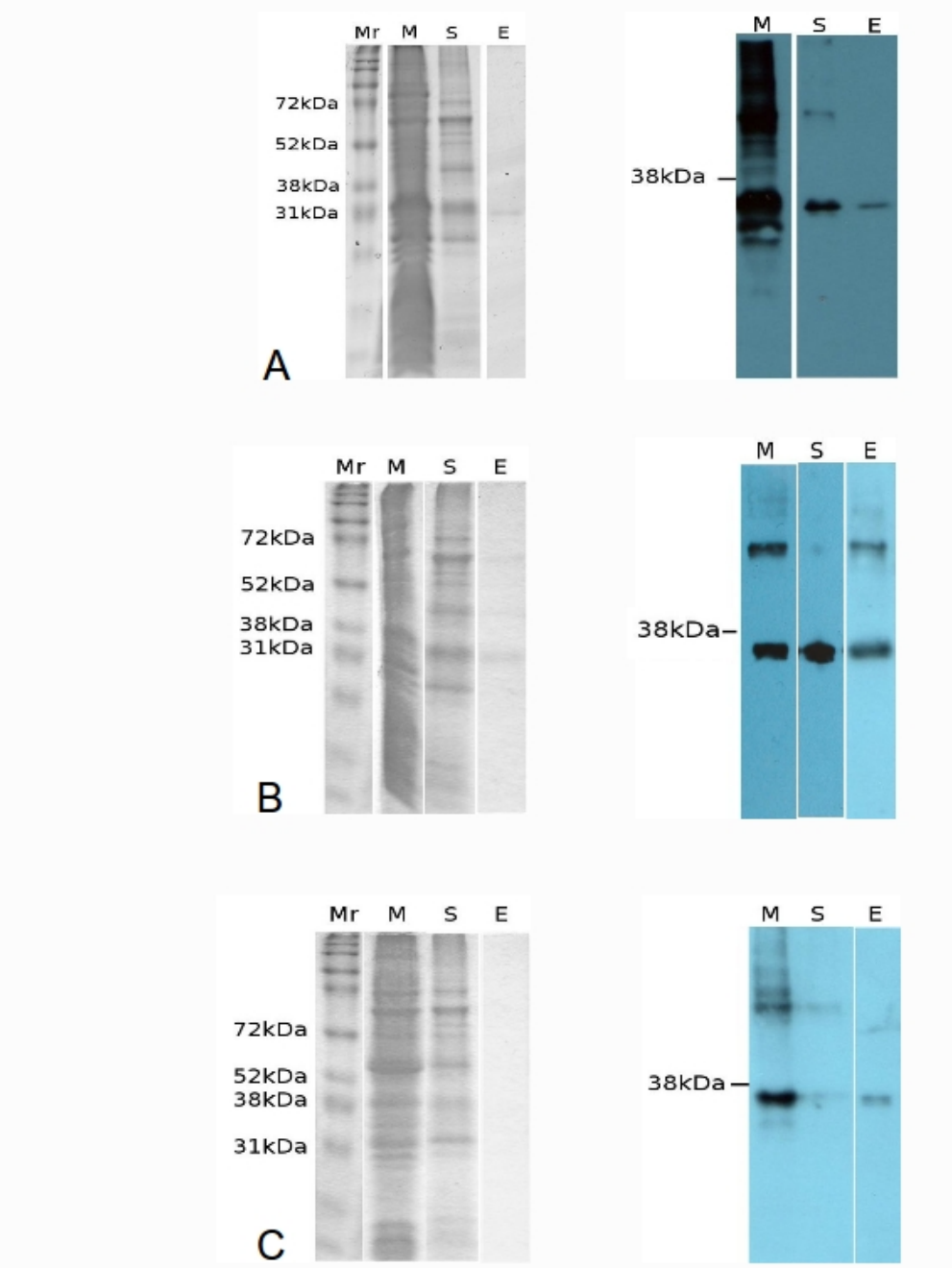

Figure 5.8 – SDS-PAGE gels and Western blots for three *S. guttatum* AOX mutants expressed in FN102. This Figure shows SDS PAGE gels (left) and Western blots (right) for C172A (A), T179A (B) and Y253F (C). Abbreviations: Mr – marker, M – membrane, S – soluble fraction, E – eluate (purified) fraction.

5.3.6 Variable temperature activity assay

The activity of membrane-bound and purified *S. guttatum* recombinant alternative oxidase expressed in FN102 was assayed at 4ºC, 40ºC, 50ºC, 90ºC and then returned to 4ºC after heating to 90ºC. Estimated protein and total protein is shown in Table 5.12a,with specific and total activities shown in Table 5.12b. 150mM ubiquinol-1 was used as the substrate and inhibition of at least 95% by 1μM octyl-gallate was demonstrated in each assay.

Sample	Protein (mg/ml)	Total protein (mg)
Membrane	52	414
Purified	0.1	1

Table 5.12a – Estimated protein for samples used in the variable temperature assays.

	Specific activity (μmol/min/mg) and [*Total activity (μmol/min)*]				
Temperature (ºC)	4	40	50	90	90 → 4
Membrane	0.58 [*242*]	0.57 [*236*]	0.8 [*317*]	0.71 [*293*]	0.26 [*106*]
Purified	15 [*15*]	4 [*4*]	10 [*10*]	0.01 [*0.01*]	1.7 [*1.7*]

Table 5.12b – The effect of temperature on activity of recombinant *S. guttatum* AOX protein expressed in FN102. This Table shows the specific and total activity for samples assayed at varying temperatures. 90 → 4 represents assay carried out after the sample had been heated to 90ºC and then cooled to 4ºC.

5.4 Discussion

5.4.1 Secondary structure

For the first time the secondary structure of the plant alternative oxidase has been demonstrated experimentally. The data obtained from circular dichroism when converted to mean residue ellipticity and plotted against wavelength provides a relatively strong signal in the 222nm region, which is associated with helical structure (Figure 5.2a). However, when comparing the data obtained from TAO (Figures 5.2b and 5.3), it is evident that there is differential absorption in the 190-200nm range, usually indicative of random coil secondary structure elements. This may be indicative of the longer unstructured N-terminal

region of the *S. guttatum* alternative oxidase, which has been implicated in the regulation of activity (Crichton *et al*., 2005). By comparison, the TAO has a much shorter unstructured region at the N-terminal.

Another factor affecting the differing far-UV absorbances observed between *S. guttatum* AOX and TAO is the contribution of solvent noise. The solvent used for CD experimentation remained the same for both proteins (0.04% DDM in dH_2O) and the choice of solvent was based on low UV absorption coupled with the ability of DDM to aid the structural stability of recombinant alternative oxidase. However, the TAO protein used for the CD experimentation had been dialysed prior to PEG precipitation, whilst the recombinant *S. guttatum* had not. As a result, it is possible that there were other ions and buffer components present in small quantities in the *S. guttatum* sample that were not present in the TAO sample – such as Tris, imidazole, chlorine ions and magnesium ions – which are known to absorb in the far UV range (*cf* Kelly *et al*., 2005). In order to overcome these effects, a smaller cell pathlength may be used if possible and alternative methods for eliminating buffer components remaining from the purification process should be investigated. Furthermore, experimentation to identify other solvents which may be used in CD analysis of recombinant *S. guttatum* AOX (and mutants thereof) would be beneficial in obtaining improved CD data in the future and may even provide insight into conditions under which the protein is most stable that may be applied to any further crystallisation attempts.

Following analysis of the raw CD data with three algorithms accessed via the DicrhoWeb server (*cf* Whitmore and Wallace, 2004; Whitmore and Wallace 2008) the evidence for helical structure in *S. guttatum* is compelling (Table 5.6) if unexpected given the apparently poor quality data. All three algorithms predict that approximately 50% of the protein is α-helix (49%, 54% and 45% by K2D, SELCON3 and CDSSTR respectively) and attribute between 10 and 20% of the total structure to β-sheet. K2D predicts the greatest amount of disorder (51%) whilst CDSSTR and SELCON3 predict approximately 20%. It is worth noting that of the three algorithms used, only K2D allowed for the selection of

wavelengths of 200nm and above and thus is the only algorithm where the noise observed in the *S. guttatum* AOX data could be avoided (as indicated by increasing HT voltage, Figure 5.2a). None of the Reference sets available at the time of analysis permitted a minimum wavelength of 200nm, so Reference set 4 (optimised for 190-240nm) was chosen for use with the CDSSTR algorithm. Similarly, all the Reference sets with the exception of one (SMP180) contain soluble proteins, so analysis of the CD data using the SMP180 Reference set and SELCON3 algorithm was chosen to reflect the fact that AOX is a membrane protein. The outcome of the analysis of *S. guttatum* AOX CD data by these algorithms is an interesting starting point which could be vastly improved in the future with the collection of higher-quality CD data.

By comparison, analysis of TAO CD data using K2D and CDSSTR algorithms calculates that approximately 36% of the protein is α-helix, 30% is β-sheet and that between 28 and 37% is random coil. This is not in agreement with the recnently solved TAO structure (Shiba *et al*., 2013) which exhibits 53% α-helical structure, and no β-structures. The difference between percentage helical structure in TAO and *S. guttatum* AOX cannot be explained by the sequence difference between the two alternative oxidase isoforms alone, and is likely to due to a combination of partial unfolding of the *S. guttatum* AOX and a more homogeneous sample used for the TAO experiments. As previously discussed in Chapter 4, the plant alternative oxidase has proven difficult to purify to the level of homogeneity to which the TAO has been purified; therefore, any potential contaminating proteins left in the *S. guttatum* sample may case interference with the circular dichroism data collection. Therefore, it is likely that these differences in protein concentration and homogeneity is the cause of the discrepancy in outcome. However, in the case of the structure prediction analysis (Table 5.8), the difference in algorithmic approach leads to a varied set of predictions which should be used with caution when ascribing potential secondary structure of the alternative oxidase.

One unexpected outcome from the circular dichroism experiments is the apparent partial retention of the helical absorbance signal at 222nm (Figure 5.4) in both *S. guttatum*

and TAO isoforms. In each case, approximately 58% and 64% (respectively) of the signal remained after heating to 90ºC. When the same sample was cooled to 10ºC following heating to 90ºC, the ellipticity was not equal to the signal observed before heating; it had decreased to approximately 75% of the original (data not shown) – indicating that there was significant unfolding during the heating process, which was not completely recovered during the cooling period. Activity data collected at different temperatures (Table 5.12b) is somewhat contradictory to the circular dichroism data collected at higher temperatures. The latter implies that secondary structure is being lost during heating, while activity in the membrane fraction actually increases between 4ºC and 50ºC temperature conditions. Once the protein had been re-cooled to 4ºC however, the activity was reduced by 77% of the maximum (at 50ºC) and 54% of the original activity at 4ºC. The increase in activity observed when heating cannot be explained by increased auto-oxidation at the increased temperature, as activity was inhibited by 98% at both 50 and 90ºC. The increase in activity could be explained by an increase in kinetic energy (supplied by the increased temperature), although this is speculative and warrants further investigation.

The loss of activity when the sample is re-cooled was not the expected outcome, as many globular proteins which unfold due to increased temperature refold to their native state spontaneously when the temperature is returned to optimum. In this case, there could be aggregation of the *E. coli* membrane – and therefore the alternative oxidase protein – due to the rapid change in temperature. It may be, that in plants and other organisms where the alternative oxidase is natively expressed there would be chaperones or heat-shock proteins available to aid in refolding should unfolding occur, which are not present in the membrane-bound sample used for these experiments. It should be noted that no expressed AOX proteins have been confirmed in prokaryotic organisms, although the gene is present in several prokaryotic genomes. The requirement for chaperones to aid in alternative oxidase protein folding *in vivo* is contraindicated by the ability of *E. coli* to express a fully folded and functional complement of alternative oxidases and further supported by the fact that approximately 10% of the original activity can be restored to the non-membrane bound

protein after heating to 90°C accompanied by a 99% loss of activity. Conversely, it could be argued that functional expression of a recombinant eukaryotic protein in *E. coli* is not proof of a spontaneously folding protein. *E. coli* systems express chaperone proteins such as GroEL which could responsible for folding directly after translation, but 10% restoration of activity in the purified alternative oxidase activity after heating could be explained by a small proportion of protein molecules refolding spontaneously, while the majority were unable to do so. Again, auto-oxidation of the substrate cannot account for activity, as more than 95% inhibition could be demonstrated in each assay by the addition of octyl-gallate.

While the apparent increase in activity at temperatures above the optimum (for most enzymes, at least) was unexpected, it is perhaps pertinent to consider the function of the alternative oxidase found in thermogenic tissue – to generate heat. While no thermogenic tissue has ever been recorded to have reached temperatures of >50°, it is not unrealistic to suggest that it may be advantageous to be able to do so. However, in consideration of the other proteins present in thermogenic tissues, raising the tissue temperature to one where most other proteins would be damaged most likely does not support the suggestion that thermogenic plants would routinely do so.

5.4.2 Crystallography

No suitable crystals were grown during this project. This can be explained by several contributory factors including low protein quantity and concentration, difficulties purifying recombinant *S. guttatum* AOX, the requirement for detergent during purification, the large region of potentially unstructured residues found at the N-terminal region of the protein, as well as practical and experimental limitations.

There were many difficulties encountered when expressing and purifying the alternative oxidase – namely low expression levels and the lengthy process of optimising the purification protocol. Even with the protocol significantly improved, protein yields were still low (<2mg per preparation) and concentrating the protein without losing too much enzyme activity is only possible using PEG. The protein produced was also not 100%

pure, which negatively impacted on the ability to crystallise the *S. guttatum* AOX. The lower boundary for protein quantity for crystallography is typically 10mg; in order to achieve this for the *S. guttatum* AOX, between 8 and 10 purification preparations would need to be pooled. In itself this is not difficult, although at one week per preparation, time was a constraint.

The requirement for detergent to be present during the purification of AOX (as described in Chapter 4 Sections 4.4.2 and 4.4.3) led to the first crystal screen experiments producing virtually no stable microcrystals and only one larger crystal (see Figure 5.6, image A) from a total of eight attempts (i.e. 768 screens). Since alternative oxidase activity is lost when detergent is removed from the protein solution, it is perhaps unwise to exclude detergent from the protocol entirely, as the lack of activity may indicate a deterioration in structure. A lack of tertiary and quaternary structure would make the formation of crystals extremely unlikely. Early attempts to remove the detergent through ultrafiltration were unsuccessful and it was only after successful precipitation with PEG that the buffer could be changed following purification and the detergent levels significantly reduced for crystallography. As previously stated (Table 4.8a) absence of detergent during solubilisation resulted in reduced specific activity, so detergent could not be completely eliminated from the protein solution. Similarly, inclusion of glycerol into later purification protocols led to the same problem as excessive detergent levels (i.e. increased protein solubility and decreased aggregation, leading to the inhibition of crystal formation); though glycerol can be relatively easily removed through PEG precipitation and the overall concentration of glycerol was reduced from 20% to 5% in the most recent and most successful purification protocols.

As previously stated, the alternative oxidase isoforms from plant species differs from the TAO significantly in the N-terminal region, with the plant sequences possessing an additional 35 residues which represents ~12% of the whole structure. These additional residues are most likely to be unstructured and as a result, the high level of conformational freedom in this region alone would decrease the likelihood of the molecules to form a

highly ordered crystal structure required to create diffraction-quality protein crystals. One possible solution to this problem would be to create a truncated version of the *S. guttatum* alternative oxidase, which lacks the N-terminal region; although there is no guarantee that this would leave the activity and native structure of the expressed protein intact.

Much knowledge has been gained about the conditions which consistently form microcrystals (i.e. microcrystals were formed on at least three occasions when the condition was used) and as this is the first time that crystallisation of the plant alternative oxidase has been attempted, this represents a significant step towards understanding how to reproducibly create high-quality AOX protein crystals. Of the crystallisation conditions listed in Appendix 1 and represented graphically in Figure 5.7 above, there are some trends in salt type and precipitant type, although pH seems to be less significant. In 5 out of the 16 conditions, there were sulphate or phosphate salts, which are ranked high in the Hofmeister series (*cf* Collins, 2004 for a recent review) of precipitating salts and in 2 of the 4 conditions where no salt was listed, the precipitants were either phosphate or sulphate. Of the 16, 6 conditions contained 0.1M NaCl, with both the anion and cation of the salt towards the middle of the Hofmeister series. This suggests that choosing either NaCl or other salts high in the Hofmesiter series may be advantageous when attempting to precipitate the protein. Regarding precipitant choice, 12 of the screen conditions contained PEG (either 30% *w/v* PEG 400 or 12% *w/v* PEG 4000), suggesting that PEG is a suitable precipitant to use; furthermore PEG precipitant experiments described in Chapter 4 indicate that PEG does not disrupt AOX protein structure. In future this knowledge may be applied to create custom screens for crystallisation of the alternative oxidase.

Finally, a major problem encountered with the crystallisation of the *S. guttatum* alternative oxidase was the tendency for any crystalline deposits (both microcrystals and larger formations) to become unstable and disintegrate when the screen plate was moved from the refrigerated unit to the microscope. Whilst this may not be a problem in cases where proteins form more stable crystals, it was a significant limitation in this project. Therefore, in an attempt to improve the likelihood of stable crystal formation, trays were

not moved for the first week. Whilst this did reduce the number of disintegrating crystals, it was not always practical and made full observation and photography of the crystals difficult. The only practical solution to this problem is to use a system such as that employed at the Membrane Protein Laboratory within the Diamond Light Source[4] where sitting and hanging drop plates are automatically checked by a robotic camera mounted inside the plate storage unit (ThermoFisher Rhombix Cs 750i) without the plate being moved. However, when crystallography was attempted in the facility (12 separate screen plates were set up), no crystals were formed which does not confirm whether the system would prevent AOX crystal disintegration.

It is worth noting that the only group to have successfully grown AOX protein crystals and gathered sufficient diffraction data to solve the structure (Shiba *et al*., 2013) began the process of producing crystals over a decade ago, whilst attempts to crystallise the *S. guttatum* AOX have been ongoing for less than half of that time.

5.4.3 Expression of mutant *S. guttatum* isoforms

The activities and SDS PAGE gels shown above in Tables 5.9, 5.10 and 5.11 and also in Figure 5.8 demonstrate the first time these particular mutants have been expressed in *E. coli*, as all previous expressions have been in the *S.pombe* yeast expression system (Albury *et al*., 1996). The specific activities of the T179A and Y253F mutants reported above are 62% and 70% less active (on average) than the *S. guttatum* wild type recombinant alternative oxidase, which is not entirely consistent with previous findings (Albury *et al*. 2001; Crichton *et al*., 2010), who reported that the mutants lost less activity compared to the wild type. The activities reported above – whilst lower than might be expected – generally support the previously described roles of the residues, although they do not add any further information to the structure-function relationship. As previously discussed in Chapter 4, expression in the non-native *E. coli* system may have an impact on the AOX isoform activities and therefore direct comparison between activities observed in

[4] http://www.diamond.ac.uk/Home/MPL/equipment.html; last accessed 16/09/12

E. coli recombinant protein and *S. pombe* recombinant protein should be viewed with caution.

Finally, the C172A *S. guttatum* mutant displayed a higher activity than most of the wild type *S. guttatum* preparations made during the course of this project, which is in direct contradiction with previous findings (Crichton *et al*., 2010), where expression of the C172A mutant resulted in lower activities than that of the wild type. Therefore, it is not possible to further elucidate the role that this particular residue plays in the structure-function relationship of the alternative oxidase.

5.4.4 Identification of a possible dimer interface

As no evidence of cysteine-associated dimerisation has been found in the recent TAO structures which indicates that there must be another mechanism – either in addition to, or instead of – the sulphide linkage proposed previously. This is likely due to hydrogen bonding between two complementary regions of the individual monomers (helices 2 and 3; Table 5.8. Table 5.5). Without detailed knowledge of exactly how and why dimerisation leads to increased activity, this does lead to the question of whether there are other physiological advantages to existing as a dimer versus a monomer. As there is no evidence to suggest that the alternative oxidase requires extensive folding interaction through chaperones (i.e. a self-folding recombinant eukaryotic protein expressed in a prokaryotic expression system), and in light of the gene coding for a single unit (not a dimer, with no identifiable dimerisation peptide signal) it can be assumed with a reasonable amount of confidence that the dimerisation occurs spontaneously *in vivo*. As such, it could be postulated that the formation is driven by a requirement for a minimal energy state. It is generally accepted that proteins existing as dimers and other oligomers have a lower minimal energy state than monomers (*cf* Goodsell and Olson, 2000) and are far more prevalent in structural databases than monomers. Crucially, 49% of the monomeric homology model surface area is solvent accessible, compared to 39% of the dimeric

homology model surface. This reduction is likely an important factor in the stabilisation of the AOX, which in turn may lead to an increase in activity.

5.4.5 Concluding remarks

For the first time, alpha helical secondary structure has been demonstrated in alternative oxidase using circular dichroism. Whilst the CD data observed for recombinant *S. guttatum* alternative oxidase appears to be of lower quality than that observed for recombinant TAO, statistical analysis of the *S. guttatum* raw data does provide evidence of a high proportion (on average 65%) of helical structure. Furthermore, the observation of an unfolding curve at 222nm through temperatures 10°-90°C without complete loss of signal at the upper temperature range, coupled with observable AOX activity above 50°C suggests a hitherto undiscovered characteristic of *S. guttatum* alternative oxidase – a degree of thermostability.

Mutant *S. guttatum* alternative oxidase has been successfully expressed and purified which is essential to the continuation of the investigation of the structural biology of the alternative oxidase. Of particular interest for future experimentation is the use of mutant *S. guttatum* alternative oxidase isoforms for crystallisation trials, should they produce more stable crystals than the wild type. Similarly, investigation of the effect of mutations on the helical content and thermostability offers an exciting future research direction.

Whilst no crystals of diffraction quality have been obtained to date for the *S. guttatum* alternative oxidase, our knowledge of the factors negatively affecting production of AOX crystals has been considerably increased. For future attempts at crystallising *S. guttatum* AOX, intensive screening of crystallisation conditions using PEG as the precipitant should be carried out, along with further investigation of the negative and positive effects of individual ions from the Hoffmeister series on successful crystallisation.

Chapter 6

General Discussion

The alternative oxidase, a monotopic integral membrane protein associated with the inner mitochondrial membrane, catalyses the oxidation of quinol to quinone and the reduction of oxygen to water and dissipates the free energy as heat. It is ubiquitous to plants and is found in several species of fungi, proteobacteria and parasitic protists such as *T. brucei* and *C. parvum;* importantly, it is not found in higher mammals. The release of heat from the catalytic function of AOX is used by thermogenic plants to volatilise aromatic compounds to attract insect pollinators. AOX is insensitive to several respiratory inhibitiors and thus facilitates the continuation of glycolysis and the Kreb's cycle when other respiratory complexes are inhibited or not functioning correctly.

The alternative oxidase found in the human parasite, *T. brucei* – the causative agent of African Sleeping Sickness – is the sole terminal oxidase during the infectious stage of the parasite's life cycle. Crucially, inhibition of the trypanosomal alternative oxidase during this stage of infection results in the death of the parasite *in vivo* and is therefore an important drug target. The alternative oxidase has also been implicated in the fungicide-resistant respiration exhibited by pathogenic fungi affecting both mammals and plants.

Given the chemotherapeutic importance of the alternative oxidase as a drug target, it is essential to understand the structure-function relationship of the enzyme and species-specific differences in protein behaviour.

Therefore, the aim of this project was to develop overexpression and purification protocols with the objective of producing purified recombinant plant alternative oxidase protein. for structural studies. These expression and purification protocols are intended to complement the existing *S. pombe* expression vector, offering a system to express functional recombinant protein that may be readily and reproducibly purified.

Also within the scope of this project was investigation of the alternative oxidase structure using bioinformatic resources; initially to attempt to replicate the previously devised model and subsequently to re-evaluate and refine the current model using new modelling techniques.

6.1 Expression of recombinant *S. guttatum* alternative oxidase

For the first time, recombinant *S. guttatum* alternative oxidase has been functionally expressed in two *E. coli* expression systems. The C41 strain, optimised for membrane protein over-expression, offers reproducible quantities of total protein (~12mg per litre of growth media) with reasonable specific and total activity (Table 4.4). The FN102 strain, chosen for its inability to synthesise haem – and therefore any other quinol oxidases – expresses on average less protein per litre of growth media than the C41 strain, but the specific and total activity of the expressed protein is consistently higher. Expression of recombinant *S. guttatum* in C41 therefore is preferable when greater quantities of protein are required, but where high activity is less important (such as crystallography, Western blotting or circular dichroism). However, when highly active protein is required in smaller quantities, such as for kinetic profiling, FN102 is the preferred strain.

Following growth, the recombinant *S. guttatum* AOX can be solubilised and further purified using affinity chromatography, with retention of total activity compared to the membrane fraction of 99% post-solubilisation and 49% post purification (Table 4.11). Identification of several key requirements for retaining protein activity and stability has been crucial to the development of a robust and reproducible purification protocol (Figure 4.6). As such, the expression of recombinant *S. guttatum* alternative oxidase in C41 and FN102 is a practical and complementary system to that of *S. pombe*, from which recombinant protein cannot be so readily extracted (Albury *et al*., 1996). Whilst extraction of AOX from native tissues provides a clear insight into the kinetics of the enzyme *in vivo* (which it is not possible to achieve using recombinant AOX expressed in a prokaryotic system), it has historically proven to be relatively unstable once released from the

mitochondrial membrane (*cf* Moore and Siedow, 1991). Expression of the alternative oxidase in C41 and FN102 offers an improved purification outcome; the protein is more stable both in the short and long term and is simpler to extract.

However, despite the advantages of expressing recombinant AOX in *E. coli*, there are also drawbacks, such as reduced specific protein activity and protein concentration compared to native extraction (*A. maculatum;* Affourtit and Moore 2004) and recombinant expression of other AOX isoforms (TAO; Kido *et al*., 2010) as summarised in Tables 4.16a and 4.16b respectively. This raises an interesting question as to why the activity of the recombinant *S. guttatum* AOX should be so low by comparison to *A. maculatum* and TAO. Higher activities observed in TAO can be explained by the necessity for the enzyme to function at a high rate in an unregulated manner, as it is the sole terminal oxidase expressed during a stage in the organism's life cycle when the only source of cellular ATP is provided by glycolysis (Clarkson *et al*., 1989; Chaudhuri *et al*., 1995; Minagawa *et al*., 1996). Similarly, the higher activity recorded for native *A. maculatum* AOX (Table 4.16a) is likely due to the combined activities of a number of different AOX isoforms expressed in native tissues during thermogenesis (Ito *et al*., 2011). This may also account for the high protein concentration observed in the *A. maculatum* solubilised and purified samples (Table 4.16a). *S. guttatum* and TAO recombinant proteins in this thesis and the data reported by Kido *et al*. (2010) respetively are under the control of the same promoter and expressed in the same strain (FN102). The significantly greater protein concentration observed of recombinant TAO (*cf* 8.95mg of purified protein) compared to recombinant *S. guttatum* alternative oxidase (typically <1mg of purified protein) may suggest that after the point of protein synthesis, *S. guttatum* recombinant alternative oxidase is becoming degraded. The exact cause of any potential degradation is not known, although the presence of *S. guttatum* AOX signal on Western blots of the membrane fraction supernatant (supernatant from the final ultracentrifugation step; Figure 4.4, lane 8) would indicate that at least some of the recombinant AOX is being lost from the membrane during growth or harvest. A very small proportion of AOX activity is also observed in the membrane supernatant fractions from

both C41 and FN102 cells (Table 4.9), which suggests that if AOX protein is present in the supernatant, most of the enzymes may well be denatured or otherwise inactivated.

The double band present on almost all gels and Western blots of recombinant *S. guttatum* (a clear exmple of which is shown in Figure 4.8, lane 2) may be the result of such degradation products. Whether these degradation products are active or inactive is not known, but the consistency with which the bands appear on Western blots would indicate that the degradation process occurs frequently and always produces similar size protein fragments. One way to investigate this would be to excise the bands from an SDS PAGE gel and analyse them using mass spectrometry.

Interestingly, the presence of ALA in the growth media for FN102 cells after induction and therefore expressing recombinant *S. guttatum* AOX, leads to a reduction in AOX specific and total activity (Table 4.4), although the effect on total protein is less pronounced. Therefore, if the ALA is either being retained in the media or the effect of the ALA (continued expression of other quinol oxidases) persists after removal, this may be negatively affecting the activity of – and possibly expression of – recombinant *S. guttatum* alternative oxidase. In order to investigate this further, the amount of ALA added to the starter culture should be decreased. If the reduction in ALA concentration leads to an increase in recombinant AOX activity this may be one strategy to increase the activity of recombinant *S. guttatum* AOX expressed in FN102. However, this may also lead to slower growth from inoculation to induction, which would make the protocol less practical and may not provide a better strategy overall.

Another factor which contributes to low observed recombinant *S. guttatum* alternative oxidase activity is the use of different substrates (Table 4.15) during spectrophotometric assays. Whilst using ubiquinol-1 as a substrate for alternative oxidase protein activity assays is preferred, other substrates such as duroquinol will suffice. The activity recorded using the latter is lower than that of ubiquinol-1 and this is most likely due to differences in chemical structure; duroquinol lacks the isoprenyl chain present in both ubiquinol-1 and decylubiquinone (containing 1 and 10 isoprenyl units in the chain

respectively) and is highly hydrophobic as a result. This may negatively affect uptake of duroquinol by the enzyme in the aqueous assay media, leading to reduced recorded specific activities. Similarly this structural difference may affect uptake into the hydrophobic quinone-binding pocket located in the membrane as this may be more selective for the ubiquinol-1 tail rather than the single six-membered ring structure of duroquinol (*cf* Hoefnagel *et al*., 1997). This preference is most likely mediated by specific residues which are responsible for facilitating the movement of the respiratory substrate into the AOX active site from the Q-pool located in the inner mitochondrial membrane.

Following the identification of a possible quinone-binding pocket between helices 1 and 4 (see "Cavities.pse"), any of these residues (150-164 and 232-255) could potentially be involved in substrate preference and this could be investigated further using mutagenesis. This is particularly worth elucidating, given that the previously identified quinone-binding residues (*cf* Fisher and Rich, 2000; L137, H141, T147, H261, R262) are not proximal to the most likely quinone-binding region.

Without knowing the exact composition of the membrane local to each expressed protein it is not possible to say whether the membrane is capable of permitting a substrate added to the media (whether ubiquinol-1 or duroquinol, both of which are hydrophobic) to pass into the membrane and subsequently into the alternative oxidase quinol binding region. When the protein has been solubilised or purified and no such membrane structure is present, it remains unclear whether the substrate passes directly into the AOX protein, or whether it must temporarily associate itself with one of the hydrophobic substances within the local media (for example PEG, DDM or glycerol). Apparent decreases in activity should therefore not necessarily be assumed to be a reflection on protein conformation, but may in fact reflect the ineffective movement of the substrate to the protein. Furthermore, relying on total protein concentration of membrane, soluble and purified fractions containing *S. guttatum* alternative oxidase rather than the exact concentration of recombinant protein has undoubtedly affected the outcome of the activity assays. As previously stated an over-estimation of protein leads to artificially lower activity, whilst

under-estimated protein concentration results in artificially inflated activity. Combined with the uncertainty of the efficiency of substrate movement within the assay media, the resulting rates of activity should be regarded as an estimate rather than a definitive figure. Whilst this has not presented a constraint during this project, it would need addressing if further and more comprehensive kinetic profiling were to be carried out.

6.2 Structural studies of the *S. guttatum* alternative oxidase

No diffraction-quality recombinant *S. guttatum* crystals were produced during this project. Small crystals could be reproducibly grown as described in Chapter 5, but these particular crystals were susceptible to disintegration whenever the plate was moved. This frustrating occurrence could be eliminated if the plates could be viewed *in situ*, as is possible at the Membrane Protein Laboratory (MPL) at the Diamond Light Source, but unfortunately the screens used at that laboratory were not the screens which produced consistent crystal growth, as these screens were discovered some time after the visit to the MPL had taken place.

It is not known exactly why the crystals formed were so small and so susceptible to degradation. One possible explanation is that the apparently unstructured N-terminal tail region of the *S. guttatum* alternative oxidase may be preventing the formation of larger, more ordered crystals. In order to ascertain the effect that the N-terminal region has on the production of stable crystals, a truncated *S.guttatum* alternative oxidase mutant which lacks the N-terminal region could be expressed recombinantly and crystallisation attempted. However, as the N-terminal region is important for the regulation of alternative oxidase activity in some isoforms (Crichton *et al*., 2005) it may be unlikely that this mutant would be fully active, if at all. Nevertheless, provided the expressed protein is fully folded, it could still be used for attempting crystallisation screening.

In light of the recent TAO crystal structure, which forms a homodimer, the oligomeric state of the *S. guttatum* alternative oxidase may be important when attempting to crystallise it. Iwata *et al*. (2012) used chemical cross-linkers to dimerise the internal

NADH-dehydrogenase (NDI1) complex. As the internal NADH-dehydrogenase is also an integral monotopic membrane protein, the use of chemical cross-linkers to potentially improve the outcome of AOX crystallisation trials could be a rewarding investigation.

For the first time, circular dichroism has been successfully used to demonstrate the α-helical nature of the *S. guttatum* alternative oxidase and TAO (Table 5.2 and Figure 5.2b). Using three CD analysis algorithms via Dichroweb, the estimated helical content for *S. guttatum* AOX is ~50%, with the remaining 50% attributed to either random coil (K2D) or a combination of β-sheet and random coil (CDSSTR and SELCON3). Following the optimisation of the buffers for CD experiments, the technique should be used to collect data for not only mutants of *S. guttatum*, but also other AOX isoforms. Additionally, the effect on secondary structure of stabilising detergents such as EDT-20 as well as pyruvate (Carré *et al*., 2011) could be determined to address whether these substances cause changes to the secondary structure rather than the tertiary or quaternary structure of the alternative oxidase.

The use of circular dichroism in this project has revealed a particularly interesting and unexpected characteristic of the alternative oxidase – apparent thermostability. Biologically, in spadix tissues, it is necessary for the alternative oxidase to have at least some heat stability, in order to dissipate the heat generated during thermogenesis. The structure of the four-helix bundle of this relatively small, simple protein is maintained within its core. Additionally, the protein is very closely associated with the membrane *in vivo*, which may help to minimise excess heating of the protein molecule as the heat would be lost through conduction to the membrane and convection to the surrounding matrix.

Regarding the extent of the thermostability – losing approximately 40% of helical conformation at 90^{o}C (Figure 5.4) – it is likely that if the protein can withstand temperatures in excess of 40^{o}C (above which most proteins begin to denature), it may be relatively easy to withstand further temperature increases. Whether this ability to maintain 60% of helical conformation at high temperatures is an evolutionary development is unclear. Thermogenic plants are found in many climates around the World, from the hot

and humid equatorial forests of Sumatra where the famous corpse flower (*Amorphophallus titanum*) grows; to the boggy wetlands of North America and Canada, home of the Western skunk cabbage (*Lysichiton americanus*); the cold snows of America, Canada, China and Japan, where the Eastern skunk cabbage (*Symplocarpus foetidus*) uses thermogenesis to melt the snow; to the mild spring-time woodlands of the UK, when the Lords and Ladies (*Arum maculatum*) appear in April and May. Perhaps, therefore, the range of ambient temperatures coupled with thermogenic activity would perhaps place selective pressure on a protein which would remain stable across a wide range of temperatures.

6.3 *In silico* modelling of the alternative oxidase – beyond the computer

Attempts to use algorithms to provide information about the alternative oxidase have in part been successful. Comparison of the homology model of recombinant *S. guttatum* alternative oxidase created using Δ^9-desaturase as a template to that of the homology model created using TAO indicates that the basic four-helix scaffold coordinating the diiron binding site is very similar (Figure 3.4b). As described previously, the section of the Δ^9-desaturase used as the template is not in any way associated with the membrane and is part of the core of a much larger multi-domain protein; therefore, whilst it was a useful template for the four-helix bundle at the core of the alternative oxidase, as a template for the membrane-associated regions of the protein Δ^9-desaturase was limited. Z-scores provided by ProSA (Table 3.2) showed the quality of the TAO-based homology model to be within an acceptable range for other proteins of similar size. However, the QMEAN4 score (Table 3.2) was low, although this could be as a result of under-representation of membrane protein models in the database against which the user-generated models are compared. By acknowledging the weakness of the models, this perhaps allows for experiments to be designed that do not assume that the model is 100% accurate, allowing a greater amount of experimental flexibility. The models are, in this case, a very useful tool, a guide – nothing more.

6.4 Readdressing the questions posed in Chapter 1 and consideration of future directions

- Is it possible to over-express recombinant *S. guttatum* alternative oxidase protein in a bacterial system?
    - Yes. Further refinement of the growth conditions for the C41 and FN102 strains should be minimal.
- Is it possible to the purify the expressed protein, to provide relatively pure protein?
    - It has been possible to purify expressed recombinant *S. guttatum* AOX to a reasonable level but further refinement is needed to ensure the reproducibility of the protocol defined in Chapter 4.
- Its is possible to crystallise recombinant *S. guttatum* alternative oxidase?
    - It has not been possible to crystallise recombinant *S. guttatum* alternative oxidase to date. Significant steps have been made towards defining a suitable crystallisation protocol, but extensive refinement is required in the future.
- Will recombinant *S. guttatum* alternative oxidase share a similar sensitivity to pyruvate as other AOX isoforms?
    - Recombinant *S. guttaum* does appear to be pyruvate sensitive. Moreover, the inclusion of pyruvate to harvest, solubilisation and purification buffers is important for maintaining protein stability. Whilst pyruvate is unsuitable for addition to CD buffers, it may prove to be an equally important component in the protocol for the crystallisation of *S. guttatum* AOX. The exact nature of pyruvate-AOX interaction is still unknown and should be an area to investigate in the future.
- What is the structure of *S. guttatum* AOX and is it similar to that of TAO and predictions made previously?
    - In lieu of crystallographic structural data for *S. guttatum* alternative oxidase, it has been possible to model the protein on the recently-elucidated TAO structure

with reasonable confidence. The previously predicted four-helix bundle coordinating the diiron active site of the AOX appears to be correct, which provides valuable information towards the understanding of the exact catalytic cycle responsible for AOX activity.

- Does recombinant *S. guttatum* expressed in a bacterial system form dimers and if so, is it possible to identify the mechanism of dimerisation?
    - It appears that recombinant *S. guttatum* AOX does form dimers. Whilst a possible dimerisation interface has been proposed in this thesis, further investigation using mutagenesis and cross-linking studies is required.
- Is it possible to replicate and expand upon previous attempts to model the alternative oxidase, taking into consideration the large volume of new AOX sequences now available in databases?
    - It has been possible to replicate the previously proposed Andersson-Nordlund (1999) general model of the alternative oxidase. Furthermore it has been possible to model the *S. guttatum* AOX on the recently-elucidated TAO structure. The addition of other alternative oxidase sequences to the databases has not improved the ability to predict AOX structure from sequence alone, but has been essential in the creation of detailed and useful multiple sequence alignments and phylogenetic trees. New sequences should be reviewed after they are published to continue understanding the nature of residue conservation and the relation of residues to structure and function.
- How do previous models of the alternative oxidase compare to the newly elucidated TAO structure?
    - The models generated previously by Andersson and Nordlund (1999) and the models generated during this project compare somewhat favourably to the TAO structure. Furthermore, the TAO structure data has provided key insights into

the nature of membrane association, dimer formation and the conservation of the diiron-coordinating four helix bundle at the heart of the alternative oxidase.

6.5 Concluding remarks

Over-expression and purification protocols have been established for recombinant *S. guttatum* alternative oxidase, thus allowing future expression and purification of other interesting AOX sequences. Several requirements have been identified to maintain AOX activity throughout solubilisation and purification, namely DDM, pyruvate, magnesium sulphate and glycerol. If ~50% of the total activity of the membrane can be retained in the purified fraction, then this purification protocol produces results comparable to the purification protocol for TAO (Kido *et al*., 2010).

Significant steps have been made towards implementation of a crystallisation protocol to produce stable crystals, but work should continue in this area with the inclusion of more mutants and other AOX proteins in the screening trial. It may prove that a mutant could crystallise more readily than the wild type, but still provide the essential crystal structure of the plant alternative oxidase.

The presence of large regions of helical structure have been confirmed through circular dichorism, which is in accordance with *in silico* predictions of the same. Whilst the exact extent of helical structure remains elusive, reliable estimates have been obtained. The thermostability discovered during the course of this project has indicated the presence of thermally robust protein, which when viewed biologically in relation to function is a logical extrapolation. Further experimentation of denaturation using heat on recombinant *S. guttatum* alternative oxidase mutants is required to see whether the exact residues which maintain large proportions of helical structure can be identified.

In silico modelling of the alternative oxidase has proven to be a useful exercise, both as a tool for experimental design, but also as a visual aid for further understanding the structure-function relationship. Caution has been used when asserting the validity of the models as anything more than guides and further modelling of the alternative oxidase as a

dynamic protein can be undertaken when the crystal structure of the plant protein is finally elucidated.

References

Abdul-Gader A., Miles A.J., Wallace B.A. 2011. A reference dataset for the analysis of membrane protein secondary structures and transmembrane residues using circular dichroism spectroscopy. *Bioinformatics* **27**:1630-1636

Abrahams J.P., Leslie A.G.W., Lutter R. and Walker J.E. 1994. Structure at 2.8Å resolution of F_1-ATPase from bovine heart mitochondria. *Nature* **370**:621-628

Affourtit C. and Moore A.L. 2004. Purification of the plant alternative oxidase from *Arum maculatum*: measurement, stability and metal requirement. *Biochimica et Biophysica Acta* **1608**:181-189

Ajayi W.U., Chaudhuri M. and Hill G.C. 2002. Site-directed mutagenesis reveals the essentiality of the conserved residues in the putative diiron active site of the trypanosome alternative oxidase. *Journal of Biological Chemistry* **277**:8187-8193

Albury M.S., Dudley P., Watts F.Z. and Moore A.L. 1996. Targeting the plant alternative oxidase protein to *Schizosazzharomyces pombe* mitochondria confers cyanide-insensitive respiration. *Journal of Biological Chemistry* **271**:17062-17066

Albury M.S., Affourtit C. and Moore A.L. 1998. A highly conserved glutamate residue (Glu-270) is essential for plant alternative oxidase activity. *Journal of Biological Chemistry* **273**:30301-30305

Albury M.S., Affourtit C., Crichton P.G. and Moore A.L. 2002. Structure of the plant alternative oxidase – site-directed mutagenesis provides new information on the active site and membrane topology. *Journal of Biological Chemistry* **277**:1190-1194

Albury M.S., Elliott C. and Moore A.L. 2009. Towards a structural elucidation of the alternative oxidase in plants. *Physiologia Plantarum* **137**:316-327

Albury M.S., Elliott C. And Moore A.L. 2010. Ubiquinol-binding site in the alternative oxidase: mutagenesis reveals features important for substrate binding and inhibition. *Biochimica et Biophysica Acta* **1797**:1922-1939

Altshcul S.F., Gish W., Miller W., Myers E.W. and Lipman D.J. 1990. Basic local alignment search tool. *Journal of Molecular Biology* **215**:403-410

Andersson M.E. and Nordlund P. 1999. A revised model of the active site of alternative oxidase. *FEBS Letters* **449**:17-22

Arechaga I., Miroux B., Karrasch S., Huijbregts R., de Kruijff B., Runswick M.J. and Walker J.E. 2000. Characterisation of new intracellular membrane in *Escherichia coli* accompanying large scale over-production of the b subunit of F_1F_0 ATP synthase. *FEBS Letters* **482**:215-219

Avissar Y.J. and Beale S.I. 1989. Identification of the enzymatic basis for delta-aminolevulinic acid auxotrophy in hemA mutant of *Escherichia coli*. *Journal of Bacteriology* **171**:2919-2924

Bahr J.T. and Bonner W.D. 1972. Cyanide-insensitive respiration: I. The steady states of skunk cabbage spadix and bean hypocotyls mitochondria. *The Journal of Biological Chemistry* **248**:3441-3445

Bairoch A., Bucher P. and Hofmann K. 1997. The PROSITE database, its status in 1997. *Nucleic Acids Resarch* **25**:217-221

Baneyx F. 1999. Recombinant protein expression in *Escherichia coli. Current Opinion in Biotechnology* **10**:411-421

Baron C. and Thompson T.E. 1975. Solubilisation of bacterial membrane proteins using alkyl glucosides and diotanoyl phosphatidylcholine. *Biochemica et Biophysica Acta: Biomembranes* **382**:276-285

Bendall D.S. and Bonner W.D. 1971. Cyanide-insensitive respiration in plant mitochondria. *Plant Physiology* **47**:236-245

Benkert P., Baisini M. and Schwede T. 2011. Toward the estimation of the absolute quality of individual protein structure models. *Bioinformatics* **27**:343-350

Bergendahl V., Glaser B.T. and Burgess R.R. 2003. A fast western blot procedure improved for quantitative analysis by direct flourescence labeling of primary antibodies. *Journal of Immunological Methods* **277**:117-125

Berthold D. and Siedow J.N. 1993. Partial purification of the cyanide-resistant alternative oxidase of skunk cabbage (*Symplocarpus foetidus*) mitochondria. *Plant Physiology* **101**:113-119

Berthold D. 1998. Isolation of mutants of the *Arabadopsis thaliana* alternative oxidase (ubiquinol:oxygen oxidoreductase) resistant to salicylhydroxamic acid. *Biochimica et Biophysica Acta* **1364**:73-83

Berthold D., Andersson M.E., and Nordlund P. 2000. New insight into the structure and function of the alternative oxidase. *Biochimica et Biophysica Acta* **1460**:241-254

Berthold D., Voevodskaya N., Stenmark P., Gräslund A., and Nordland P. 2002. EPR studies of the mirochondrial alternative oxidase. Evidence for a diiron carboxylate centre. *Journal of Biological Chemistry* **277**:43608-43614

Berthold D.A. and Stenmark P. 2003. Membrane-bound diiron carboxylate proteins. *Annual Review of Plant Biology* **54**:497-517

Bill R.M., Henderson P.J.F., Iwata S., Kunji E.R.S., Michel H., Neutze R., Newstead S., Poolman B., Tate C.G. and Vogel H. 2011. Overcoming barriers to membrane protein structure determination. *Nature Biotechnology* **29**:335-340

Bondi A. 1964. van der Waals volumes and radii. *The Journal of Physical Chemistry* **68**:441-451

Bonner W.D., Clarke S.D. and Rich P.R. 1986. Partial purification and characterisation of the quinol oxidase activity in *Arum maculatum* mitochondria. *Plant Physiology* **80**:838-842

Boyer P.D. 1975. A model for conformational coupling of membrane potential and proton translocation to ATP synthesis and to active transport. *FEBS Letters* **58**:1-6

Brink C., Hodgkin D.C., June L., Pickworth J., Robertson J.H. and White J.G. 1954. X-ray crystallographic evidence on the structure of vitamin B_{12}. *Nature* **174**:1169-1171

Buchan D.W., Ward S.M., Lobley A.E., Nugent T.C., Bryson K. and Jones D.T. 2010. Protein annotation and modelling servers at University College London. *Nucleic Acids Research* **38**:W563-568

Caffrey M. 2009. Crystallising membrane proteins for structure determination: use of lipidic mesophases. *Annual Review of Biophysics* **38**:29-51

Carol P., Stevenson D., Bisanz C., Breitenbach J., Sandmann G., Mache P., Coupland G. and Kuntz M. 1999. Mutations in the arabadopsis gene *IMMUTANS* cause a variegated phenotype by inactivating a chloroplast terminal oxidase associated with phenotype desaturation. *The Plant Cell* **11**:57-68

Carol P. and Kuntz P. 2001. A plastid terminal oxidase comes to light: implications for carotenoid biosynthesis and chlororespiration. *TRENDS in Plant Science* **6**:31-36

Carpenter E.P., Beis K., Cameron A.D. and Iwata S. 2008. Overcoming the challenges of membrane protein crystallography. *Current Opinion in Structural Biology* **18**:581-588

Carré J.E., Affourtit C. and Moore A.L. 2011. Interaction of purified plant alternative oxidase from *Arum maculatum* with pyruvate. *FEBS Letters* **585**:397-401

Chance B. and Williams G.R. 1956. The respiratory chain and oxidative phosphorylation. *Advances in Enzymology and Related Subjects of Biochemistry* **17**:65-134

Chang C.T., Wu C.S.C. and Yang J.T. 1978. Circular dichroic analysis of protein conformation: inclusion of the β-turns. *Analytical Biochemistry* **91**:13-31

Chaudhuri M., Ajayi W., Temple S. and Hill G.C. 1995. Identification and partial purification of a stage specific 33 kDa mitochondrial protein as the alternative oxidase of the *Trypanosoma brucei brucei* bloodstream trypomastigotes. *Journal of European Microbiology* **42**:467-472

Chaudhuri M. and Hill G.C. 1996. Cloning, sequencing and functional activity of the *Trypanosoma brucei brucei* alternative oxidase. *Molecular and Biochemical Parasitology* **83**:125-129

Chaudhuri M., Ajayi W. and Hill G.C. 1998. Biochemical and molecular properties of the *Trypanosoma brucei* alternative oxidase. *Molecular and Biochemical Parasitology* **95**:53-68

Chaudhuri M., Ott R.D., Saha L., Williams S. and Hill G.C. 2005. The trypanosome alternative oxidase exists as a monomer in *Trypanosoma brucei* mitochondria. *Parasitology Research* **96**:178-183

Chaudhuri M., Ott R.D. and Hill G.C. 2006. Trypanosome alternative oxidase: from molecule to function. *Trends in Parasitology* **22**:484-491

Chayen N.E. 2005. Methods for separating nucleation and growth in protein crystallisation. *Progress in Biophysics and Molecular Biology* **88**:329-337

Chen Y.H., Yang J.T. and Chau K.H, 1974. Determination of the helix and β form of proteins in aqueous solution by circular dichroism. *Biochemistry* **13**:3350-3359

Cherezov V., Rosenbaum D.M, Hanson M.A., Rasmussen S.G., Thian F.S., Kobilka T.S., Choi H.J., Kuhn P., Weis W.I., Kobilka B.K. *et al*. 2007. High resolution crystal structure of an engineered human β-2-adrenergic G-protein-coupled receptor. *Science* **318**:1258-1265

Cherezov V. 2011. Lipidic cubic phase techologies for membrane protein structural studies. *Current Opinion in Structural Biology* **21**:559-566

Chernov A.A. 2003. Protein crystals and their growth. *Journal of Structural Biology* **142**:3-21

Chothia C. and Lesk A.M. 1986. The relation between the divergence of sequence and the structure in proteins. *The EMBO Journal* **5**:823-826

Chou P.Y. and Fasman G.D. 1974. Prediction of protein conformation. *Biochemistry* **13**:222-245

Clarkson A.B., Bienen E.J., Pollakis G. and Grady R.W. 1989. Respiration of bloodstream forms of the parasite *Trypanosoma brucei brucei* is dependent on a plant-like alternative oxidase. *The Journal of Biological Chemistry* **264**:17770-17776

Clifton R., Lister R., Parker K.L., Sappl P.G., Elhafez D., Millar A.H., Day D.A. and Whelan J. 2005. Stress-induced co-expression of alternative respiratory chain components in *Arabadopsis thaliana*. *Plant Molecular Biology* **58**:193-212

Clifton R., Millar A.H. and Whelan J. 2006. Alternative oxidases in Arabidopsis: a comparative analysis of differential expression in the gene family provides new insights into function of non-phoshorylating bypasses. *Biochimica et Biophysica Acta* **1757**:730-741

Cogdell R.J. and Scheer H. 1985. Circular dichroism of light-harvesting complexes from purple photosynthetic bacteria. *Photochemistry and Photobiology* **42**:669-678

Cohen S.N., Chang A.C.Y. and Hsu L. 1972. Nonchromosomal antibiotic resistance in bacteria: genetic transformation of *Escherichia coli* by R-factor DNA. *Proceedings of the National Academy of Sciences* **69**:2110-2114

Cole C., Barber J.D. and Barton G.J. 2008. The Jpred3 secondary structure prediction server. *Nucleic Acid Research* **35**:W197-201

Collins K.D. 2004. Ions from the Hofmeister series and osmolytes: effects on proteins in solution and in crystallisation process. *Methods* **34**:300-311

Collins K.D. 2006. Ion hydration: implications for cellular function, polyelectrolytes, and protein crystallisation. *Biophysical Chemistry* **119**:271-281

Combet C., Blanchet C., Geourjon C. and Deléage G. 2000. NPS@: Network protein sequence analysis. *Trends In Biochemical Sciences* **25**:147-150

Considine M.J., Holtzapffel R.C., Day D.A., Whelan J. and Millar A.H. 2002. Molecular distinction between alternative oxidase from monocots and dicots. *Plant Physiology* **129**:949-953

Cooley R.B., Arp D.J. and Karplus P.A. 2010. Evolutionary origin of a secondary structure: π-helices as cryptic but widespread insertional variations of α-helices that enhance protein functionality. *Journal of Molecular Biology* **404**:232-246

Crichton P.G., Affourtit C., Albury M.S., Carré J.E. and Moore A.L. 2005. Constitutive activity of *Sauromatum guttatum* alternative oxidase in *Schizosaccharomyces pombe* implicates residues in addition to conserved cysteines in α-keto acid activation. *FEBS Letters* **579**:331-336

Crichton P.G., Albury M.S., Affourtit C. and Moore A.L. 2010. Mutation of *Sauromatum guttatum* alternative oxidase reveals features important for oxygen binding and catalysis. *Biochemica et Biophysica Acta: Bioenergetics* **1797**:732-737

Cuff J.A., Clamp M.E., Siddiqui A.S., Finlay M. and Barton G.J. 1998. JPred: a consensus secondary structure prediction server. *Bioinformatics* **14**:892-893

Deisenhofer J., Epp O., Miki K., Huber R. and Michel H. 1985. Structure of the protein subunits in the photosynthetic reaction centre of *Rhodopseudomonas viridis* at 3Å resolution *Nature* **318**:618-624

Dong H., Nilsson L. and Kurland C.G. 1995. Gratuitous overexpression of genes in *Escherichia coli* leads to growth inhibition and ribosome destruction. *Journal of Bacteriology* **177**:1497-1504

Drew D.E., von Heijne G., Nordlund P. and de Gier J.W. 2001. Green fluorescent protein as an indicator to monitor membrane protein overexpression in *Escherichia coli*. *FEBS Letters* **507**:200-224

Efremov R.G., Baradaran R. and Sazanov L.A. 2010. The architechture of respiratory complex I. *Nature* **465**:441-445

Elthon T.E. and McIntosh L. 1986. Characterization and solubilization of the alternative oxidase of *Sauromatum guttatum* mitochondria. *Plant Physiology* **82**:1-6

Elthon T.E., Nickles R.L. and McIntosh L. 1989. Monoclonal antibodies to the alternative oxidase of higher plant mitochondria. *Plant Physiology* **89**:1311-1317

Fairlamb A.H. 2003. Chemotherapy of human african trypanosomaisis: current and future prospects. *Trends in Parasitology***19**:488-494

Felsenstein J. 1989. PHYLIP - Phylogeny Inference Package (Version 3.2). *Cladistics* **5:** 164-166

Finnegan P.M., Unbach A.L. and Wilce J.A. 2003. Prokaryotic origins for the mitochondrial alternative oxidase and plastid terminal oxidase nuclear genes. *FEBS Letters* **555**:425-430

Finnegan P.M., Soole K.L. and Umbach A.L. 2004. Alternative mitochondrial electron transport proteins in higher plants. In Day D.A., Millar A.H., and Whelan J. (Eds) *Plant Mitochondria: From Gene To Function*, Advances in Photosynthesis and Respiration, Kluwer, Dordrecht, The Netherlands **17**:163-230

Fisher N. and Rich P.R. 2000. A motif for quinone binding sites in respiratory and photosynthetic systems. *Journal of Molecular Biology* **296**:1153-1162

Fukai Y., Amino H., Hirawake H., Yabu Y., Ohta N., Minagawa N., Sakajo S., Yoshimoto A., Nagai K., Takamiya S., Kojima S. and Kita K. 1999. Functional expression of the ascofuranone-sensitive *Trypanosoma brucei brucei* alternative oxidase in the cytoplasmic membrane of *Escherichia coli*. *Comparative Biochemistry and Physiology Part C* **124**:141-148

Fukai Y., Nihei C., Yabu Y., Suzuki T., Ohta N., Minagawa N., Nagai K. and Kita K. 2002. Strain specific difference in amino acid sequences of trypanosome alternative oxidase. *Parasitology International* **51**:195-199

Fukai Y., Nihei C., Kawai K., Yabu Y., Suzuki T., Ohta N., Minagawa N., Nagai K. and Kita K. 2003. Overproduction of highly active trypanosome alternative oxidase in *Escherichia coli* heme-deficient mutant. *Parasitology International* **52**:237-241

Gajewski E., Steckler D.K. and Goldberg R.N. 1986. Thermodynamics of the hydrolysis of adenosine 5'-triphosphate to denosine 5'-diphosphate. *Journal of Biological Chemistry* **261**:12733-12737

Garnier J., Osguthorpe D.J. and Robson B. 1978. Analysis of the accuracy and implications of simple methods for predicting the secondary structure of globular proteins. *Journal of Molecular Biology* **120**:97-120

George J.W., Brosh R.M. and Matson S.W. 1994. A dominant negative allele of *Escherichia coli* uvrD gene encoding DNA helicase II. *Journal of Molecular Biology* **235**:424-435

Gibbons C., Montgomery M.G., Leslie A.G.W. and Walker J.E. 2000. The structure of the central stalk in bovine F(1)-ATPase at 2.4Å resolution. *Nature Structural Biology* **7**:1055-1061

Ginalski K. 2006. Comparative modelling for protein structure prediction. *Current Opinion in Structural Biology* **16**:172-177

Gomes C.M., le Gall J., Xavier A.V. and Teixeira M. 2001. Could a di-iron containing four-helix bundle protein have been a primitive oxygen reductase? *Chembiochem* **2**:583-587

Goodsell D.S. and Olson A.J. 2000. Structural symmetry and protein function. *Annual Review of Biophysics and Biomolecular Structure* **29**:105-53

Gouy M., Suindon S. and Gascuel O. 2010. Seaview version 4: a multiplatform graphical user interface for sequence alignment and phylogenetic tree building. *Molecular Biology and Evolution* **27**:221-224

Grant N., Onda Y., Kakizaki Y., Ito K., Watling J. and Robinson S. 2009. Two cys or not two cys? That is the question: alternative oxidase in the thermogenic plant sacred lotus. *Plant Physiology* **150**:987-995

Grant P.T. and Sargent J.R. 1960. Properties of L-α-glycerophosphate oxidase and its role in the respiration of *Trypanosoma rhodesiense*. *The Biochemical Journal* **76**:229-237

Grant P.T. and Sargent J.R. 1961. Respiratory systems in the trypanosomidae. *The Biochemical Journal* **81**:200-206

Greenfield N.J. 2006a. Using circular dichroism collected as a function of temperature to determine the thermodynamics of protein unfolding and binding interactions. *Nature Protocols* **1**:2527-2535

Greenfield N.J. 2006b. Using circular dichroism spectra to esimate protein secondary structure. *Nature Protocols* **1**:2876-2890

Grisshammer R. and Tate C.G. 1995. Overexpression of integral membrane proteins for structural studies. *Quarterly Reviews of Biophysics* **28**:315-422

Guex N. and Peitsch M.C. 1997. Swiss-Model and the Swiss-PDbViewer: an environment for comparative protein modelling. *Electrophoresis* **18**:2714-2723

Guzzo A.V. 1965. Influence of amino-acid sequence on protein structure. *Biophysical Journal* **5**:809-822

Haas C. and Drenth J. 1999. Understanding protein crystallisation on the basis of the phase diagram. *Journal of Crystal Growth* **196**:388-394

Helmer-Citterich M. and Tramontano A. 1994. Puzzle: a new method for automated protein docking based on surface shape complementarity. *Journal of Molecular Biology* **235**:1021-1031

Hiser C. and McIntosh L. 1990. Alternative oxidase of potato is an integral membrane protein synthesized *de novo* during aging of tuber slices. *Plant Physiology* **93**:312-318

Hodgkin D.C, Pickworth J., Robertson J.H., Trueblood K.N., Prosen R.J. and White J.G. 1955. The crystal structure of the hexacarboxylic acid derived from B_{12} and molecular structure of the vitamin. *Nature* **176**:325-328

Hoefnagel M.H.N., Rich P.R., Zhang Q. and Wiskich J.T. 1997. Substrate kinetics of the plant mitochondrial alternative oxidase and the effects of pyruvate. *Plant Physiology* **115**:1145-1153

Holmes M.A., Le Trong I., Turley S., Sieker L.C. And Stenkamp R.E. 1991. Structures of deoxy and oxy hemerythrin at 2.0 Å resolution. *Journal of Molecular Biology***218**:583-593

Holtzapffel R.C., Castelli J., Finnegan P.M., Millr A.H., Whelan J. and Day D.A. 2003. A tomato alternative oxidase protein with altered regulatory properties. *Biochimca et Biophysica Acta* **1606**:153-162

Humphrey W., Dalke A. and Schulten K. 1996. VMD - Visual Molecular Dynamics. *Journal of Molecular Graphics* **14**:33-38.

Huq S. and Palmer J.M. 1978. Isolation of a cyanide-resistant duroquinol oxidase from *Arum maculatum* mitochondria. *FEBS Letters* **95**:217-220

Ikuma H. 1972. Electron transport in plant respiration. *Annual Review of Plant Physiology* **23**:419-436

Ito K., Ogata T., Kakizaki Y., Elliott C., Albury M.S. and Moore A.L. 2011. Identification of a gene for pyruvate-insenstive mitochondrial alternative oxidase expressed in the thermogenic appendices in *Arum maculatum*. *Plant Physiology* **157**:1721-1732

Iwata M., Lee Y., Yamashita T., Yagi T., Iwata S., Cameron A.D. and Maher M.J. 2012. The structure of the yeast NADH dehydrogenase (Ndi1) reveals overlapping binding sites for water- and lipid-soluble substrates. *Proceedings of the National Academy of Sciences* **109**:15247-15252

Iwata S., Ostermeier C., Ludwig B. and Michel H. 1995. Structure at 2.8Å resolution of cytochrome *c* oxidase from *Paracoccus denitrificans*. *Nature* **376**:660-669

Iwata S., Lee J.W., Okada K., Lee J.K., Iwata M., Rasmussen B., Link T.A., Ramaswamy S. and Jap B.K. 1998. Complete structure of the 11-subunit bovine mitochondrial cytochrome bc1 complex. *Science* **281**:64-71

Jacob F. and Monod J. 1961. Genetic regulatory mechanisms in the synthesis of proteins. *Journal of Molecular Biology* **3**:318-356

James W.O. and Elliott D.C. 1955. Cyanide-resistant mitochondria from the spadix of an *Arum. Nature* **175**:89

Jancarik J. and Kim S.-H. 1991. Sparse matrix sampling: a screening method for crystallisation of proteins. *Journal of Applied Crystallography* **24**:409-411

Jayasinghe S., Hristova K. and White S.H. 2001. Mptopo:a database of membrane protein topology. *Protein Science* **10**:455-458

Jeanmougin F., Thompson J.D., Gouy M., Higgins D.G. and Gibson T.J. 1998. Multiple sequence alignment with Clustal X. *Trends in Biochemical Sciences* **23**:403-405

Jones B.T. 1999. Protein secondary structure prediction based on position-specific scoring matrices. *Journal of Molecular Biology* **292**:195-202

Josse E., Simkin A.J., Gaffé J., Labouré A., Kuntz M. and Carol P. 2000. A plastid terminal oxidase associated with carotenoid desaturation during chromoplast differentiation. *Plant Physiology* **123**:1427-1436

Kabsch W. and Sander C. 1983. Dictionary of protein secondary structure: pattern recognition of hydorgen-bonded and geometrical features. *Biopolymers* **22**:2577-2637

Källberg M., Wang H., Wang S., Peng J., Wang Z., Lu H and Xu J. 2012. Template-based protein structure modelling using the RaptorX web server. *Nature Protocols* **7**:1511-1522

Katona G., Andréasson U., Landau E.M., Andréasson L.E. and Neutze R. 2003. Lipidic cubic phase crystal stucture of the photosynthetic reaction centre from *Rhodobacter sphaeroides* at 2.35Å resolution. *Journal of Molecular Biology* **331**:681-692

Keilin D. and Hartree E.F. 1938. Letters to the Editor: cytochrome *a* and cytochrome oxidase. *Nature* **141**:870-871

Kelley L.A. and Sternberg M.J.E. 2009. Protein structure prediction on the Web: a case study using the Phyre server. *Nature Protocols* **4**:363-371

Kelly S.M., Jess T.J. and Price N.C. 2005. How to study proteins by circular dichroism. *Biochimica at Biophysica Acta* **1751**:119-139

Kendrew J.C., Bodo G., Dintzis H.M., Parrish R.G. and Wyckoff H. 1958. A three-dimensional model of the myoglobin molecule obtained by X-ray analsysis. *Nature* **181**:662-666

Kendrew J.C., Dickerson R.E., Strandberg B.E., Hart H.G., Davies D.R., Phillips D.C. and Shore V.C. 1960. Structure of myoglobin: a three-dimensional fourier synthesis at 2Å resolution. *Nature* **185**:422-427

Kido Y., Shiba T., Inaoka D.K., Sakamoto K., Nara T., Aoki T., Honma T., Tanaka A., Inoue M., Matsuoka S., Moore A.L., Harada S. and Kita K. 2010. Cyrstallisation and preliminary crystallographic analysis of cyanide-insensitive alternative oxidase from *Trypanosoma brucei brucei*. *Acta Crystallographica Section F: Structural Biology and Crystallization Communications* **66**:275-278

Kilikian B.V., Suárez C.W., Liria C.W. and Gombert A.K. 2000. Process strategies to improve heterologous protein production in *Escherichia coli* under lactose of IPTG induction. *Process Biochemistry* **35**:1019-1025

Kotelchuck D and Scheraga H.A. 1969. The influence of short-range interactions on protein conformation, II – a model for predicting the α-helical regions of proteins. *Proceedings of the National Academy of Sciences* **62**:14-21

Kumar A.M. and Söll D. 1992. *Arabadopsis* alternative oxidase sustains *Escherichia coli* respiration. *Proceedings of the National Academy of Sciences* **89**:10842-10846

Laemmli U.K. 1970. Cleavage of structural proteins during the assembly of head of bacteriophage T4. *Nature* **227**:680-685

Lambers H. 1982. Cyanide-resistant respiration: a non-phosphorylating electron transport pathway acting as an energy overflow. *Physiologia Plantarum* **55**:478-485

Lambowitz A.M., Sabourin J.R., Bertrand H., Nickels R. and McIntosh L. 1989. Immunological identification of the alternative oxidase of *Neurospora crassa* mitochondria. *Molecular and Cellular Biology* **9**:1362-1364

Landau E.M. and Rosenbusch J.P. 1996. Lipidic cubic phases: a novel concept for the crystallisation of membrane proteins. *Proceedings of the National Academy of Sciences* **93**:14532-14535

Lee B. and Richards F.M. 1971. The interpretation of protein structures: estimation of static accessibility. *Journal of Molecular Biology* **55**:379-400

Lipscomb J.D. 1994. Biochemistry of the soluble methane monooxygenase. *Annual Review of Microbiology* **48**:371-399

Lindqvist Y., Huang W., Schneider G. and Shanklin J. 1996. Crystal structure of Δ^9 stearoyl-acyl carrier protein desaturase from castor seed and its relationship to other di-iron proteins. *The EMBO Journal* **15**:4081-4092

Lowry O.H., Rosebrough N.J., Farr A.L. and Randall R.J. 1951. Protein measurement with the folin phenol reagent. *Journal of Biological Chemistry* **193**:165-275

Macindoe G., Mavridis L., Venkatraman V., Devignes M. and Ritchie D.W. 2010. HexServer: an FFT-based protein docking server powered by graphics processors. *Nucleic Acids Research* **38**:W445W449

le Maire M., Champeil P. and Møller J.V. 2000. Interaction of membrane proteins and lipids with solubilising detergents. *Biochimica et Biophysica Acta* **1508**:86-111

Martí-Renom M.A., Stuart A.C., Fiser A., Sánchez R., Melo F. and Šali A. 2000. Comparative protein structure modelling of genes and genomes. *Annual Review of Biophysics and Biomolecular Structure* **29**:291-325

Maxwell D.P., Wang Y. and McIntosh. 1999. The alternative oxidase lowers mitochondrial reactive oxygen production in plant cells. *Proceedings of the National Academy of Sciences* **96**:8271-8276

McDonald A.E., Sieger S.M. and Vanlerberghe G.C. 2002. Methods and approaches to study the plant mitochondrial alternative oxidase. *Physiologia Plantarum* **116**:135-143

McDonald A.E. and Vanlerberghe G.C. 2004. Branched mitochondrial electron transport in the Animalia: presence of alternative oxidase in several animal phyla. *IUBMB Life* **56**:333-341

McDonald A.E. and Vanlerberge G.C. 2006. Origins, evolutionary history and taxonomic distribution of alternative oxidase and plastoquinol terminal oxidase. *Comparative Biochemistry and Physiology Part D* **1**:357-364

Meeuse B.J.D. 1975. Thermogenic respiration in Aroids. *Annual Review of Plant Physiology* **26**:117-126

Meeuse B.J.D. and Raskin I. 1988. Sexual reproduction in the arum lily family, with emphasis on thermogenicity. *Sexual Plant Reproduction* **1**:3-15

Midgett C.R. and Madden D.R. 2007. Breaking the bottleneck: Eukaryotic membrane protein expression for high-resolution structural studies. *Journal of Structural Biology* **160**:265-274

Millar A.H., Wiskich J.T., Whelan J. and Day D.A. 1993. Organic acid activation of the alternative oxidase of plant mitochondria. *FEBS Letters* **329**:259-262

Minagawa N., Sakajo H., Komiyama T. and Yoshimoto A. 1990. Essential role of ferrous iron in cyanide-resistant respiration in *Hansenula anomala*. *FEBS Letters* **267**:114-116

Minagawa N., Yabu Y., Kita K., Nagai K., Ohta N., Meguro K., Sakajo S. and Yoshimoto A. 1996. An antibiotic, ascofuranone, specifically inhibits respiration and *in vitro* growth of long slender bloodstream forms of *Trypanosoma brucei brucei*. *Molecular and Biochemical Parasitology* **81**:127-136

Miroux B. and Walker J. 1996. Over-production of proteins in *Escherichia coli*: mutant hosts that allow synthesis of some membrane proteins and globular proteins at high levels. *Journal of Molecular Biology* **260**:289-298

Mitchell P. 1961. Coupling of phosphorylation to electron and hydrogen transfer by a chemi-osmotic type of mechanism. *Nature* **191**:144-148

Moore A.L., Bonner W.D. and Rich P.R. 1978. The determination of the proton-motive force during cyanide-insensitive respiration in plant mitochondria. *Archives of Biochemistry and Biophysics* **186**:298-306

Moore A.L., Dry I.B and Wiskich J.T. 1988. Measurement of the redox state of the ubiquinone pool in plant mitochondria. *FEBS Letters* **235**:76-80

Moore A.L. and Siedow J.N. 1991. The regulation and nature of the cyanide-resistant alternative oxidase of plant mitochondria. *Biochimica et Biophysica Acta* **1059**:121-140

Moore A.L., Umbach A.L. and Siedow J.N. 1995a. Structure-function relationships of the alternative oxidase of plant mitochondria: a model of the active site. *Journal of Bioenergetics and Biomembranes* **27**:367-377

Moore A.L., Umbach A.L. and Siedow J.N. 1995b. A structural model of the alternative oxidase of plant mitochondria. *Biochemical Society Transactions* **23**:151S

Moore A.L., Carré J.E., Affourtit C., Albury M.S., Crichton P.G., Kita K. and Heathcote P. 2008. Compelling EPR evidence that the alternative oxidase is a diiron carboxylate protein. *Biochimica et Biophysica Acta – Bioenergetics* **1777**:327-330

Moore A.L., Shiba T., Young L., Harada S., Kita K. and Ito K. 2013. Unravelling the Heater – New Insights into the Structure of the Alternative Oxidase *Annual Reviews in Plant Biology* **64**: In Press

Morris G.M., Huey R., Lindstrom W., Sanner M.F., Belew R.K., Goodsell D.S. and Olson A.J. 2009. Autodock4 and AutoDockTools4: automated docking with selective receptor flexiblity. *J. Computational Chemistry* **16**: 2785-27 91.

Morrow J.F., Cohen S.F., Chang A.C.Y, Boyer H.W., Goodman H.M. and Helling R.B. 1974. Replication and transcription of eukaryotic DNA in *Escherichia coli*. *Proceedings of the National Academy of Sciences* **71**:1743-1747

Moult J., Pedersen J.T., Judson R. and Fidelis K. 1995. A large-scale experiment to assess protein structure prediction models. *Proteins* **23**:ii-iv

Nakamura K., Sakamoto K., Kido Y., Fujimoto Y., Suzuki T., Suzuki M., Yuba Y., Ohta N., Tsuda A., Onuma M. and Kita K. 2005. Mutational analysis of the *Trypanosoma vivax* alternative oxidase: The $E(X)_6Y$ motif is conserved in both mitochondrial alternative oxidase and the plastid terminal oxidase and is indispensable for enzyme activity. *Biochemical and Biophysical Research Communications* **334**:593-600

Newstead S., Ferrandon S. and Iwata S. 2008. Rationalising α-helical membrane protein crystallisation. *Protein Science* **17**:466-472

Nihei C., Fukai Y. and Kita K. 2002. Trypanosome alternative oxidase as a target of chemotherapy. *Biochimica et Biophysica Acta* **1587**:234-239

Nihei C., Fukai Y., Kawai K., Osanai A., Yabu Y., Suzuki T., Ohta N., Minagawa N., Nagai K. and Kita K. 2003. Purification of active recombinant trypanosome alternative oxidase. *FEBS Letters* **538**:35-40

Nordlund P., Dalton H. and Eklund H. 1992. The active site structure of methane monooxygenase is closely related to the binuclear iron centre of ribonucleotide reductase. *FEBS Letters* **307**:257-262

Nordlund P. and Eklund H. 1993. Structure and function of the *Escherichia coli* ribonucleotide reductase protein R2. *Journal of Molecular Biology* **232**:123-164

Nordlund P. and Eklund H. 1995. Diiron-carboxylate proteins. *Current Opinion in Structural Biology* **5**:758-766

Nugent T. and Jones D.T. 2012. Membrane protein structural bioinformatics. *Journal of Structural Biology* **179**:327-337

Pauling L., Corey R.B., Branson H.R. 1951. The structure of proteins; two hydrogen-bonded helical configurations of the polypeptide chain. *Proceedings of the National Academy of Sciences* **37**:205-211

Peng J. and Xu J. 2011. Raptorx: exploiting structure information for protein alignment by statistical inference. *Proteins* **79**:161-171

Perrière G. and Gouy M. 1996. WWW-query: an online retrieval system for biological sequence banks. *Biochimie* **78**:364-369

Picot D., Loll P.J. and Garavito M. 1994. The X-ray crystal structure of the membrane protein prostaglandin H_2 synthase-1. *Nature* **367**:243-249

Polidoros A.N., Mylona P.V. and Arnholdt-Schmitt B. 2009. *Aox* gene structure, transcript variation and expression in plants. *Physiologia Plantarum* **137**:342-353

Privé G.G. 2007. Detergents for the stabilisation and crystallisation of membrane proteins. *Methods* **41**:388-397

Prothero J.W. 1966. Letters to the editor. *Biophysical Journal* **6**:367-370

Purvis A.C. and Shewfelt R.L. 1993. Does the alternative pathway ameliorate chilling injury in sensitive plant tissues? *Physiologia Plantarum* **88**:712-718

Ramachandran G.N., Ramakrishnan C. And Sasisekharan V. 1963. Stereochemistry of polypeptide chain configurations. *Journal of Molecular Biology* **7**:95-99

Rasmusson A.G., Møller I.M. and Palmer J.M. 1990. Component of the alternative oxidase localized to the matrix durface of the inner membrane of plant mitochondria. *FEBS Letters* **259**:311-314

Rastogi V.K. and Girvin M.E. 1999. Structural changes linked to proton translocation by subunit c of the ATP synthase. *Nature* **402**:263-268

Reynolds J.A. and Tanford C. 1976. Determination of molecular weight of the protein moeity in protein-deterfent complexes without direct knowledge of detergent binding. *Proceedings of the National Academy of Sciences* **73**:4467-4470

Rhoads D.M. and McIntosh L. 1991. Isolation and characterization of a cDNA clone encoding an alternative oxidase protein of *Sauromatum guttatum* (Schott). *Proceedings of the National Academy of Sciences* **88**:2122-2126

Rhoads D.M., Umbach A.L., Sweet C.R, Lennon A.M., Rauch G.S. and Siedow J.N. 1998. Regulation of the cyanide-resistant alternative oxidase from plant mitochondria – identification of the cysteine residue involved in α-keto acid stimulation and intersubunit disulphide bond formation. *Journal of Biological Chemistry* **273**:30750-30756

Rich P.R. and Moore A.L. 1976. The involvement of the protonmotive ubiquinone cycle in the respiratory chain of higher plants and its relation to the branchpoint of the alternate pathway. *FEBS Letters* **65**:339-344

Rich P. R. 1978. Quinol oxidation in *Arum maculatum* mitochondria and its application to the assay, solubilisation and partial purification of the alternative oxidase. *FEBS Letters* **96**:252-256

Rich P.R. 1981. Electron transfer reactions between quinols and quinones in aqueous and aprotic media. *Biochimica et Biophysica Acta* **637**:28-33

Rich P.R. 1984. Electron and proton transfers through quinones and cytochrome *bc* complexes. *Biochimica and Biophysica Acta* **768**:53-79

Rieske J.S., Lipton S.H., Baum H. and Silman H.I. 1967. Factors affecting the binding of antimycin A to complex III of the mitochondrial respiratory chain. *The Journal of Biological Chemistry* **242**:4888-4896

Roberts C.W., Roberts F., Henriquez F.L., Akiyoshi D., Samuel B.U., Richards T.A., Milhouse W., Kyle H., McIntosh L., Hill G.C., Chaudhrui M., Tzipori S. and McLoed R. 2004. Evidence for mitochondrial-dervied alternative oxidase in the apicomplexan parasite *Cryptosporidium parvum*: a potential anti-microbial agent target.*International Journal of Parasitology* **34**:297-308

Rosenzweig A.C., Frederick C.A., Lippard S.J. and Nordlund P. 1993. Crystal structure of a bacterial non-haem iron hydroxylase that catalyses the biological oxidation of methane. *Nature* **366**:537-543

Rosevear P., VanAken T., Baxter J. and Ferguson-Miller S. 1980. Alkyl glycoside detergents: a simpler synthesis and their effects on kinetic and physical properties of cytochrome *c* oxidase. *Biochemistry* **19**:4108-4115

Rost B. and Sander C. 1993. Improved prediction of protein secondary strtucture by use of sequence profiles and neural networks. *Proceedings of the National Academy of Sciences* **90**:755-7562

Rost B. 1996. Predicting one-dimensional protein structure by profile-based neural networks. *Methods in Enzymology* **266**:525-539

Rost. B., Yachdav G. and Liu J. 2004. The PredictProtein server. *Nucleic Acids Research* **W32**:W321-326

Rupp B. and Wang J. 2004. Predictive models for protein crystallisation. *Methods* **34**:390-407

Ruprecht J., Yaknovskaya V., Maklashina E., Iwata S. and Cecchini G. 2009. Structure of *Escherichia coli* succinate:quinone oxidoreductase with an occupied and empty quinone-binding sute. *Journal of Biological Chemistry* **284**:29836-29846

Russo E. 2003. Special report. *Nature* **421**:456-457

Sakajo S., Minagawa N. and Yoshimoto A. 1991. Molecular cloning of cDNA for antimycin A-inducible mRNA and its role in the cyanide-resistant respiration in *Hansenula anomala*. *Biochemica et Biophysica Acta* **1090**:102-108

Sali A. and Blundell T.L. 1993. Comparative protein modelling by satisfaction of spatial restraints. *Journal of Molecular Biology* **234**:779-815

Sander C. and Schneider R. 1991. Database of homology-derived protein structures and the structural meaning of sequence alignment. *Proteins* **9**:56-68

Schonbaum G.R., Bonner W., Storey B.T. and Bahr J.T. 1971. Specific inhibition of the cyanide-insentive respiratory pathway in plant mitochondria by hydroxamic acids. *Plant Physiology* **47**:124-128

Schwede T., Kopp J., Guex N. and Peitsch M.C. 2003. Swiss-model: an automated protein homology-modelling server. *Nucleic Acids Research* **31**:3381-3385

Shiba T., Kido Y., Sakamoto K., Takahashi G.,, Inaoka D.K., Tsuge C., Tatsumi R., Balogun E.O., Nara T., Aoki T., Honma T., Tanaka A., Inoue M., Matsuoka S., Saimoto H., Moore A.L., Harada S. and Kita K. 2013. Structure of the trypanosome cyanide-insensitive alternative oxidase, a promising drug target. *Proceedings of the National Academy of Sciences* : In Press

Shoichet B.K., Bodian D.L. and Kuntz I.D. 1991. Molecular docking using shape descriptors. *Journal of Computational Chemistry* **3**:380-397

Shoichet B.K. and Kuntz I.D. 1991. Protein docking and complementarity. *Journal of Molecular Biology* **221**:327-346

Shrake A. and Rupley J.A. 1973. Environment and exposure to solvent of protein atoms; lysozyme and insulin. *Journal of Molecular Biology* **79**:351-371

Siedow J.N. and Bickett D.M. 1981. Structural features required for inhibition of cyanide-insensitive electron transfer by propyl gallate. *Archives of Biochemistry and Biophysics* **207**:32-39

Siedow J.N., Umbach A.L. and Moore A.L. 1995. The active site of the cyanide-resistant oxidase from plant mitochondria contains a binuclear iron centre. *FEBS Letters* **362**:10-14

Sippl M.J. 1990. Calculation of conformational ensembles from potentials of mean force. *Journal of Molecular Biology* **213**:859-883

Sippl M.J. 1993. Recognition of errors in three-dimensional structures of proteins. *Proteins* **17**:355-362

Smith P.K., Krohn R.I., Hermanson G.T., Mallia A.K., Gartner F.H., Provenzano M.D., Fujimoto E.K., Goeke N.M., Olson B.J. and Klenk D.C. 1985. Measurement of protein using bicinchroninic acid. *Analytical Biochemistry* **150**:76-85

Söding J., Biegert A. and Lupas A.N. 2005. The HHPred interactive server for protein homology detection and structure prediction. *Nucleic Acids Research* **33**:W244-W248

Söding J. 2005. Protein homology detection by HMM-HMM comparison. *Bioinformatics* **21**:951-960

Sousa R. 1995. Use of glycerol, polyols and other protein structure stabilising agents in protein crystallisation. *Acta Crystallographica* **D51**:271-277

Sreerama N., Venyaminov S.Y. and Woody R.W. 1999. Estimation of the number of α-helical and β-strand segments in proteins using circular dichroism spectrocopy. *Protein Science* **8**:370-380

Sreerama N. and Woody R.W. 2000. Estimation of protein secondary structure from circular dichroism spectra: comparison of CONTIN, SELCON and CDSSTR methods with an expanded reference set. *Analytical Biochemistry* **287**:252-260

Sreerama N. and Woody R.W. 2004. On the analysis of membrane protein circular dichroism spectra. *Protein Science* **13**:100-112

Srinivasan S., March C.J. and Sudarsanam S. 1993. An automated method for modelling protein on known templates using distance geometry. *Protein Science* **2**:277-289

Stechmann A., Hamblin K., Pérez-Brocal V., Gaston D., Richmond GS., van der Giezen M., Clark C.G. and Roger A.J. 2008. Organelles in Blastocystis that blur the distinction between mitochondria and hydrogenosomes. *Current Biology* **18**:580-585

Storey B.T. 1976. Respiratory chain of plant mitochondria: XVIII – Point of interaction of the alternative oxidase with the respiratory chain. *Plant Physiology* **58**:521-525

Stubbe J. 2003. Di-iron tyrosyl radical ribonucleotide reductases. *Current Opinion in Chemical Biology* **7**:183-188

Studier F.W. and Moffat B.A. 1986. Use of bacteriophate T7 RNA polymerase to direct selective high-level expression of cloned genes. *Journal of Molecular Biology*. **189**:113-130

Studier F.W., Rosenberg A.H., Dunn J.J. and Dubendorff J.W. 1990. Use of T7 RNA polymerase to direct expression of cloned genes. *Methods in Enzymology***185**:60-89

Suzuki T., Hashimoto T., Yabu Y., Kido Y., Sakamoto K., Nihei C., Hato M., Suzuki S., Amano Y., Nagai K., Hosokawa T., Minagawa N., Ohta N. and Kita K. 2004. Direct evidence for cyanide-insensitive quinol oxidase (alternative oxidase) in apicomplexan parasite *Cryptosporidium parvum*: phylogenetic and therapeutic implications. *Biochemical and Biophysical Research Communications* **313**:1044-1052

Svensson-Ek M., Abramson J., Larsson G., Törnroth A., Brzezinski P. and Iwata S. 2002. The X-ray crystal structures of wild-type and EQ(I-286) mutant cytochrome *c* oxidases from *Rhodobacter sphaeroides*. *Journal of Molecular Biology* **321**:329-339

Swords N.A. and Wallace B.A. 1993. Circular-dichroism analyses of membrane proteins: examination of environmental effects on bacteriorhodopsin spectra. *Biochemical Journal* **289**:215-219

Tanudji M., Sjöling S., Glaser E. And Whelan J. 1999. Signals required for the import and processing of the alternative oxidase into mitochondria. *Journal of Biological Chemistry* **274**:1286-1293

Terpe K. 2006. Overview of bacterial expression systems for heterologous protein production: from molecular and biochemical fundamentals to commercial systems. *Appl Microbiol Biotechnol* **72**:211-222

Thompson J.D., Higgins D.G. and Gibson T.J. 1994. Clustal W: improving the sensitivity of progressive multiple sequence alignment through sequence weighting, position-specific gap penalties and weight matrix choice. *Nucleic Acids Research* **22**:4673-4680

Tovchihrechko A. and Vasker I.A. 2006. Gramm-x public web server for protein-protein docking. *Nucleic Acids Research* **34**:W310-W314

Umbach A.L. and Siedow J.N. 1993. Covalent and noncovalent dimmers of the cyanide-resistant alternative oxidase protein in higher plant mitochondria and their relationship to enzyme activity. *Plant Physiology* **103**:845-854

Umbach A.L., Wiskich J.T and Siedow J.N. 1994. Regulation of alternative oxidase kinetics by pyruvate and intermolecular disulfide bond redox status in soybean seedling mitochondria. *FEBS Letters* **348**:181-184

Umbach A.L., Gonzàlez-Meler M.A., Sweet C.R. and Siedow J.N. 2002. Activation of the plant mitochondrial alternative oxidase: insights from site-directed mutagenesis. *Biochemica et Biophysica Acta: Bioenergetics* **1554**:118-128

van Buuren K.J.H., Zuurendonk P.F., van Gelder B.F. and Muijsers A.O. 1972. Biochemical and biophysical studies on cytochrome aa_3: binding of cyanide to cytochrome aa_3. *Biochimica et Biophysica Acta* **256**:243-257

Vanlerberghe G.C. and McIntosh L. 1997. Alternative oxidase: from gene to function. *Annual Review of Plant Physiology and Plant Molecular Biology* **48**:703-734

Veiga A., Arrabaça J.D. and Loureiro-Dias M.C. 2003. Cyanide-resistant respiration, a very frequent pathway in yeast. *FEMS Yeast Research* **3**:239-245

Vincent J.B., Olivier-Lilley G.L. and Averill B.A. 1990. Proteins containing oxo-bridged dinuclear iron centres: a bioinorganic perspective. *Chemical Reviews* **90**:1447-1467

Wagner A.M., Krab K., Wagner M.J. and Moore A.L. 2008. Regulation of thermogenesis in flowering Araceae: The role of the alternative oxidase. *Biochimica et Biophysica Acta: Bioenergetics* **1777**:993-1000

Wakagi T. 2003. Sulerythrin, the smallest family member of the rubrerythrin family, from a strictly aerobic and thermoacidophilic archeon, *Sufolobus tokodaii* strain 7. *FEMS Microbiology Letters* **222**:33-37

Wallace B.A., Lees J.G., Orry A.J.W., Lobley A. and Janes R.W. 2003. Analyses of circular dichroism spectra of membrane proteins. *Protein Science* **12**:875-884

Wallner B. and Elofsson A. 2005. All are not equal: a benchmark of different homology modelling programs. *Protein Science* **14**:1315-1327

Whitmore L. and Wallace B.A. 2004. Dichroweb, an online server for protein secondary structure analyses from circular dichroism spectroscopic data. *Nucleic Acids Research* **2004**:W668-673

Whitmore L. and Wallace B.A. 2008. Protein secondary structure analyses from circular dichroism spectroscopy: Methods and reference databases. *Biopolymers* **89**:392-400

Wiederstein M. and Sippl M.J. 2007. ProSA-web: interactive web service for the recognition of errors in three-dimensional structures of proteins. *Nucleic Acids Research* **35**:W407-W410

Wilkins R.G. 1992. Binuclear iron centres in proteins. *Chemistry Society Reviews* **21**:171-178

Williams B.A.P., Elliott C., Burri L., Kido Y., Kita K., Moore A.L. and Keeling P.J. 2010. Wide distribution of the mitochondrial alternative oxidase in microsporidia parasites. *Plos Pathogens* **6**:2 e1000761

Winn M.D. *et al*. 2011. Overview of the CCP4 suite and current developments. *Acta Crystallographica Section D* **D67**:235-242

Yabu Y., Yoshida A., Suzuki T., Nihei C., Kawai K, Minagawa N., Hosokawa T, Nagai K, Kita K and Ohta N. 2003. The efficacy of ascofuranone in a consecutive treatment on *Trypanosoma brucei brucei* in mice. *Parasitology International* **52**:155-164

Yadav S. and Ahmed F. 2000. A new method for the determination of stability parameters of proteins from their heat-induced denaturation curves. *Analytical Biochemistry* **283**:207-213

Yoshikawa S., Shinzawa-Itoh K., Nakashima R., Yaono R., Yamashita E., Inoue N., Yao M., Fei M.J., Libeu C.P., Mizushima T., Yamaguchi H., Tomizaki T. and Tsukihara T. 1998. Redox-coupled crystal structure changes in bovine heart cytochrome c oxidase. *Science* **280**:1723-1729

Zhang Q.S., Hoefnagel M.H.N. and Wiskich J.T. 1996. Alternative oxidase from *Arum* and soybean: its stabilisation during purification. *Physiologia Plantarum* **96**:551-558

Zheng Y., Fung R.W.M., Wang S.Y. and Wang C.Y. 2008. Transcript levels of antioxidative genes and oxygen radical scavenging enzyme activities in chilled zucchini squash in response to superatmospheric oxygen. *Postharvest Biology and Technology* **47**:151-158

Zimm B.H. and Bragg J.K. 1959. Theory of the phase transition between helix and random coil in polypeptide chains. *The Journal of Chemical Physics* **31**:526-535

Appendix

A. Full *S. guttatum* alternative oxidase sequence (P22185):

```
MMSSRLVGTALCRQLSHVPVPQYLPALRPTADTASSLLHGCSAAAPAQRAGLWPPSWFSP
PRHASTLSAPAQDGGKEKAAGTAGKVPPGEDGGAEKEAVVSYWAVPPSKVSKEDGSEWRW
TCFRPWETYQADLSIDLHKHHVPTTILDKLALRTVKALRWPTDIFFQRRYACRAMMLETV
AAVPGMVGGVLLHLKSLRRFEHSGGWIRALLEEAENERMHLMTFMEVAQPRWYERALVLA
VQGVFFNAYFLGYLLSPKFAHRVVGYLEEEAIHSYTEFLKDIDSGAIQDCPAPAIALDYW
RLPQGSTLRDVVTVVRADEAHHRDVNHFASDVHYQDLELKTTPAPLGYH
```

B. Crystal screen solutions producing microcrystals (Section 4.3.4):

Screen	Salt	pH	Precipitant
Memstart 9	-	6.5	-
Memstart 10	0.1M $(NH_4)_2SO_4$	7.5	K_2HPO_4 + Na_2HPO_4
Memstart 15	0.1M $(NH_4)_2SO_4$	4.6	4M formate
Memstart 21	0.1M NaCl	5.6	30% PEG 400
Memstart 22	0.1M $LiSO_4$	5.6	30% PEG 400
Memstart 23	0.1M $LiSO_4$	6.5	30% PEG 400
Memstart 24	0.1M $MgSO_4$	7.5	30% PEG 400
Memstart 29	0.1M $(NH_4)_2SO_4$	4.6	12% PEG 4000
Memstart 31	0.1M NaCl	5.6	12% PEG 4000
Memstart 35	0.2M $MgCl_2$	8.5	12% PEG 4000
Memstart 41	0.1M $(NH_4)_2HPO_4$	8.5	12% PEG 4000
Memsys 8	0.1M NaCl	6.5	30% PEG 400
Memsys 16	0.1M NaCl	7.5	30% PEG 400
Memsys 24	0.1M NaCl	9.5	30% PEG 400
Memsys 25	0.1M NaCl	9.5	1.5M $NaPO_4$
Memsys 28	0.1M NaCl	5.5	12% PEG 4000

C. Sequences used in multiple alignments can be found on the CD at the back of this thesis.

D. ProSA-web output graphs for homology models (Section 5.3.3):

Left: for *S. guttatum* alternative oxidase using Δ^9-desaturase as a template; Right for *S. guttatum* alternative oxidase using TAO as a template (black dot represents z-score for the model).